Self-Assembly of Synthetic Zinc Chlorophylls

– Structure Control for Light Harvesting –

Dissertation

Department of Materials and Applied Chemistry,
Graduate School of Science and Technology,
Nihon University

2015

Yoshinao Shinozaki
Supervised by Prof. Joe Otsuki

Preface

This dissertation entitled "*Self-Assembly of Synthetic Zinc Chlorophylls: Structure Control for Light Harvesting*" is described based on the research performed under the direction of Professor Joe Otsuki at the Supramolecular Chemistry Laboratory (Department of Materials and Applied Chemistry, Graduate School of Science and Technology) in the period 2010–2015.

Construction of the artificial light-harvesting antenna models is of interest not only to understand fundamental light-harvesting processes in nature and also to improve the efficiency of artificial photosynthesis. The models with diverse structure have been constructed for such purpose. The geometry of the antennae is an important factor for energy transfer because orientations and distances among the light-harvesting chromophores in the antennae significantly influence its efficiency. Therefore systematic investigation of the contribution of the geometry to the energy transfer is required for exploring the promising antennae. Thus the author described this dissertation focusing on tuning the energy transfer efficiency within the antennae by control of their geometry. Self-assembly of synthetic zinc chlorophyll derivatives appended by *N*-heterocycles *via* intermolecular coordination interaction between the nitrogen atom in the heterocyclic moiety and the zinc atom in the center of chlorophyll ring was utilized to construct the novel antenna models. Because the orientations among the zinc chlorophyll components in the assemblies change by altering the *N*-heterocyclic moiety in the zinc chlorophyll derivative, it was expected that the efficiency within the assemblies should change simultaneous with change in their higher-order structures. Thus the author described characterization of the assemblies formed by self-assembly of the zinc chlorophyll derivatives in Chapters 2 and 3 followed by control of higher-order structures of the coordination polymers formed in the crystal in Chapter 4 based on the insight obtained from Chapters 2 and 3. On the other hand, Chapters 5 and 6 were described for the purpose of utilization of the assemblies in solution as the antennae. While the insight into the molecular design suitable for the purpose in Chapter 6 was obtained in Chapter 5, the

antenna function of the assemblies comprising the zinc chlorophyll derivatives suitably designed was demonstrated in Chapter 6.

The author expresses his deepest gratitude to all researchers involving to him up to the present date below.

Most of the author's research life occupied the time that spent with Professor Joe Otsuki. This dissertation was realized by his advices and tutelage on this research as well as his attitudes and ambition to chemistry. Therefore the greatest thanks should be given to him. The author must sincerely thank to many researchers corroborating with him: Dr. Kosuke Sugawa (Nihon Univ.), Dr. Gary J Richards (Tsukuba Univ.), Dr. Keizo Ogawa (Nihon Univ.), Dr. Akihito Yamano (Rigaku), Dr. Kazuaki Ohara (Tokushima Bunri Univ.), Prof. Kentaro Yamaguchi (Tokushima Bunri Univ.), Dr. Shin-ichiro Kawano (Nagoya Univ.), Prof. Kentaro Tanaka (Nagoya Univ.), Dr. Yasuyuki Araki (Tohoku Univ.), Prof. Takehiko Wada (Tohoku Univ.), Prof. Koji Araki (Univ. Tokyo), Dr. Isao Yoshikawa (Univ. Tokyo), Prof. Taro Tsubomura (Seikei Univ.), Dr. Takayoshi Watanabe (Chiba Cancer Center), Prof. Hiroki Nagase (Chiba Cancer Center), Dr. Kyoko Fujiwara (Nihon Univ.), Dr. Naoya Ishibashi (Nihon Univ.), Dr. Toru Oba (Utsunomiya Univ.), Miss Rei Nakayama (Nihon Univ.), Dr. Hiroki Ikake, Dr. Kei Ohkubo (Osaka Univ.), and Prof. Shunichi Fukuzumi (Osaka Univ.). This work was not accomplished without their contributions. Best wishes from the author for their continued success. Moreover the author thanks to all judges for this dissertation, especially to Prof. Atsuyoshi Nishina (Nihon Univ.) and Prof. Hiizu Iwamura (Nihon Univ.). The author is finally grateful to the members sharing joys and sorrows in the Supramolecular Chemistry Laboratory during the period from 2010 to 2015, although their names do not given, and wishes the precious memories not to fade no matter how many years pass by.

February 2015

Yoshinao Shinozaki

Contents

Chapter 1

Introduction

1-0 General Introduction

Most of the world's energy supply relies on fossil and nuclear sources in the present situation.[1,2] Although the society faces the issues of resource limitation and environmental pollution, we have to continue to be dependent on the supply for our living without a breakthrough in alternative energy production while caring about the preservation of these sources for the next generation.[2] Utilization of sunlight can fulfill social energy demands in an environmentally benign manner due to its abundance, non-polluting property, and sustainability when the technologies are developed for conversion of solar energy to clean fuels.[3-6] In natural world, in fact, photosynthesis allows such conversion using sunlight, in which oxygen and carbohydrates are produced by oxidation of water and carbon dioxide.[7]

Artificial solar energy conversion such as light-driven water splitting,[8-10] photovoltaics and photoelectrochemical cells[11,12] have not yet made a strong contribution to the energy supply because of their low conversion efficiencies although there are extensive efforts to improve their efficiencies over the decades.[2,13] On the other hand, natural photosynthetic system demonstrates remarkably high efficiencies for light-driven catalytic reactions like water oxidation reaction whose efficiency is more than 80% under certain conditions.[14] This high efficiency is caused by highly frequently generated photo-induced charge separation state of reaction center as a primary step in photosynthesis.[3] However, in fact, most of charge separation is not due to direct photoexcitation of reaction center but rather due to excitation energy transfer from light-harvesting antennae to the reaction center.[15]

Light-harvesting antennae are large assemblies consisting of mainly (bacterio)chlorophyll molecules, whose photoexcitation energy is transferred within and among the antennae with high efficiencies until it reaches a reaction center.[3,16] In addition to such funneling function of excitation energy, large area of the antennae enables to give a substantially increased cross-section for light absorption.[3] To translate natural antenna functions into artificial systems, researchers have been making effort to learn natural light harvesting and mimic its functions by synthetic antenna models.[17-19]

Thus, we firstly describe light-harvesting antennae in natural photosynthesis, and

understand the relationship between their structures and functions (1-1). Although it is shown that there are several types of antennae, light-harvesting antenna complexes (LH) 1 and 2 will mainly be mentioned because their structural analyses are most progressed. The following section is about artificial antenna models (1-2). We describe the strategies of construction of large antenna structures needed for effective collection of photons as well as their functions and properties.

1-1 Light-Harvesting Antennae in Natural Photosynthesis

Photosynthesis is multifarious processes in which oxygen and carbohydrates are produced from water and carbon dioxide using sunlight, which can be divided into three processes: (i) light-harvesting processes; (ii) charge generation and separation processes; and (iii) catalytic reaction processes.[7] The light harvesting is a key for success of photosynthesis, in which protein–chromophore complexes called light-harvesting (antenna) complexes perform collection of photons from sunlight and concentration of local excitation energy to reaction center. Furthermore the antenna complexes simultaneously carry out photoprotection by dissipation of excess energy as heat.[20] Although structure analyses of photosynthetic organisms have been performed, the structures of the antennae are not fully clarified due to their diversity and complexity. However, because the structure analyses of light-harvesting complexes LH1 and LH2 has been one of intense research issues,[21-24] their structures have recently been revealed by X-ray crystallography at near atomic resolution, allowing us to understand the detailed mechanism of nature's light harvesting.[25-30] The following sections thus show structures of LHs focusing on (bacterio)chlorophyll ((B)Chl) molecules (1-1-1), and then explain the light-harvesting mechanism on the basis of the understanding their structures (1-1-2).

1-1-1 Light-Harvesting Complexes (LHs) 1 and 2

Light-harvesting complexes (LHs) are integral membrane proteins containing chromophores including carotenoids and (B)Chls. LHs are the components of the

photosynthetic antenna system,[31,32] where LHs serve as the absorber of the sunlight for initiation of photosynthesis. In purple photosynthetic bacteria, the light-harvesting system contains mainly two types of light-harvesting complexes.[29] The first type, LH1, is called a core antenna, which is stoichiometrically associated with the reaction center (RC) to form core complex RC-LH1. The other type of light-harvesting complex, LH2, which is called a peripheral antenna, surrounds the RC-LH1 core complex in variable amounts.[22,28,30] Although the structures of the complexes vary slightly with species, the complexes are constructed following the same principle. The LHs consist of oligomeric assembly of unit heterodimers comprising α- and β-apoproteins bound to light-absorbing BChls and Carotenoids by non-covalent interactions.[28,30,33] This section describes the crystal structures of LH2 of *Rhodopseudomonas acidophila* and RC-LH1 in *Rhodopseudomonas palustris* focusing on BChls, and their photophysical features participating in light harvesting.

Structure of LH2 in Rhodopseudomonas acidophila[30]

The crystal structure of LH2 in *Rhodopseudomonas acidophila strain* 10050 was reported by N. W. Isaacs *et al*. in 1995 (Figure 1-1).[30] The structure of LH2 has a nine-fold symmetry. The nine sets of α- and β-apoproteins are arranged radially to form a cylinder, where α- and β-apoproteins position on the inward and outward sides, respectively. An αβ-apoprotein unit incorporates two Bchl-*a* molecules with a slipped cofacial orientation between α and β-apoproteins: totally eighteen BChl-*a* molecules form an inner ring. The remaining nine Bchl-*a* molecules pack with between the β-apoproteins to form an outer ring. The BChl-*a* molecules are fixed by the proteins with non-covalent bonds including a metal-ligand coordination bond. The magnesium atom in Bchl-*a* is coordinated by the imidazolyl group of histidine residues or the carbonyl group in methionine residues on the proteins.

The two groups of Bchl-*a*'s are identified by their absorption maxima. The groups of eighteen (B850) and nine (B800) Bchl-*a*'s show the maxiama at 850 nm and 800 nm, respectively. This difference in the absorption maxima partly is attributed to interchromophore interaction. The B800 Bchl-*a* molecules are almost isolated from other BChls thus are

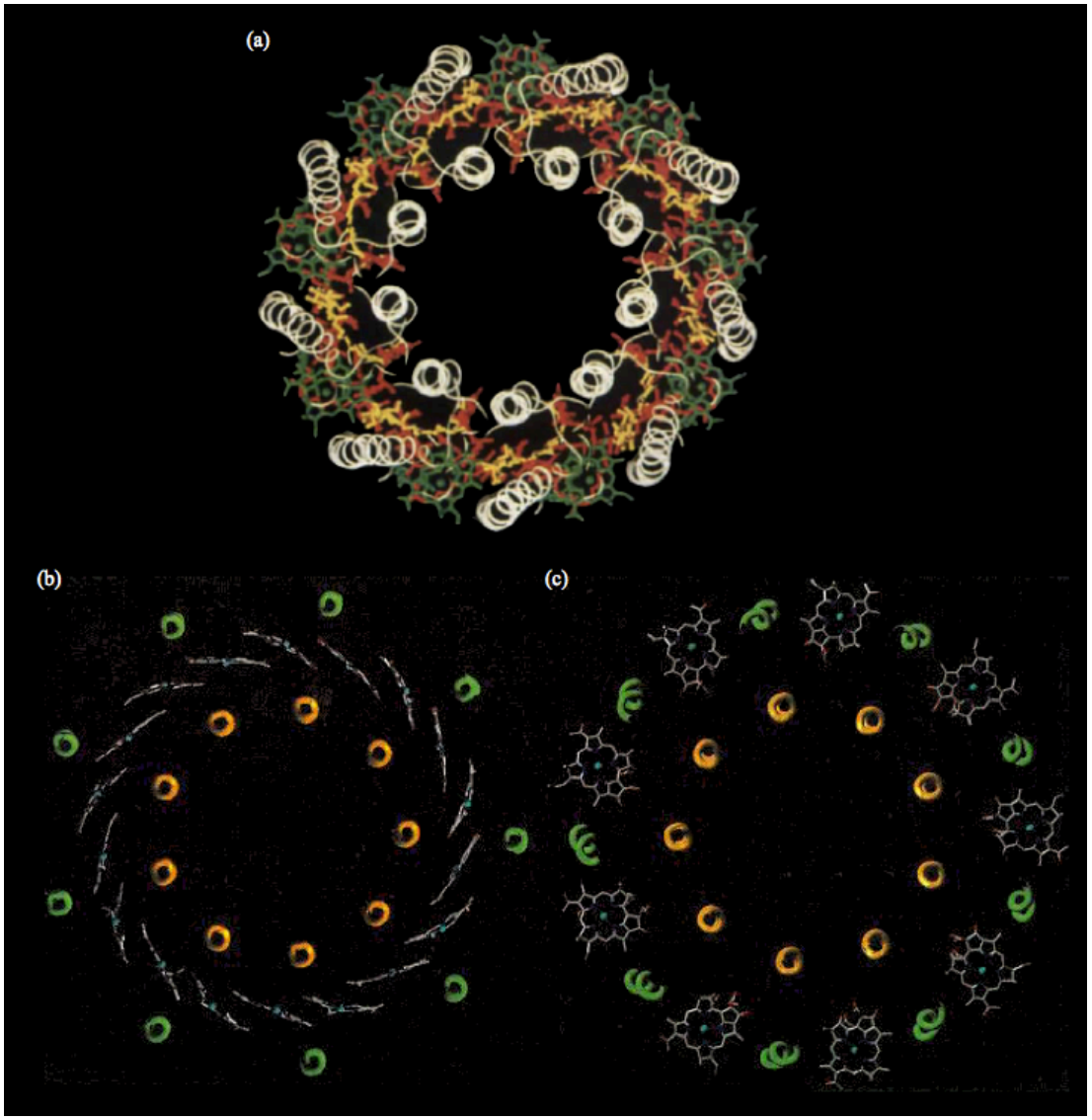

Figure 1-1. (a) Crystal structure of LH2 in *Rhodopseudomonas acidophila strain* 10050. The B850 BChl-*a* molecules (b) and the B800 BChl-*a* molecules (c) in LH2. The α- and β-apoproteins are represented by yellow and green cylinders, respectively. [15,19]

Peproduced from [30, 36] with permission from Nature (No. 3474180996399) and Elsevier (No. 3474174154), 2014.

regarded as being in an almost monomeric state. The central Mg–Mg distance of the closest pair of B800 and B850 molecules is 17.6 Å, and that of two B800 molecules is 21 Å. On the other hand, the B850 Bchl-*a* molecules form one system by π-orbital overlapping as indicated by the short Mg–Mg distance between the adjacent BChl-*a* pair (8.7 Å).[34] As the results of the Coulombic coupling of the transition dipole moments which can occur between such closely interacting pigments makes the absorption maxima red-shifted.[34]

Structure of RC-LH1 in Rhodopseudomonas palustris[28,35]

Although the crystal structure of RC-LH1 is not fully determined unlike that of LH2, the LH1 is fundamentally constructed following the same principle with that of LH2. The crystal structure of RC-LH1 in *Phodopseudomonas palustris* reported by A. W. Roszak *et al.* is shown in Figure 1-2. The LH1 consists of fifteen αβ-apoprotein units incorporating two BChl-*a* molecules per unit, where α- and β-apoproteins are arranged inside and outside of LH1, respectively. The assembly of αβ-apoprotein units make an elliptical structure with a gap rather than a circle. The αβ-apoprotein units are radially positioned from the RC at the center of LH1. Very recently, another crystal structure of RC-LH1 was reported by S. Niwa *et al*.[29] In this report, sixteen αβ-apoprotein units constitute LH1 without the gate-like gap.

The BChl-*a* molecules in LH1 are arranged between the protein walls in a manner similar to B850 in LH2. The BChl-*a* group in LH1 is called B875 showing absorption maxima at 875 nm.[36] This further red-shift compared to absorption maxima of other BChl-*a* groups is due to slight differences in chemical environments of the LH2 and LH1 BChl-*a* binding sites.[35] The RC also contains BChl-*a*'s, which exist as a dimer so-called special pair (P870) whose absorption maxima is at 870 nm.[21] It is worth noting that the P870 locates in the same plane with B875 and B850, that shows cooperative energy transfer of BChl-*a*s in the LHs to the P870 for light harvesting.[30,35]

1-1-2 Mechanism of Light Harvesting

The light-harvesting system in purple bacteria comprises a reaction center–core antenna

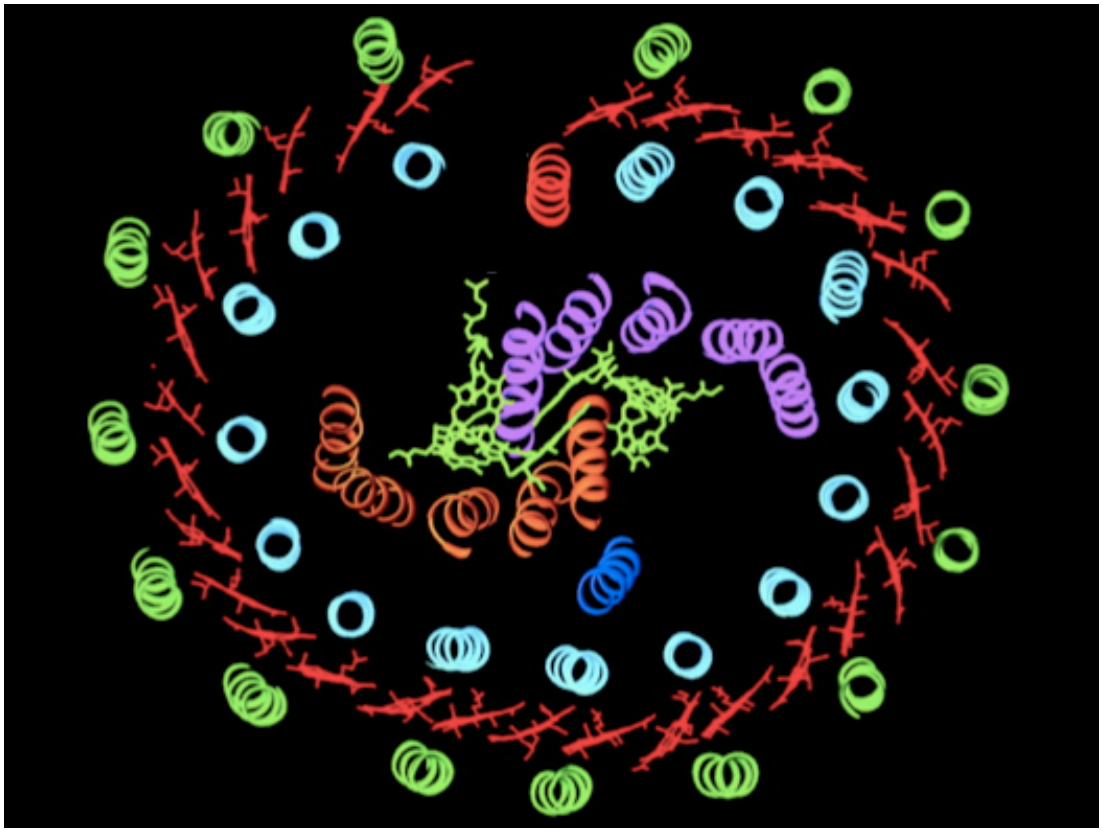

Figure 1-2. Schematic model of the RC-LH1 in *Rhodopseudomonas palustris.* Peproduced from [28] with permission from AAAS (No. 3474210986282), 2014.

complex RC-LH1 and peripheral antenna LH2s surrounding RC-LH1 in variable amounts as mentioned above (Figure 1-3). This system thus contains three antenna groups of BChl-*a*s with different excited state energies, B800, B850, and B875, which are manipulated by the surrounding environment to amplify the range of absorption wavelengths.[37,38] These groups organize along energy gradient to ensure the funneling of the excitation energy to the reaction center. The B875 in LH1 with the lowest energy accepts energy from B850 in LH2, while B850 accepts the energy from B800 with the highest energy by excitation energy transfer. It should be noted that an exciton moves through energy hopping, which is defined as energy transfer among energetically equivalent molecules, around a ring before interring energy transfer.[39,40] The energy arrived at B875 is finally available for transfer from LH1 to P870 in RC. The mechanism of the upfill energy transfer step from B875 to P870 in RC has not yet been fully clarified.

The consecutive energy transfer to P870 must be performed rapidly because the following catalytic events require multiple electron transfer from the single P870, its photoexcitation rate thus exceeds the rate of charge recombination.[3] The energy transfer dynamics within the light-harvesting system have been studied by means of several techniques including spectral hole burning, pump–probe, and three-pulse photon echo techniques as well as theoretical modeling.[41] The first energy transfer step, B800→B850, occurs in a few picosecond range. Sundström *et al.* proved the transfer rate in LH2 of *Rhodobacter sphaeroide* to be ~0.7 ps by a transient absorption measurement.[42] Other techniques also give similar results. As an example, Grondelle *et al.* found the rate to be 600–700 fs from the transient gating and three-pulse echo peak shift for the LH2 in *Rhodopseudomonus acidiphilia* and *Rhodospirillum molischianum*.[43] The energy transfer of B850→B875 occurs more slowly than that of B800→B850. Hess *et al.* estimated the transfer rate in *Rhodobacter sphaeroide* to be ~3 ps by using a two-color pomp-probe measurement.[44] As similar result was reported by Nagarajan *et al.* by using *Rhodobacter sphaeroide* lacking RC, the rate being ~5 ps.[45] The energy transfer rate of LH2→LH2 was obtained only by a calculation employing an effective Hamiltonian approach to the best of our knowledge, and was determined to be 7–10 ps by Schulten and

co-workers.[46,47] This is due to experimental difficulty in studying the LH2→LH2 energy transfer since there is no spectral change associated with this process.[42] Whereas the ring-to-ring energy transfer mentioned so far can be described by weak-coupling theories such as the Förster theory since the distances between the rings are large compared to the dimensions of BChl molecules, such weak-coupling theories are inadequate to be applied to the energy transfer within a ring (energy hopping) as the BChl molecules in the B850 or B875 strongly couple as mentioned above.[48,49] Although the mode of energy transfer taking place within the B850 and B875 rings is less clear,[48,49] it is mentioned that these energy hopping occur in ~100 fs.[48,49] The uphill energy transfer form B875→P870, energy trapping, is final and the rate-limiting step in the overall energy flow to RC. The trapping rate was estimated to be in several ten ps. The time-resolved fluorescence measurements by V. Sundström *et al.* demonstrated that the trapping occurs in 40–50 ps.[50] Now it is understood that the trapping by RC has high efficiency but still being variable (70–90%). It is proposed that this slow rate is a consequence of the size of the RC, which prevents itself from approaching the LH1.[42] The opposite process, detrapping, would be minor, but should occur because of the uphill energy gradient. The detrapping rate was determined to be 10-13 ps (~20%) by V. Sundström *et al.*[50]

1-2 Artificial Antenna Models

Naturally occurring antenna complexes as described so far serve as the apotheosis for the design of the artificial antenna model.[51] The development of efficient antennae requires an appropriate design including the selection of the light-harvesting chromophores as well as the overall geometry of the antenna.[52]

The tetrapyrrolic compounds are a suitable building block for constructing molecular array due to their excellent light-harvesting ability in term of wide absorption and high extinction coefficient. The porphyrin and chlorophyll arrays thus are the most promising candidate for light-harvesting antennae.[53-60] The zinc complexes or the non-metallated derivatives are particularly suitable as the component chromophores compared with the magnesium complexes used in natural antenna system in term of chemical stability. Furthermore, as the

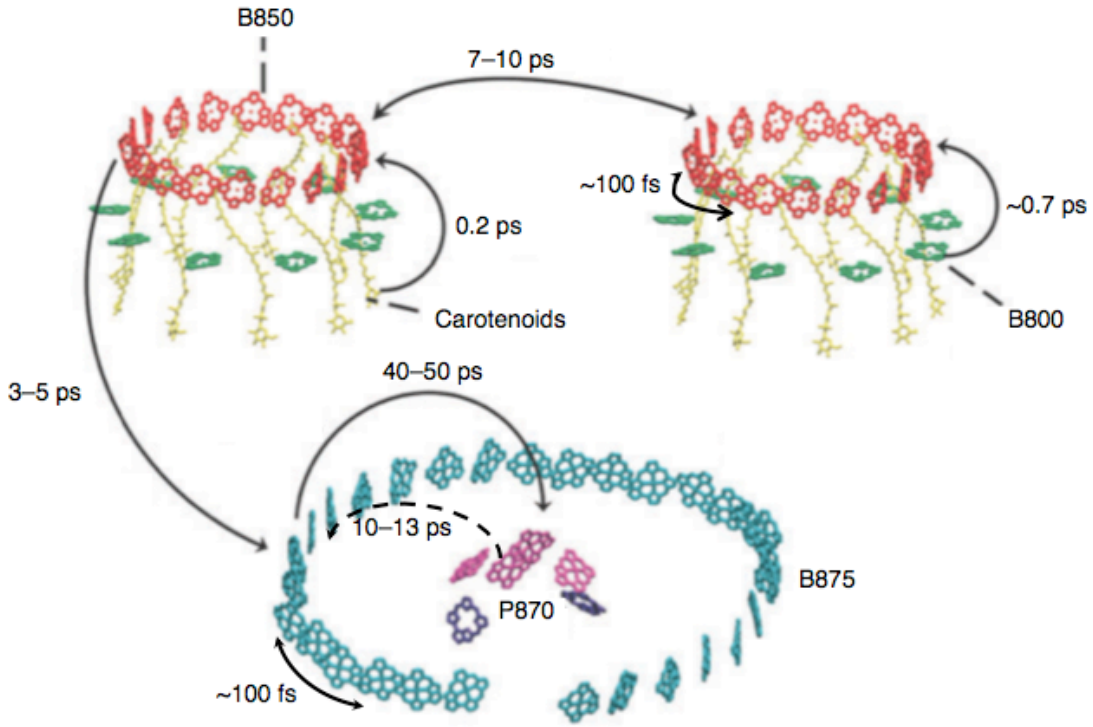

Figure 1-3. Overall energy transfer within the LH system in photosynthetic purple bacteria. Reproduced from [14] with permission from RSC (No. 3474591226996), 2014.

examples shown below, use of the zinc complexes is preferable to utilize the coordination bond between the metal atom and an apical ligand for construction of the array due to its high association constant as compared that of the magnesium complexes. Therefore, in this section, we focus on porphyrin and chlorophyll arrays and review the reports on their arrays sorted by their structure together with their performance as light-harvesting antennae.

LHs-Like Antennae

Cyclic porphyrin oligomers are the interesting candidates for the artificial light-harvesting antennae which are intended to mimic structural aspects of the ring-shaped chlorophyll arrays in photosynthetic purple bacteria.[61] Osuka and coworker reported the cyclic porphyrin oligomers **CZ4**, **CZ6**, and **CZ8**, in which the porphyrins are directly linked at the meso position (Scheme 1-1), and related cyclic porphyrin arrays. The unique meso–meso coupling of porphyrins was performed by the Ag(I)-prompted oxidative coupling reaction, which regioselectively occurs only at the meso position. **CZ4** and **CZ8** were obtained by the intramolecular cyclization and the cyclic dimerization of the linear tetramer **4a**, respectively, whereas **CZ6** was synthesized by the intermolecular dimerization of the linear trimer **3a**. At the optimized concentration of these linear species, which is a critical factor for the cyclization reaction, the cyclic oligomers were obtained in high yield (74%/**CZ4**, 22%/**CZ6**, 29%/**CZ8**). The excitation energy hopping times in these cyclic oligomers were investigated by transient absorption and transient anisotropy absorption measurements. The fact that the hopping within these cyclic oligomers efficiently occurs in 100–400 fs arises from the strong excitonic coupling between the porphyrin components.

The pentagonal and hexagonal cyclic arrays **5** and **6** were reported by Kobuke *et al* (Chart 1-1).[18,62] The pentagon and hexagon formed by self-assembly of a zinc porphyrin dimer with two imidazolyl groups *via* the intermolecular coordination interaction between the imidazolyl group and the zinc center in the porphyrin moiety. These arrays were fully characterized by the gel permeation chromatography, the small-angle X-ray scattering, and the atomic force microscopy as well as the ^{1}H-NMR measurement.[62] Further the pentagon and hexagon arrays

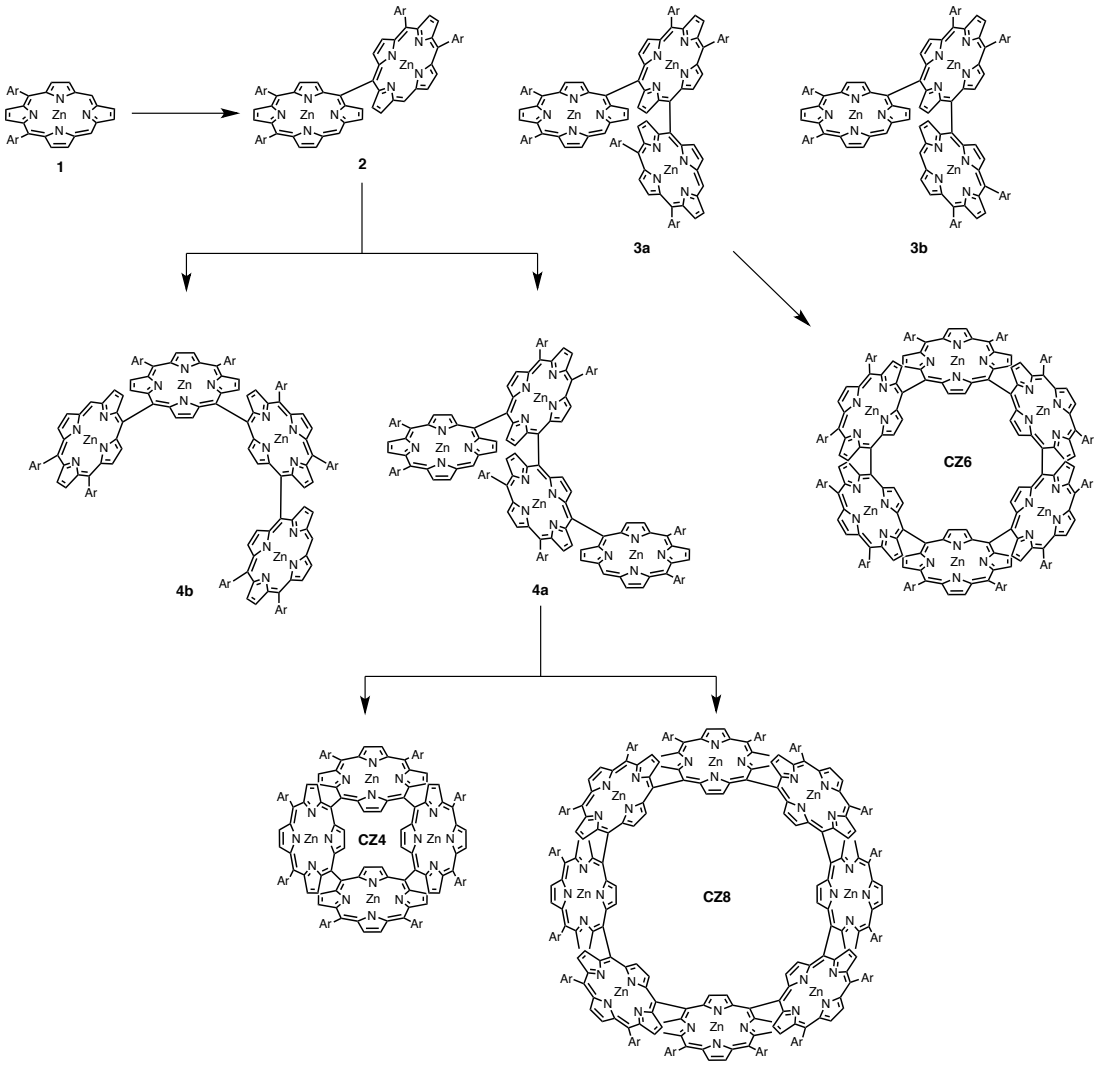

Scheme 1-1. Synthesis of the cyclic zinc porphyrin arrays **CZ4**, **CZ6**, and **CZ8**.

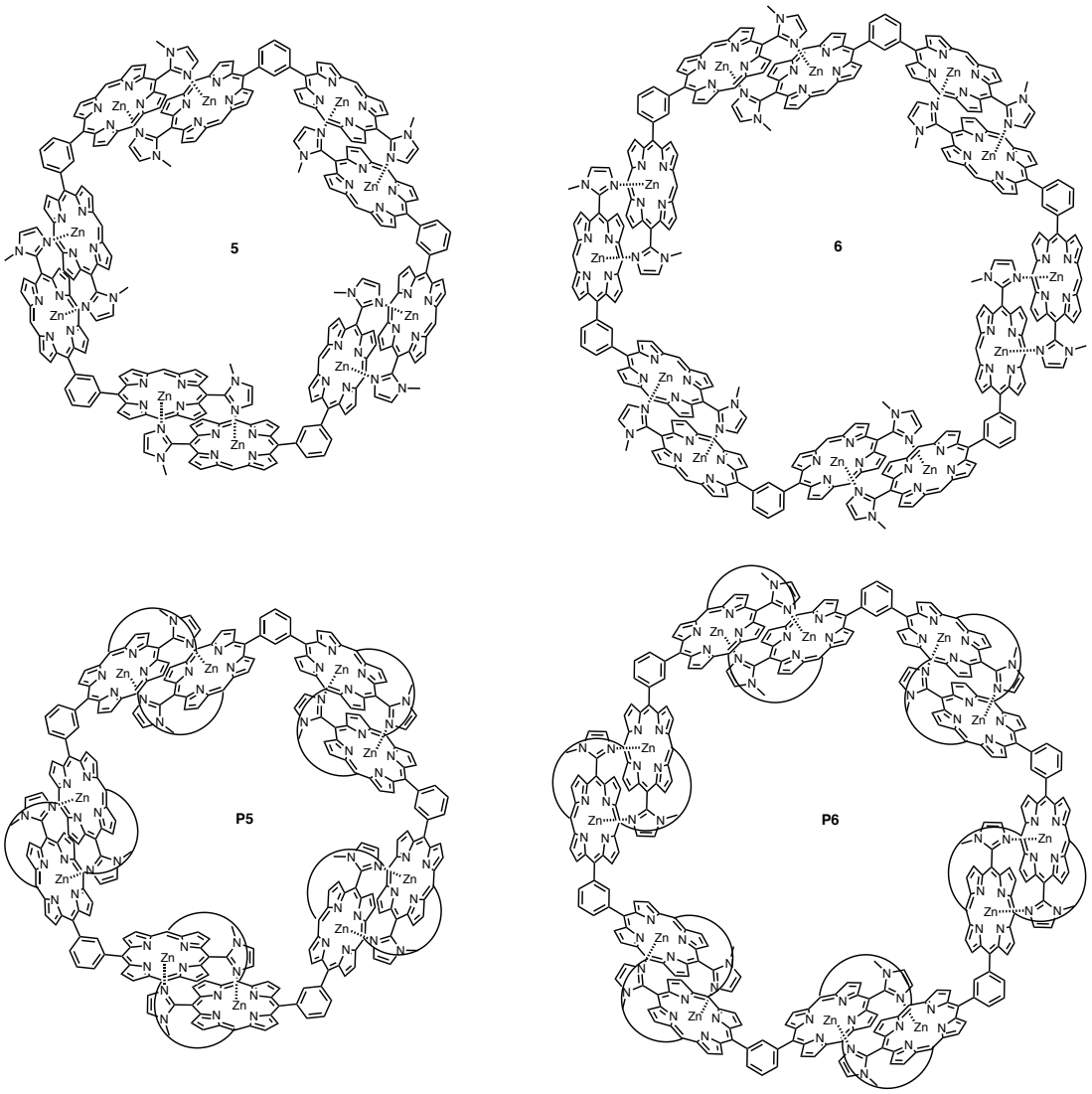

Chart 1-1. The pentagonal and hexagonal arrays **5** and **6** consisting of the zinc porphyrin dimer, and their analogues **P5** and **P6** stabilized by the metathesis reaction.

P**5** and **P6** with high stability were also reported a few years later (Chart 1-1).[63] The porphyrin dimers in these polygons are covalently linked by a metathesis reaction to prevent dissociation of the intermolecular coordination. The excitation energy hopping times in these arrays **5** and **6** were determined to be ~8 and ~5 ps, respectively. The short hopping time of **6** compared to that of **5** is accounted for in term of different dipole–dipole coupling strength between cofacial porphyrin dimer units or the transient fluctuation caused by twist motions of the unit with respect to the linker group.

Star-Shaped Antennae

Lindesy and coworkers reported the multiporphyrin arrays **Zn_8Fb** and **Zn_{20}Fb** consisting of *n* zinc porphyrin units (*n* = 8, or 20) and one free-base porphyrin unit (Chart 1-2), in which porphyrins are ligated *via* diarylethyne linkers.[64] These arrays were synthesized by the convergent method using the Sonogashira coupling of the wings comprising zinc porphyrins and one free-base porphyrin. The energy transfer within the dyad **ZnFb**, triad **ZnZnFb** (Chart 1-3), and oligomers **Zn_8Fb** and **Zn_{20}Fb** was investigated by transient absorption measurements. The short-lived components with 3–10 ps time constants whose amplitudes increase with increasing the photon flux were assigned to the singlet–singlet annihilation rate within the peripheral zinc porphyrin wings around the free-base porphyrin core for the arrays except for the dyad **ZnFb**. The average overall energy transfer rates from the zinc porphyrin wings to the free-base porphyrin core in the arrays are slower as the number of zinc porphyrin components in an array increases (45 ps/**ZnFb**, 90 ps/**ZnZnFb**, 105 ps/**Zn_8Fb**, 220 ps/**Zn_{20}Fb**). The trend that the rate is slower for longer arrays can be attributed to the fact that more reversible energy transfer is possible between the zinc porphyrin units as the zinc porphyrin wings are longer.

Otsuki and coworkes supramolecularly constructed multiporphyrin **$(ZnPA)_4$FbPC** from a free-base porphyrin with tetracarboxylate groups and the four zinc porphyrin with an amidium group *via* the intermolecular hydrogen bond formation (Chart 1-4).[65,66] The energy transfer time between the free-base porphyrin and the zinc porphyrins was estimated as ~8 ps by the

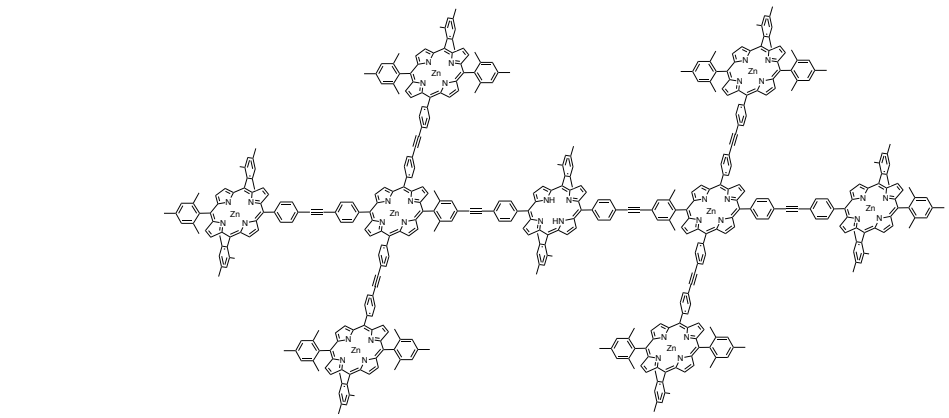

Zn_8Fb

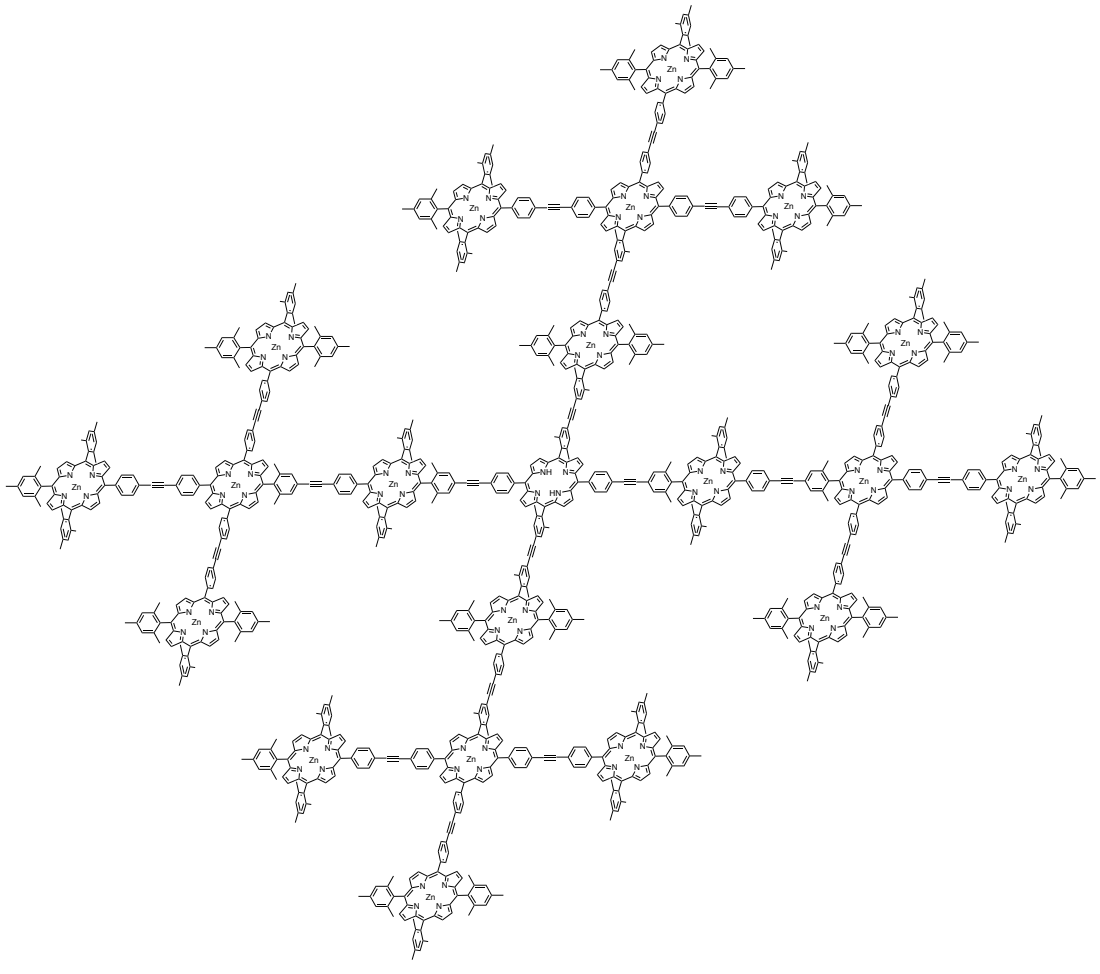

$Zn_{20}Fb$

Chart 1-2. Porphyrin arrays **Zn_8Fb** and **$Zn_{20}Fb$**.

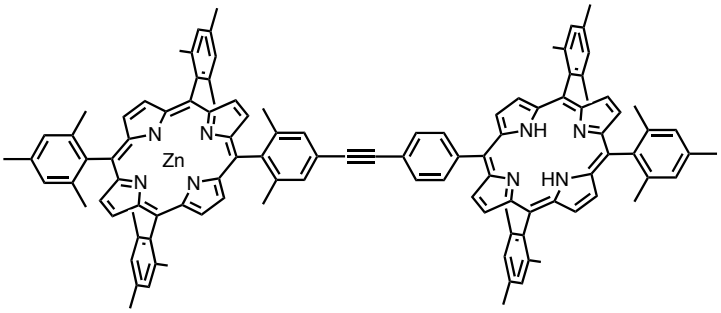

ZnFb

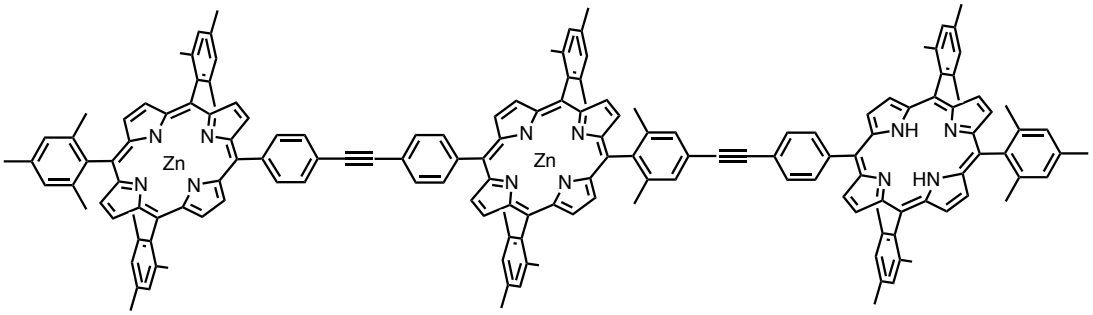

ZnZnFb

Chart 1-3. Porphyrin dyad **ZnFb** and triad **ZnZnFb**.

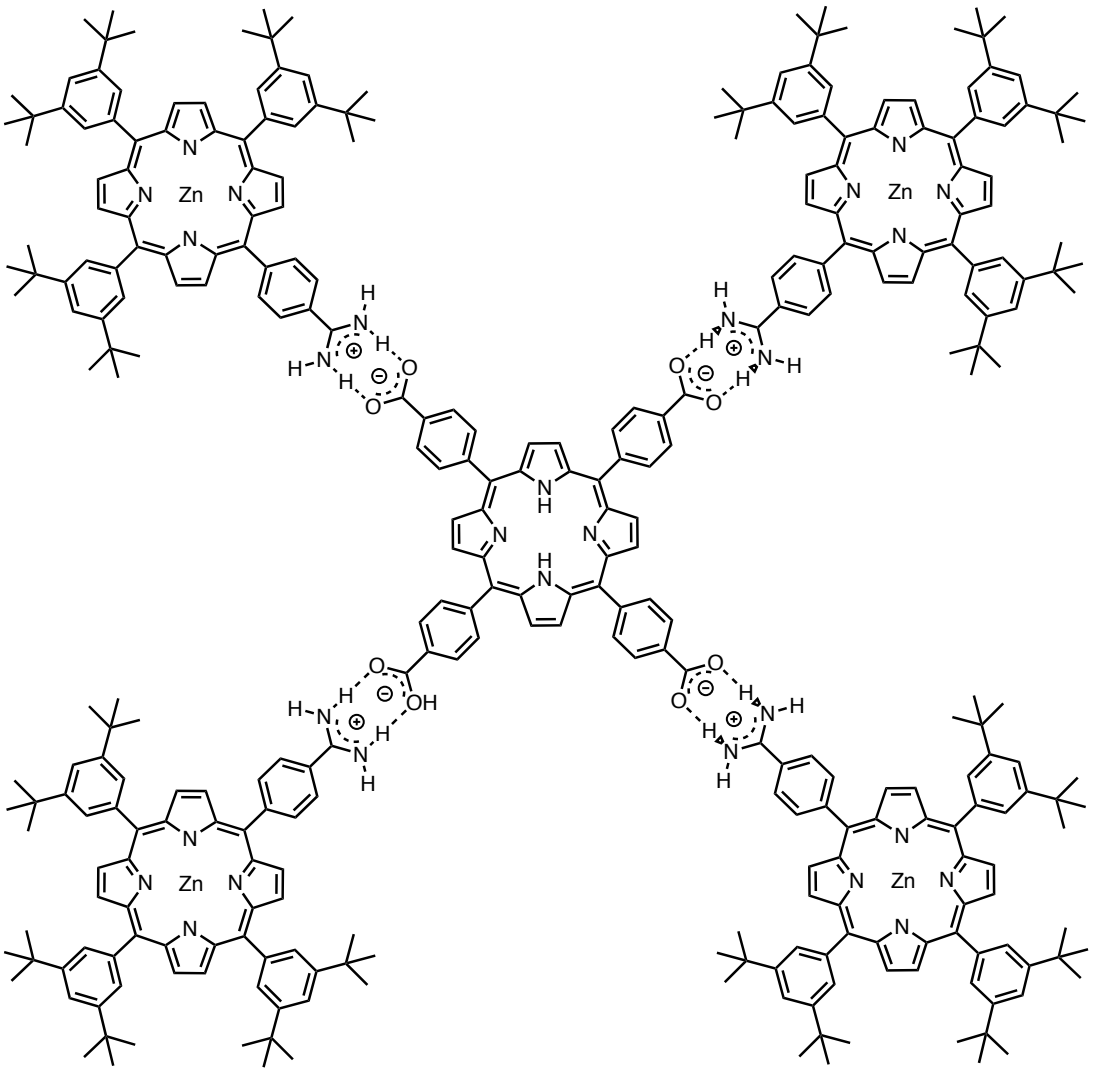

$(ZnPA)_4FbPC$

Chart 1-4. Supramolecular porphyrin pentad **$(ZnPA)_4FbPC$** formed *via* intermolecular hydrogen bonds.

time-resolved fluorescence measurement. This energy transfer time is obviously faster than that estimated based on the Förster energy transfer theory (~1.5 ns), thus suggesting that the energy transfer through the carboxylate–amidinium salt bond is involved in the unusual fast energy transfer.

Chlorosome-Like Antennae

Chlorosome is an antenna complex found in green photosynthetic bacteria, which contains rod-like aggregates consisting of BChl-*c*, BChl-*d*, and BChl-*e*.[67] Although the structure of the aggregate has not been fully clarified, it is obvious that BChl molecules exist as J-aggregates according to their significantly red-shifted $Q_y(0,0)$ band and so on.[67,68] The Tamiaki group has particularly addressed the construction of model chlorosomes by self-assembly of the zinc chlorophyll (ZnChl) derivatives (Chart 1-5).[69] It was clarified that the chlorosome-like J-aggregate (Chart 1-5) formed by the multiple intermolecular interaction of the ZnChl derivatives and their homologues including (i) the intermolecular axial coordination of the alcoholic (OR) oxygen at the position 3^1 to the zinc atom at the center of ZnChl molecule, (ii) the π-π stacking interaction between adjacent ZnChl molecules, and (iii) the hydrogen bond formation between the hydrogen atom in the OH group at the position 3^1 and the carbonyl oxygen at the position 13^1 if the substituent at the position 3^1 is the OH group.[70,71]

The J-aggregate of ZnChl is not just a model for chlorosome but is modified to be applied to artificial antennae. Würthner and coworkers successfully amplified the light absorption ability of the aggregate by functionalization of the ZnChl derivatives **1**–**3** with the naphthalene diimide (NDI) dyes (Chart 1-6).[72] The self-assembly of the ZnChl derivatives **1**–**3** gave the chlorosome-like aggregate with its periphery modified by the NDI dyes (Figure 1-4). Although the absorption of the J-aggregate of ZnChls in a range of ~450–650 nm is generally low in intensity relative to that of the Soret and $Q_y(0,0)$ bands, it was significantly improved by sum of the absorption of the NDI dyes which have a complementary absorption spectrum to that of the chlorophylls. Further the large spectral overlap of the absorption of the inner ZnChl aggregate and the emission of the NDI moiety suggested that the energy transfer from the NDI dye to the ZnChl aggregate can occur in the Förster mechanism. Indeed, it is

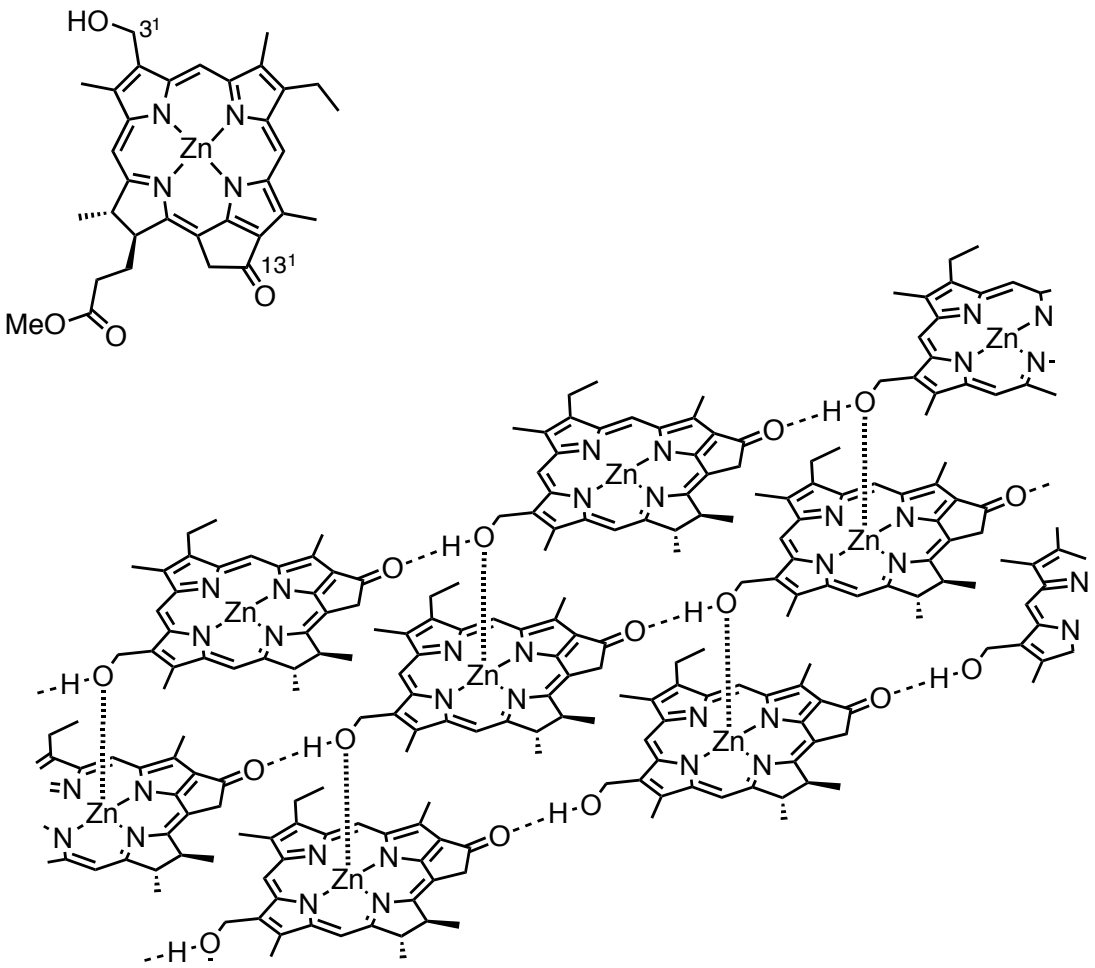

Chart 1-5. The zinc chlorophyll derivative appended by the hydroxyl group at the position 3^1 and their J-aggregate.

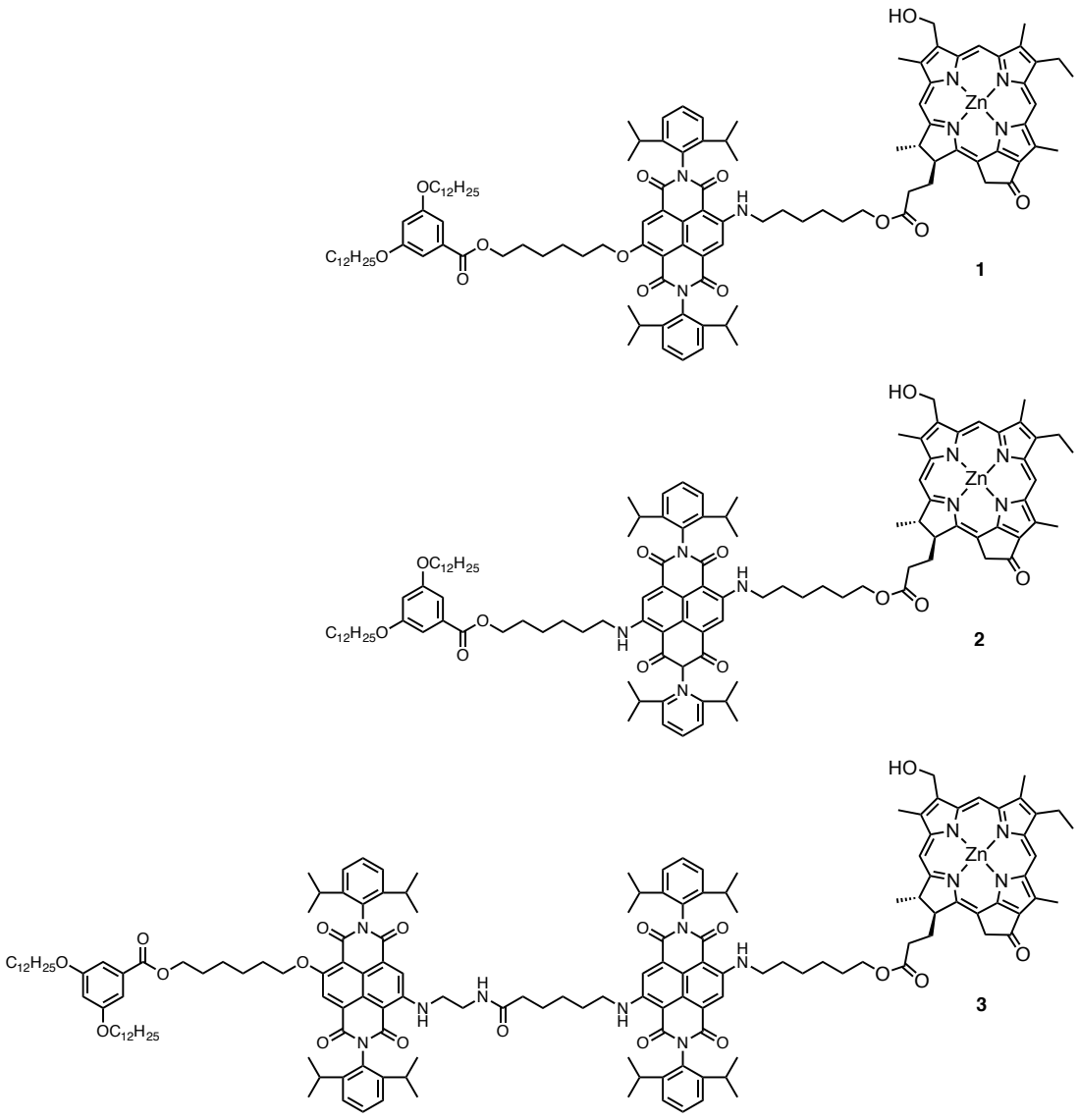

Chart 1-6. The zinc chlorophyll–NDI dye conjugates **1**–**3**.

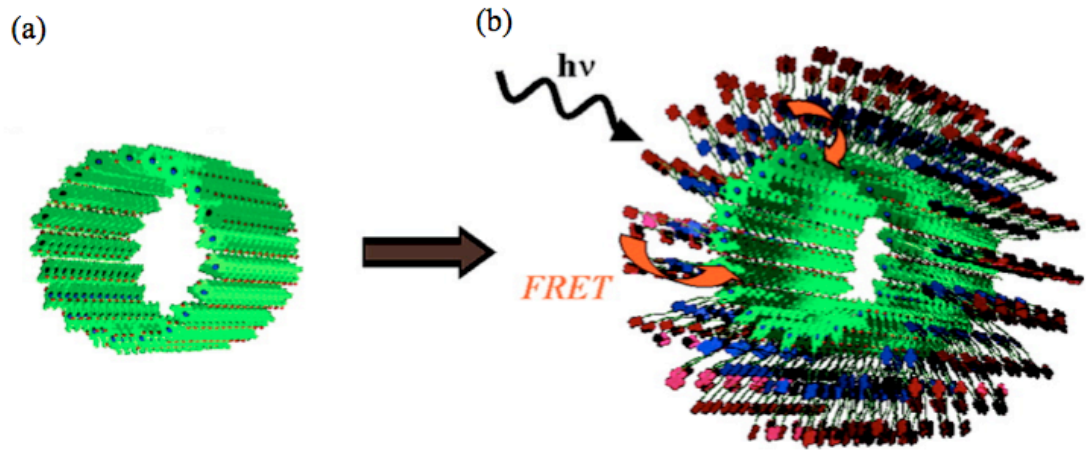

Figure 1-4. Schematic models of (a) the J-aggregate of the zinc chlorophyll derivative in Chart 1-5 and (b) the aggregate of **3**. Reproduced from [72] with permission from ACS, 2014.

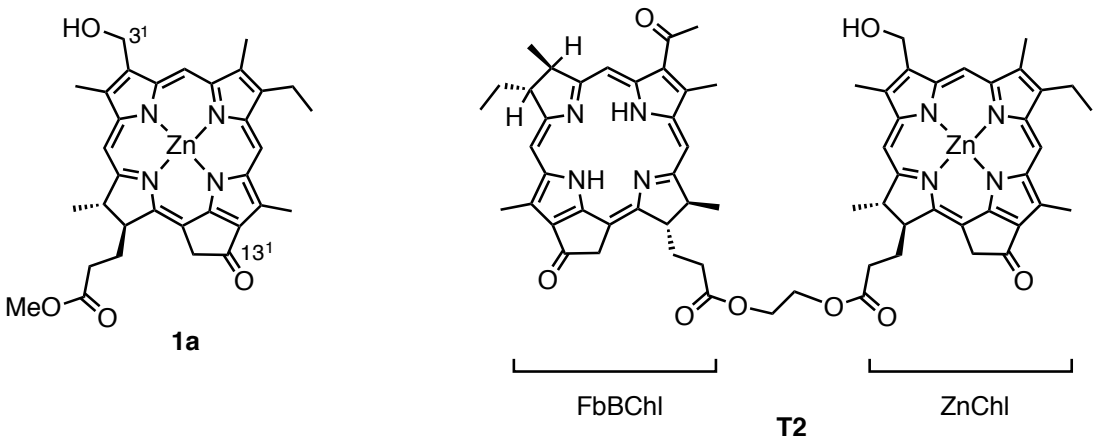

Chart 1-7. The zinc chlorophyll **1a** and the ZnChl–FbBChl dyad **T2**

confirmed that the excitation energy of the NDI moieties is transferred to the inner ZnChl aggregate in very high efficiency (>99%) by the time-resolved fluorescence measurements.

Another artificial antenna model using the chlorosome-like aggregate was reported by Tamiaki and coworkers.[73] They successfully incorporated a free-base bacteriochlorophyll (FbBChl) as an energy trap into the ZnChl aggregate utilizing the dynamic feature of the self-assembly of the ZnChl molecules. The co-aggregate of ZnChl **1a** and the dyad **T2** consisting of the ZnChl moiety and the FbBChl moiety (Chart 1-7) was prepared by the precipitation from a solution containing **1a** and **T2** in a certain ratio (25/1). The energy transfer time and its efficiency from the ZnChl aggregate to the FbBChl trap were estimated by the time-resolved fluorescence measurements to be 7 ps and ~70%, respectively, under reducing condition to avoid oxidative quenching.

1-3 Object and outline of this Dissertation

The light-harvesting antennae in nature and their artificial models have been reviewed in this chapter. Highly efficient energy transfer within the molecular arrays is required to concentrate the excited energy into an energy trap in the antennae. The diverse structures of antenna models as shown in section 1-2 indicate the geometry suitable for the antennae is still being explored. Further, most of the examples as shown above have not been verified in their effect on the actual light–energy conversion at the present, and, at the same time, their application potentiality as the antennae has been investigated only in the molecular level, which may be due to the difficulty in the introduction of the antenna to the actual device.

Attention is also paid to polymeric structures as one of the attractive candidates of the light-harvesting antennae, and several polymer-based antennae thus have been fabricated so far.[74-76] The polymers are used as a backbone for arranging light-harvesting chromophores in most cases.[77-80] The conformational flexibility of the backbone and relatively high degree of freedom in the position of the chromophores, however, cause undesirable energy dissipation like an excimer formation, preventing the success of the energy transfer over extended distances and making the energy transfer difficult to control.[81,82]

The antenna models we describe in this dissertation are based on the results obtained in Chapters 2 and 3 that the higher-order structures of the coordination polymers formed by self-assembly of a ZnChl derivative appended by *N*-heterocycle in the solid state *via* the intermolecular coordination interaction between the nitrogen atom in the heterocycle and the zinc ion at the center of chlorin ring vary by altering the *N*-heterocyclic moiety.[83,84] The structural changes of the polymers by altering the coordination site is notable advantage for the light-harvesting antenna models because we can tune the energy transfer efficiency in the polymer by control of the higher-order structures of the coordination polymer as demonstrated in the later chapters, among which we particularly focused on the "Control" in Chapter 4.[85] Another structural merit of the polymer for the light-harvesting antennae is that the reactive sites certainly remain at either end of the polymers. The reactive site is essential for introducing the light-harvesting antennae to the actual devices, and in turn has potential for further functionalization of the polymers.

It is also noteworthy that the ZnChls forms the cyclic oligomers in solution while the polymers in the solid state. As mentioned in Section 1-2, the cyclic arrays of the chromophores are also possible candidate for the artificial antennae. Chapters 5 and 6 describe the basis of the cyclic oligomers as the antennae. We address the construction of soluble cyclic oligomers in Chapter 5 improving the poor solubility of the assemblies described in the previous chapters, while the functionalization of the oligomers in Chapter 6.

1-4 References

(1) Chu, S.; Majumdar, A. *Nature* **2012**, *488*, 294.

(2) Dresselhaus, M. S.; Thomas, I. L. *Nature* **2001**, *414*, 332.

(3) Scholes, G. D.; Fleming, G. R.; Olaya-Castro, A.; van Grondelle, R. *Nat. Chem.* **2011**, *3*, 763.

(4) Yoon, T. P.; Ischay, M. A.; Du, J. *Nat. Chem.* **2010**, *2*, 527.

(5) Fukuzumi, S.; Ohkubo, K. *J. Mater. Chem.* **2012**, *22*, 4575.

(6) McConnell, I.; Li, G.; Brudvig, G. W. *Chem. Biol.* **2010**, *17*, 434.

(7) Tachibana, Y.; Vayssieres, L.; Durrant, J. R. *Nat. Photon.* **2012**, *6*, 511.

(8) Youngblood, W. J.; Lee, S.-H. A.; Kobayashi, Y.; Hernandez-Pagan, E. A.; Hoertz, P. G.; Moore, T. A.; Moore, A. L.; Gust, D.; Mallouk, T. E. *J. Am. Chem. Soc.* **2009**, *131*, 926.

(9) Maeda, K.; Domen, K. *J. Phys. Chem. C* **2007**, *111*, 7851.

(10) Kudo, A.; Miseki, Y. *Chem. Soc. Rev.* **2009**, *38*, 253.

(11) Grätzel, M. *Inorg. Chem.* **2005**, *44*, 6841.

(12) Hagfeldt, A.; Grätzel, M. *Chem. Rev.* **1995**, *95*, 49.

(13) Mathew, S.; Yella, A.; Gao, P.; Humphry-Baker, R.; CurchodBasile, F. E.; Ashari-Astani, N.; Tavernelli, I.; Rothlisberger, U.; NazeeruddinMd, K.; Grätzel, M. *Nat. Chem.* **2014**, *6*, 242.

(14) Frischmann, P. D.; Mahata, K.; Würthner, F. *Chem. Soc. Rev.* **2013**, *42*, 1847.

(15) Gust, D.; Moore, T. A.; Moore, A. L. *Acc. Chem. Res.* **2009**, *42*, 1890.

(16) Papiz, M. Z.; Prince, S. M.; Howard, T.; Cogdell, R. J.; Isaacs, N. W. *J. Mol. Biol.* **2003**, *326*, 1523.

(17) Ziessel, R.; Harriman, A. *Chem. Commun.* **2011**, *47*, 611.

(18) Satake, A.; Kobuke, Y. *Org. Biomol. Chem.* **2007**, *5*, 1679.

(19) Adronov, A.; Frechet, J. M. J. *Chem. Commun.* **2000**, 1701.

(20) Pascal, A. A.; Liu, Z.; Boress, K.; van Oort, B.; van Amerongen, H.; Wang, C.;

Horton, P.; Robert, B.; Chang, W.; Ruban, A. *Nature*, **2005**, *436*, 134.

(21) Bahatyrova, S.; Frese, R. N.; Siebert, C. A.; Olsen, J. D.; van der Werf, K. O.; van Grondelle, R.; Niederman, R. A.; Bullough, P. A.; Otto, C.; Hunter, C. N. *Nature* **2004**, *430*, 1058.

(22) Scheuring, S.; Rigaud, J.-L.; Sturgis, J. N. *EMBO J.* **2004**, *23*, 4127.

(23) Richter, M. F.; Baier, J.; Southall, J.; Cogdell, R. J.; Oellerich, S.; Köhler, J. *Proc. Nati. Acad. Sci. USA* **2007**, *104*, 20280.

(24) Jungas, C.; Ranck, J.-L.; Rigaud, J.-L.; Joliot, P.; Verméglio, A. *EMBO J.* **1999**, *18*, 534.

(25) Deisenhofer, J.; Epp, O.; Miki, K.; Huber, R.; Michel, H. *Nature* **1985**, *318*, 618.

(26) Liu, Z.; Yan, H.; Wang, K.; Kuang, T.; Zhang, J.; Gui, L.; An, X.; Chang, W. *Nature* **2004**, *428*, 287.

(27) Qian, P.; Papiz, M. Z.; Jackson, P. J.; Brindley, A. A.; Ng, I. W.; Olsen, J. D.; Dickman, M. J.; Bullough, P. A.; Hunter, C. N. *Biochemistry* **2013**, *52*, 7575.

(28) Roszak, A. W.; Howard, T. D.; Southall, J.; Gardiner, A. T.; Law, C. J.; Isaacs, N. W.; Cogdell, R. J. *Science* **2003**, *302*, 1969.

(29) Niwa, S.; Yu, L.-J.; Takeda, K.; Hirano, Y.; Kawakami, T.; Wang-Otomo, Z.-Y.; Miki, K. *Nature* **2014**, *508*, 228.

(30) McDermott, G.; Prince, S. M.; Freer, A. A.; Hawthornthwaite-Lawless, A. M.; Papiz, M. Z.; Cogdell, R. J.; Isaacs, N. W. *Nature* **1995**, *374*, 517.

(31) Prince, S. M.; Papiz, M. Z.; Freer, A. A.; McDermott, G.; Hawthornthwaite-Lawless, A. M.; Cogdell, R. J.; Isaacs, N. W. *J. Mol. Biol.* **1997**, *268*, 412.

(32) Olsen, J. D.; Tucker, J. D.; Timney, J. A.; Qian, P.; Vassilev, C.; Hunter, C. N. *J. Biol. Chem.* **2008**, *283*, 30772.

(33) Koepke, J.; Hu, X.; Muenke, C.; Schulten, K.; Michel, H. *Structure* **1996**, *4*, 581.

(34) Freer, A.; Prince, S.; Sauer, K.; Papiz, M.; Lawless, A. H.; McDermott, G.; Cogdell, R.; Isaacs, N. W. *Structure* **1996**, *4*, 449.

(35) Law, C. J.; Roszak, A. W.; Southall, J.; Gardiner, A. T.; Isaacs, N. W.; Cogdell, R. J. *Mol. Membr. Biol.* **2004**, *21*, 183.

(36) Kühlbrandt, W. *Structure* **1995**, *3*, 521.

(37) van Grondelle, R. *Biochimi. Biophys. Acta* **1985**, *811*, 147.

(38) Ritz, T.; Damjanović, A.; Schulten, K. *ChemPhysChem* **2002**, *3*, 243.

(39) Cogdell, R. J.; Isaacs, N. W.; Howard, T. D.; McLuskey, K.; Fraser, N. J.; Prince, S. M. *J. Bacteriol.* **1999**, *181*, 3869.

(40) Cogdell, R.; Fyfe, P.; Barrett, S.; Prince, S.; Freer, A.; Isaacs, N.; McGlynn, P.; Hunter, C. N. *Photosynth. Res.* **1996**, *48*, 55.

(41) van Grondelle, R.; Novoderezhkin, V. I. *Phys. Chem. Chem. Phys.* **2006**, *8*, 793.

(42) Sundström, V.; Pullerits, T.; van Grondelle, R. *J. Phys. Chem. B* **1999**, *103*, 2327.

(43) Salverda, J. M.; van Mourik, F.; van der Zwan, G.; van Grondelle, R. *J. Phys. Chem. B* **2000**, *104*, 11395.

(44) Hess, S.; Chachisvilis, M.; Timpmann, K.; Jones, M. R.; Fowler, G. J.; Hunter, C. N.; Sundström, V. *Proc. Natl. Acad. Sci. USA* **1995**, *92*, 12333.

(45) Nagarajan, V.; Parson, W. W. *Biochemistry* **1997**, *36*, 2300.

(46) Hu, X.; Ritz, T.; Damjanović, A.; Schulten, K. *J. Phys. Chem. B* **1997**, *101*, 3854.

(47) Ritz, T.; Park, S.; Schulten, K. *J. Phys. Chem. B* **2001**, *105*, 8259.

(48) Jimenez, R.; Dikshit, S. N.; Bradforth, S. E.; Fleming, G. R. *J. Phys. Chem.* **1996**, *100*, 6825.

(49) Jimenez, R.; van Mourik, F.; Yu, J. Y.; Fleming, G. R. *J. Phys. Chem. B* **1997**, *101*, 7350.

(50) Timpmann, K.; Freiberg, A.; Sundström, V. *Chem. Phys.* **1995**, *194*, 275.

(51) Cogdell, R. J.; Lindsay, J. G. *Trends in Biotechnol.* **1998**, *16*, 521.

(52) Li, F.; Yang, S. I.; Ciringh, Y.; Seth, J.; Martin, C. H.; Singh, D. L.; Kim, D.; Birge, R. R.; Bocian, D. F.; Holten, D.; Lindsey, J. S. *J. Am. Chem. Soc.* **1998**, *120*, 10001.

(53) Lin, V. S.-Y.; DiMagno, S. G.; Therien, M. J. *Science* **1994**, *264*, 1105.

(54) Mozer, A. J.; Griffith, M. J.; Tsekouras, G.; Wagner, P.; Wallace, G. G.; Mori, S.;

Sunahara, K.; Miyashita, M.; Earles, J. C.; Gordon, K. C.; Du, L.; Katoh, R.; Furube, A.; Officer, D. L. *J. Am. Chem. Soc.* **2009**, *131*, 15621.

(55) Imahori, H. *J. Phys. Chem. B* **2004**, *108*, 6130.

(56) Choi, M.-S.; Aida, T.; Yamazaki, T.; Yamazaki, I. *Chem. Eur. J.* **2002**, *8*, 2667.

(57) Wasielewski, M. R.; Svec, W. A. *J. Org. Chem* **1980**, *45*, 1969.

(58) Kelley, R. F.; Goldsmith, R. H.; Wasielewski, M. R. *J. Am. Chem. Soc.* **2007**, *129*, 6384.

(59) Gunderson, V. L.; Smeigh, A. L.; Kim, C. H.; Co, D. T.; Wasielewski, M. R. *J. Am. Chem. Soc.* **2012**, *134*, 4363.

(60) D. Kim., E. *Multiporphyrin Arrays*; Pan Stanford Publishing: Singapore, 2012.

(61) Choi, M.-S.; Yamazaki, T.; Yamazaki, I.; Aida, T. *Angew. Chem. Int. Ed.* **2004**, *43*, 150.

(62) Takahashi, R.; Kobuke, Y. *J. Am. Chem. Soc.* **2003**, *125*, 2372.

(63) Hwang, I.-W.; Park, M.; Ahn, T. K.; Yoon, Z. S.; Ko, D. M.; Kim, D.; Ito, F.; Ishibashi, Y.; Khan, S. R.; Nagasawa, Y.; Miyasaka, H.; Ikeda, C.; Takahashi, R.; Ogawa, K.; Satake, A.; Kobuke, Y. *Chem. Eur. J.* **2005**, *11*, 3753.

(64) del Rosario Benites, M.; Johnson, T. E.; Weghorn, S.; Yu, L.; Rao, P. D.; Diers, J. R.; Yang, S. I.; Kirmaier, C.; Bocian, D. F.; Holten, D.; Lindsey, J. S. *J. Mater. Chem.* **2002**, *12*, 65.

(65) Otsuki, J.; Iwasaki, K.; Nakano, Y.; Itou, M.; Araki, Y.; Ito, O. *Chem. Eur. J.* **2004**, *10*, 3461.

(66) Otsuki, J. *J. Porphyrin Phthalocyanines* **2009**, *13*, 1069.

(67) Tamiaki, H. *Coord. Chem. Rev.* **1996**, *148*, 183.

(68) Orf, G.; Blankenship, R. *Photosynth. Res.* **2013**, *116*, 315.

(69) Yagai, S.; Tomohiro, M.; Shimono, Y.; Tamiaki, H. *Photochem. Photobiol.* **2001**, *73*.

(70) Tamiaki, H.; Holzwarth, A. R.; Schaffner, K. *J. Photochem. Photobiol. B: Biol.* **1992**, *15*, 355.

(71) Miyatake, T.; Tanigawa, S.; Kato, S.; Tamiaki, H. *Tetrahedron Lett.* **2007**, *48*, 2251.

(72) Röger, C.; Miloslavina, Y.; Brunner, D.; Holzwarth, A. R.; Würthner, F. *J. Am. Chem. Soc.* **2008**, *130*, 5929.

(73) Prokhorenko, V. I.; Holzwarth, A. R.; Müller, M. G.; Schaffner, K.; Miyatake, T.; Tamiaki, H. *J. Phys. Chem. B* **2002**, *106*, 5761.

(74) Becker, K.; Lupton, J. M. *J. Am. Chem. Soc.* **2006**, *128*, 6468.

(75) Chen, M.; Ghiggino, K. P.; Mau, A. W. H.; Rizzardo, E.; Thang, S. H.; Wilson, G. J. *Chem. Commun.* **2002**, 2276.

(76) Stewart, G. M.; Fox, M. A. *J. Am. Chem. Soc.* **1996**, *118*, 4354.

(77) Adronov, A.; Robello, D. R.; Fréchet, J. M. J. *J. Polym. Sci., Part A: Polym. Chem.* **2001**, *39*, 1366.

(78) Ng, D.; Guillet, J. E. *Macromolecules* **1982**, *15*, 724.

(79) Serin, J.; Schultze, X.; Adronov, A.; Fréchet, J. M. J. *Macromolecules* **2002**, *35*, 5396.

(80) Chen, M.; Ghiggino, K. P.; Thang, S. H.; Wilson, G. J. *Angew. Chem. Int. Ed.* **2005**, *44*, 4368.

(81) Watkins, D. M.; Fox, M. A. *J. Am. Chem. Soc.* **1994**, *116*, 6441.

(82) Adronov, A.; Gilat, S. L.; Fréchet, J. M. J.; Ohta, K.; Neuwahl, F. V. R.; Fleming, G. R. *J. Am. Chem. Soc.* **2000**, *122*, 1175.

(83) Shinozaki, Y.; Richards, G.; Ogawa, K.; Yamano, A.; Ohara, K.; Yamaguchi, K.; Kawano, S.-i.; Tanaka, K.; Araki, Y.; Wada, T.; Otsuki, J. *J. Am. Chem. Soc.* **2013**, *135*, 5262.

(84) Shinozaki, Y.; Yoshikawa, I.; Araki, K.; Ohara, K.; Yamaguchi, K.; Kawano, S.-i.; Tanaka, K.; Araki, Y.; Wada, T.; Otsuki, J. *Chem. Lett.* **2014**, *43*, 862.

(85) Shinozaki, Y.; Yoshikawa, I.; Araki, K.; Sugawa, K.; Otsuki, J. *CrystEngComm* **2014**, *16*, 9155.

Chapter 2

Self-Assembly of a Zinc Chlorophyll Derivative Appended by Pyridine

2-0 Summary

The self-assembled structures of a zinc chlorophyll derivative appended by vinylpyridine in solution and in crystal were investigated. Self-assembly occurred *via* an intermolecular axial coordination of the nitrogen atom in the pyridine moiety to the zinc center in another chlorophyll molecule in both solution and the crystal. The cyclic tetramers formed as a predominant species in chloroform, which was identified by use of ^{1}H-NMR measurements including diffusion ordered spectroscopy (DOSY), vapor pressure osmometry (VPO), and cold-spray ionization mass spectrometry (CSI-MS). On the other hand, the coordination polymers with double-helical motif formed in the crystal, which was clarified by X-ray crystal structure analysis. A calculation of relative efficiency of the Förster energy transfer that could occur within the double helix indicated that the *inter*strand pathways are more efficient than *intra*strand pathways. These results indicate that the double-helical motif is one of promising models for the artificial light-harvesting antennae.

2-1 Introduction

Supramolecular assemblies of porphyrin analogues have drawn considerable attention not only for the understanding of natural photosynthetic function but also for development of synthetic architectures for light harvesting and manipulation of excitation energy in material science.[1,2] Nature uses assemblies of chlorophyll and its analogues as light-harvesting antennae and electron relays in photosynthetic bacteria and chloroplast in plants.[3] One type of light-harvesting antenna consists of chlorophyll–protein complexes, such as LH1 and LH2 in purple photosynthetic bacteria as well as light-harvesting complexes found in plants (1-1).[4] Chlorosomes found in green photosynthetic bacteria belong to another type of antenna.[5] They consists of agglomerates of bacteriochlorophyll molecules called rod elements that are constructed only through pigment–pigment interactions without a protein scaffold.

A number of model compounds to mimic the structure and function of chlorosomes have been prepared (1-2).[6-11] Most of the synthetic analogues prepared to date closely follow their natural counterparts and retain the functional groups believed to be crucial for the formation of higher-order structures, including the 3^1-hydroxy group. In the meantime, less attention has been paid to the design of structurally diverse chlorophyll derivatives that could also form novel, highly ordered assemblies. We have examined the zinc complex of a chlorophyll derivative bearing a pyridine moiety as a much less explored coordination site in comparison with hydroxide groups, which may provide more robust platforms for artificial antenna system.[12-17] Thus, in this chapter, we describe the self-assemblies of the pyridine-appended zinc chlorophyll derivative **ZnPy** (Chart 2-1) in solution and in the crystal.

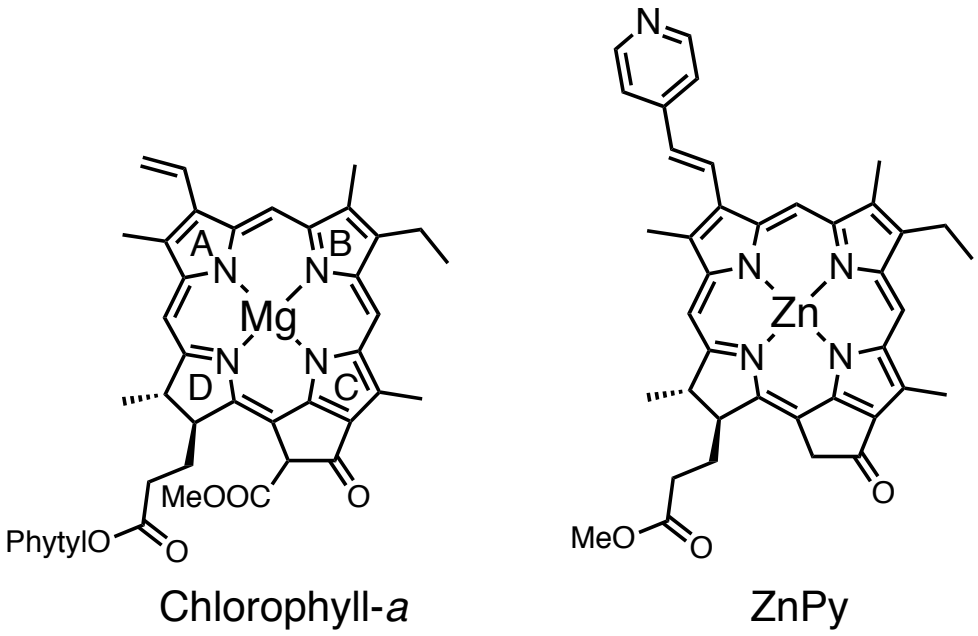

Chart 2-1. Chemical structures of chlorophyll-*a* and **ZnPy**.

2-2 Results and Discussion

2-2-1 Syntheses

The synthetic procedure of **ZnPy** is shown in Scheme 2-1. The commercially available dry Spirulina powder was used as a source of pheophytin-*a* which is the free-base

counterpart of chlorophyll-*a*. The pheophytin-*a* was extracted from the Spirulina powder with hot acetone in the form of a mixture containing lipid, sugar, and other pigments and so on.[18] The mixture was roughly purified by flash column chromatography using silica gel as a stationary phase. The methyl pheophorbide-*a* was obtained by transesterification of the phytyl ester to the methyl ester in methanol in the presence of sulfuric acid as the acid catalyst. The pyrolysis of methyl pheophorbide-*a* in 2,4,6-trimethylpyridine (collidine) caused demethoxycobonylation of the methy ester group at the 13^2 position to give methyl pyropheophorbide-*a*, quantitatively. The use of pyridine as the solvent instead of collidine gave a similar result, which is benefical in term of the cost. The vinyl group in the position 3 of methyl pyropheophorbide-*a* was transformed to the formyl group by the Lemieux–Johnson oxidation using osumium tetraoxide (OsO_4) and sodium periodide ($NaIO_4$) to give methyl pyropheophirbide-*d*.[10,19] Although we tried alternative synthetic method using thiophenol reported by the Oba group due to the high toxicity of volatile OsO_4,[20-22] the yield varied widely in some batches. The free-base chlorophyll appended by pyridine (**FbPy**) was obtained by the aldol-like condensation of 4-methypyridine (4-picoline) with the formyl group in the methyl pyropheophorbide-*d*,[23,24] which was performed in acetic anhydride in the presence of a catalytic amount of acetic acid. A complex mixture containing an only small amount of the desired compound was obtained when we used 1.5 equivalent amount of 4-picoline. We have therefore modified the reaction condition such that a large excess of 4-picoline (1500 equiv) was used to obtain a tractable crude material with an additional merit of shorter reaction time. Finally, the zinc ion was inserted into the center of the free-base using zinc acetate dihydrate ($Zn(OAc)_2 \bullet 2H_2O$),[25-27] the zinc complex **ZnPy** was quantitatively obtained. The free-base complex **FbPy** and the zinc complex **ZnPy** were fully characterized by NMR measurements and APCI-HRMS, and their purities were checked by HPLC.

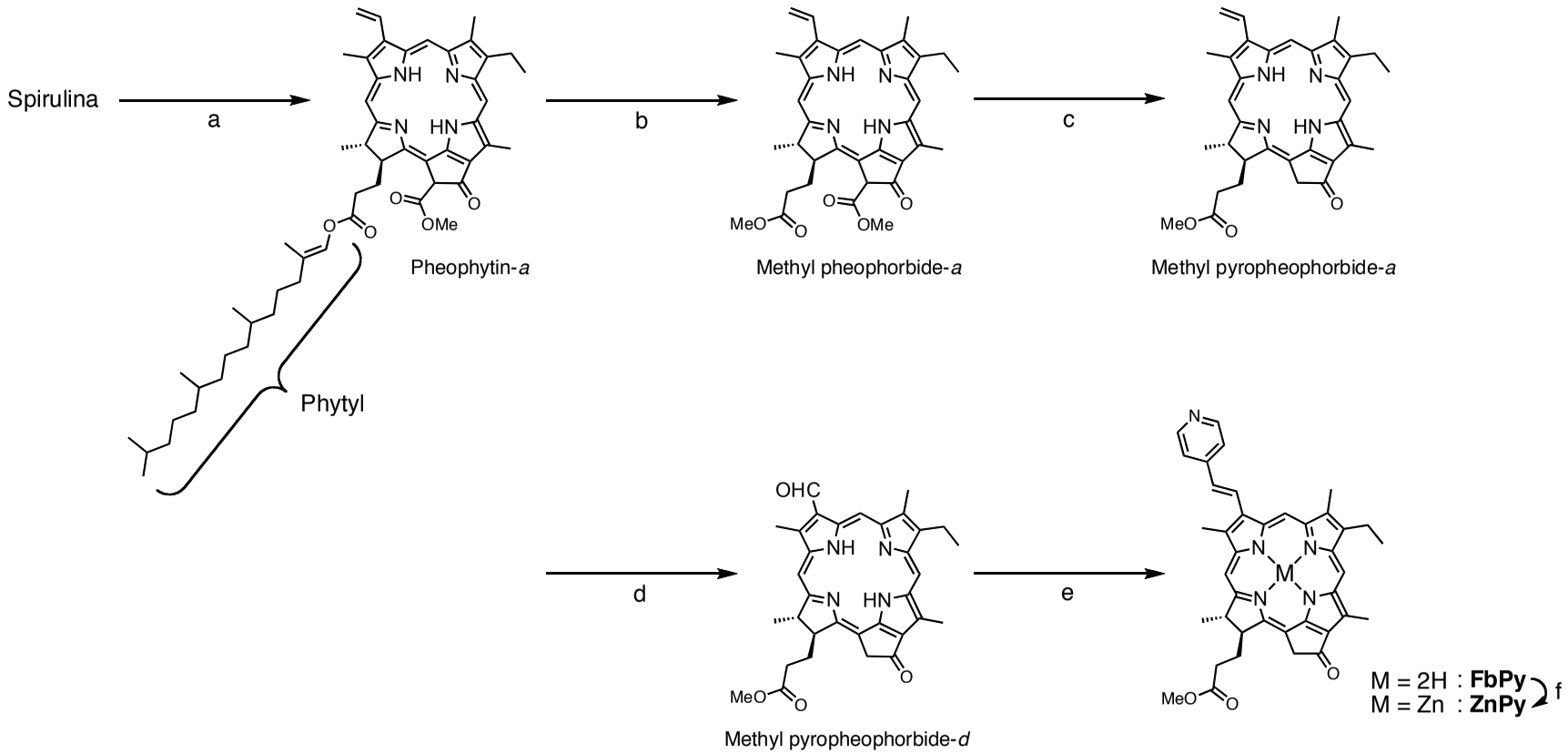

Scheme 2-1. Synthetic procedures of the free-base chlorophyll **FbPy** and its zinc complex **ZnPy**. a) acetone, reflux. b) H_2SO_4, MeOH, overnight. c) collidine, reflux. d) OsO_4, $NaIO_4$, AcOH, THF, H_2O, overnight. e) 4-picoline, AcOH, Ac_2O, reflux, 3 h. f) $Zn(OAc)_2 \bullet 2H_2O$, MeOH, $CHCl_3$, 3 h.

2-2-2 Self-Assembly in Solution

The ^{1}H-NMR spectra of the free-base **FbPy** in $CDCl_3$ are shown in Figure 2-1. The signals for the α and β protons of the pyridine moiety appeared at 8.81 and 7.68 ppm, respectively. Although these signals in the zinc complex **ZnPy** appeared in a similar region in tetrahydrofran-d_8 (THF-d_8), they underwent marked upfield shifts to 3.40 and 6.11 ppm, respectively, in $CDCl_3$. Signals corresponding to other protons were also upfield-shifted by successively smaller amounts as the distance between the protons and the pyridine group increased (Figure 2-2). The magnitudes of the upfield shifts for the pyridine protons and the trend observed for the other protons in $CDCl_3$ are consistent with a self-assembled structure in which the pyridine moiety of a molecule **ZnPy** coordinates to the zinc center of another molecule **ZnPy**. These upfield chemical shifts, including those for the α and β protons of the pyridine moiety, showed little change over a temperature range of 223–348 K (Figure 2-3). Furthermore, these values were also independent of concentration over a range of 0.1–10 mM (Figure 2-4). The insensitivity of the chemical shifts to changes in temperature and concentration over wide ranges, combined with the appearance of a single set of proton signals for the molecular structure, is inconsistent with the formation of linear oligomeric structures in solution but instead points to the assembly of a stable, well-defined discrete cyclic oligomer (or different-membered cyclic oligomers) held together through pyridine–zinc axial coordination.

Diffusion coefficient (D) of $(6.37 \pm 0.20) \times 10^{-10}$ and $(3.43 \pm 0.05) \times 10^{-10}$ m^2 s^{-1} were obtained for the free-base **FbPy** and the zinc complex **ZnPy**, respectively, in $CDCl_3$ (10 mM, 298 K) by means of diffusion ordered spectroscopy measurements (Figure 2-5). The hydrodynamic radii (r) were then estimated using the Stokes–Einstein equation (eq 1),[28]

$$r = k_B T / 6\pi\eta D \quad (1)$$

where k_B, T, and η are the Boltzmann constant, absolute temperature, and viscosity of the

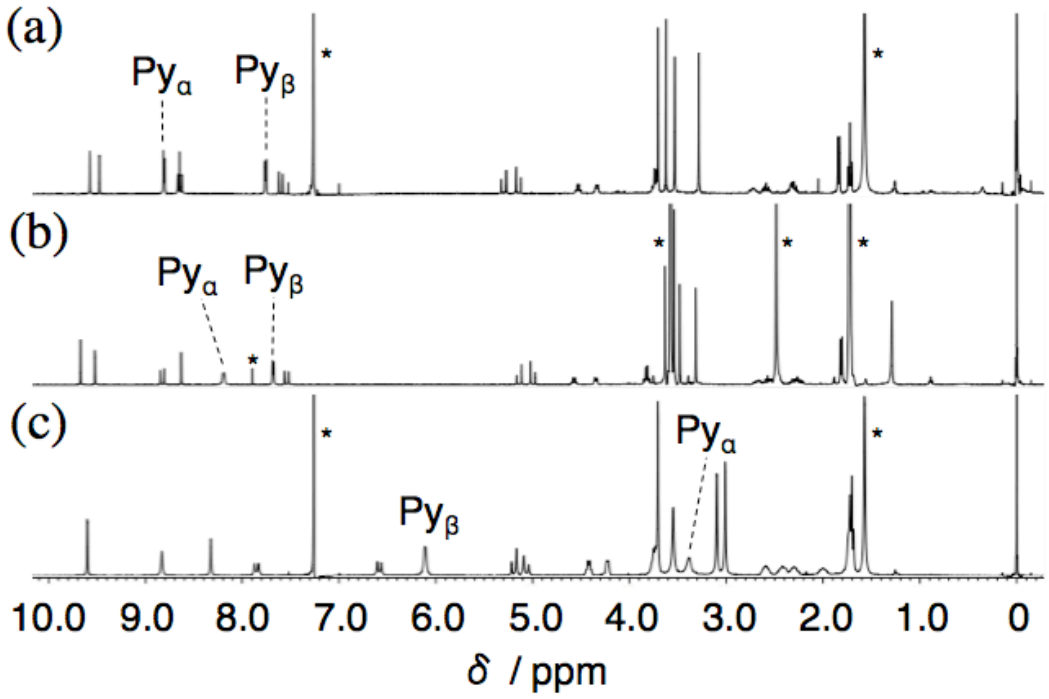

Figure 2-1. ^{1}H NMR spectrum of the free-base **1** in $CDCl_3$ (a) and those of the zinc complex **2** in THF-d_8 (b) and in $CDCl_3$ (c). Asterisks indicate solvent and water peaks.

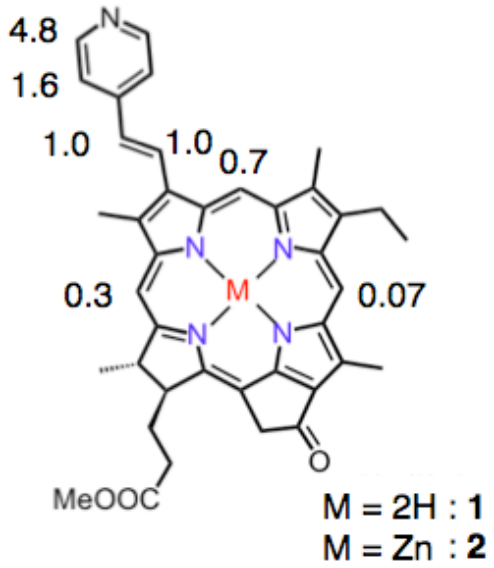

Figure 2-2. Chemical shift differences for zinc complex **2**: δ(THF-d_8)–δ($CDCl_3$).

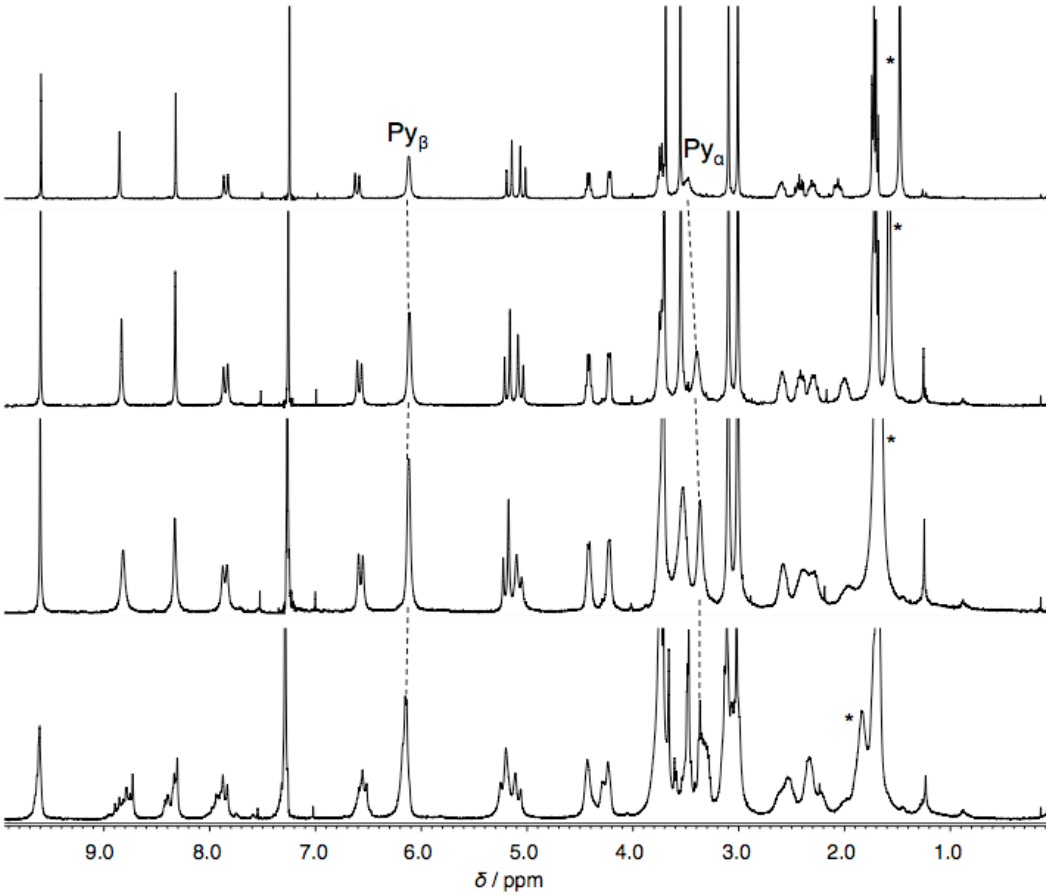

Figure 2-3. ^{1}H NMR spectra of **ZnPy** in $CDCl_3$ at (a) 323 K, (b) 298 K, (c) 273 K, and (d) 223 K. [**ZnPy**] = ca. 10 mM. Asterisks indicate the peaks of water.

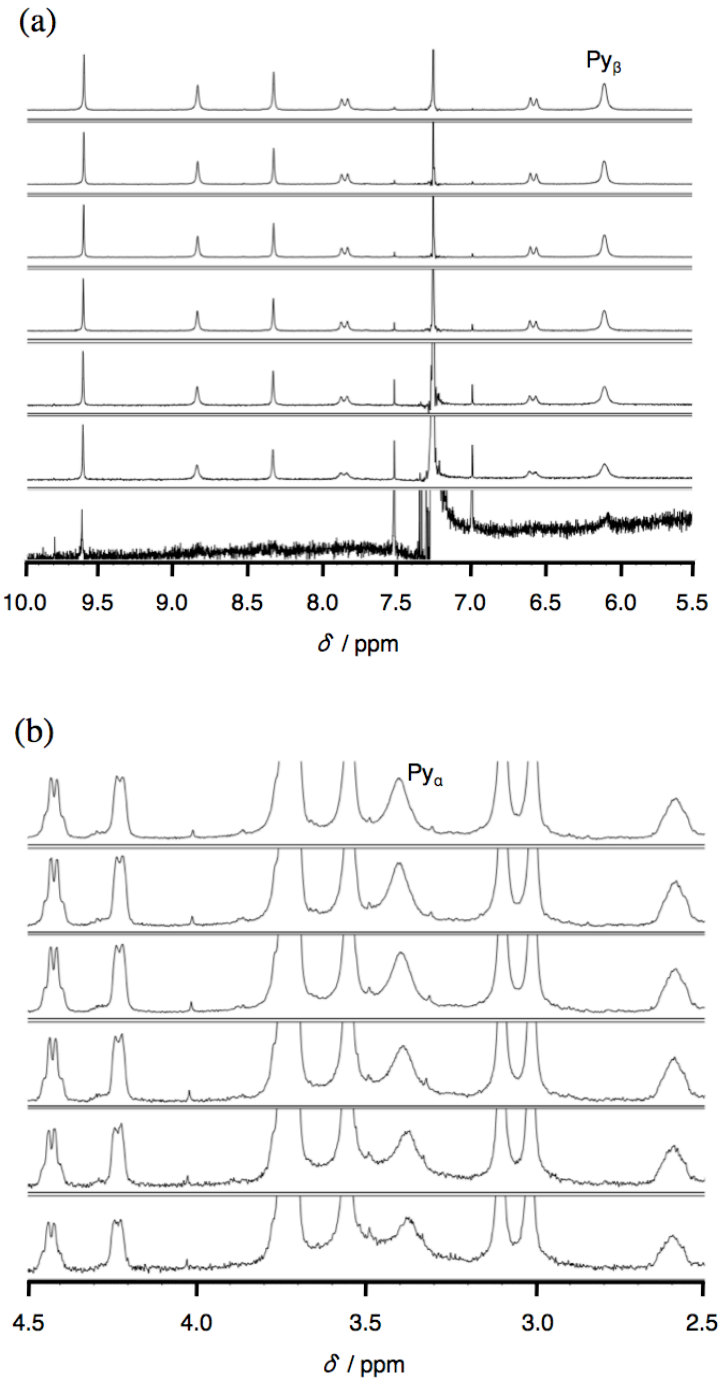

Figure 2-4. Concentration dependence of ^{1}H NMR spectra of **ZnPy** in $CDCl_3$ at 298 K. (a) Aromatic region at the concentrations of 10, 7.5, 5.0, 2.5, 1.0, 0.5, and 0.1 mM from top to bottom. (b) Aliphatic region at the concentration of 10, 7.5, 5.0, 2.5, 1.0, and 0.5 mM, from top to bottom.

medium, respectively. The *r* values obtained for **FbPy** and **ZnPy** were 6.32 and 11.8 Å, respectively. The radius for **FbPy** is consistent with the dimensions of the monomeric species (Figure 2-6), whereas the radius for **ZnPy** is about twice that for **FbPy**, which is more or less in accord with the dimension of the cyclic tetramer.

The vapor pressure osmometry (VPO) data for zinc methyl pyropheophorbide-*a* (M = 612 g mol^{-1}) without pyridine moiety and **ZnPy** (M = 689 g mol^{-1}) in $CHCl_3$ at 37 ℃ indicated the masses of the species in solution to be 828 ± 67 and 2600 ± 190 g mol^{-1}, respectively, the latter being in good agreement with the value for the tetramer of **ZnPy** (M = 2756 g mol^{-1}) (Figure 2-7). Cold spray ionization mass spectrometry (CSI-MS)[29] detected ions from the monomer up to the pentamer (Figure 2-8–2-10). From all the evidence combined, we concluded that **ZnPy** exists as stable, cyclic oligomers in solution, with the tetramer being the predominant species.

2-2-3 Photophysical Properties

The free-base compound **FbPy** and its zinc complex **ZnPy** showed typical absorption spectra (ca. 10 μM) for the chlorin derivatives in $CHCl_3$, toluene and pyridine as shown in Figure 2-11: the most intense Soret band around 400 nm and four Q bands in 450–700 nm, among which the $Q_y(0,0)$ band is the most intense.[30,31] While the spectral feature of **FbPy** was almost insensitive to the solvents, that of **ZnPy** was affected by them. The spectra of **ZnPy** in non-coordinatable $CHCl_3$ and toluene showed broad features whereas that in pyridine showed sharp feature, indicating that **ZnPy** molecules form self-aggregates in $CHCl_3$ and toluene whereas those exist as monomers in pyridine due to the coordination of pyridine molecule to the zinc center of **ZnPy** molecule.[12,25]

Preliminary time-resolved measurements were performed to probe the excited-state dynamics of the assembly. Excitation of **ZnPy** leads to the formation of the singlet excited state, as demonstrated by the transient absorption (TA) spectra (Figure 2-12), which were taken in toluene as the compound decomposed in $CHCl_3$ under our TA

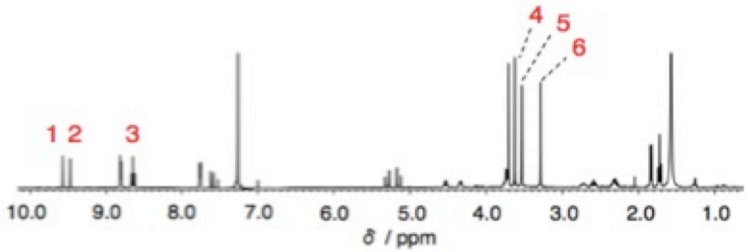

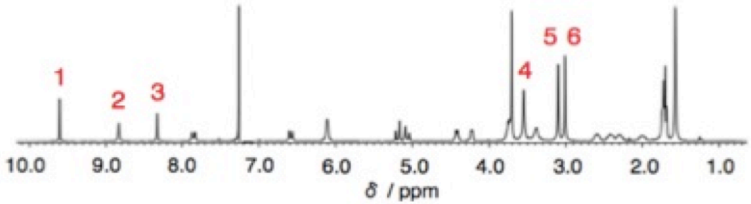

Peak Number	D / $m^2s^{-1} \times 10^{-10}$
1	6.72±0.07
2	6.24±0.05
3	6.49±0.08
4	6.08±0.05
5	6.35±0.06
6	6.34±0.07
Average D	6.37±0.06

Peak Number	D / $m^2s^{-1} \times 10^{-10}$
1	3.47±0.04
2	3.40±0.05
3	3.34±0.03
4	3.43±0.05
5	3.42±0.05
6	3.48±0.04
Average D	3.42±0.04

Figure 2-5. Self-diffusion coefficients for (a) the free-base **FbPy** and (b) the zinc complex **ZnPy** (ca. 10 mM, 298 K) in $CDCl_3$.

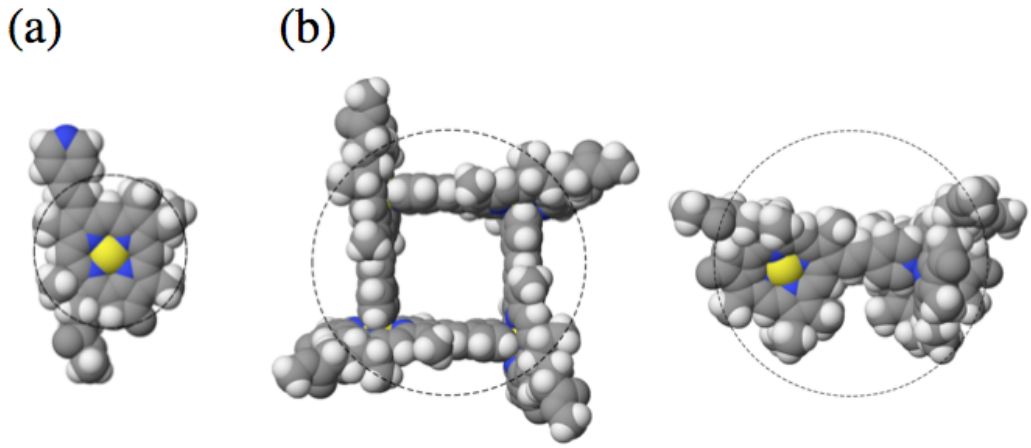

Figure 2-6. Molecular models of the monomeric (a) and cyclic tetrameric (b) zinc complex **ZnPy**. The circles indicate the hydrodynamic radiuses estimated by the DOSY measurements.

(a)

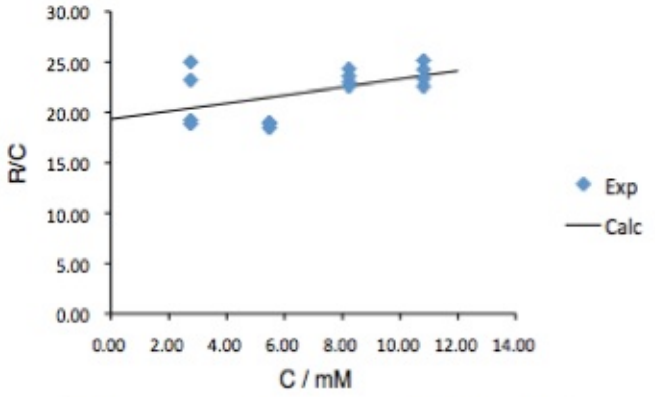

Slope	Intercept	Mw / g mol^{-1}
0.40	19.32 E03	828 (±67)

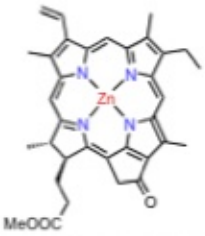

Molecular Weight: 612.06876

(b)

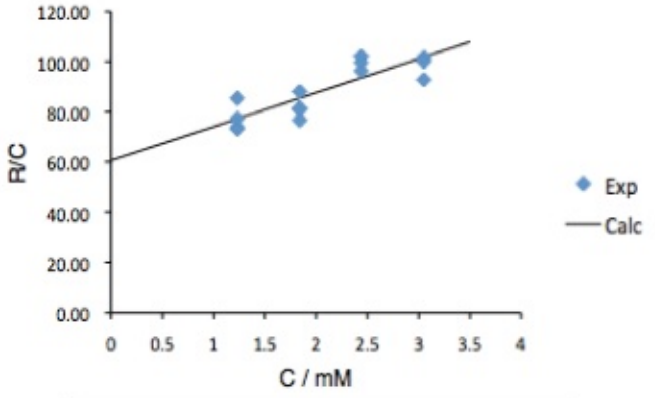

Slope	Intercept	Mw / g mol^{-1}
13.5	60.58 E03	2600 (±190)

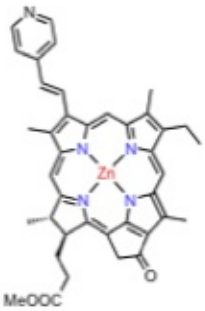

Molecular Weight: 689.15278

Figure2-7. Data analysis of VPO measurements for (a) zinc complex of methyl pyropheophorbide-*a* as a non-coordinatable reference compound and (b) **ZnPy**.

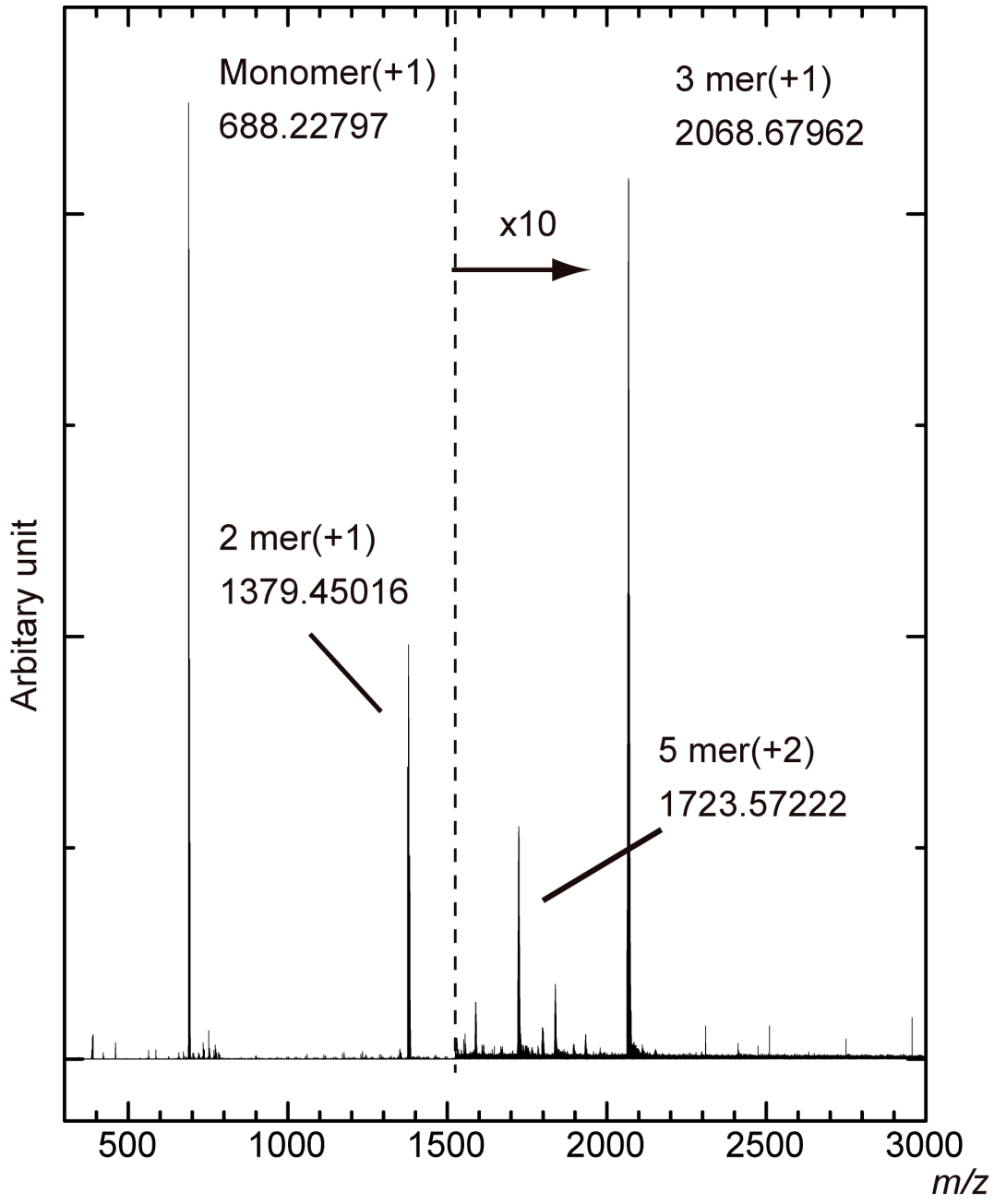

Figure 2-8. CSI-MS spectrum of **ZnPy**. Three molecular ion peaks (m/z = 688, 1379, 2068) were observed as +1 charged state. An ion peak assigned to 5 mer was observed as +2 charged state. The region m/z > 1520 was enlarged by 10 times for clarity.

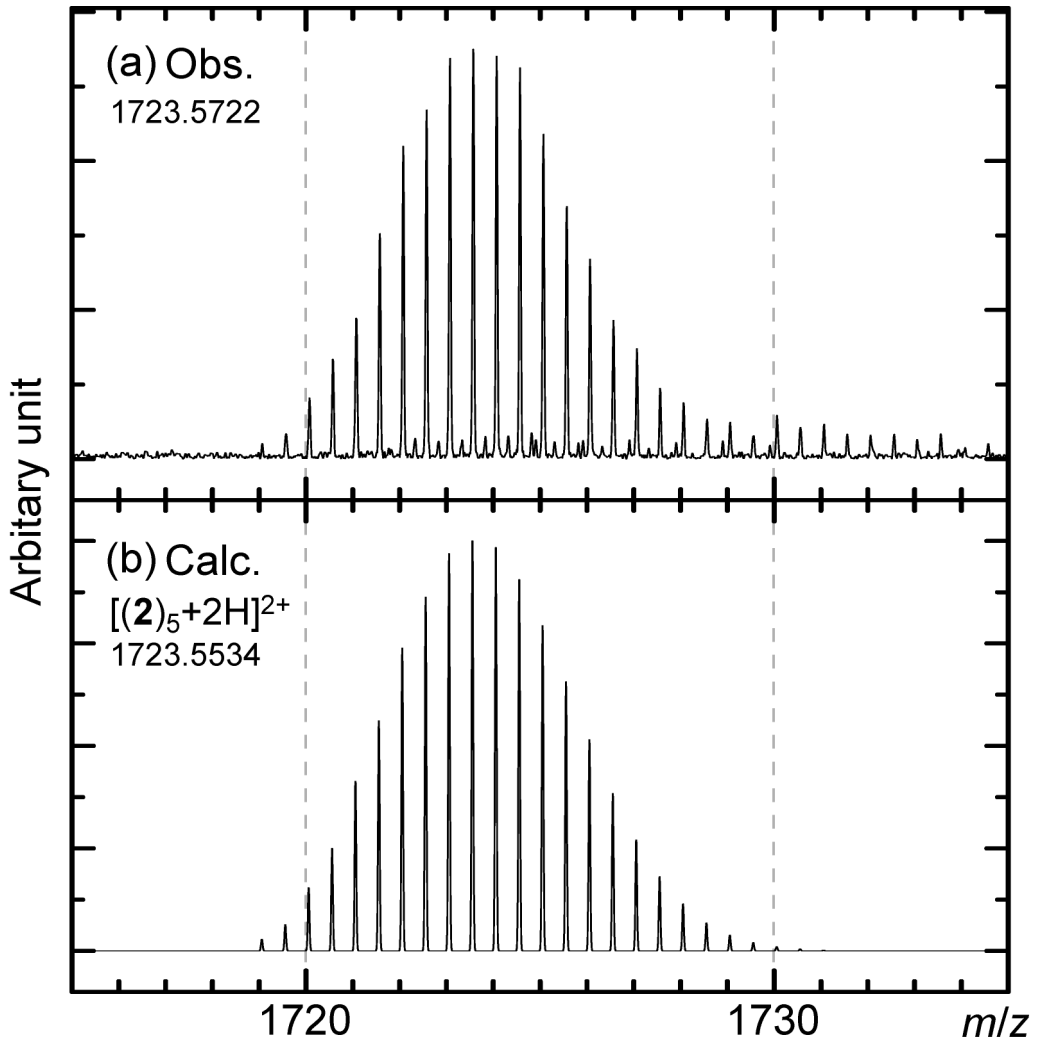

Figure 2-9. Comparison of the observed pentameric molecular ion peaks (a) with the isotope pattern calculated from $[(\mathbf{ZnPy})_5+2H]^{2+}$ (b).

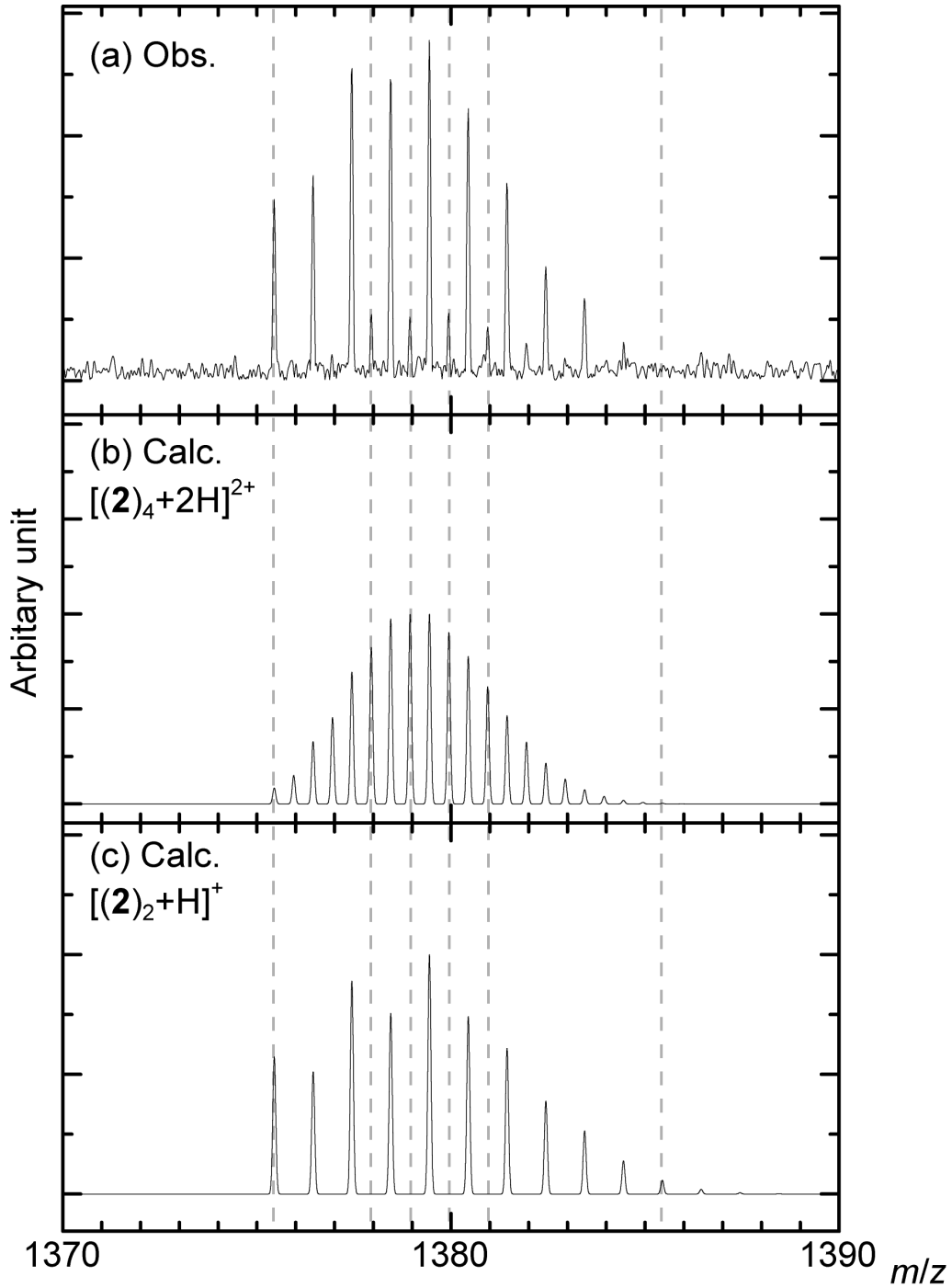

Figure 2-10. Comparison of the observed tetrameric molecular ion peaks (a) with the isotope pattern calculated from $[(\mathbf{ZnPy})_4+2H]^{2+}$ (b) and $[(\mathbf{ZnPy})_2+H]^{+}$, indicating that the observed peaks are the superposition of these two species.

measurement condition. The insensitive decay rate of the singlet-excited state of **ZnPy** to the laser power indicates that singlet–singlet annihilation does not occur within the cyclic oligomers (Figure 2-12). The Wasielewski group reported that the singlet–singlet annihilation occurs within a cyclic tetramer consisting of a zinc chlorophyll derivative with a pyridine group at the position 20.[12,15] The difference would be ascribed to the different orientations of the zinc chlorophyll molecules in our cyclic oligomers and those of Wasielewski's. The fluorescence of **ZnPy** (41 μM) in $CHCl_3$ decayed biexponentially with a major lifetime of 3.3 ns (92%) and a minor, fast component of 0.47 ns (8%) (Figure 2-13). In pyridine, the fast component was drastically different: a fast rising component appeared (0.19 ns, 10%), while the long component was slightly affected (3.6 ns, 90%). The rise was also observed in $CHCl_3$ in the presence of a small amount of pyridine (1–2%), which would disrupt the assembly. Thus, the difference in the dynamics of the excited states in $CHCl_3$ and pyridine is not an effect of the medium but may be ascribed to the cyclic organization of the assembly. Further study will be needed to clarify the nature of the rising component and the effects of the assembly upon it.

2-2-4 Self-Assembly in the Crystal

Quite interestingly, the X-ray crystal structure analysis of a single crystal obtained from $CHCl_3$ layered with CH_3CN using a liquid–liquid diffusion method revealed that the zinc complex **ZnPy** formed double-stranded coordination helices in the crystal as shown in Figure 2-14 and their crystallographic data are summarized in Table 2-1. Two non-equivalent chlorophyll molecules are contained in the unit cell (Figure 2-15). The coordination geometry of the zinc ion of each molecule is that of a square pyramid. That the bond length between the zinc ion and the reduced pyrrole nitrogen is the longest is in accord with those in a reported zinc tetraphenylchlorin–pyridine complex (ZnTPC(Py)).[32] The out–of–cetral nitrogens plane displacements of the zinc ion are 0.26 and 0.30 Å, which are somewhat less than that of ZnTPC(Py) (0.33 Å) (Table 2-2). Each

(a)

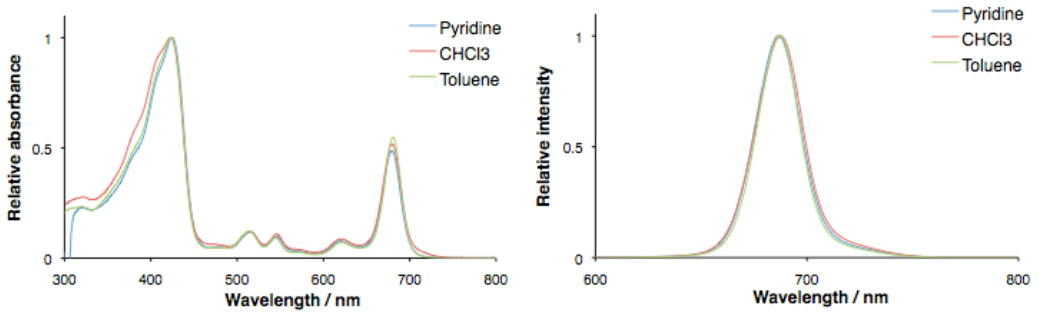

(b)

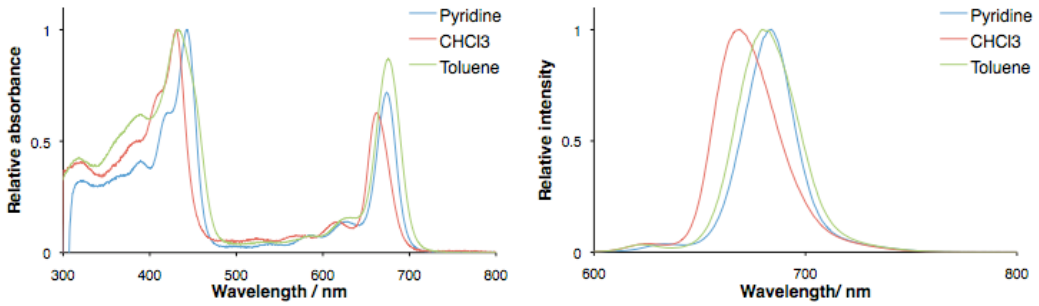

Figure 2-11. Normalized absorption and fluorescence spectra of (a) **FbPy** and (b) **ZnPy** in pyridine (blue), $CHCl_3$ (red), and toluene (green) (ca. 10 M, 298 K). Excited at the Soret band for fluorescence in the absorption spectra. In the case of $CHCl_3$, solid K_2CO_3 was added to ensure that adventitiously produced acid was quenched.

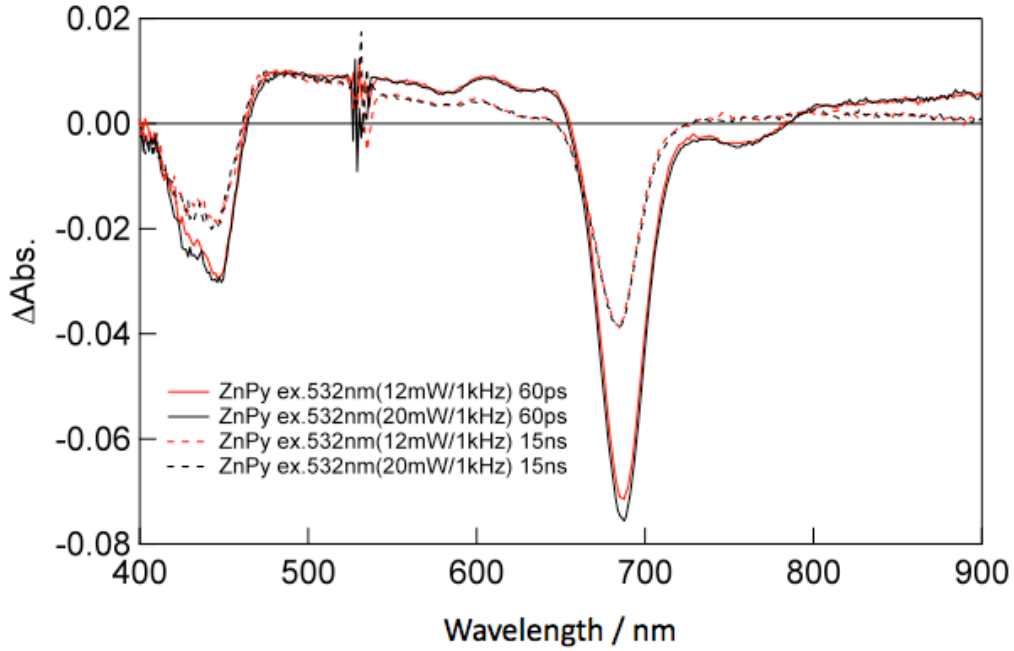

Figure 2-12. Transient absorption spectra of **ZnPy** in toluene.

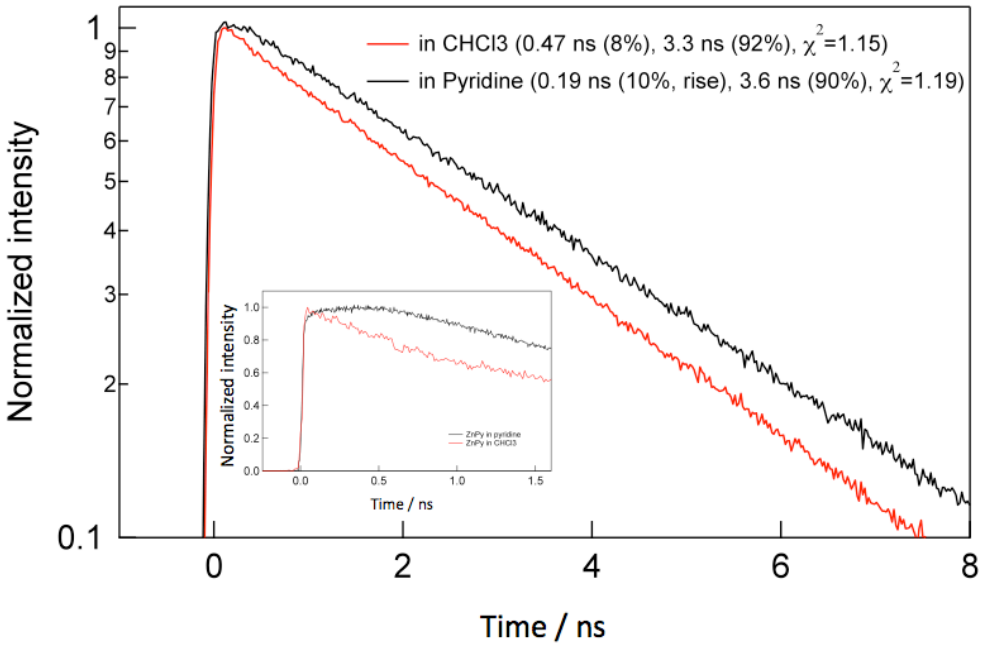

Figure 2-13. Fluorescence decay curves of **ZnPy** in $CHCl_3$ (41 μM) and in pyridine (70 μM).

of

of the non-equivalent chlorophyll molecules forms a double helix, resulting in two non-equivalent helices, one of them being shown in bluish colors in Figure 2-14a and 2-14b. Both of the double helices have similar gross features as follows. The pyridine group in one molecules coordinates axially to the zinc ion in the next molecule. The array of coordination makes a right-handed helical structure with a pitch consisting of three **ZnPy** molecules. Two such helices wrap around one another, forming a double-helical structure. The two chains within the same double helix run in the same direction, that is the pyridine–Zn bonds orientate in the same direction, as indicated by the two arrows in Figure 2-14a. On the other hand, the other non-equivalent double-helix runs in the opposite direction, as shown in reddish colors in Figure 2-14c and 2-14d. The chlorophyll molecules in one double-helix make π-π stacking interactions with molecules in the other oppositely running double helix, with the intermacrocycle separation being ~3.6 Å, apparently mutually stabilizing the helices.

Only a very limited number of crystal structures of chlorophyll assemblies are known thus far. Knapp and co-workers reported a coordination polymer of a 3^1-oxime derivative of zinc chlorophyll held together by axial coordination by the 13^1-carbonyl group.[33] Recently, Tamiaki and co-workers reported another coordination polymer of a zinc bacteriochlorophyll derivative held together by coordination of the 17-propionyl carbonyl group to the zinc ion.[34] Both of them form staircase-like structures without any helical turns. It is interesting to note that a tetraphenylporphyrin derivative functionalized with a vinylpyridine moiety at the β-position also forms a staircase structure without any twist.[35]

2-2-5 Potentiality for Light-Harvesting Antenna

The double-stranded helical structure obtained in this work has some implication in the design of artificial antenna for efficient light harvesting. The axial coordination strategy *via* a coordination site coplanar with chlorophyll plane as exemplified by **ZnPy** has an

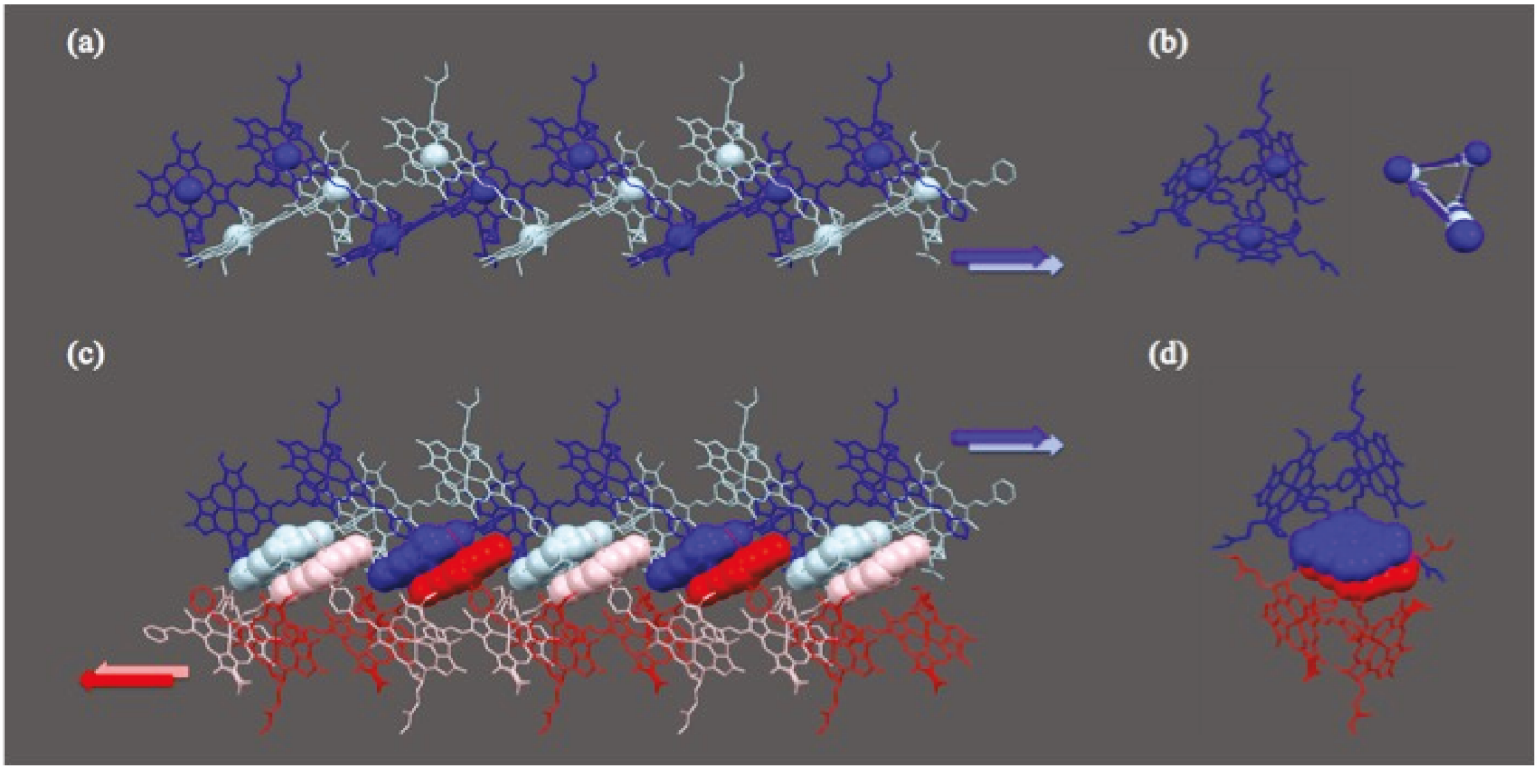

Figure 2-14. Double stranded helical structure of zinc complex **ZnPy**. The colored arrows indicate the coordination direction (pyridine→Zn) of the correspondingly colored helices. Hydrogen atoms and solvent molecules have been omitted for clarity. (a) and (b): One of the double helices. Zinc atoms are shown by space-filling models. (c) and (d): Two different helices pack with π-π stacking interactions. Stacked chlorin rings are shown by space-filling models. (a) and (c) are views perpendicular to the *c*-axis, while (b) and (d) are views along the *c*-axis.

Table 2-1. Crystallographic Data of **ZnPy**

Empirical formula	$C_{39}H_{37}N_5O_3Zn\ (CH_3CN)_{0.5}$
Formula weight	689.15
Color, Habit	Brown, Plate-like
Crystal system	Trigonal
Space group	$P3_2$ (#145)
Unit cell dimensions / Å	a = 20.097(3) b = 20.097(3) c = 14.3196(19)
Volume / Å^3	5008.7(12)
Z	6
Density (calc) / g cm^{-3}	1.412
Absorption coefficient / mm^{-1}	0.782
F(000)	2226
Crystal size / mm^3	0.15 × 0.10 × 0.05
θ for data collection	1.84 to 26.02
Index ranges	$-23 \le h \le 10$, $-15 \le k \le 24$, $-14 \le l \le 17$
Reflections collected	10698
Independent reflections	8134 [R(int) = 0.0501]
Completeness	97.4% (θ = 25.49°)
Absorption correction	Multi-scan (REQAB; Rigaku, 1998)
Refinement method	Full-matrix least-squares on F^2
Data/restraints/parameters	8134/70/843
Goodness-of-fit on F^2	1.102
Final R indices [$I>2\sigma(I)$]	R_1 = 0.0727
R indices (all data)	wR_2 = 0.1465
Largest diff. peak and hole / e Å^{-3}	1.328 and –0.706

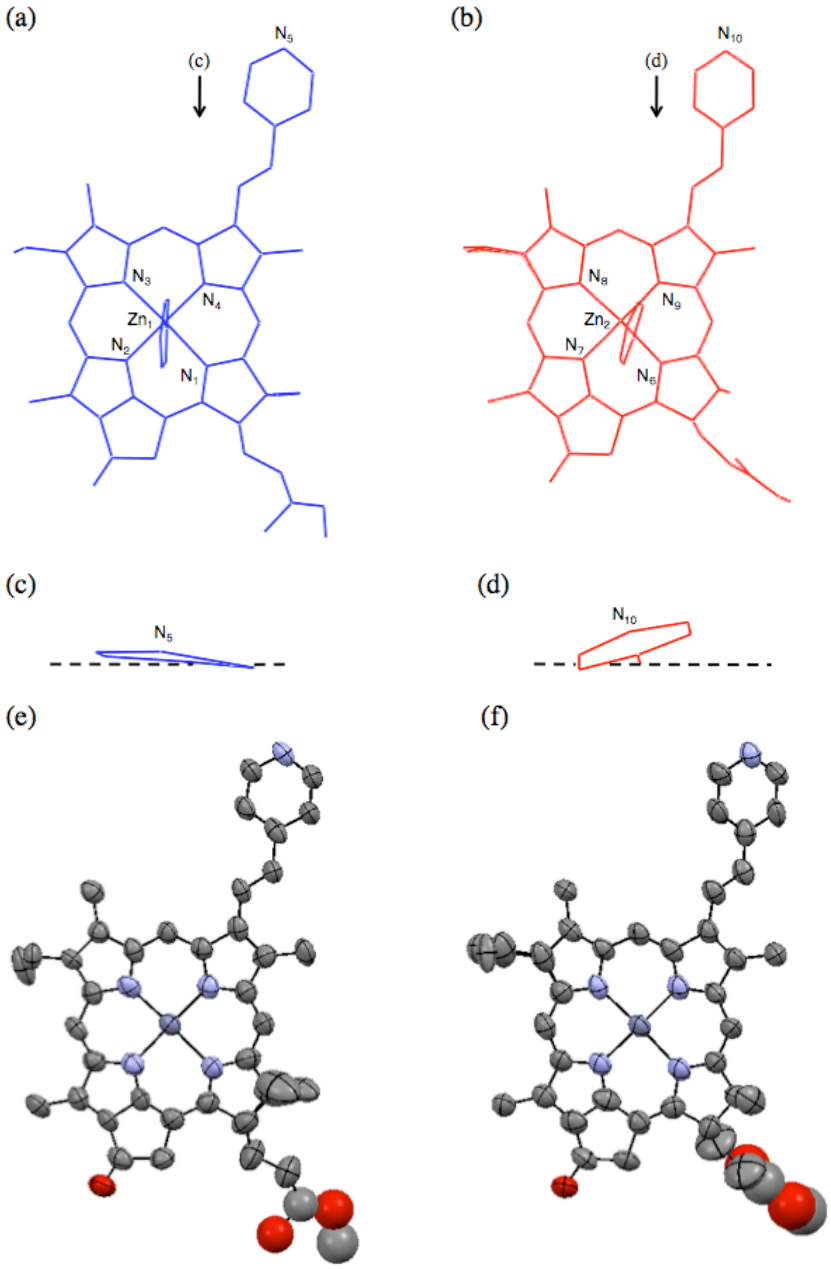

Figure 2-15. Monomer units in the non-equivalent double helices. (a) and (b) show the views perpendicular to the Chl mean plane from the coordinating pyrdine side. (c) and (d) present the tilt of the pyridyl moiety with respect to the Chl mean plane, which is represented by the dashed line. The blue and red colors correspond to the helices in the same colors in Figure 2-14. (e) and (f) show the structures in ORTEP for (a) and (b), respectively. Thermal ellipsoids represent 50% probability. The hydrogen atoms are omitted for clarity.

Table 2-2. Selected Structural Parameters of **ZnPy** for the Coordination Environment

Bond distance / Å			
Zn1 [a]		Zn2 [b]	
$Zn_1–N_1$	2.21(3)	$Zn_2–N_6$	2.18(3)
$Zn_1–N_2$	2.00(3)	$Zn_2–N_7$	2.01(3)
$Zn_1–N_3$	2.07(3)	$Zn_2–N_8$	2.07(3)
$Zn_1–N_4$	1.98(3)	$Zn_2–N_9$	2.02(3)
$Zn_1–N_5^{i}$	2.15(2)	$Zn_2–N_{10}^{ii}$	2.14(0)
$N_1N_2N_3N_4$ palne–Zn_1	0.26	$N_6N_7N_8N_9$ palne–Zn_2	0.30
$N_1N_2N_3N_4$ palne–N_5^{i}	2.40	$N_6N_7N_8N_9$ palne–N_{10}^{ii}	2.42
Angle / °			
Zn1 [a]		Zn2 [b]	
$\angle N_1–Zn_1–N_2$	87.1(11)	$\angle N_6–Zn_2–N_7$	87.3(12)
$\angle N_1–Zn_1–N_3$	166.8(11)	$\angle N_6–Zn_2–N_8$	164.1(10)
$\angle N_1–Zn_1–N_4$	90.3(11)	$\angle N_6–Zn_2–N_9$	90.3(11)
$\angle N_1–Zn_1–N_5^{i}$	92.2(12)	$\angle N_6–Zn_2–N_{10}^{ii}$	90.7(9)
$\angle N_2–Zn_1–N_3$	88.2(11)	$\angle N_7–Zn_2–N_8$	86.7(11)
$\angle N_2–Zn_1–N_4$	163.9(11)	$\angle N_7–Zn_2–N_9$	162.4(11)
$\angle N_2–Zn_1–N_5^{i}$	95.9(11)	$\angle N_7–Zn_2–N_{10}^{ii}$	98.9(12)
$\angle N_3–Zn_1–N_4$	90.8(11)	$\angle N_8–Zn_2–N_9$	91.1(11)
$\angle N_3–Zn_1–N_5^{i}$	100.6(11)	$\angle N_8–Zn_2–N_{10}^{ii}$	104.8(9)
$\angle N_4–Zn_1–N_5^{i}$	100.1(10)	$\angle N_9–Zn_2–N_{10}^{ii}$	98.5(10)

[a] Blue in Figure 2-15. [b] Red in Figure 2-15. Symmetry codes: (i) 1–*x*+*y*, 1–*x*, –2/3+*z*. (ii) 2–*y*, 1+*x*–*y*, 2/3+*z*.

intrinsic weakness in conducting light-harvesting antenna, because the chromophores organized in this coordination model are arranged in mutually perpendicular orientations. The perpendicular orientation is unfavorable for the Förster-type energy transfer, which relies on dipole–dipole interactions. Approximating the transition moments as lying in the direction of the diagonal line connecting the nitrogen in pyrrole A having the vinylpyridine group and the nitrogen C (Chart 2-1),[36] we have calculated the factor κ^2/r^6, which are expected to be in proportional to the energy transfer rate, among the chromophores in the double helices in the crystal (Figure 2-16). Here, κ^2 is the orientation factor and r is the interchromophore center-to-center distance. As expected, energy transfer along the *intre*strand pathways is not efficient with the κ^2/r^6 values of 7–9 $\times$ 10^{-9} Å^{-6} between the nearest neighbors in the same strand due to vanishingly small orientation factor κ^2 = 0.03–0.05. However, the κ^2/r^6 factors are two-orders of magnitude larger (225 $\times$ 10^{-9} Å^{-6} and 162 $\times$ 10^{-9} Å^{6}) between nearest neighbors residing in the complementary strands. Even the κ^2/r^6 factors between the next nearest-neighbors residing in the complementary stands are large (166 $\times$ 10^{-9} Å^{-6} and 157 $\times$ 10^{-9} Å^{-6}) due to favorable orientations (κ^2 = 1.42 and 1.51, respectively). Thus, the double-helical architecture confers efficient, contiguous *inter*strand energy transfer pathways, in which energy migrates among chromophores belonging to complementary strands alternatively in the double helix, even in the case that *intra*strand energy transfer is slow. This analysis demonstrates that the double helices have a functional significance as a light-harvesting antenna in addition to the esthetic beauty. In this particular crystal structure, *inter*-double-helix pathways should be even more efficient owing to the π-π overlap (Figure 2-14c and 2-14d) and parallel orientation.

2-3 Conclusion

We herein described self-assembly of the zinc chlorophyll derivative appended by pyridine as a self-coordinatable moiety **ZnPy** in solution and in the crystal. **ZnPy** formed

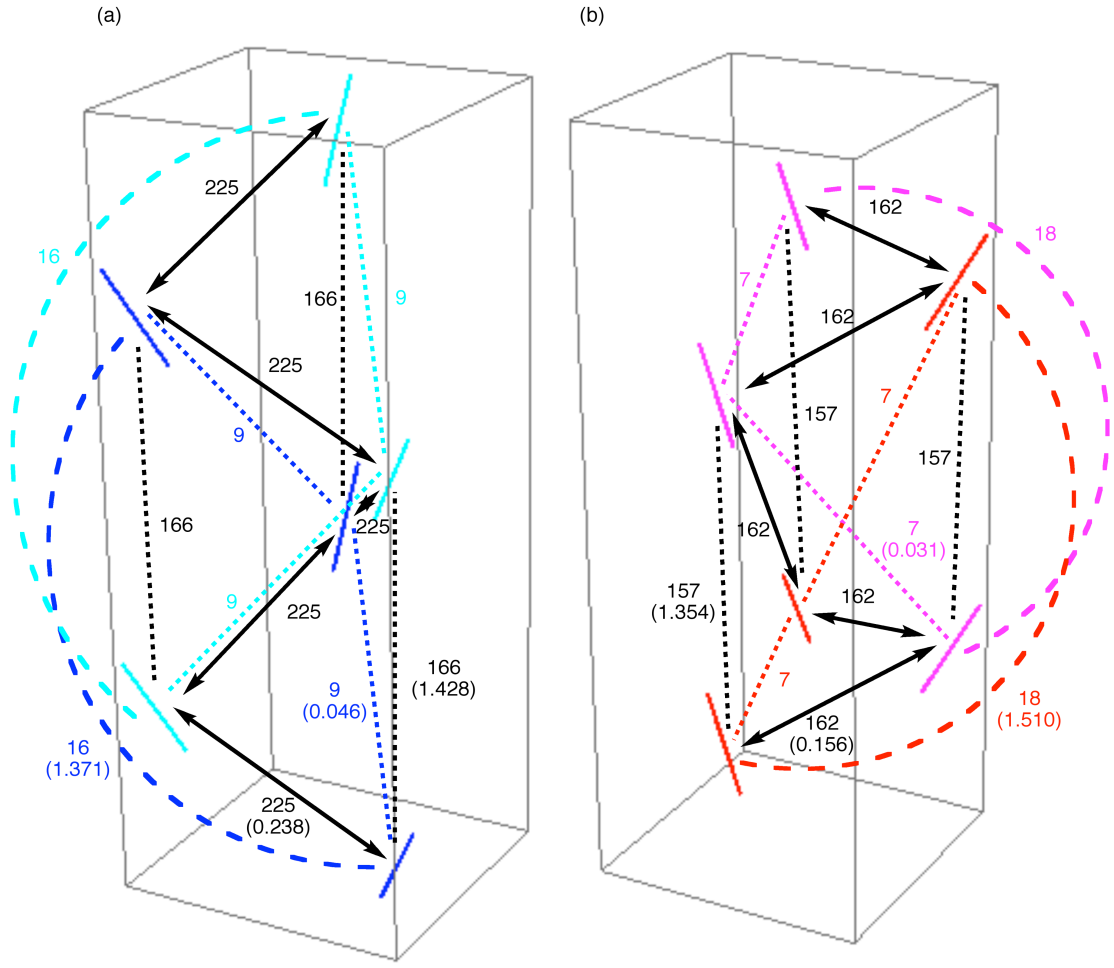

Figure 2-16. Values of $(\kappa^2/r^6 \times 10^9)$ in $Å^{-6}$ and the orientation factor κ^2 (in parentheses) in the crystal, where r is the interchromophore distance. Colors match those used in Figure 2-14. Short solid lines are those connecting N_2 and N_4 (a) or N_7 and N_9 (b), representing approximate transition dipole moments of the Q_y transition. Colored dotted lines represent *intra*strand pathways. Black lines represent *inter*strand pathways, among which the arrowed lines indicate the most efficient pathways. The cuboids are not related to the crystallographic axes but are just meant to aid the eye.

cyclic tetramers as a predominant species in solution and the coordination polymers with double-helical motif in the crystal by intermolecular axial coordination of one pyridine moiety in a zinc chlorophyll molecule to the zinc center in another molecule. The analysis for the relative energy transfer rate demonstrated the possibility that the double-helical structure confers the efficient *inter*strand energy transfer.

2-4 Experiment

2-4-1 General

All reactions were conducted under argon atmosphere. $CHCl_3$ and THF were distilled over NaH and benzophenone ketyl, respectively. Other reagents and solvents purchased for syntheses were used without further purification. Spectroscopic grade $CHCl_3$, toluene, and infinity pure grade pyridine were purchased from Wako. Deuterated solvets, $CDCl_3$ and THF-d_8 were purchased from Sigma-Aldrich. High-performance liquid chromatography (HPLC) was performed with a Shimazu HPLC 20A apparatuses using a solvent system consisting of H_2O and MeOH with flow rates of 1.0 and 10.0 mL/min for analysis and preparation, respectively. ^{1}H-NMR inclusing DOSY spectra were recorded with a 400 MHz JEOL ECX400 spectrometer, and chemical shifts were reported as ppm relative to internal tetramethylsilane. The peaks were assigned with the help of COSY, NOESY, HMQC, HMBC, and DEPT. High resolution mass spectrometry analyses were performed with an Agilant G1969A mass spectrometer using positive atmospheric chemical ionization (APCI). UV-vis and fluorescence data were obtained using Shimazu UV-2400PC and PF 5300PC spectrometers, respectively. The molecular models were made with PM3 or MM3 using CAChe software (version 6.1.12.33). The fluorescence lifetimes were measured by a photon counting method with a streak scope (Hamamatsu Photonics, C4334-01) using the second harmonic generation (SHG, 390 nm) of a Ti:sapphire laser (Spectra-Physics, Tsunami 3950-L2S, fwhm 150 fs) as an excitation source. Accumulation of photons from 675 nm to 775 nm was performed to display

fluorescence decay in all data. Picosecond transient absorption measurement was carried out with a ps transient absorption spectrometer (Ultrafast system, EOS) equipped with a LD-pumped Nd:YAG laser (Ekapla PL2210A). Excitation wavelength and pulse width were 532 nm and 25 ps, respectively. The operation frequency was 1 kHz. The sample concentration was set as approximately 170 μM. CSI-MS measurement was performed using Fourier transform ion cyclotron resonance mass spectrometer (FT-ICR MS; Apex-Qe 9.4 T, Bruker Daltonics, Inc. Billerica, MA, USA). A $CHCl_3$/MeOH (99:1) solution of **ZnPy** (1.5 mM) was subjected to CSI-MS. Measurement condition was as follows: positive mode; capillary voltage, 4.5 kV; dry gas flow rate w.5 L/min; nebulizer gas flow rate, 1.5 L/min; sample flow rate, 60 μL/h; desolvation plate temperature, 35 ℃. Vapor pressure osmometry was measured using a GONOTEC OSMAT 070. Benzil was used as s stsndard and a calibration curve at 37 ℃ in term of *R* in Ohm versus molal osmatic concentration (moles per kg $CHCl_3$) was constructed up to 0.01 molal. Single crystal diffraction analysis data were collected at 273.0 K with Rigaku Saturn724+ diffractometer by using Mo *K*α radiation (λ = 0.71075 Å). The structures were solved by a direct method.

2-4-2 Syntheses

FbPy. A mixture of methy pyropheophorbide-*d* (12.5 mg, 0.023 mmol), picoline (3.3 mL, 34 mmol), Ac_2O (10 mL), and two drops of AcOH was heated at reflux for 3 h. The progress of reaction was monitored using HPLC. The solvent and excess picoline were evaporated *in vacuo* to give a brown viscous oil (38 mg). The crude mixture was purified by column chromatography (silica, hexane/EtOAc = 2/1→1/1→1/3) followed by HPLC (octadecylsilyl, MeOH/H_2O = 9/1) to afford a purple solid (7.8 mg, 0.013 mmol, 55%).

^{1}H-NMR ($CDCl_3$, 298 K): δ = 9.58 (s, 1H, 10), 9.48 (s, 1H, 5), 8.81 (d, *J* = 6.4, 2H, Py_α), 8.65 (s, 1H, 20), 8.65 (d, *J* = 16.5 Hz, 1H, 3^1), 7.76 (d, *J* = 6.4 Hz, 2H, Py_β), 7.60 (d, *J* = 16.5 Hz, 1H, 3^2), 5.30 (d, *J* = 19.7 Hz, 1H, 13^2), 5.14 (d, *J* = 19.7 Hz, 1H, 13^2), 4.53

(m, 1H, 18-H), 4.33 (m, 1H, 17-H), 3.73 (quartet, J = 7.3 Hz, 2H, 8-$\underline{CH_2}CH_3$), 3.70, 3.62, 3.53, 3.28 (s, each 3H, ring CH_3 × 3, 17^2-$COOCH_3$), 2.73, 2.59, 2.30 (m, 1H, 1H, 2H, 17-CH_2CH_2), 1.84 (d, J = 7.3 Hz, 3H, 18-CH_3), 1.71 (t, J = 7.3 Hz, 3H, 8-$CH_2\underline{CH_3}$), 0.35 (bs, 1H, NH), and –1.72 (bs, 1H, NH) ppm; APCI–HRMS: m/z = 626.3130 $[M+H]^+$ (100%), calcd for $C_{39}H_{40}N_5O_3$ = 626.3132. HPLC (octadecylsilyl, MeOH/H_2O = 9/1, isocratic): t_R = 9.18 min.

ZnPy. To a solution of **FbPy** (62 mg, 0.10 mmol) in $CHCl_3$ (70 mL), a saturated solution of $Zn(OAc)_2$•$2H_2O$ in MeOH (7.0 mL) was added. The resulting mixture was stirred for 3 h. An aqueous solution of 4% $NaHCO_3$ was added, and the mixture was stirred for 30 min. The organic layer was separated and was washed with brine (100 mL × 3) and H_2O (100 mL × 3). The solvent was evaporated after drying with Na_2SO_4 to give a purple solid (69 mg). The crude mixture was purified with column chromatography (silica, 3–10% acetone/$CHCl_3$) to afford a green-purple solid (62 mg, 0.090 mmol, 91%).

^{1}H-NMR ($CDCl_3$, 298 K): δ = 9.60 (s, 1H, 10), 9.83 (s, 1H, 5), 8.32 (s, 1H, 20), 7.85 (d, J = 16.3 Hz, 1H, 3^1), 6.59 (d, J = 16.3 Hz, 1H, 3^2), 7.76 (bs, 2H, Py_β), 5.19 (d, J = 19.7 Hz, 1H, 13^2), 5.06 (d, J = 19.7 Hz, 1H, 13^2), 4.42 (m, 1H, 18-H), 4.22 (m, 1H, 17-H), 3.74 (quartet, J = 7.8 Hz, 2H, 8-$\underline{CH_2}CH_3$), 3.70, 3.55, 3.10, 3.01 (s, each 3H, ring CH_3 × 3, 17^2-$COOCH_3$), 3.40 (bs, 2H, Py_α), 2.60, 2.41, 2.29, 1.99 (m, each 1H, 17-CH_2CH_2), and 1.71 (m, 6H, 18-CH_3, 8-$CH_2\underline{CH_3}$) ppm; APCI–HRMS: m/z = 688.2274 $[M+H]^+$ (100%), calcd for $C_{39}H_{38}N_5O_3Zn$ = 688.2266. HPLC (octadecylsilyl, MeOH/H_2O = 17/3, isocratic) t_R = 9.86 min.

2-5 References

(1) D. Kim., E. *Multiporphyrin Arrays*; Pan Stanford Publishing: Singapore, 2012.

(2) Otsuki, J. *J. Porphyrin Phthalocyanines* **2009**, *13*, 1069.

(3) Scholes, G. D.; Fleming, G. R.; Olaya-Castro, A.; van Grondelle, R. *Nat. Chem.* **2011**, *3*, 763.

(4) McDermott, G.; Prince, S. M.; Freer, A. A.; Hawthornthwaite-Lawless, A. M.; Papiz, M. Z.; Cogdell, R. J.; Isaacs, N. W. *Nature* **1995**, *374*, 517.

(5) Balaban, T. S.; Tamiaki, H.; Holzwarth, A. R. *Top Curr. Chem.* **2005**, *258*, 1.

(6) Tamiaki, H.; Holzwarth, A. R.; Schaffner, K. *J. Photochem. Photobiol. B: Biol.* **1992**, *15*, 355.

(7) Tamiaki, H.; Holzwarth, A. R.; Schaffner, K. *Photosynth. Res.* **1994**, *41*, 245.

(8) Jochum, T.; Reddy, C. M.; fer, A. E.; Buth, G.; Szmytkowski, J. d.; Kalt, H.; Moss, D.; Balaban, T. S. *Proc. Natl. Acad. Sci.* **2008**, *105*, 12736.

(9) Balaban, M. C.; Eichho1fer, A.; Buth, G.; Hauschild, R.; Szmytkowski, J.; Kalt, H.; Balaban, T. S. *J. Phys. Chem. B* **2008**, *112*, 5512.

(10) Tamiaki, H.; Miyata, S.; Kureishi, Y.; Tanikag, R. *Tetrahedron* **1996**, *52*, 12421.

(11) Miyatake, T.; Tanigawa, S.; Kato, S.; Tamiaki, H. *Tetrahedron Lett.* **2007**, *48*, 2251.

(12) Kelley, R. F.; Goldsmith, R. H.; Wasielewski, M. R. *J. Am. Chem. Soc.* **2007**, *129*, 6384.

(13) Kelley, R. F.; Lee, S. J.; Wilson, T. M.; Nakamura, Y.; Tiede, D. M.; Osuka, A.; Hupp, J. T.; Wasielewski, M. R. *J. Am. Chem. Soc.* **2008**, *130*, 4277.

(14) Gunderson, V. L.; Smeigh, A. L.; Kim, C. H.; Co, D. T.; Wasielewski, M. R. *J. Am. Chem. Soc.* **2012**, *134*, 4363.

(15) Jensen, R. A.; Kelley, R. F.; Lee, S. J.; Wasielewski, M. R.; Hupp, J. T.; Tiede,

D. M. *Chem. Commun.* **2008**, 1886.

(16) Sengupta, S.; Würthner, F. *Acc. Chem. Res.* **2013**, *46*, 2498.

(17) Röger, C.; Miloslavina, Y.; Brunner, D.; Holzwarth, A. R.; Würthner, F. *J. Am. Chem. Soc.* **2008**, *130*, 5929.

(18) Smith, K. M.; Goff, D. A.; Simpson, D. J. *J. Am. Chem. Soc.* **1985**, *107*, 4946.

(19) Kunieda, M.; Tamiaki, H. *J. Org. Chem.* **2008**, *73*, 7686.

(20) Fukusumi, T.; Takei, N.; Tateno, Y.; Aoki, T.; Ando, A.; Kozakai, K.; Shima, H.; Mizoguchi, T.; Ito, S.; Ikeda, T.; Tamiaki, H.; Oba, T. *J. Porphyrins Phthalocyanines* **2013**, *17*, 1188.

(21) Oba, T.; Uda, Y.; Matsuda, K.; Fukusumi, T.; Ito, S.; Hiratani, K.; Tamiaki, H. *Bioorg. Med. Chem. Lett.* **2011**, *21*, 2489.

(22) Oba, T.; Tateno, Y.; Ihara, M.; Fukusumi, T.; Takei, N.; Ito, S. *Tetrahedron Lett.* **2014**, *55*, 725.

(23) Li, J. Z.; Wang, J. J.; Yoon, I.; Cui, B. C.; Shim, Y. K. *Bioorg. Med. Chem. Lett.* **2012**, *22*, 1846.

(24) Li, J.-Z.; Cui, B.-C.; Wang, J.-J.; Shim, Y. K. *Bull. Korean Chem. Soc.* **2011**, *32*, 2465.

(25) Tamiaki, H.; Yagai, S.; Miyatake, T. *Bioorg. Med. Chem.* **1998**, *6*, 2171.

(26) Shoji, S.; Hashishin, T.; Tamiaki, H. *Chem. Eur. J.* **2012**, *18*, 13331.

(27) Sasaki, S.-i.; Mizutani, K.; Kunieda, M.; Tamiaki, H. *Tetrahedron* **2012**, *68*, 7133.

(28) Oliva, A. I.; Gómez, K.; Gonzáleza, G.; Ballester, P. *New J. Chem.* **2008**, *32*, 2159.

(29) Yamaguchi, K. *J. Mass Spectrom.* **2003**, *38*, 473.

(30) Sasaki, S.-i.; Mizutani, K.; Kunieda, M.; Tamiaki, H. *Tetrahydron* **2011**, *67*, 6065.

(31) Yagai, S.; Tomohiro, M.; Shimono, Y.; Tamiaki, H. *Photochem. Photobiol.*

2001, *73*.

(32) Spaulding, L. D.; Andrews, L. C.; Williams, G. J. B. *J. Am. Chem. Soc.* **1977**, *99*, 6918.

(33) Knapp, S.; Huang, B.; Emge, T. J.; Sheng, S.; Krogh-Jespersen, K.; Potenza, J. A.; Schugar, H. J. *J. Am. Chem. Soc.* **1999**, *121*, 7977.

(34) Jesorka, A.; Holzwarth, A. R.; Eichhöfer, A.; Reddy, C. M.; Kinoshita, Y.; Tamiaki, H.; Katterle, M.; Naubrond, J.-V.; Balaban, T. S. *Photochem. Photobiol. Sci.* **2012**, *11*, 1069.

(35) Burrell, A. K.; Officer, D. L.; Reid, D. C. W.; Wild, K. Y. *Angew. Chem. Int. Ed.* **1998**, *37*, 114.

(36) Linke, M.; Lauer, A.; von Haimberger, T.; Zacarias, A.; Heyne, K. *J. Am. Chem. Soc.* **2008**, *130*, 14904.

Chapter 3

Self-Assembly of a Zinc Chlorophyll Derivative Appended by Oxazole

3-0 Summary

This chapter describes self-assembly of a novel zinc chlorophyll derivative appended by oxazole as a self-coordinatable moiety. The cyclic oligomers including trimers as a predominant species formed in solution, whereas the coordination polymer with a staircase motif was produced in the crystal mediated by intermolecular axial coordination of a nitrogen atom in the oxazole moiety to the zinc ion in another zinc chlorophyll molecule. The higher-order structures of the zinc chlorophyll assemblies thus correlates with the structure of *N*-heterocycle in the chlorophyll molecule.

3-1 Introduction

Artificial antenna models have been fabricated by self-assembly of several chromophores including chlorophyll derivatives.[1-5] A majority of chlorophyll-based assemblies have been constructed to obtain insights into structures and functions of chlorosome (1-2), which formed by zinc-alcoholic oxygen coordination.[6-9] We thus focused on construction of novel zinc chlorophyll-based self-assembly mediated by zinc–aromatic nitrogen coordination as demonstrated in Chapter 2. Generally, nitrogen-based donors coordinate more strongly than the oxygen-based donors to the zinc atom. Further, the rigidity of aromatic ligands would help restrict the possible structures of assemblies. These traits make *N*-containing aromatic heterocycles more attractive than hydroxyl oxygen in constructing robust and well-defined chlorophyll assemblies. We demonstrated the self-assembly of a zinc chlorophyll derivative **ZnPy** with vinylpyridine as a coordination site in Chapter 2.[1] The vinylpyridine derivative formed cyclic tetramers as predominant species in solution, while it formed double-helical coordination polymers by self-assembly through the intermolecular axial coordination of the nitrogen in the pyridine moiety to the zinc center in another chlorophyll molecule. In this chapter, we describe the coordination-directed assemblies of an oxazole-appended zinc chlorophyll derivative **ZnOx** (Chart 3-1) in solution as well as in the crystal. The oxazole moiety has a couple of geometrical features different from those of the vinylpyridine moiety as a coordination site: (i) a shorter linker between the chlorophyll scaffold and the

coordination site and (ii) a more angled coordination orientation, i.e., the nitrogen lone pair directs away from the line along the chlorin–oxazole bond. Furthermore, the oxazole moiety has not been used as an axial ligand in the porphyrin/chlorophyll chemistry to the best of our knowledge.

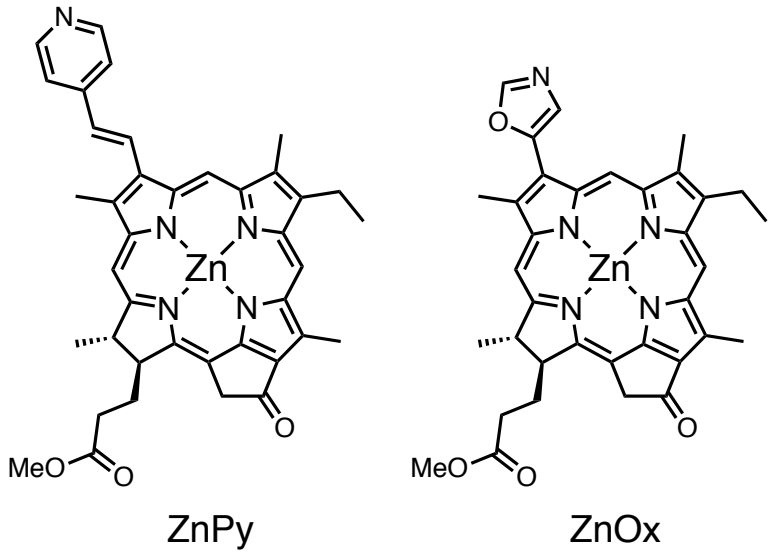

Chart 3-1. Chemical structures of **ZnPy** and **ZnOx**

3-2 Results and Discussion

3-2-1 Syntheses

The synthetic route of the free-base chlorophyll **FbOx** and its zinc complex **ZnOx** is shown in Scheme 3-1. Methyl pyropheophorbide-*d* was synthesized from pheophytin-*a* through three steps: (i) the transesterification of phytyl ester at the position 17^2 to the methyl ester in methanol in the presence of sulfuric acid;[10] (ii) the demethoxycarbonylation of the methyl ester group at the position 13^2 by refluxing in collidine;[10] and (iii) the oxidation of the vinyl group at the position 3 to the formyl group by the Lemieux–Johnson oxidation using osumium tetraoxide (OsO_4) and sodium periodide ($NaIO_4$) as mentioned in Chapter 2.[11] The formyl group in methy pyropheophorbide-*d* was transformed to the 5-substituted oxazole group by the van Leusen oxazole synthesis using van Leusen regent, *p*-toluenesulfonylmethyl isocyanide (TosMIC), to give the free-base chlorophyll appended by oxazole **FbOx** in high yield (70%).[12,13] The zinc ion was inserted into the center of the chlorophyll ring of **FbOx** to

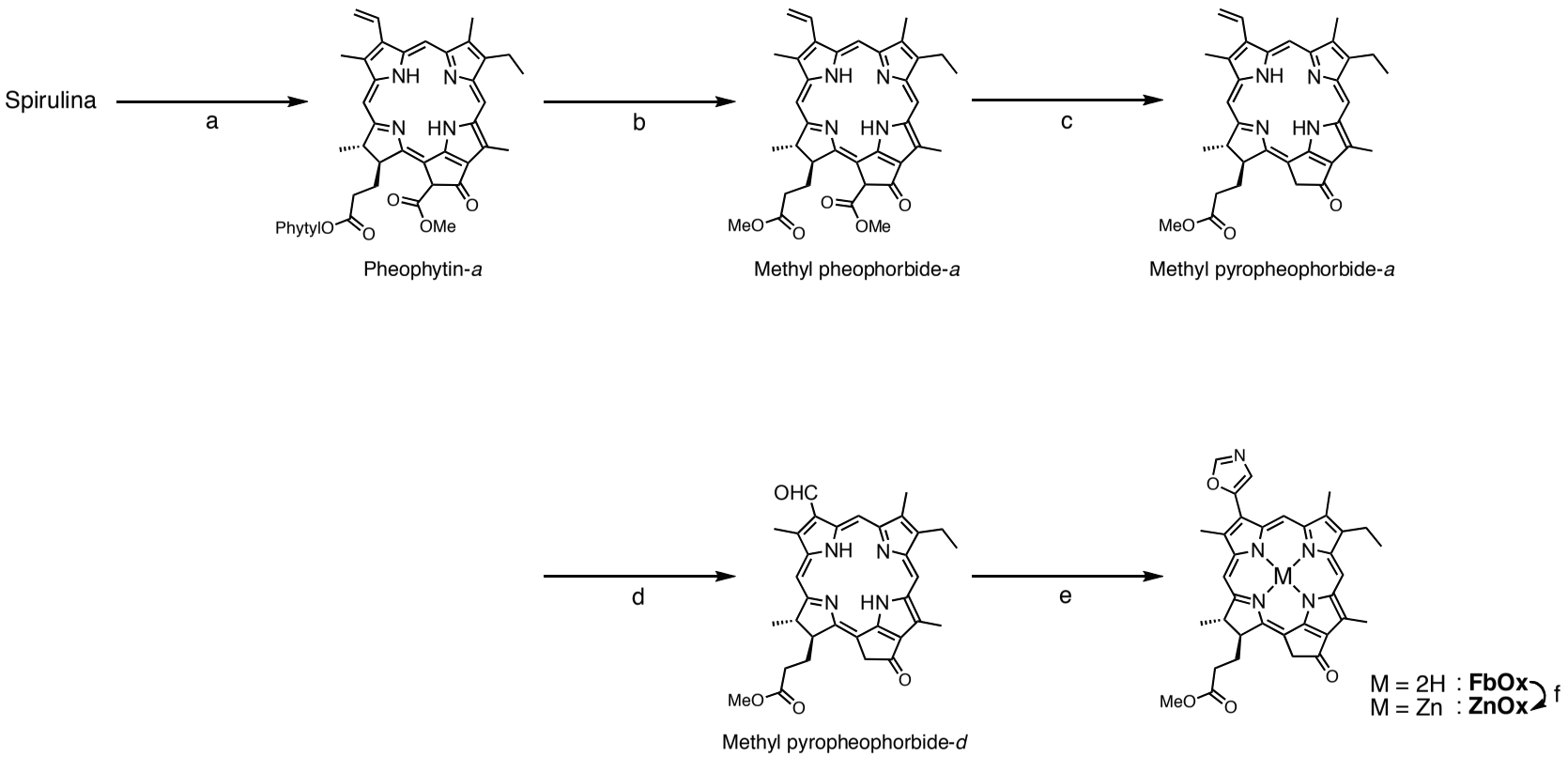

Scheme 3-1. Synthetic procedures of the free-base chlorophyll **FbOx** and its zinc complex **ZnOx**. a) acetone, reflux. b) H_2SO_4, MeOH, overnight. c) collidine, reflux. d) OsO_4, $NaIO_4$, AcOH, THF, H_2O, overnight. e) TosMIC, K_2CO_3, MeOH, reflux, 3 h. f) $Zn(OAc)_2 \bullet 2H_2O$, MeOH, $CHCl_3$, 3 h.

afford the zinc complex **ZnOx**, quantitatively.[14]

3-2-2 Self-Assembly in Solution

ZnOx showed typical absorption spectrum for the chlorin derivatives in $CHCl_3$ as shown in Figure 3-1: the most intense Soret band around 400 nm and four Q bands in 450–700 nm which, among which the $Q_y(0,0)$ band is the most intense.[15] The bands were bathochromically shifted upon increasing concentration (2.0–400 μM) as shown in Figure 3-1. The bathochromic shift still continued at 400 μM. The fluorescence spectra also red-shifted with increasing concentration to 400 μM (Figure 3-2). Bathochromic shifts in the absorption and fluorescence spectra were also observed in the case of reference compound, zinc methyl pyropheophorbide-*a*, after addition of 1% pyridine (Figure 3-3).[16] Similar bathochromic shifts were also observed for other zinc chlorophyll derivatives coordinated by pyridine. Thus we have assigned the bathochromic shifts to the self-coordination of **ZnOx**. The ^{1}H-NMR peaks of the oxazole protons Ox-a and Ox-b next to nitrogen atom in non-coordinatable $CDCl_3$ were shifted upfield from those in coordinatable pyridine-d_5 by 4.61 ppm and 4.67 ppm (298 K, ca. 10 mM; Figure 3-4), indicating that the nitrogen atom in the oxazole moiety is involved in the self-coordination. We have investigated the effect of concentration of **ZnOx** in $CDCl_3$ on ^{1}H-NMR chemical shifts in more detail (Figure 3-5–3-8). The equilibrium for this system, in which both linear and cyclic oligomers and polymers are likely to be formed, may be represented as

$$\begin{array}{ccccccc} \mathrm{M} & \overset{\mathrm{M}}{\rightleftarrows} & \mathrm{M}_2 & \overset{\mathrm{M}}{\rightleftarrows} & \mathrm{M}_3 & \overset{\mathrm{M}}{\rightleftarrows} & \mathrm{M}_4 \overset{\mathrm{M}}{\rightleftarrows} \cdots \\ & & \downarrow\uparrow & & \downarrow\uparrow & & \downarrow\uparrow \\ & & \mathrm{C}_2 & & \mathrm{C}_3 & & \mathrm{C}_4 \end{array} \qquad \begin{cases} K_{\mathrm{i}} = [\mathrm{M}_n]/\left([\mathrm{M}_{n-1}][\mathrm{M}]\right) \\ K_{\mathrm{c},n} = [\mathrm{C}_n]/[\mathrm{M}_n] \end{cases}$$

where M_n and C_n represent linear and cyclic *n*-mers. The K_i is the intermolecular binding constant, which we assumed to be independent of the oligomer size and thus may be obtained from a model study. The K_i value of the coordination of 5-phenyloxazole to zinc pyropheophorbide-*a* was determined to be 890 M^{-1} (298 K, Figure 3-8). It was impossible to

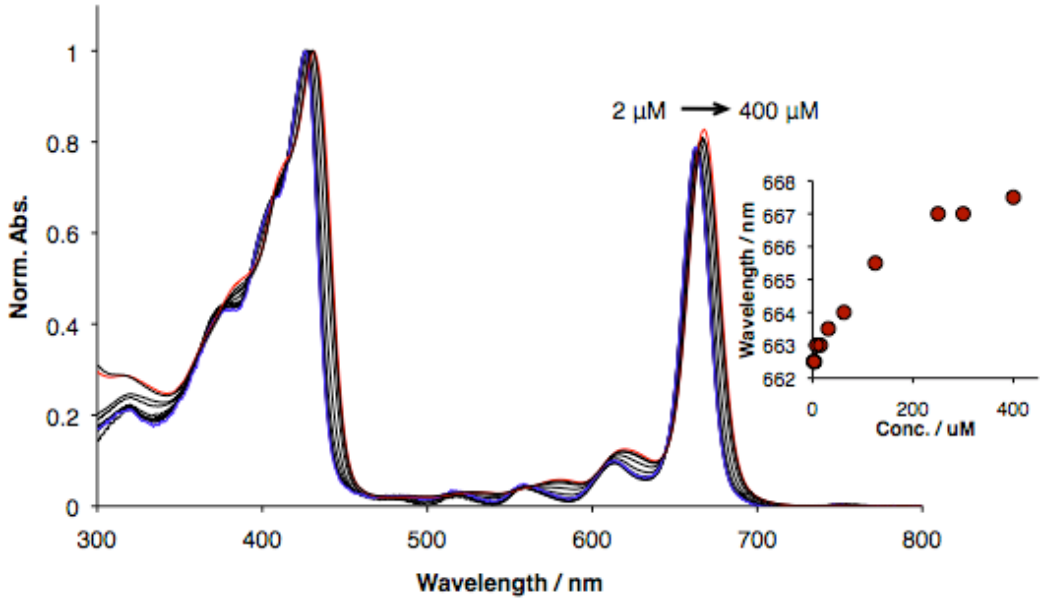

Figure 3-1. Absorption spectra of **ZnOx** in $CHCl_3$ in a concentration from 2.0 (blue) to 400 (red) µM. The inset shows λ_{max} of the $Q_y(0,0)$ band.

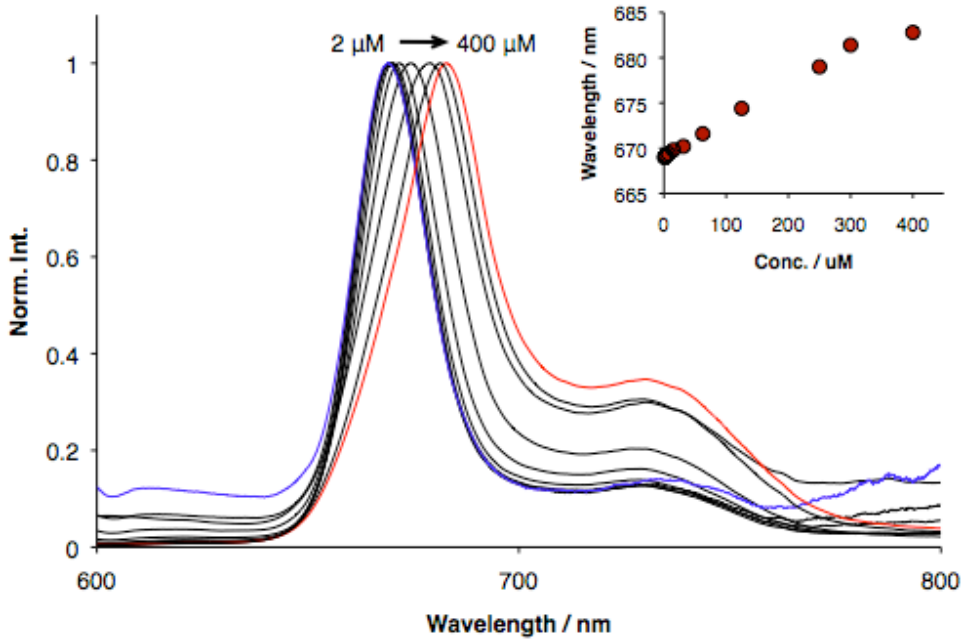

Figure 3-2. Fluorescence spectra of **ZnOx** in $CHCl_3$ in a concentration range from 2.0 (blue) to 400 (red) µM (λ_{ex} = 533 nm). The inset shows λ_{max}. A reflection configuration was used for measurement of the spectra using 1 mm cuvette.

(a)

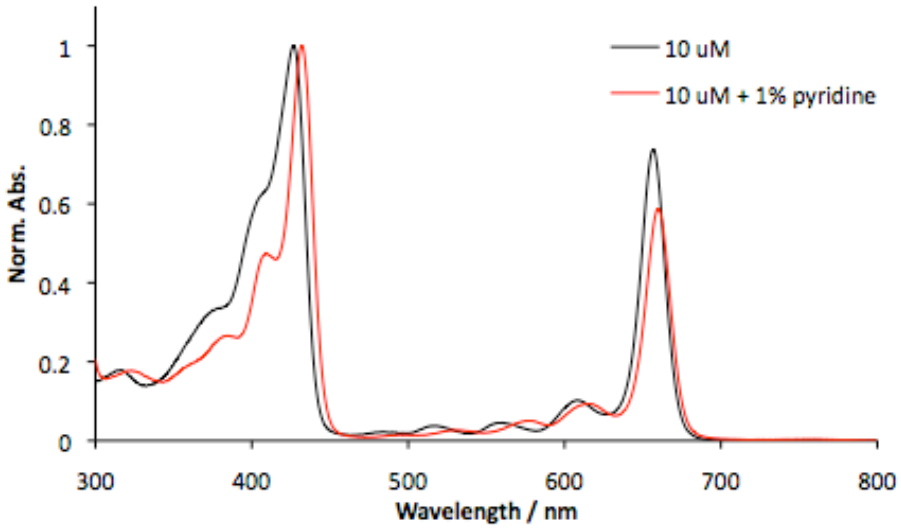

(b)

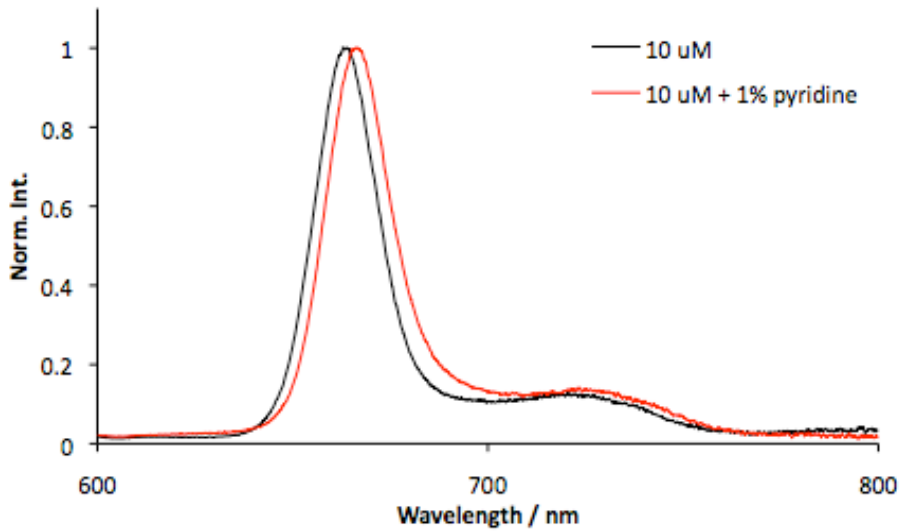

Figure 3-3. Influence of addition of pyridine on the (a) absorption and (b) fluorescence spectrum of zinc methyl pyropheophorbide-*a* (10 μM) in $CHCl_3$.

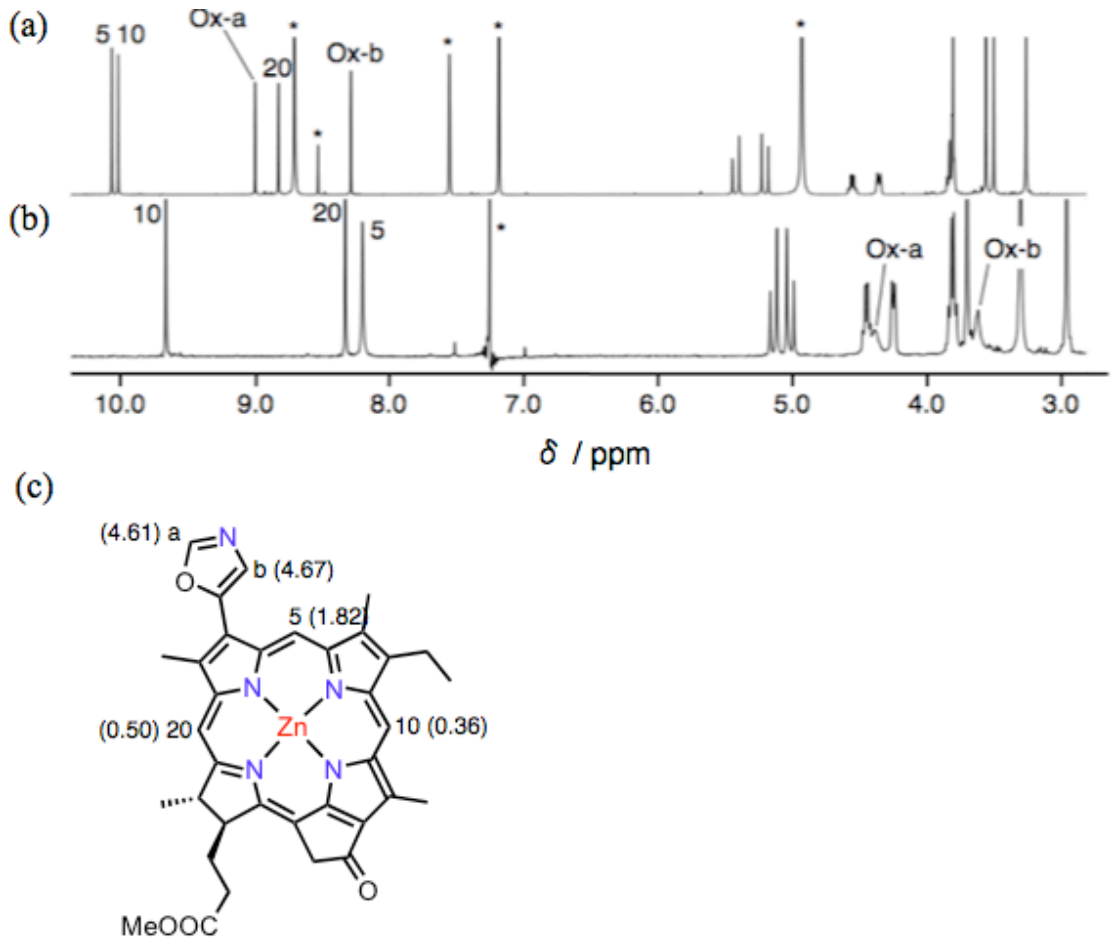

Figure 3-4. ^{1}H-NMR spectra for **ZnOx** (a) in pyridine-d_5 and (b) in $CDCl_3$ (298 K, ca 10 mM). Asterisks indicate water and residual solvent peaks. (c) Chemical shift differences for **ZnOx**. The values of $\Delta\delta$ / ppm = $\delta_{\text{Pyridine-d5}} - \delta_{\text{CDCl3}}$ are shown in parentheses.

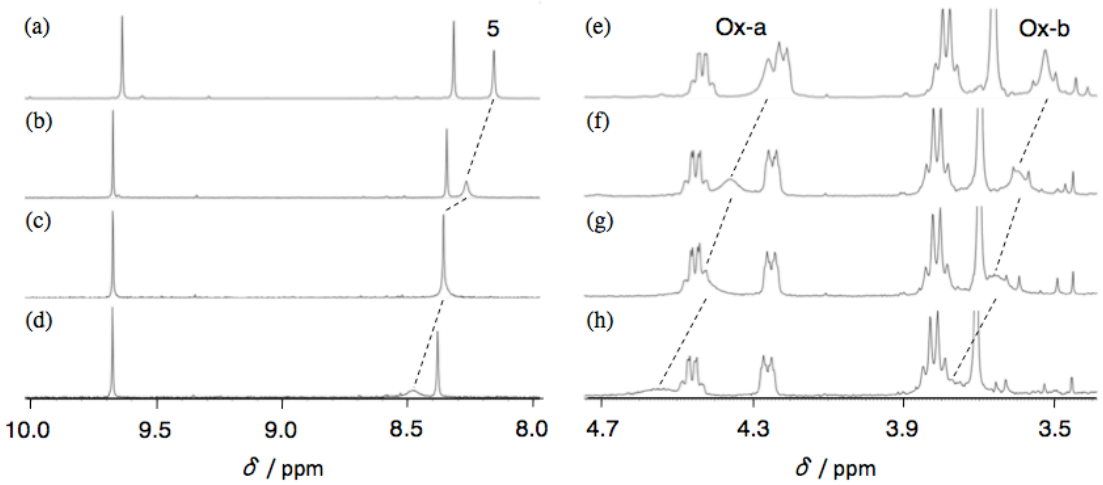

Figure 3-5. ^{1}H-NMR spectra of **ZnOx** at various concentrations in $CDCl_3$ at 298 K. (a)-(d) show a downfield region at (a) 38.7 mM, (b) 2.4 mM, (c) 1.2 mM, and (d) 0.6 mM. (e)-(h) show an upfield region at (e) 38.7 mM, (f) 9.6 mM, (g) 7.2 mM, and (h) 3.6 mM. The dashed lines indicate the movement of the peaks of protons at the position of meso-5, Ox-a, and Ox-b.

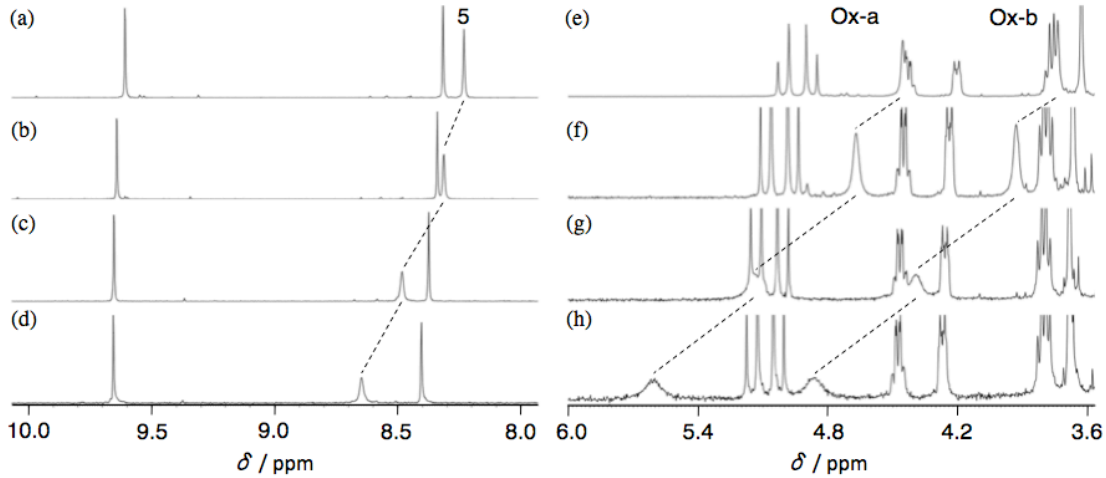

Figure 3-6. ^{1}H-NMR spectra of **ZnOx** at various concentrations in $CDCl_3$ at 348 K; (a), (d) 50.2 mM, (b), (f) 11.9 mM, (c), (g) 3.6 mM, and (d), (h) 1.8 mM. The dashed lines indicate the movement of the peaks of protons at the position of meso-5, Ox-a, and Ox-b.

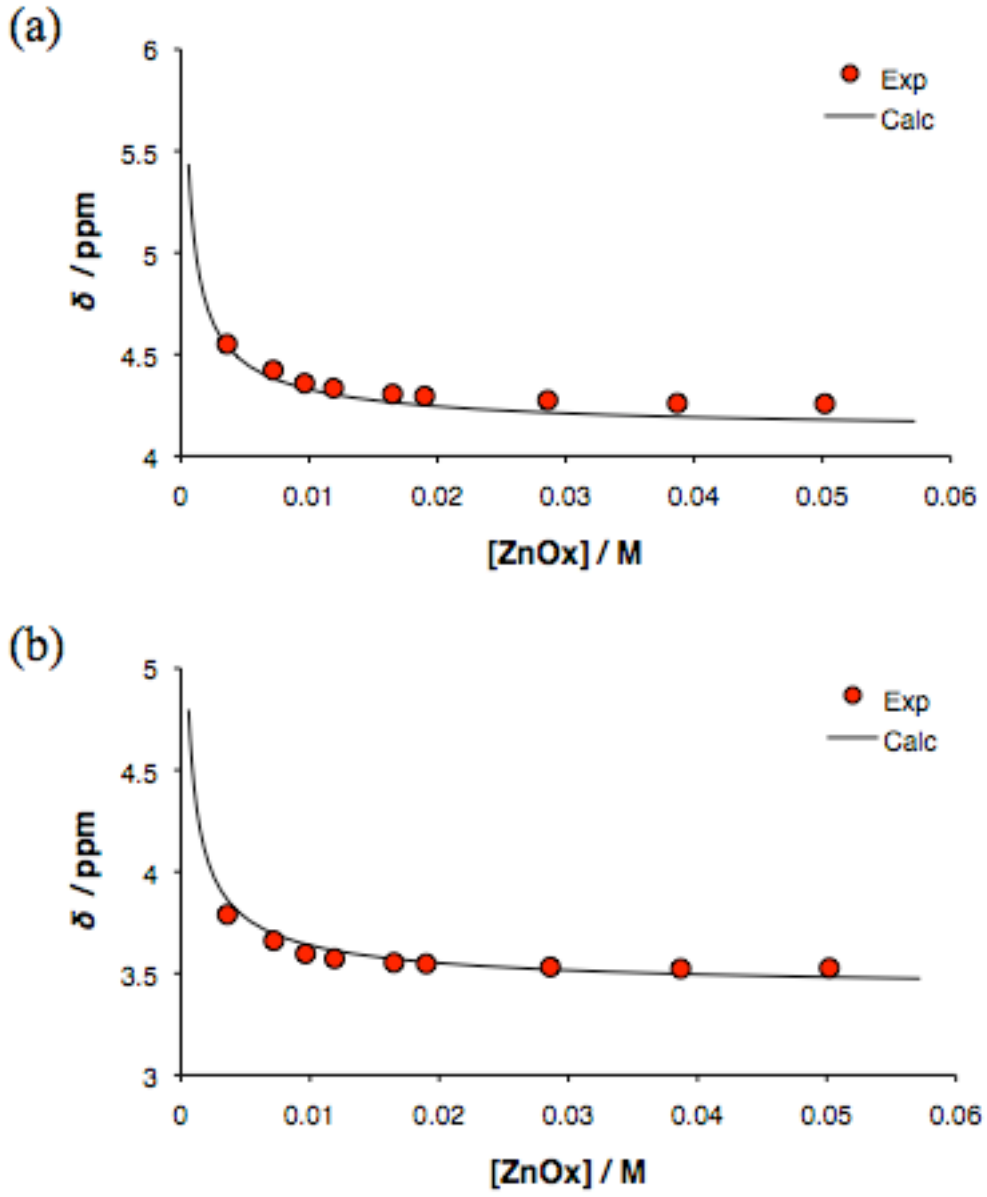

Figure 3-7. ^{1}H-NMR chemical shift changes of the **ZnOx** protons as a function of concentration at the position of (a) Ox-a and (b) Ox-b in $CDCl_3$ at 298 K.

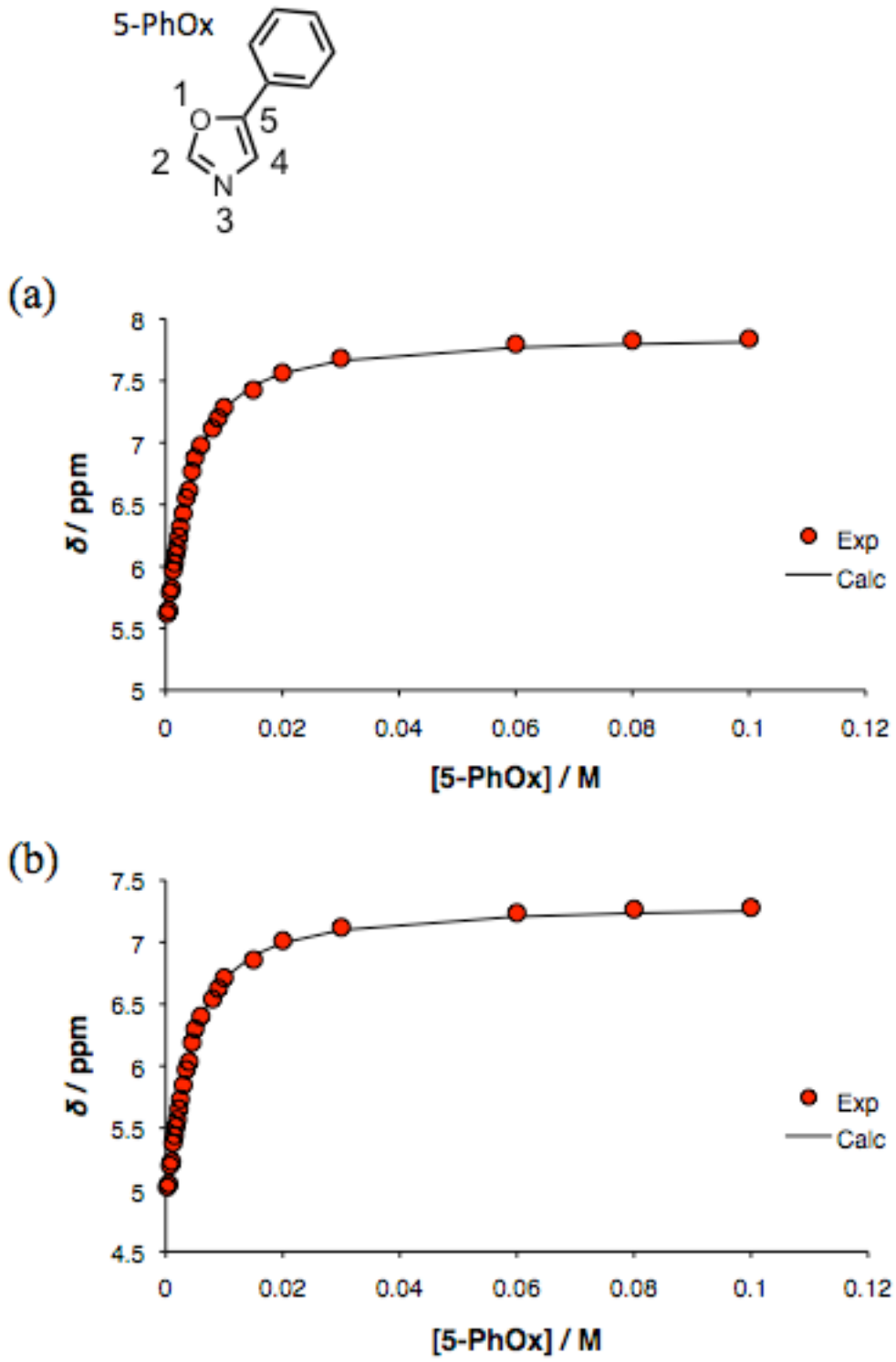

Figure 3-8. Titration of zinc methyl pyropheophorbide-*a* (ZnMPPa) (1.7 mM) with 5-phenyloxazole (5-PhOx) as the ligand in $CDCl_3$ at 298 K. The chemical shift changes of the 5-phenyloxazole protons at the position of (a) 2 and (b) 4 are plotted.

fit the concentration dependence of ^{1}H-NMR chemical shifts of **ZnOx** (Figure 3-7) using this value of K_i, if we assumed the formation of the linear oligomers and polymers only. We then have to conclude that the cyclic oligomers are formed.

The diffusion constant D of the zinc complex **ZnOx** was obtained with the ^{1}H-NMR diffusion-ordered spectroscopy (DOSY) (Figure 3-9). The value of D (6.01 (±0.4)×10^{-10} m^2 s^{-1}) for **ZnOx** at 1 mM was comparable with that of **FbOx** (30 mM, D = 6.42 (±0.02)×10^{-10} m^2 s^{-1}). The value of D decreased significantly on going from 1 mM to 5 mM and then reached a plateau (5–30 mM), followed by gradual decrease in the more dense region (>30 mM) with overall changes consistent with the change in the chemical shift. The hydrodynamic radiuses r were estimated using the D values by use of the Stokes–Einstein equation (1), where k_B, T, and η are the Boltzmann constant, the temperature, and viscosity of the medium, respectively.[17-19]

$$r = k_B T / 6\pi\eta D \quad (1)$$

The value of r at 1 mM **ZnOx** was 6.7 (±0.5) Å, which is consistent with the size of the monomer as shown in Figure 3-10a. This value, however, is somewhat larger than that (6.3 (±0.02) Å) obtained for the free-base **FbOx**. The results indicate that **ZnOx** molecules begin to form assemblies at 1 mM, which is corroborated by the absorption and fluorescence spectra described above. The values of r at 20 mM and 50 mM of **ZnOx** were 11.2 (±0.1) Å (D = 3.59 (±0.01)×10^{-10} m^2 s^{-1}) and 13.5 (±0.1) Å (D = 2.99 (±0.02)×10^{-10} m^2 s^{-1}), respectively, which were about twice as large as that at 1 mM, which are consistent with the trimer and tetramer models as shown in Figures 3-10b and 3-10c. The cold-spray ionization mass spectrometry (CSI-MS) showed peaks for the trimer as well as weak peaks for the tetramer (Figure 3-11). The vapor pressure osmometry (VPO) measured in a range of 10–30 mM provided the molecular weight corresponding to the trimer (Figure 3-12). Taken together, we concluded that **ZnOx** formed cyclic oligomers, mostly trimers and tetramers, in the range of 5–50 mM. To estimate the fractions of cyclic and linear species, we fitted the NMR data (Figure 3-7), assuming that the cyclic species consists only of trimers for simplicity. We obtained the equilibrium constant $K_{c,3}$ = 28, which signifies the stability of the cyclic species over linear

(a)

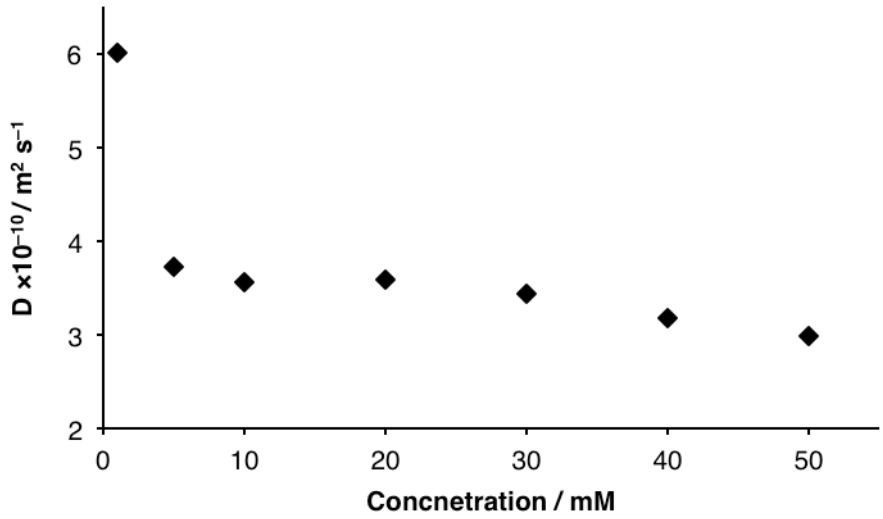

(b)

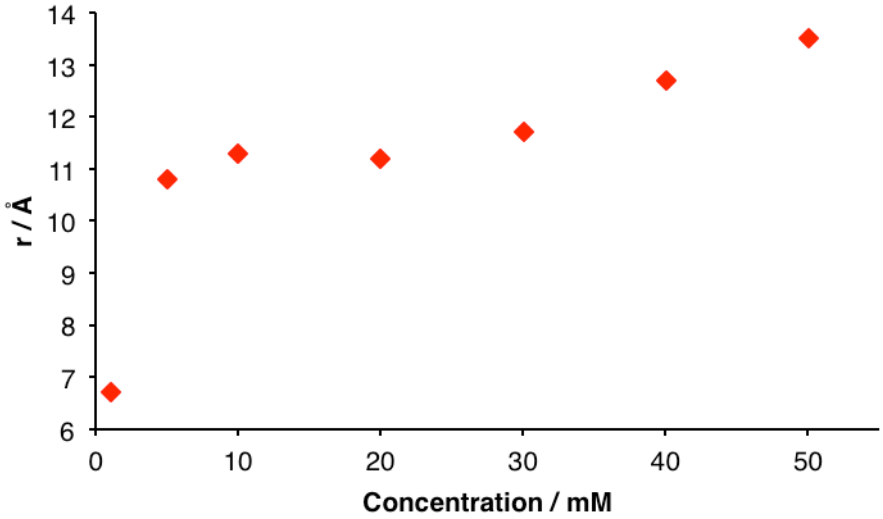

Figure 3-9. Concentration dependence of (a) the diffusion coefficient (*D*) and (b) the hydrodynamic radius (*r*) for **ZnOx** in $CDCl_3$ at 298 K.

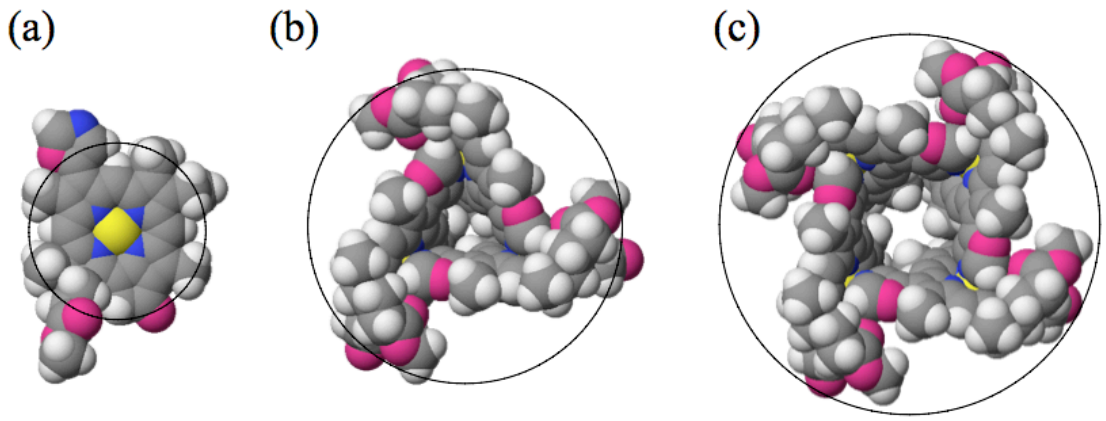

Figure 3-10. Molecular models of (a) monomeric **ZnOx** molecule, (b) cyclic trimer, and (c) cyclic tetramer constructed by MM3 force-field calculation. The circle indicate the calculated hydrodynamic radius on the basis of the diffusion coefficients at 20 mM and 50 mM.

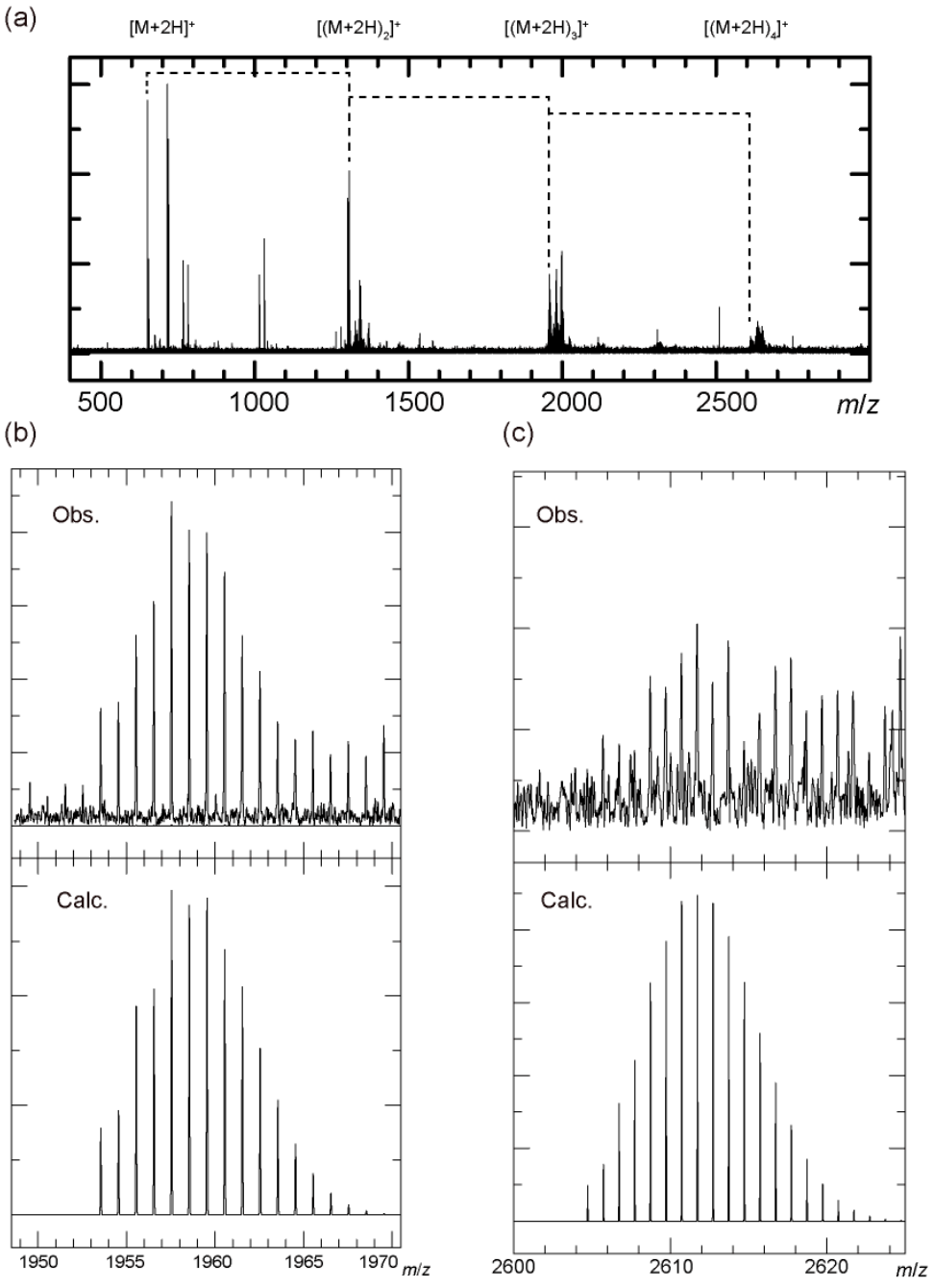

Figure 3-11. CSI-MS Spectra of **ZnOx**. The peaks corresponding to the trimer and tetramer and their simulation isotope pattern are shown in (b) and (c), respectively.

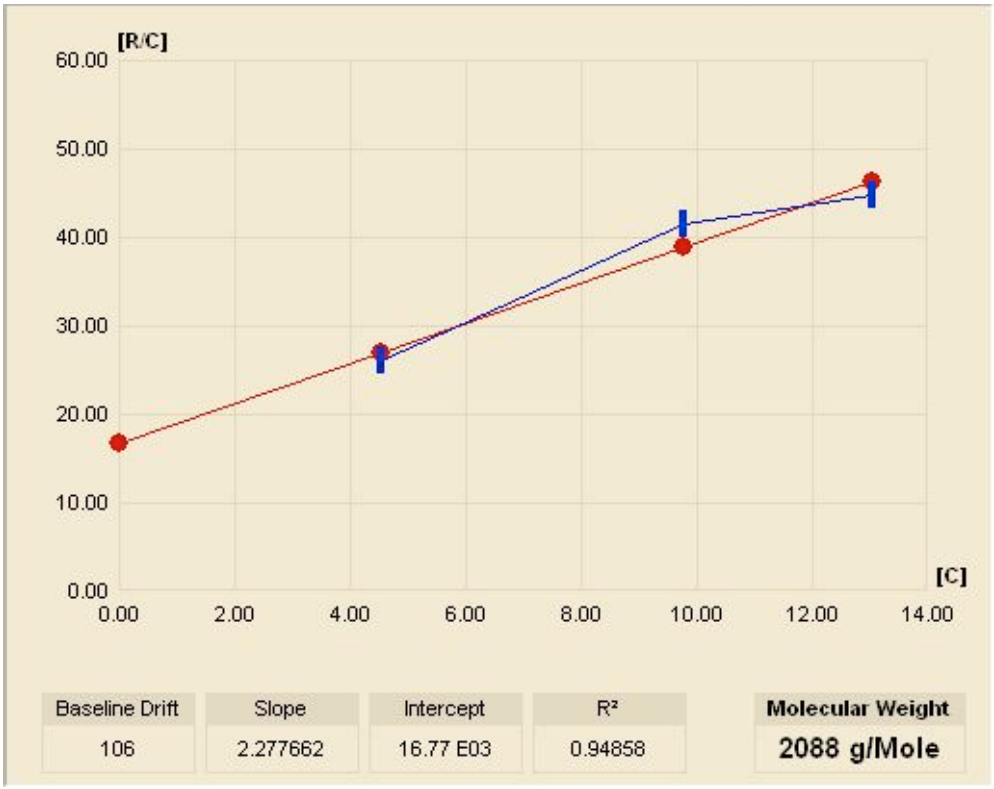

Figure 3-12. Data analysis of VPO measurements for **ZnOx** (MW = 653.08) in $CDCl_3$ at 37 ^oC.

species. The simulation indicated that more than 90% of **ZnOx** are in the cyclic trimer in the range of 5–75 mM. A simulation including the cyclic tetramer also gave similar results.

3-2-3 Self-Assembly in the Crystal

Controlling not only the microscopic arrangement of chlorophyll molecules in the assembly but also the macroscopic morphology of the assembly is important in designing artificial light-harvesting antenna system.[20] Two types of crystals of **ZnOx** with different morphologies were reproducibly obtained using different protocols in which: (i) a chloroform solution of **ZnOx** covered with toluene as an antisolvent was exposed to hexane vapor; and (ii) solvents were slowly evaporated from a solution of **ZnOx** in chloroform and toluene. The flower-shaped crystal aggregates were formed using protocol (i) as shown in Figure 3-13a. The petal-like features extend from the center of the aggregate, where fine crystals disorderly agglomerate. The edge portion of the petal-like feature revealed striped thin layers (Figure 3-13b). On the other hand, the rhombic-shaped crystals as shown in Figure 3-13c were deposited using protocol (ii). The magnified image for the edge region also revealed the layered structures similar to those found in the flower-like aggregate (Figure 3-13d).

The X-ray analysis revealed that these two variants had the same unit cell parameters, indicating that the crystal structures are identical (Figure 3-14). The crystals belong to the space group $P2_12_12_1$. The nitrogen atom of the oxazole moiety in a **ZnOx** molecule coordinates to the zinc atom of another **ZnOx** molecule, giving rise to the staircase-like coordination polymer as shown in Figure 4b. The coordination bond length of N_{Ox}–Zn is 2.16 Å, which is similar to the lengths in a previously reported zinc tetraphenylchlorin–pyridine complex (2.17 Å) and the axially coordinated pyridine-appended zinc chlorophyll derivatives (2.14–2.15 Å).[1,21] The coordination geometry of the zinc atom is a distorted square pyramid. The bond length between the zinc atom and nitrogens N_1, N_3, and N_5 are 2.02, 2.03, and 2.06 Å, respectively, while that between the zinc atom and N_2 is as long as 2.23 Å, which is typical for zinc complexes of chlorin.[22] In general, the bond length to the nitrogen of the reduced pyrrole ring is the longest among the four bonds between the zinc and the pyrrole nitrogens.

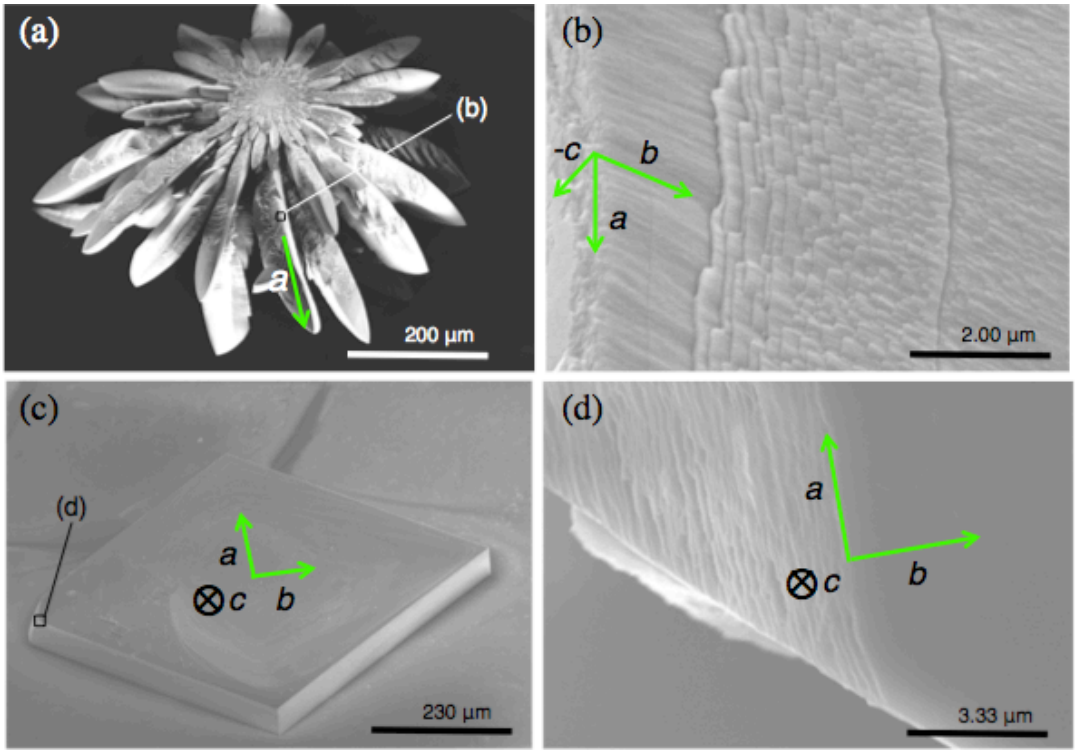

Figure 3-13. FE-SEM images of **ZnOx** crystals. (a) The flower-like crystal aggregates. (b) Magnification of the squared portion in (a). (c) The rhombic crystal. (d) Magnification of the portion indicated in (c). The green arrows represent the direction of the crystallographic axes.

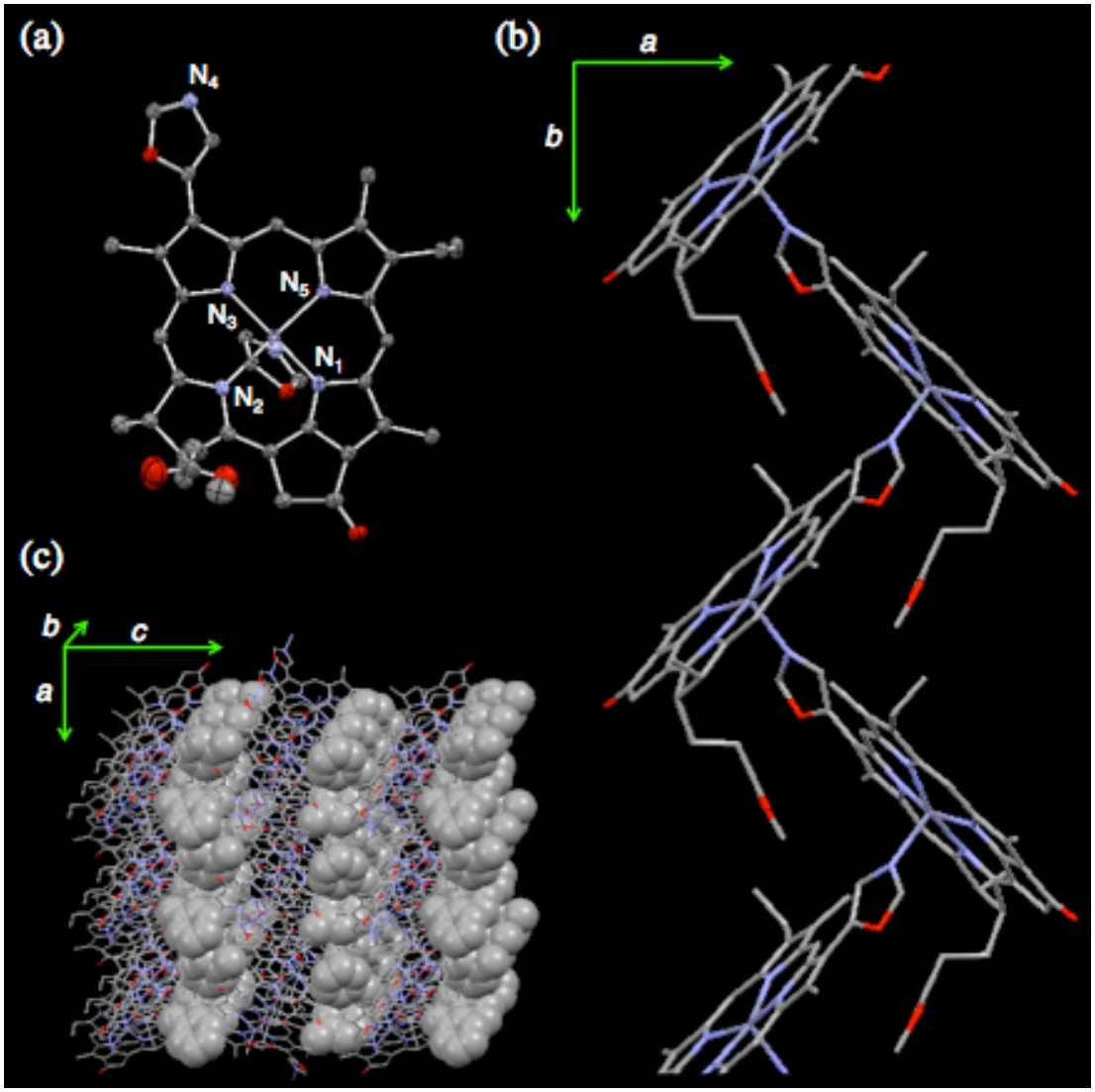

Figure 3-14. Crystal structure of **ZnOx** coordination polymer. The hydrogen atoms are omitted for clarity. (a) ORTEP representation of **ZnOx** molecule coordinated by the oxazole moiety. Thermal ellipsoids represent 50% probability. (b) View along the *c*-axis. (c) Layered structure consisting of **ZnOx** coordination polymers and toluene molecules. Toluene molecules are shown by space-filling model.

Table 3-1. Crystallographic data for **ZnOx**

Compound	**ZnOx**
Empirical formula	$C_{35}H_{33}N_5O_4Zn$ (toluene)$_1$
Formula weight	745.17
Color, Habit	Blue, prism
Crystal system	Orthorhombic
Space group	P 2_1 2_1 2_1
Unit cell dimensions / Å	a = 10.330(3)
	b = 13.652(4)
	c = 24.842(6)
Volume / Å^3	3501.9(17)
Z	4
Density (calc) / g cm^{-3}	1.413
Absorption coefficient / mm^{-1}	0.753
F(000)	1560
Crystal size / mm^3	0.35×0.20×0.08
θ for data collection	3.0 to 27.50
Index ranges	$-13 \le h \le 13$, $-17 \le k \le 17$, $-26 \le l \le 32$
Reflections collected	27184
Independent reflections	7968
Completeness	99.8% (θ = 27.42°)
Absorption correction	Numerical
Max. and min. transmission	0.9422 and 0.7784
Refinement method	Full-matrix least-squares on F^2
Data/restraints/parameters	7968/0/469
Goodness-of-fit on F^2	1.080
Final R indices [$I>2\sigma(I)$]	R_1 = 0.0532

The displacement of zinc atom from the $N_1N_2N_3N_4$ mean plane is 0.31 Å. The polymers and the clathrated toluene molecules independently make layers in parallel with the crystallographic *ab* plane, resulting in the layered structure. Each **ZnOx** layer consists of the coordination polymers extending along the *b*-axis. Notably, the staircase-like coordination polymer of a zinc chlorophyll derivative mediated by the intermolecular N–Zn coordination bond has not been reported previously, although similar coordination polymers of zinc porphyrin derivatives have been reported. To date, only a few crystal structures of zinc chlorophyll-based coordination polymer have been reported besides our previous report including the coordination polymers reported by the Knapp group and the Tamiaki group as mentioned in Chapter 2.[23,24]

The relationship between the morphology of the **ZnOx** crystals and the crystallographic axes are shown in Figure 3-13. The *a*-axis of the unit cell corresponds to the long axis of the petal-like feature while the *b*- and *c*-axes correspond to the shorter axes. In the rhombic crystal, the crystallographic axes *a*-, *b*-, and *c*-axes correspond to the short diagonal, long diagonal, and height of the rhombic prism, respectively (Figure 3-13c). Lamellar structures observed in edge regions of crystal turned out to be in parallel with the *ab* plane which is in parallel with the layers consisting of the **ZnOx** polymers and those consisting of toluene molecules in the crystal structure, resulting in the easy cleavage plane.

3-3 Conclusion

We herein elucidated the self-assembled structures of the novel oxazole-appended zinc chlorophyll complex **ZnOx** in solution and in the crystal. **ZnOx** forms the cyclic oligomers in chloroform, whereas it forms the staircase-like coordination polymers in the crystal. Given the fact that the zinc chlorophyll derivative appended by vinyl pyridine **ZnPy** formed the coordination polymers with a double-helical motif as shown in Chapter 2, the higher-order structures of the coordination polymers are sensitive to the structure of the *N*-heterocyclic moiety in the zinc chlorophyll components. This indicates that we can tune the higher-order structures of the coordination polymer by altering the coordination site as well as its

orientations in the chlorophyll molecules. Since the orientations among the chromophores in light-harvesting arrays are a crucial factor for the energy transfer as demonstrated in Chapter 2,[25-27] the control of the orientation is an all-important issue for design of the light-harvesting antenna models. We demonstrate the "control" of the higher-order structures of the polymers in Chapter 4.

3-4 Experiment

3-4-1 General

All reactions were conducted under argon atmosphere. Chloroform and tetrahydrofran were distilled over NaH and benzophenone ketyl, respectively. Other reagents and solvents for preparation of compounds were used as purchased without further purification.

Spectroscopic grade chloroform was purchased from Wako. $CDCl_3$ and pyridine-d_5 were purchased from Sigma-Aldrich. ^1H NMR and DOSY spectra were recorded with a 400 MHz JEOL ECX 400 spectrometer, and chemical shifts were reported in ppm relative to internal tetramethylsilane. The peaks were assigned using COSY, NOESY, HMQC, HMBC, and DEPT. Mass spectrometry analysis was performed with an Agilent G1969A mass spectrometer using the APCI ionization method in the positive mode. HPLC was performed with a Shimadzu HPLC 20A apparatuses using a solvent system consisting of H_2O and MeOH, and the flow rates were 1.0 and 10.0 mL/min for analysis and preparation, respectively. UV-vis spectra and fluorescence spectra were obtained using a Shimadzu UV-2400PC spectrometer and JASCO FP-8600 fluorometer, respectively. Cold-spray ionization mass spectrometry (CSI-MS) measurement was performed using a Fourier transform ion cyclotron resonance mass spectrometer (FT-ICR MS; Apex-Qe 9.4 T, Bruker Daltonics, Inc. Billerica, MA, USA). The heater of the desolvation assembly was turned off to keep room temperature around the spray chamber in the ionization process and the temperature of nebulizer gas N_2 was set at 35 °C. General measurement conditions were as follows: positive mode; capillary voltage, 4.5 kV; dry gas flow rate, 5.0 L/min; nebulizer gas flow rate, 1.5 L/min; and sample flow rate, 120 mL/h. The **ZnOx** solution (0.1 mg/mL, $CHCl_3/CH_3OH$ = 4/1, v/v) was injected

into CSI-MS. Vapor pressure osmometry (VPO) was measured using a Gonotec Osmomat 070 osmometer. The calibration curve was made using benzil as the standard in $CHCl_3$ at 37 ℃. The molecular models were obtained with MM2 and MM3 for the monomeric model and the cyclic oligomeric model, respectively, using CAChe software (version 6.1.12.33). The single crystal diffraction analysis data were collected at 93 K with a Rigaku VariMax Dual with Saturn diffractometer using Mo Kα radiation (0.71075 Å). All structural solutions were performed with the crystallographic software package SHELX-97.[28]

3-4-2 Syntheses

FbOx. To a solution of methyl pyropheophorbide-*d* (203 mg, 0.37 mmol) in MeOH (100 mL) K_2CO_3 (154 mg, mmol), and TosMIC (111 mg, 0.57 mmol) were added in portion, and the resulting mixture was refluxed for 3 h under Ar. The reaction mixture was cooled to r.t., then was poured into $CHCl_3$ (100 mL) and was washed with brine (100 mL × 3). The organic layer was dried with Na_2SO_4 and was evaporated to give a brown solid (283 mg). The crude mixture was purified with column chromatography (silica, 3% acetone in $CHCl_3$) to afford a purple solid (155 mg, 0.26 mmol, 70%).

^{1}H NMR ($CDCl_3$, 298 K): δ = 9.67 (s, 1H, meso), 9.57 (s, 1H, meso), 8.70 (s, 2H, 20-H), 8.47 (s, 1H, Ox-a), 7.97 (s, 1H, Ox-b), 5.31 (d, J = 19.3 Hz, 1H, 13^2), 5.16 (d, J = 19.3 Hz, 1H, 13^2), 4.55 (m, 1H, 18-H), 4.35 (m, 1H, 17-H), 3.71 (quartet, J = 7.3 Hz, 2H, 8-$\underline{CH_2}CH_3$), 3.70, 3.62, 3.53, 3.25 (s, each 3H, ring CH_3 × 3, 17^2-$COOCH_3$), 2.72, 2.59, 2.32 (m, 1H, 1H, 2H, 17-CH_2CH_2), 1.84 (d, J = 7.3 Hz, 3H, 18-CH_3), 1.71 (t, J = 7.3 Hz, 3H, 8-$CH_2\underline{CH_3}$), 0.20 (bs, 1H, NH), and -1.83 (bs, 1H, NH) ppm; HRMS: m/z = 590.2734 $[M+H]^+$ (100%), calcd for $C_{35}H_{36}N_5O_3$ 590.2767; HPLC (octadecylsilyl, MeOH/H_2O = 17/3, isocratic): t_R = 16.6 min.

ZnOx. To a solution of **FbOx** (150 mg, 0.25 mmol) in $CHCl_3$ (150 mL) saturated solution of $Zn(OAc)_2 \cdot 2H_2O$ (15 mL) was added. After stirring for 3 h under Ar, 4% $NaHCO_3$ (100 mL) was added into the mixture and was stirred for 10 min. The organic layer was separated, and was washed with brine (100 mL × 3). The organic layer was dried with Na_2SO_4 and was evaporated to give a green-blue solid (180 mg). The crude mixture was purified with column

chromatography (silica, 3% acetone in $CHCl_3$) to afford a green-blue solid (160 mg, 0.25 mmol, 97%).

^{1}H NMR ($CDCl_3$, 298 K): δ = 9.67 (s, 1H, 10-H), 8.33 (s, 1H, 20-H), 8.20 (bs, 1H, 5-H), 5.14 (d, J = 20.2 Hz, 1H, 13^2), 5.02 (d, J = 20.2 Hz, 1H, 13^2), 4.45 (m, 1H, 18-H), 4.39 (bs, 1H, Ox-a), 4.25 (m, 1H, 17-H), 3.81 (quartet, J = 7.3 Hz, 2H, 8-$\underline{CH_2}CH_3$), 3.70, 3.30, 2.96, 2.70 (s, each 3H, ring CH_3 × 3, 17^2-$COOCH_3$), 3.62 (bs, 1H, Ox-b), 2.61, 2.46, 2.28, 2.10 (m, each 1H, 17-CH_2CH_2), and 1.75 (m, 6H, 18-CH_3, 8-$CH_2\underline{CH_3}$) ppm; HRMS: m/z = 652.1910 $[M+H]^+$ (100%), calcd for $C_{35}H_{34}N_5O_3Zn$ 652.1902; HPLC (octadecylsilyl, MeOH/H_2O = 8/2, isocratic) t_R = 13.0 min.

3-4-3 Curve Fitting

The curve fitting was based on a model developed by Ercolani *et al.*[29-31]

$$\begin{array}{ccccccc} M & \overset{M}{\rightleftarrows} & M_2 & \overset{M}{\rightleftarrows} & M_3 & \overset{M}{\rightleftarrows} & M_4 \overset{M}{\rightleftarrows} \ldots \\ & & \downarrow\uparrow & & & & \\ & & C_3 & & & & \end{array} \qquad \begin{cases} K_i = [M_n]/([M_{n-1}][M]) \\ K_{c,3} = [C_3]/[M_3] \end{cases}$$

Where M_n are linear polymers and C_3 is the cyclic trimer. The equilibrium constant K_i and $K_{C,3}$ are defined as above. K_i is assumed to be identical for all n. The model includes linear polymers with n up to infinity but only the trimer as the cyclic species for simplicity. The equation to solve is

$$[M]_T = \frac{1}{K_i}\frac{x}{(1-x^2)} + 3\frac{K_{c,3}}{K_i}x^3 \text{, where } x = K_i[M]$$

where $[M]_T$ is the total (initial) concentration of the monomer unit.

3-5 References

(1) Shinozaki, Y.; Richards, G.; Ogawa, K.; Yamano, A.; Ohara, K.; Yamaguchi, K.; Kawano, S.-i.; Tanaka, K.; Araki, Y.; Wada, T.; Otsuki, J. *J. Am. Chem. Soc.* **2013**, *135*, 5262.

(2) Kelley, R. F.; Goldsmith, R. H.; Wasielewski, M. R. *J. Am. Chem. Soc.* **2007**, *129*, 6384.

(3) Jensen, R. A.; Kelley, R. F.; Lee, S. J.; Wasielewski, M. R.; Hupp, J. T.; Tiede, D. M. *Chem. Commun.* **2008**, 1886.

(4) Gunderson, V. L.; Wasielewski, M. R. *Chem. Phys. Lett.* **2013**.

(5) Gunderson, V. L.; Smeigh, A. L.; Kim, C. H.; Co, D. T.; Wasielewski, M. R. *J. Am. Chem. Soc.* **2012**, *134*, 4363.

(6) Tamiaki, H.; Holzwarth, A. R.; Schaffner, K. *J. Photochem. Photobiol. B: Biol.* **1992**, *15*, 355.

(7) Sengupta, S.; Würthner, F. *Acc. Chem. Res.* **2013**, *46*, 2498.

(8) Sengupta, S.; Würthner, F. *Chem. Commun.* **2012**, *48*, 5730.

(9) Sengupta, S.; Ebeling, D.; Patwardhan, S.; Zhang, X.; von Berlepsch, H.; Böttcher, C.; Stepanenko, V.; Uemura, S.; Hentschel, C.; Fuchs, H.; Grozema, F. C.; Siebbeles, L. D. A.; Holzwarth, A. R.; Chi, L.; Würthner, F. *Angew. Chem. Int. Ed.* **2012**, *51*, 6378.

(10) Smith, K. M.; Goff, D. A.; Simpson, D. J. *J. Am. Chem. Soc.* **1985**, *107*, 4946.

(11) Tamiaki, H.; Miyata, S.; Kureishi, Y.; Tanikag, R. *Tetrahedron* **1996**, *52*, 12421.

(12) Weitman, M.; Lerman, L.; Cohen, S.; Nudelman, A.; Major, D. T.; Gottlieb, H. E. *Tetrahedron* **2010**, *66*, 1465.

(13) Sisko, J.; Kassick, A. J.; Mellinger, M.; Filan, J. J.; Allen, A.; Olsen, M. A. *J. Org. Chem.* **2000**, *65*, 1516.

(14) Sasaki, S.-i.; Mizutani, K.; Kunieda, M.; Tamiaki, H. *Tetrahydron* **2011**, *67*, 6065.

(15) Sasaki, S.-i.; Takebe, H.; Mizoguchi, T.; Tamiaki, H. *Tetrahedron Lett.* **2005**, *46*, 7687.

(16) Tamiaki, H.; Yagai, S.; Miyatake, T. *Bioorg. Med. Chem.* **1998**, *6*, 2171.

(17) Oliva, A. I.; Gómez, K.; Gonzáleza, G.; Ballester, P. *New J. Chem.* **2008**, *32*, 2159.

(18) Sprafke, J. K.; Odell, B.; Claridge, T. D. W.; Anderson, H. L. *Angew. Chem. Int. Ed.* **2011**, *50*, 5572.

(19) Ohkawa, H.; Takayama, A.; Nakajima, S.; Nishide, H. *Org. Lett.* **2006**, *8*, 2225.

(20) Medforth, C. J.; Wang, Z.; Martin, K. E.; Song, Y.; Jacobsen, J. L.; Shelnutt, J. A. *Chem. Commun.* **2009**, 7261.

(21) Spaulding, L. D.; Andrews, L. C.; Williams, G. J. B. *J. Am. Chem. Soc.* **1977**, *99*, 6918.

(22) Taniguchi, M.; Mass, O.; Boyle, P. D.; Tang, Q.; Diers, J. R.; Bocian, D. F.; Holten, D.; Lindsey, J. S. *J. Mol. Struct.* **2010**, *979*, 27.

(23) Knapp, S.; Huang, B.; Emge, T. J.; Sheng, S.; Krogh-Jespersen, K.; Potenza, J. A.; Schugar, H. J. *J. Am. Chem. Soc.* **1999**, *121*, 7977.

(24) Jesorka, A.; Holzwarth, A. R.; Eichhöfer, A.; Reddy, C. M.; Kinoshita, Y.; Tamiaki, H.; Katterle, M.; Naubrond, J.-V.; Balaban, T. S. *Photochem. Photobiol. Sci.* **2012**, *11*, 1069.

(25) Wu, P. G.; Brand, L. *Anal. Biochem.* **1994**, *218*, 1.

(26) Dale, R. E.; Eisinger, J.; Blumberg, W. E. *Biophys. J* **1979**, *26*, 161.

(27) Förster, T. *J. Biomed. Opt.* **2012**, *17*, 011002.

(28) Sheldrick, G. M. *Acta Cryst.* **2008**, *A64*, 112.

(29) Ercolani, G. *J. Phys. Chem. B* **1998**, *102*, 5699.

(30) Ercolani, G.; Ioele, M.; Monti, D. *New. J. Chem.* **2001**, *25*, 783.

(31) Ercolani, G.; Mandolini, L.; Mencarelli, P.; Roelens, S. *J. Am. Chem. Soc.* **1993**, *115*, 3901.

Chapter 4

Control of Higher-Order Structures of Zinc Chlorophyll Coordination Polymers

4-0 Summary

In this chapter, we describe the control of the higher-order structures of supramolecular coordination polymers of zinc chlorophyll derivatives by rational design of molecular structure; positional isomers differing in the location of the coordination site leads to staircase-like or helical structures as revealed by X-ray crystallography.

4-1 Introduction

Artificial light-harvesting antennae have been constructed to mimic the function of light-harvesting antennae and for the models to understand natural light-harvesting mechanism.[1-3] The models should consist of higher-order assemblies of a number of pigment molecules like porphyrins and chlorophylls.[4-6] One of the major strategies to construct such assemblies is to use intermolecular coordination interactions (1-2).[7,8]

We demonstrated the self-assembly of a zinc chlorophyll derivative **ZnPy** with a vinylpyridine moiety *via* intermolecular axial coordination of the nitrogen atom in the vinylpyridine moiety to the zinc center in another chlorophyll molecule in Chapter 2.[9] **ZnPy** formed the coordination polymers with a double-helical motif. It was suggested that the double-helical motif provides an efficient conduit for Förster-type energy transfer, which is sensitive to the interchromophore orientation and distance.[10] Therefore, tuning higher-order structure of the zinc chlorophyll coordination polymer merits special attention for searching for motifs that enable more efficient light harvesting. We thus altered the coordination moiety in the structure of zinc chlorophyll to explore the roots of the helical induction of the coordination polymers. The zinc chlorophyll derivative **ZnOx** appended by oxazole as a coordination moiety formed the staircase-like coordination polymer as shown in Chapter 3.[11] This result indicates that the structure of the coordination moiety in the zinc chlorophyll molecule is one of the determinant factors of the higher-order structures of the coordination polymers. Herein, we describe the control of higher-order structures employing two zinc chlorophyll derivatives **Zn3Py** and **Zn4Py** appended by phenylpyridine through the ethynyl linker (Chart 4-1). We have designed

these compounds differing only in the position of the coordinatable nitrogen atom anticipating that altering the angle made between the chlorophyll plane and the axis of the ligand would have a consequence in the higher-order structure.

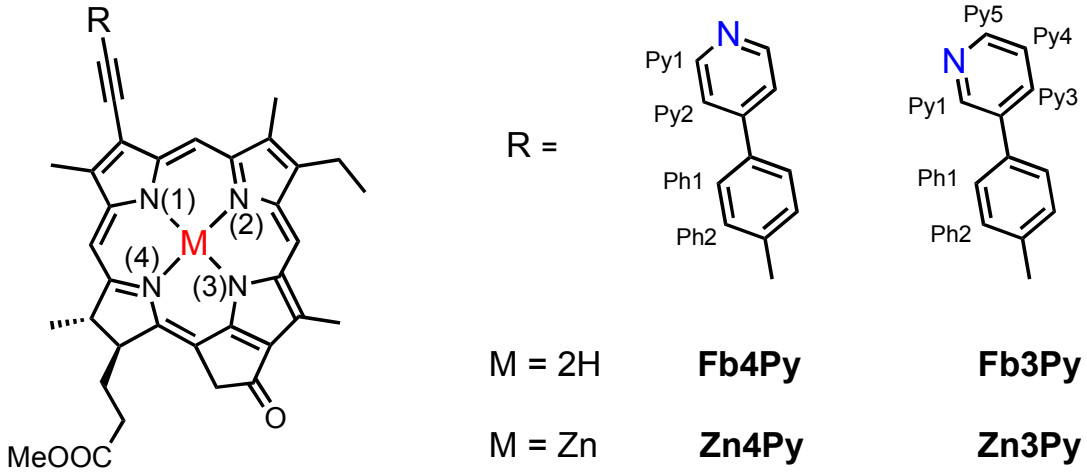

Chart 4-1. Chemical structures of the zinc chlorophyll derivatives **Zn3Py** and **Zn4Py** appended by phenylpyridine.

4-2 Results and Discussion

4-2-1 Syntheses

The synthetic routes of the zinc chlorophyll derivatives **Zn3Py** and **Zn4Py** appended by phenylpyridine are shown in Scheme 4-1. Methyl pyropheophorbide-*d* was synthesized from methyl pyropheophorbide-*a* following the procedure shown in Chapters 2 and 3.[12,13] The ethynylation of the formyl group at the position 3 in the methyl pyropheophorbide-*d* was performed by the Seyferth–Gilbert Homologation reaction using the Bestmann–Ohira reagent,[14,15] which was prepared from chloroacetone through three steps following reported procedures.[16] Although the homologation was smoothly proceeded, the ethynyl chlorophyll derivative was difficult to be isolated due the residual methyl pyropheophorbide-*d*. As the step following the homologation should not be interfered by the presence of methyl pyropheophorbide-*d*, we used the mixture to the next step. The Sonogashira coupling reactions of the ethynyl chlorophyll derivative with 3-

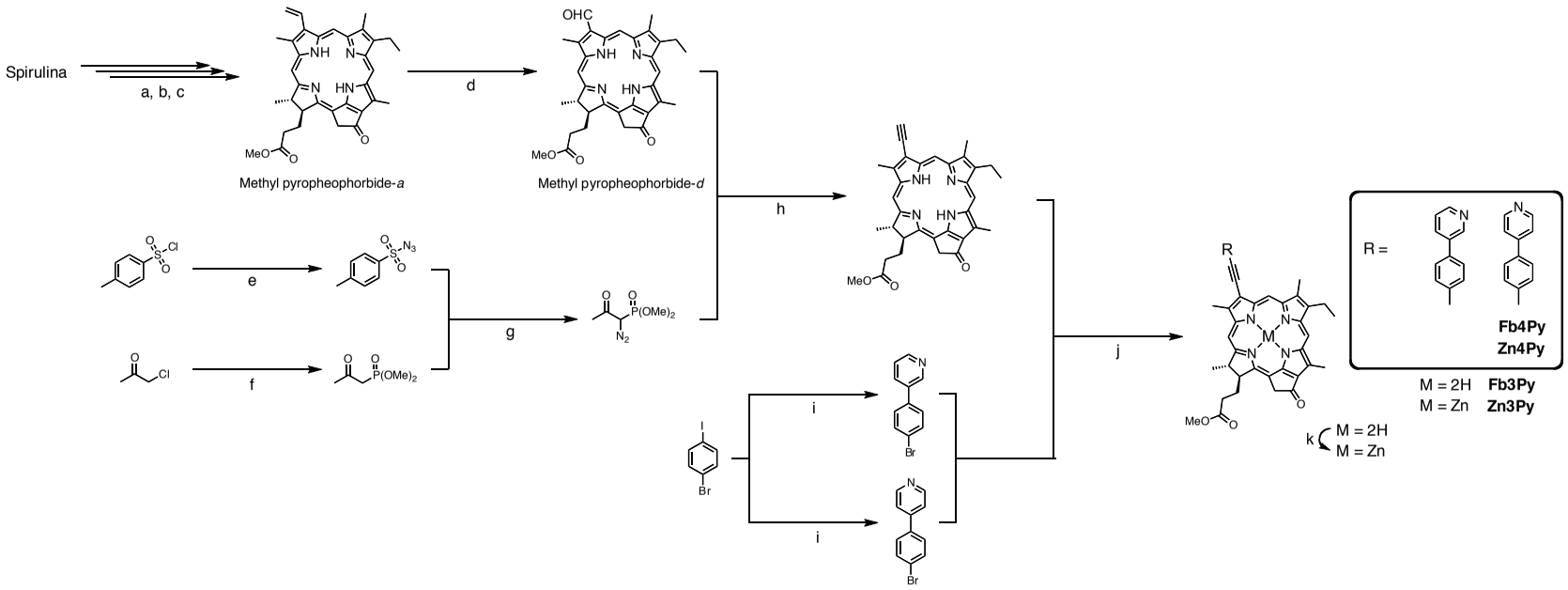

Scheme 4-1. Synthetic procedures of the zinc complexes **Zn3Py** and **Zn4Py**. a) acetone, reflux. b) H_2SO_4, MeOH, overnight. c) collidine, reflux. d) OsO_4, $NaIO_4$, AcOH, THF, H_2O, overnight. e) NaN_3, acetone, 2 h f) KI, CH_3CN, acetone, $P(OMe)_3$, 22 h. g) K_2CO_3, CH_3CN, 6 h. h) $CsCO_3$, THF, MeOH, 3 h. i) Pyridine boronic acid Na_2CO_3, $Pd(PPh)_3$, H_2O, EtOH, toluene, reflux, overnight. j) $Pd_2(dba)_3$, P(*o*-tolyl)$_3$, Et_3N, toluene, reflux, 24 h. k) $Zn(OAc)_2 \cdot 2H_2O$, MeOH, $CHCl_3$, 3 h.

and 4-(4-bromophenyl)pyridine, which was prepared by the selective Suzuki coupling of pyridine boronic acid with *p*-bromoiodobenzene,[17] were performed in the copper-free condition since the copper can be coordinated into the center of the chlorophyll ring to give free-base derivative **Fb3Py** and **Fb4Py** appended by phenylpyridine at the position 3 in moderate yields (41% for **Fb3Py** and 75% for **Fb4Py**, respectively).[14,15] The residual methyl pyropheophorbide-*d* in the previous step was easily removed by column chromatography. The zinc complexes **Zn3Py** and **Zn4Py** were quantitatively obtained by zinc insertion using $Zn(OAc)_2 \bullet 2H_2O$.[18,19]

4-2-2 Axial Coordination in Solution

^{1}H-NMR spectra for the zinc complex and free-base derivatives **Fb3Py**, **Zn3Py**, **Fb4Py**, and **Zn4Py** in $CDCl_3$ are shown in Figure 4-1. The proton signals were assigned by COSY, NOESY, HMQC, HMBC, and DEPT. The signals for the phenylpyridine group appeared in the aromatic region for the free-base chlorophylls, while the corresponding signals for the zinc complexes appeared in significantly upfield regions. The upfield shifts were particularly large for the signals of the protons adjacent to the nitrogen in the pyridine ring (Py1 in **Zn4Py** and Py1 and Py5 in **Zn3Py**, see Chart 4-1). The magnitude of the upfield shifts became smaller as the distance from the nitrogen in the pyridine ring was longer. This trend indicates the axial coordination of the pyridine moiety to the zinc center in another chlorophyll molecule as mentioned in Chapters 2 and 3.[9,11] Detailed analysis of the self-assembled species was prevented by the poor solubility of the zinc complexes in $CDCl_3$.

4-2-3 Self-Assembly in the Crystal

We obtained a needle-like single crystal of **Zn4Py** deposited from a THF/toluene solution exposed to methanol vapor and a rhombic-shaped single crystal of **Zn3Py** from a THF solution exposed to diethyl ether vapor. The X-ray crystal structure analysis of the crystals clarified the assembled structures of these compounds in the solid state. Disorder

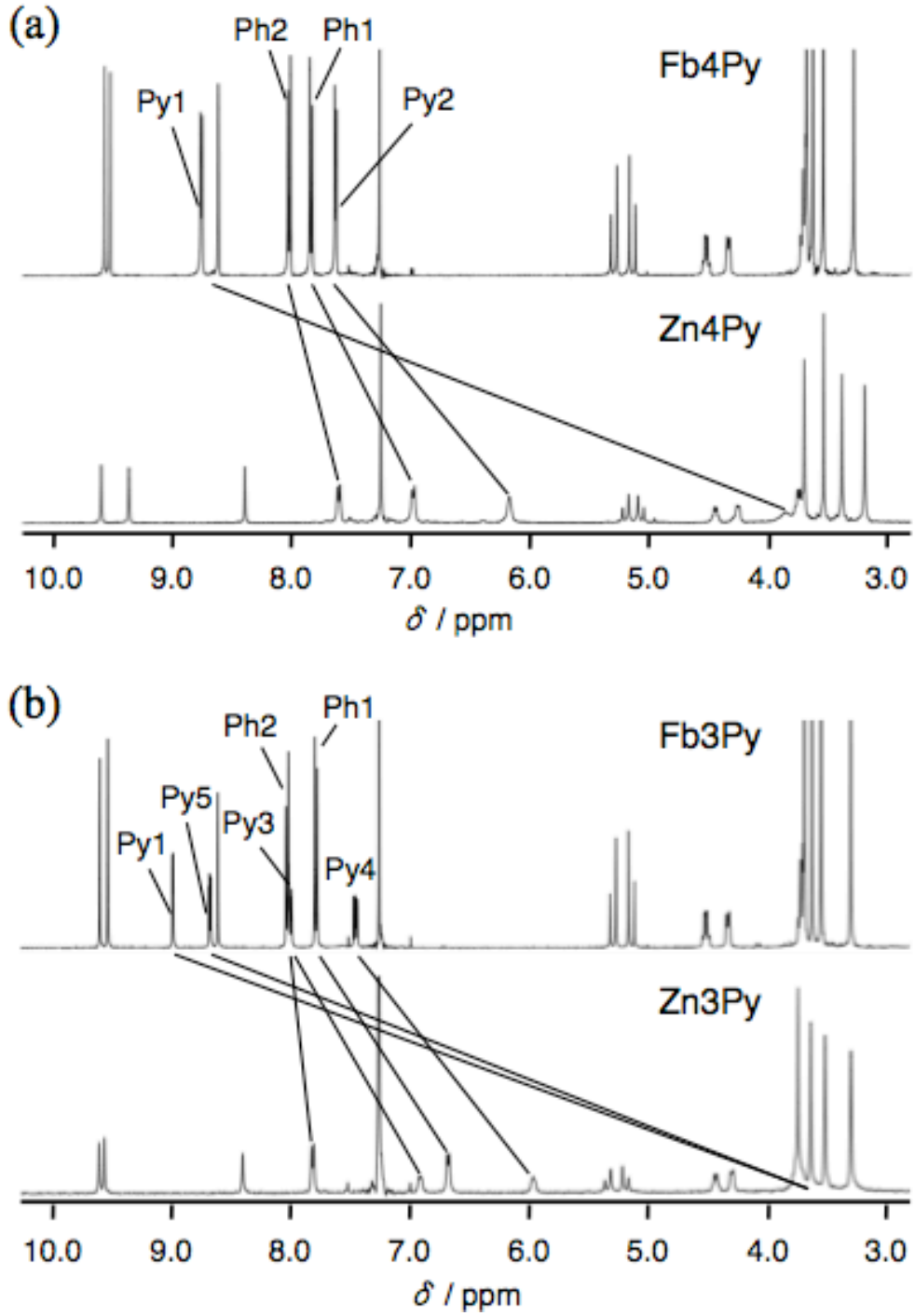

Figure 4-1. ^{1}H-NMR spectra of (a) **Fb4Py** and **Zn4Py**, (b) **Fb3Py** and **Zn3Py** in $CDCl_3$ at 298 K (ca 10 mM for free-base compounds, saturated solution for zinc complexes due to poor solubility). The solid lines indicate the upfield shift upon zinc insertion. See Chart 4-1 for proton labels.

was found in the methyl propionate residue and solvent molecules, part of which might have been lost, resulting in relatively large R values (**Zn4Py**: R_1 = 0.11, wR_2 = 0.24; **Zn3Py**: R_1 = 0.08, wR_2 = 0.20). The quality of the crystals was, nevertheless, sufficient for the present purpose of investigating the assembled structures (Tables 4-1 and 4-2).

Zn4Py molecules crystallized into space group $P2_1$. Wide channels are observed along the *a*-axis, which are probably occupied by solvent molecules, whose positions could not be determined (Figure 4-2). There are two inequivalent molecules in the unit cell, each forming a coordination polymer through the intermolecular axial coordination of the pyridine moiety to the zinc atom in another chlorophyll molecule, as shown in red or blue in Figures 4-2a and 4-2b. The polymer chains form staircase-like structure, as the pyridine group coordinates to the chlorophyll plane nearly perpendicularly. The axial coordination angles between the N_{py}–Zn bond and the chlorophyll N_4 plane are 85° (red) and 87° (blue), respectively. These polymers are antiparallel in the sense that the directions of pyridine→Zn coordination are in the –*b* and +*b* directions for the red and blue polymers, respectively. The chlorophyll molecules in a polymer stack with molecules in the adjacent antiparallel polymers with interplanar separation being ~3.4 Å. It is noted that the pyridyl group coordinates to the zinc ion from the α-face, which is anti to the propionate residue in the chlorophyll, in one polymer (red), while it coordinates from the β-face, which is *syn* to the propionate residue, in the other polymer (blue) as shown in Figure 4-2c.

Zn3Py molecules also crystallized into space group $P2_1$. This crystal also contains disordered solvent molecules. Similar to **Zn4Py**, there are two inequivalent molecules in the unit cell, each forming a coordination polymer through the intermolecular axial coordination. Interestingly, the polymers are helical as shown in red or blue in Figures 4-3a and 4-3b. The axial coordination angles between the N_{py}–Zn bond and the chlorophyll N_4 plane are 88° in both red and blue polymers. One polymer (red) extends in the –*b* direction with the coordination from the β-face (Figure 4-3c), forming a right-handed helix, while the other polymer (blue) extends in the +*b* direction with the

Table 4-1. Crystallographic Data for **Zn3Py**.

Empirical formula	$C_{102}H_{106}N_{10}O_9Zn_2$
Formula weight	1746.70
Color, Habit	Black, Rhombic
Crystal system	Monoclinic
Space group	$P2_1$
Unit cell dimensions / Å	a = 14.904(4) b = 14.159(3) c = 21.949(5)
Z	2
Absorption coefficient / mm^{-1}	0.589
F(000)	1840
Crystal size / mm^3	0.25×0.16×0.13
θ for data collection	3.0 to 27.5
Index ranges	$-17 \le h \le 19$, $-18 \le k \le 18$, $-24 \le l \le 27$
Reflections collected	37583
Independent reflections	19583
Completeness	97.5% (θ = 27.48°)
Absorption correction	Numerical
Refinement method	Full-matrix least-squares on F^2
Flack parameter	0.061(11)
Data/restraints/parameters	19583/341/999
Goodness-of-fit on F^2	1.021
Final R indices [$I>2\sigma(I)$]	R_1 = 0.0787
R indices (all data)	wR_2 = 0.2032
Largest diff. peak and hole / e $Å^{-3}$	1.066 and –0.811

Table 4-1. Crystallographic Data for **Zn4Py**.

Empirical formula	$C_{45}H_{39}N_5O_3Zn$
Formula weight	763.18
Color, Habit	Black, Needle
Crystal system	Monoclinic
Space group	$P2_1$
Unit cell dimensions / Å	a = 10.372(7) b = 22.684(14) c = 18.375(11)
Z	4
Absorption coefficient / mm^{-1}	0.630
F(000)	1592
Crystal size / mm^3	0.34×0.050×0.020
θ for data collection	2.10 to 25.30
Index ranges	$-12 \le h \le 12$, $-27 \le k \le 27$, $-22 \le l \le 21$
Reflections collected	29029
Independent reflections	14538
Completeness	92.4% (θ = 25.26°)
Absorption correction	multi-scan
Refinement method	Full-matrix least-squares on F^2
Flack parameter	0.10(2)
Data/restraints/parameters	14538/333/968
Goodness-of-fit on F^2	1.046
Final R indices [$I>2\sigma(I)$]	R_1 = 0.1136
R indices (all data)	wR_2 = 0.2384
Largest diff. peak and hole / e $Å^{-3}$	0.803 and –0.528

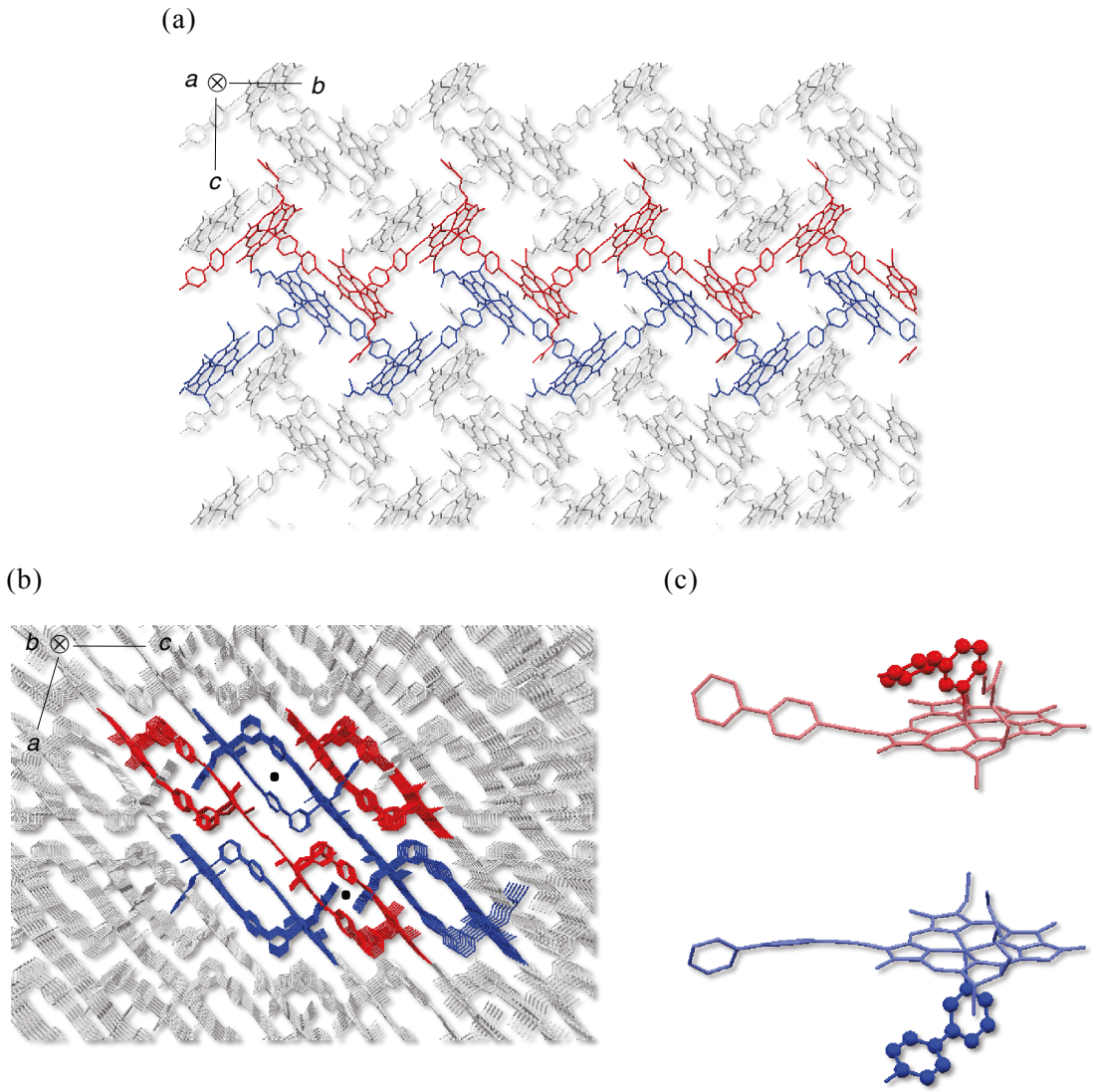

Figure 4-2. Crystal structure of **Zn4Py**. Hydrogen atoms and solvent molecules are omitted for clarity. (a) View along the *a*-axis showing the staircase-like coordination polymers. (b) View along the *b*-axis. (c) Inequivalent **Zn4Py** molecules.

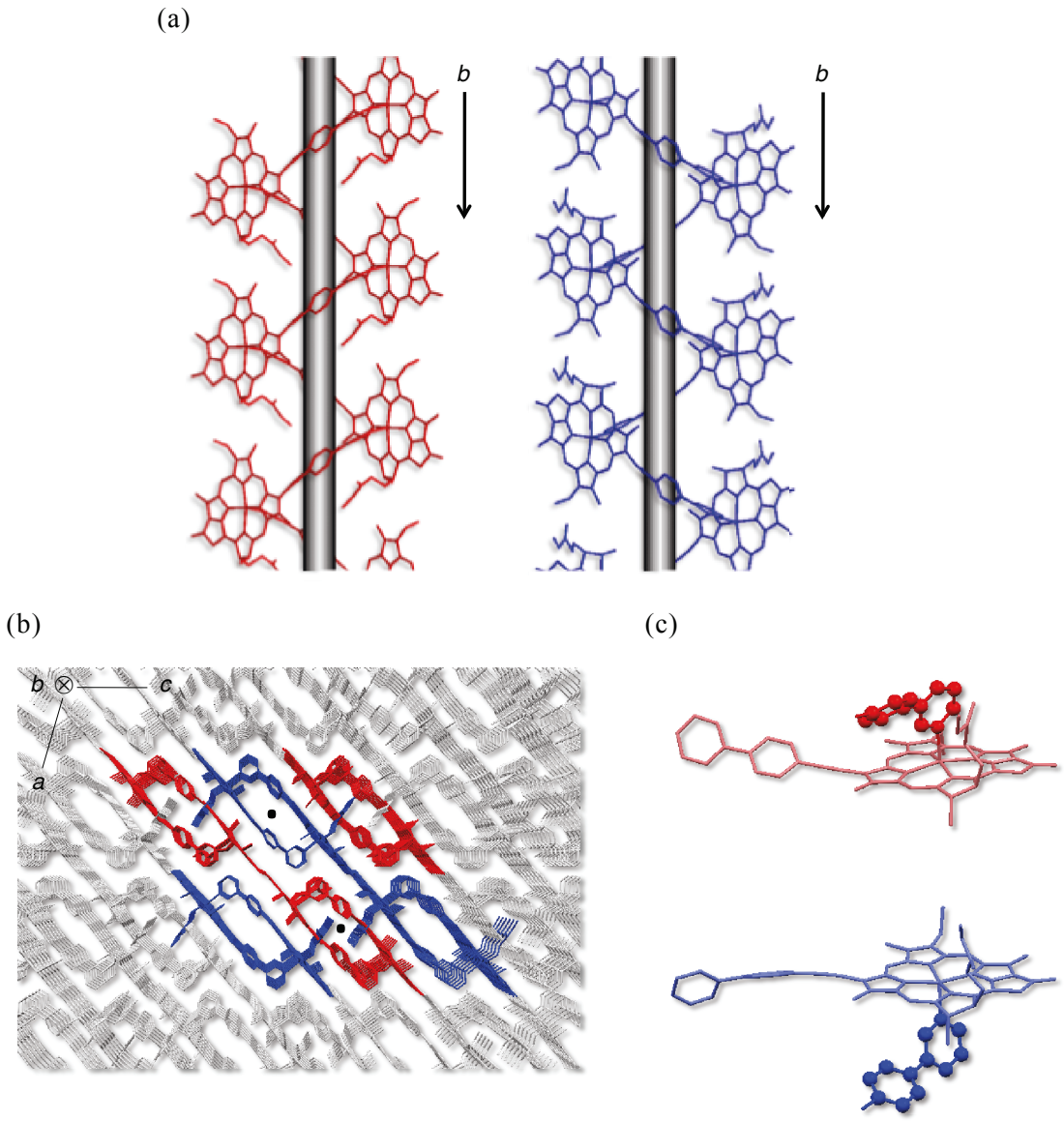

Figure 4-3. Crystal structure of **Zn3Py**. Hydrogen atoms and solvent molecules are omitted for clarity. (a) Views perpendicular to the *b*-axis showing the helical coordination polymers. Red and blue polymers have right and left-handed helicities, respectively. (b) View along the *b*-axis showing the packing of the coordination polymers. (c) Inequivalent **Zn3Py** molecules.

coordination from the α-face forming a left-handed helix. A helical polymer is surrounded by four helical polymers with the opposite helicity, two of them being stacked with the central polymer as shown in Figure 4-3b with an interchlorophyll separation of ~3.3 Å.

The two different motifs of the polymer structure derive from the different molecular structures. The axial coordination angle between the bond N_{py}–Zn and the chlorophyll N_4 plane are almost vertical in both cases: ~86° for the staircase and 88° for the helix, but the intramolecular angles N_{py}–Ct_{py}–$Ct(N_4)$ are respectively ~170° and ~110° due to the different position of the nitrogen atom in the pyridine ring, where Ct indicates centroid. The nearly linear arrangement of N_{py}–Ct_{py}–$Ct(N_4)$ in **Zn4Py** leads to nearly perpendicular interchlorophyll angles (N_4 plane *vs* N_4 plane: 77° for red; 85° for blue), resulting in the staircase-like motif, whereas the bent arrangement of N_{py}–Ct_{py}–$Ct(N_4)$ in **Zn3Py** leads to nearly parallel interchlorophyll angles (3° for red; 6° for blue), resulting in the helical motif.

4-2-4 Potentiality for Light-Harvesting Antenna

The relative efficiency of Förster-type energy transfer within the coordination polymers were estimated by use of the factor $\kappa^2 r^{-6} \times 10^9/Å^{-6}$, which is proportional to the efficiency, where κ^2 and r are the orientation factor and the center-to-center distance between the transition moments, respectively (Figure 4-4).[9,20,21] Nevertheless, we did not take into account the Dexter-type energy transfer because direct orbital overlap between the zinc chlorophyll molecules in the polymers is negligibly small or no due to absence of HOMO orbital density at the zinc center.[22] It was assumed that the $Q_y(0,0)$ transition moment lies at the center of the chlorophyll in the direction of the N(1)–N(3) axis.[23] The values of $\kappa^2 r^{-6} \times 10^9/Å^{-6}$ for the staircase-like polymers of **Zn4Py** are quit small due to the unfavorable, mutually vertical orientation of the transition moments between the neighboring chlorophyll molecules related by coordination (0.7 for red; 2×10^{-3} for blue). The next neighbors are parallel, but the molecules are already far apart (0.03 for red; 0.4

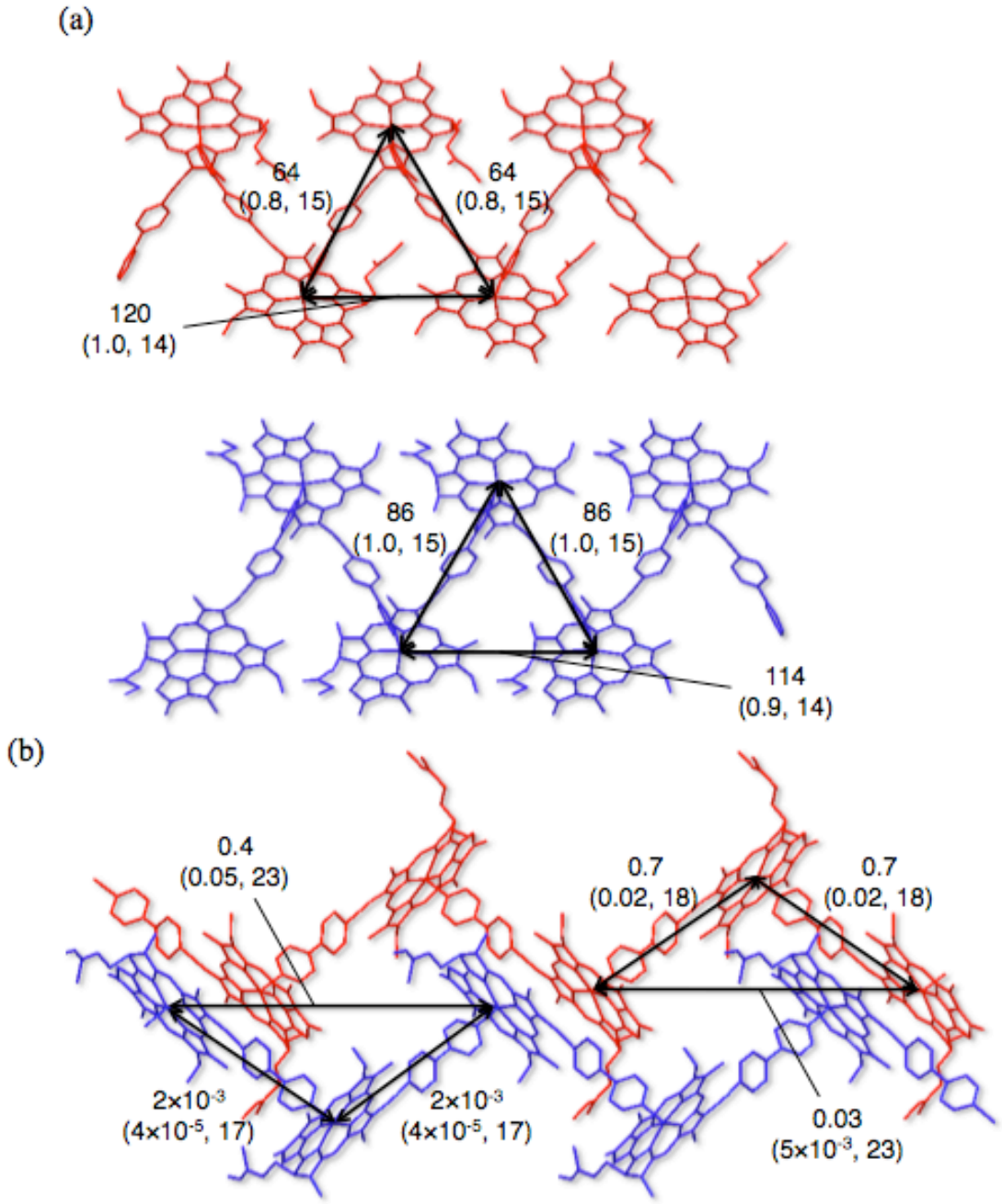

Figure 4-4. Values of ($k^2/r^6 \times 10^9$) (in $Å^{-6}$) as a measure of relative efficiencies of Förster-type energy transfer in the coordination polymers of (a) **Zn3Py** and (b) **Zn4Py**. The arrows represent the pair of donor and acceptor molecules. The orientation factor κ^2 and the distance r (in Å) are shown in parenthesis.

for blue). On the other hand, the helical polymers of **Zn3Py** provide favorable values for the energy transfer. The transition moments in the polymers are either nearly parallel or antiparallel between any chlorophyll pairs (176° between the neighbors and 0° between the next neighbors for red; 167° between the neighbors and 0° between the next neighbors for blue). Furthermore, the intermolecular distances for the helical polymers of **Zn3Py** are smaller (15 Å between the direct neighbors; 14 Å between the next neighbors) than those for the staircase-like **Zn4Py** polymers (18 Å; 23 Å). Therefore, the helical structure is a promising motif as light-harvesting model.

4-3 Conclusion

We have demonstrated that the control of higher-order structures of zinc chlorophyll coordination polymers formed by the intermolecular axial coordination may be possible by rational positioning of the coordination site and consequent alteration of the interchlorophyll angle. We also suggest that helical structures of the coordination polymer can offer favorable arrangement of chlorophyll molecules for light-harvesting applications.

4-4 Experiment

4-4-1 General

All reactions were conducted under argon atmosphere. All reagents and solvents purchased for syntheses were used without further purification. $CDCl_3$ was purchased from Sigma-Aldrich. ^1H NMR spectra were recorded with a 400 MHz JEOL ECX 400 spectrometer, and chemical shifts were reported in ppm relative to internal tetramethylsilane (TMS). The peaks were assigned with the help of COSY, NOESY, HMQC, HMBC, and DEPT. Gel permeation chromatography was performed with Japan Analytical Industry LC-9201 apparatuses equipped with Jaigel-1H and Jaigel-2H columns. High-resolution mass spectrometry analyses were performed with an Agilent G1969A mass spectrometer using positive atmospheric chemical ionization (APCI). The

fluorescence spectra were recorded with a JASCO FP-8600 fluorometer. The single crystal diffraction analysis data were collected at 93 K with a Rigaku VariMax Dual with Saturn diffractometer using Mo Kα radiation (0.71075 Å). The structures were solved by direct method using SIR2004[24] for **Zn3Py** or SIR2011[25] for **Zn4Py**, and refined by the full-matrix least-squares method using SHELXL-97.[26,27] Contributions of disordered solvents on the reflection data were removed by the SQUEEZE command in the program PLATON.[28]

4-4-2 Syntheses

Sonogashira Coupling. To a degassed solution of ethynylchlorophyll (100 mg, 0.186 mmol) and bromophenylpyridine (89 mg, 0.38 mmol) in toluene (60 mL) and Et_3N (12 mL) were added P(*o*-tolyl)$_3$ (66 mg, 0.22 mmol) and $Pd_2(dba)_3$ (26 mg, 0.028 mmol). The mixture was then refluxed for 24 h. After cooling to r.t., the solvent was eliminated in *vacuo* to give a black solid. The crude mixture was purified by column chromatography to afford the product as a brown solid.

Fb3Py: Yield: 41%. ^{1}H-NMR ($CDCl_3$): δ / ppm = 9.60 (s, 1H, meso), 9.54 (s, 1H, meso), 9.00 (d, J = 1.4 Hz, 1H, Py), 8.68 (dd, J = 1.4, 5.5 Hz, 1H, Py), 8.61 (s, 1H, meso), 8.03 (d, J = 8.3 Hz, 2H, Ph), 8.01 (dd, J =1.4, 5.5 Hz, 1H, Py), 7.79 (d, J = 8.3 Hz, 2H, Ph), 7.46 (m, 1H, Py), 5.30 (d, J = 20.2 Hz, 1H, 13^2), 5.14 (d, J = 20.2 Hz, 1H, 13^2), 4.52 (m ,1H, 18-H), 4.22 (m, 1H, 17-H), 3.71 (quartet, J = 7.8 Hz, 2H, 8-$\underline{CH_2}CH_3$), 3.69, 3.62, 3.55, 3.30 (each s, each 3H, ring CH_3×3, COOMe), 2.76–2.68, 2.62–2.54, 2.35–2.26 (each m, 1H, 1H, 2H, 17^1, 17^2), 1.84 (d, J = 7.3 Hz, 3H, 18-CH_3), 1.71 (t, J = 7.8 Hz, 3H, 8-$CH_2\underline{CH_3}$), 0.30 (bs, 1H, NH), and -1.84 (bs, 1H, NH); APCI-HRMS: calcd for $C_{45}H_{41}N_5O_3$, MH^+, 700.3288, found 700.3291; GPC: V_R = 163.4 mL (100%).

Fb4Py: Yield: 75%. ^{1}H-NMR ($CDCl_3$): δ / ppm = 9.60 (s, 1H, meso), 9.52 (s, 1H, meso), 8.75 (d, J = 6.0 Hz, 2H, Py), 8.61 (s, 1H, meso), 8.02 (d, J = 8.5 Hz, 2H, Ph), 7.83 (d, J = 8.5 Hz, 2H, Ph), 7.63 (d, J = 6.0 Hz, 2H, Py), 5.29 (d, J = 19.7 Hz, 1H, 13^2), 5.14 (d, J = 19.7 Hz, 1H, 13^2), 4.52 (m, 1H, 18-H), 4.33 (m, 1H, 17-H), 3.70 (quartet, J =

7.8 Hz, 2H, 8-$\underline{CH_2}CH_3$), 3.68, 3.62, 3.54, 3.28 (each s, each 3H, CH_3×3, COOMe), 2.76–2.67, 2.63–2.55, 2.36–2.26 (each m, 1H, 1H, 2H, 17^1, 17^2), 1.84 (d, J = 7.3 Hz, 3H, 18-CH_3), 1.71 (t, J = 7.8 Hz, 3H, 8-$CH_2\underline{CH_3}$), 0.26 (bs, 1H, NH), and -1.87 (bs, 1H, NH); APCI-HRMS: calcd for $C_{45}H_{41}N_5O_3$, MH^+, 700.3288, found 700.3273; GPC : V_R = 167.6 mL (100%).

Zinc Insertion. To a solution of the free-base compounds (50 mg, 0.07 mmol) in $CHCl_3$ (56 mL) was added sat. $Zn(OAc)_2$•$2H_2O$ in MeOH (5 mL). After stirring for 3 h, 4% $NaHCO_3$ was added. The organic layer was separated, and was washed with H_2O. The solvent was eliminated in *vacuo* to quantitatively give the product as a green solid.

Zn3Py: ^{1}H-NMR ($CDCl_3$): δ/ppm = 9.61 (s, 1H, meso), 9.56 (s, 1H, meso), 8.40 (s, 1H, meso), 7.82 (d, J = 7.3 Hz, 2H, Ph), 6.92 (d, J = 5.5 Hz, 1H, Py), 6.68 (d, J = 7.3 Hz, 2H, Ph), 5.97 (bt, J = 6.0 Hz, 1H, Py), 5.34 (d, J = 19.2 Hz, 1H, 13^2), 5.19 (d, J = 19.2 Hz, 1H, 13^2), 4.43 (m, 1H, 18-H), 4.30 (m, 1H, 17-H), 3.74 (m, 2H, Py, 3-$\underline{CH_2}CH_3$), 3.74, 3.63, 3.51, 3.30 (each s, each 3H, ring CH_3×3, COOMe), 3.30 (bs, 1H, Py), 2.72–2.64, 2.54–2.46, 2.38–2.29, 2.24–2.16 (each m, each 1H, 17^1, 17^2), and 1.76–1.69 (m, 6H, 8-$CH_2\underline{CH_3}$, 18-CH_3); APCI-HRMS: calcd for $C_{45}H_{40}N_5O_3Zn$, MH^+, 762.2423, found 762.2414.

Zn4Py: ^{1}H-NMR ($CDCl_3$): δ/ppm = 9.59 (s, 1H, meso), 9.36 (s, 1H, meso), 8.39 (s, 1H, meso), 7.60 (d, J = 8.0 Hz, 2H, Ph), 6.97 (d, J = 8.0 Hz, 2H, Ph), 6.17 (bs, 2H, Py), 5.19 (d, J = 19.7 Hz, 1H, 13^2), 5.07 (d, J = 19.7 Hz, 1H, 13^2), 4.44 (m ,1H, 18-H), 4.25 (m, 1H, 17-H), 3.85 (bs, 2H, Py), 3.74 (quartet, J = 7.3 Hz, 2H, 8-$\underline{CH_2}CH_3$), 3.70, 3.53, 3.38, 3.19 (each s, each 3H, ring CH_3×3, COOMe), 2.63–2.58, 2.43–2.38, 2.36–2.26, 2.08–2.00 (each m, each 1H, 17^1, 17^2), 7.3 (d, J = 7.3 Hz, 3H, 18-CH_3), and 1.70 (t, J = 7.3 Hz, 3H, 8-$CH_2\underline{CH_3}$); APCI-HRMS: calcd for $C_{45}H_{40}N_5O_3Zn$, MH^+, 762.2423, found 762.2400.

4-5 References

(1) Scholes, G. D.; Fleming, G. R.; Olaya-Castro, A.; van Grondelle, R. *Nat Chem* **2011**, *3*, 763.

(2) Choi, M.-S.; Yamazaki, T.; Yamazaki, I.; Aida, T. *Angew. Chem. Int. Ed.* **2004**, *43*, 150.

(3) Ziessel, R.; Harriman, A. *Chem. Commun.* **2011**, *47*, 611.

(4) Kobuke, Y. *Eur. J. Inorg. Chem.* **2006**, 2333.

(5) Aratani, N.; Kim, D.; Osuka, A. *Acc. Chem. Res.* **2009**, *42*, 1922.

(6) Imahori, H. *J. Phys. Chem. B* **2004**, *108*, 6130.

(7) Fukuzumi, S.; Ohkubo, K. *J. Mater. Chem.* **2012**, *22*, 4575.

(8) Frischmann, P. D.; Mahata, K.; Würthner, F. *Chem. Soc. Rev.* **2013**, *42*, 1847.

(9) Shinozaki, Y.; Richards, G.; Ogawa, K.; Yamano, A.; Ohara, K.; Yamaguchi, K.; Kawano, S.-i.; Tanaka, K.; Araki, Y.; Wada, T.; Otsuki, J. *J. Am. Chem. Soc.* **2013**, *135*, 5262.

(10) Dale, R. E.; Eisinger, J.; Blumberg, W. E. *Biophys. J* **1979**, *26*, 161.

(11) Shinozaki, Y.; Yoshikawa, I.; Araki, K.; Ohara, K.; Yamaguchi, K.; Kawano, S.-i.; Tanaka, K.; Araki, Y.; Wada, T.; Otsuki, J. *Chem. Lett.* **2014**, *43*, 862.

(12) Smith, K. M.; Goff, D. A.; Simpson, D. J. *J. Am. Chem. Soc.* **1985**, *107*, 4946.

(13) Tamiaki, H.; Miyata, S.; Kureishi, Y.; Tanikag, R. *Tetrahedron* **1996**, *52*, 12421.

(14) Sasaki, S.-i.; Mizutani, K.; Kunieda, M.; Tamiaki, H. *Tetrahedron Lett.* **2008**, *49*, 4113.

(15) Sasaki, S.-i.; Mizutani, K.; Kunieda, M.; Tamiaki, H. *Tetrahydron* **2011**, *67*, 6065.

(16) Patil, U. D. *Synlett* **2009**, *17*, 2880.

(17) Wang, Y.; Frattarelli, D. L.; Facchetti, A.; Cariati, E.; Tordin, E.; Ugo, R.; Zuccaccia, C.; Macchioni, A.; Wegener, S. L.; Stern, C. L.; Ratner, M. A.; Marks, T. J. *J. Phys. Chem. C* **2008**, *112*, 8005.

(18) Tamiaki, H.; Yagai, S.; Miyatake, T. *Bioorg. Med. Chem.* **1998**, *6*, 2171.

(19) Yagai, S.; Tomohiro, M.; Shimono, Y.; Tamiaki, H. *Photochem. Photobiol.* **2001**, *73*.

(20) Otsuki, J. *J. Porphyrin Phthalocyanines* **2009**, *13*, 1069.

(21) Wu, P. G.; Brand, L. *Anal. Biochem.* **1994**, *218*, 1.

(22) Kelley, R. F.; Goldsmith, R. H.; Wasielewski, M. R. *J. Am. Chem. Soc.* **2007**, *129*, 6384.

(23) Linke, M.; Lauer, A.; von Haimberger, T.; Zacarias, A.; Heyne, K. *J. Am. Chem. Soc.* **2008**, *130*, 14904.

(24) Burla, M. C.; Caliandro, R.; Camalli, M.; Carrozzini, B.; Cascarano, G. L.; DeCaro, L.; Giacovazzo, C.; Polidori, G.; Spagna, R. *J. Appl. Cryst.* **2005**, *38*, 381.

(25) Burla, M. C.; Caliandro, R.; Camalli, M.; Carrozzini, B.; Cascarano, G. L.; DeCaro, L.; Giacovazzo, C.; Polidori, G.; Spagna, R. *J. Appl. Cryst.* **2007**, *40*, 609.

(26) Sheldrick, G. M. *Acta Cryst.* **2008**, *A64*, 112.

(27) Sheldrick, G. M. *Acta Cryst.* **2008**, *A64*, 112.

(28) Spek, A. L. *Acta Cryst.* **2009**, *D65*, 148.

4-6 Appendix

Table 4-A1. Selected Structural Parameters of **Zn3Py**.

	Red	Blue
	Angle / °	
$\angle N_1–Zn–N_2$	91.24	90.45
$\angle N_2–Zn–N_3$	86.75	87.61
$\angle N_3–Zn–N_4$	89.30	88.33
$\angle N_4–Zn–N_1$	88.57	89.50
	Distance / Å	
$N_1–Zn$	1.997	2.038
$N_2–Zn$	2.049	2.095
$N_3–Zn$	2.022	2.015
$N_4–Zn$	2.187	2.164
$N_{Py}–Zn$	2.146	2.135
$N_1N_2N_3N_4–Zn$	0.281	0.280

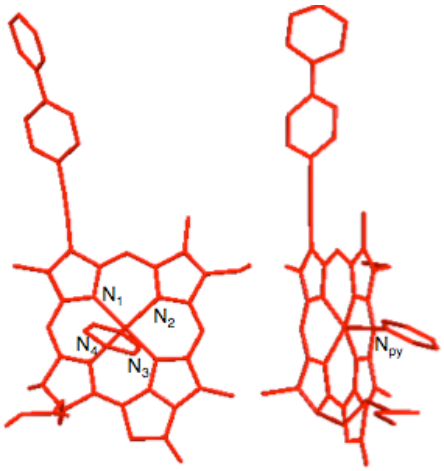

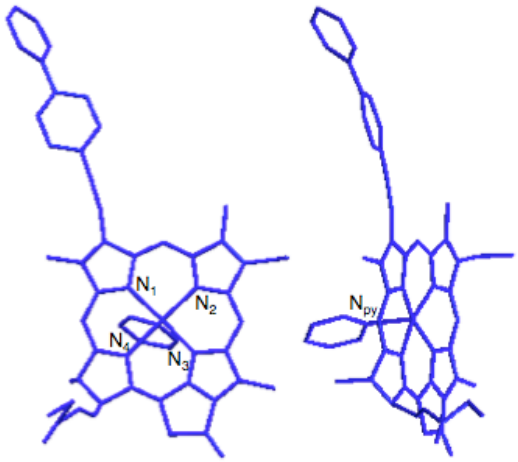

Table 4-A2. Selected Structural Parameters of **Zn4Py**.

	Red	Blue
	Angle / °	
$\angle N_1–Zn–N_2$	91.27	91.58
$\angle N_2–Zn–N_3$	88.04	87.12
$\angle N_3–Zn–N_4$	87.87	89.35
$\angle N_4–Zn–N_1$	88.90	88.36
	Distance / Å	
$N_1–Zn$	2.033	1.995
$N_2–Zn$	2.072	2.056
$N_3–Zn$	2.012	1.992
$N_4–Zn$	2.186	2.210
$N_{Py}–Zn$	2.179	2.161
$N_1N_2N_3N_4–Zn$	0.276	0.262

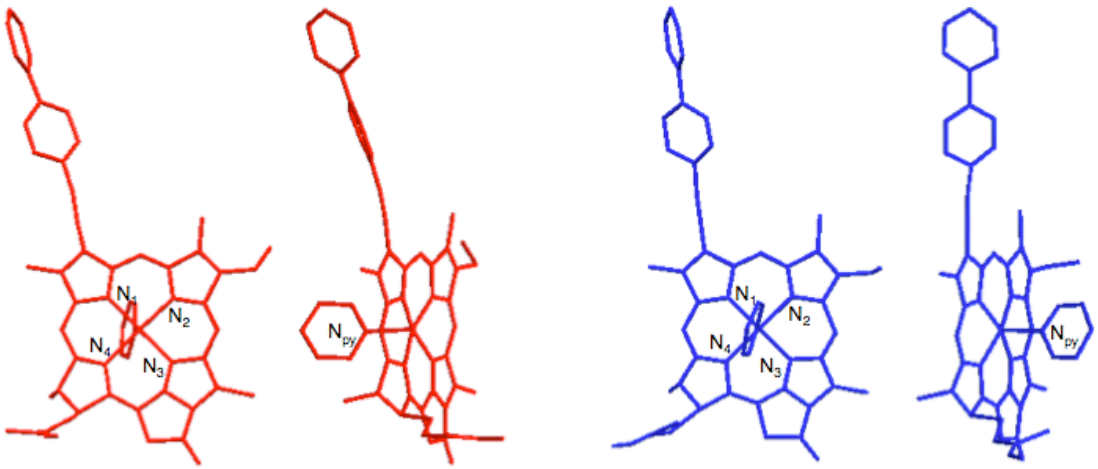

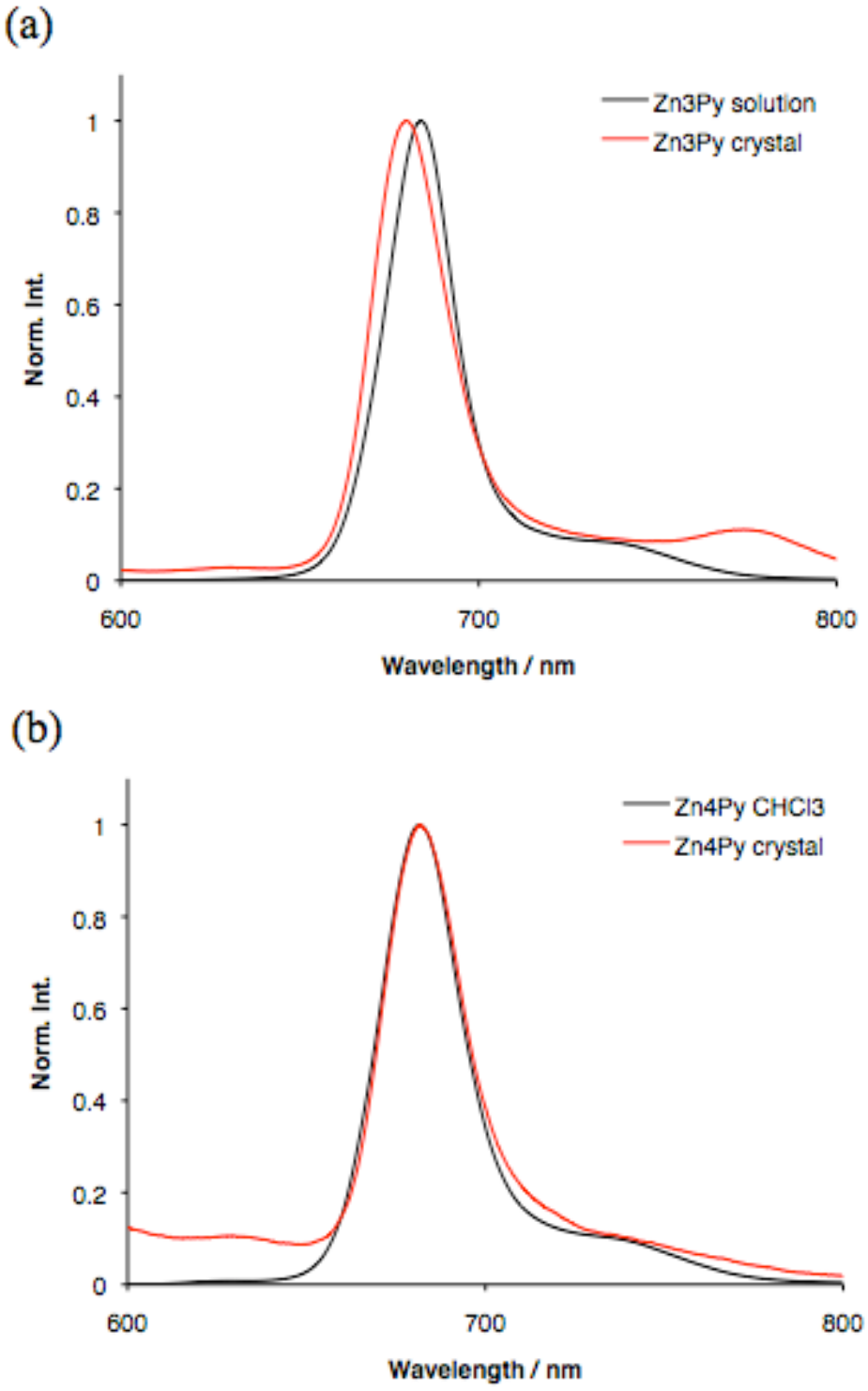

Figure 4-A1. Fluorescence spectra of (a) **Zn3Py** (λ_{ex} = 439 nm) and (b) **Zn4Py** ((λ_{ex} = 432 nm) in $CHCl_3$ (ca. 10 μM) and their crystals. The spectra of the crystals were measured in liquid paraffin by a reflection configuration.

Chapter 5

Construction of Soluble Zinc Chlorophyll Cyclic Tetramers

5-0 Summary

We constructed soluble cyclic tetramers by self-assembly of dendron-modified zinc chlorophyll derivatives *via* intermolecular coordination interaction between the nitrogen atom in the pyridine moiety to the zinc center in another zinc chlorophyll molecule, which were identified by ^{1}H-NMR techniques including diffusion-ordered spectroscopy (DOSY), fluorescence, absorption, and circular dichroism (CD) spectroscopies.

5-1 Introduction

Green photosynthetic bacteria use LH1 and LH2 (LHs) as the light-harvesting antennae consisting of chlorophyll molecules, which are circularly arranged by complexation with proteins (1-1).[1,2] While the large surface of the antennae that is striked by photons enables efficient light absorption, the intermolecular orientation of the chlorophyll molecules in the antennae is made to be preferable for efficient energy transfer.[3,4] Cyclic antenna models have also attracted attention due to their structural resemblance with LHs together with chlorosome-like aggregates (1-2).[5,6]

We mainly described on the structural analyses of the self-assemblies of the zinc chlorophyll derivatives and the potentiality of the coordination polymers in the crystal for light-harvesting antennae in Chapters 2–4, while the cyclic oligomers formed in solution should also have the potential applicability for the antenna model. However, to apply the cyclic oligomers as an antenna model, their poor solubility must be an issue to be resolved. Therefore, we herein construct the soluble cyclic tetramers by introduction of the dendron into the zinc chlorophyll molecule appended by pyridine in the Chapter 2 and investigate whether the dendron moiety in the dendron-modified zinc chlorophyll derivatives (Chart 5-1) influences their self-assembly in solution by means of the ^{1}H-NMR techniques including diffusion-ordered spectroscopy (DOSY), electronic absorption, fluorescence, and circular dichroism (CD) spectroscopies.

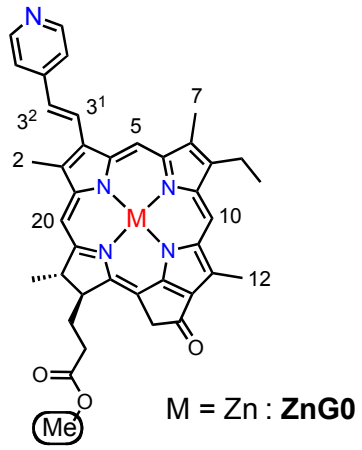

	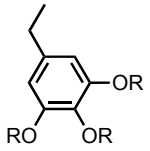	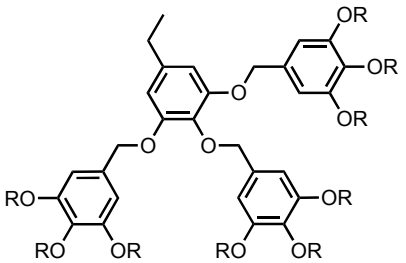
R = $C_{12}H_{25}$	M = 2H : **FbG1C12** M = Zn : **ZnG1C12**	M = 2H : **FbG2C12** M = Zn : **ZnG2C12**
R = $(CH_2CH_2O)_3CH_3$	M = 2H : **FbG1TEG** M = Zn : **ZnG1TEG**	M = 2H : **FbG2TEG** M = Zn : **ZnG2TEG**

Chart 5-1. Zinc chlorophyll derivatives functionalized by dendrons.

5-2 Results and Discussion

5-2-1 Syntheses

The series of the zinc chlorophyll derivatives equipped with the dendron were synthesized following Scheme 5-1. Methyl pyropheophorbide-*d* **CHOG0** was prepared from pheophytin-*a* as a starting material through three steps as described in Chapters 2–4.[7,8] The methyl ester group at the position 17^2 was hydrolyzed in concentrated hydrochloric acid (conc. HCl) to give the free carboxylic acid derivative, pyropheophorbide-*d*. The dendronized benzyl alcohol

derivatives **G1C12**, **G2C12**, **G1TEG**, and **G2TEG** were synthesized by a stepwise convergent method following reported procedures.[9] The hydroxyl groups in methyl gallate were substituted by bromododecane or tosylated triethylene glycol, and the methyl ester group was then reduced using lithium aluminum hydride (LiAlH) to give G1 generation benzyl alcohol derivatives **G1C12** and **G1TEG**. The G2 generation benzyl alcohol derivatives **G2C12** and **G2TEG** were prepared by similar manner to that of G1 generation derivatives: (i) the substitution of hydroxyl groups in methyl gallate by benzyl bromide or chloride derivative which were prepared by the substitution reactions of the G1 generation benzyl alcohol **G1C12** and **G1TEG** with hydrogen bromide (HBr) or thionyl chloride ($SOCl_2$), respectively; and (ii) the reduction of the methy ester group using LiAlH. The carboxylic acid is esterified with 1st (G1)–2nd (G2) generation oxylbenzyl alcohol derivatives with dodecyl chains (C12) or triethylene glycol chains (TEG) by use of 1-(3-dimethylaminopropyl)-3-ethylcarbodiimide hydrochloride (EDC•HCl) and 4-dimethylaminopyridine (DMAP) in chloroform to give the intermediates **CHOG1C12**, **CHOG2C12**, **CHOG1TEG**, and **CHOG2TEG** (hereafter collectively called **CHOD**) in moderate yields (~50%).[10] 4-Picoline was condensed with the formyl group in **CHOD** in carboxylic acid anhydride (Ac_2O) in the presence of catalytic amount of acetic acid (AcOH) *via* the aldol-like condensation to afford the free-base derivatives **FbG1C12**, **FbG2C12**, **FbG1TEG**, and **FbG2TEG** (hereinafter collectively called **FbD**) as described in Chapter 2.[11,12] The final step is simple zinc insertion with excess $Zn(OAc)_2$•$2H_2O$ in chloroform and methanol to afford the zinc chlorophyll derivatives **ZnG1C12**, **ZnG2C12**, **ZnG1TEG**, and **ZnG2TEG** (hereafter collectively called **ZnD**).[13] The free-base derivatives **FbD** were purified by column chromatography followed by gel permeation (GPC) or high performance liquid chromatography (HPLC) if needed. Because of the column chromatography of the zinc complexes **ZnD** absorb into the stational phase, those were purified only by reprecipitation. The compounds were characterized with ^{1}H-NMR and MS spectrometry.

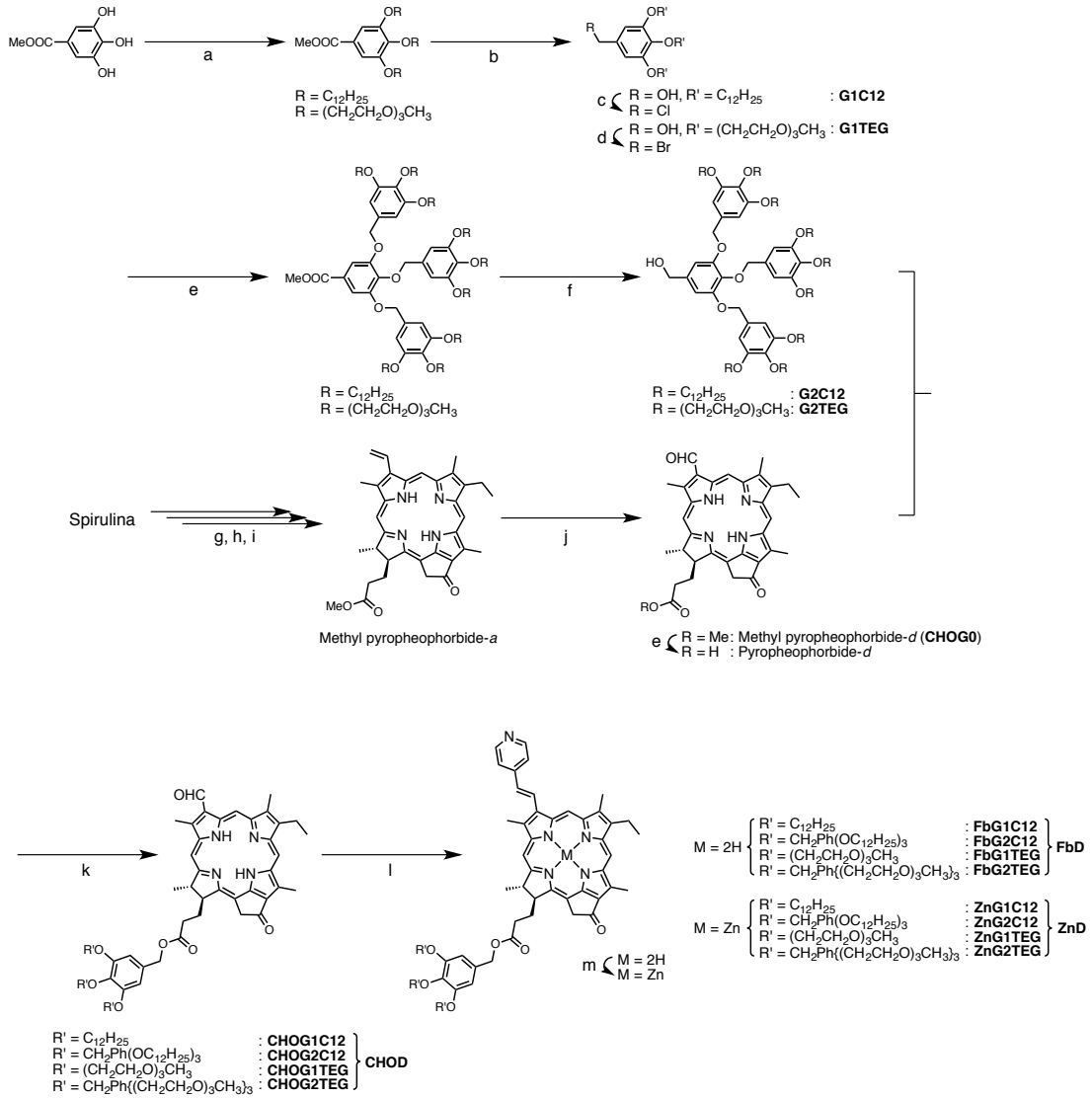

Scheme 5-1. Synthetic procedures of dendron-equipped zinc chlorophyll derivatives appended by pyridine. (a) 1-bromododecane, K_2CO_3, acetone, reflux, 24 h. $CH_3(OCH_2CH_2)_3OTs$, 18-crown-6, K_2CO_3, acetone, reflux, 2 days. (b) LAH, THF, 3 h. (c) HBr, AcOH, $CHCl_3$, 1 h. (d) $SOCl_2$, $CHCl_3$, 4 h. (e) methyl gallate, KI, K_2CO_3, acetone, reflux, 24 h. Methyl gallate, K_2CO_3, DMF, 65 ^{O}C. (f) LiAlH, THF, 3 h. (g) acetone, reflux, 10 days. (h) H_2SO_4, MeOH, overnight. (i) 2,4,6-trimethylpyridine, reflux, 3 h. (j) OsO_4, $NaIO_4$, AcOH, THF, H_2O, overnight. (k) conc. HCl, 3 h. (l) corresponding benzyl alcohol derivative, EDC•HCl, DMAP, $CHCl_3$, overnight. (m) 4-picoline, Ac_2O, AcOH, reflux, 3 h. (n) $Zn(OAc)_2$•$2H_2O$, MeOH, $CHCl_3$, 3 h.

5-2-2 Intermolecular Axial Coordination

The **ZnD** showed typical absorption spectra for a zinc chlorophyll derivative in benzene: the most intense Soret band around 400 nm and the four Q bands at 450–700 nm among which the $Q_y(0,0)$ band is the most intense (Figure 5-1).[14] The absorption spectra were bathochromically shifted with increasing concentration in the range of 5–250 μM (Figure 5-1), and the red-shift then reached plateau at >100 μM. A similar behaviour was also observed in the fluorescence spectra at the concentration range of 5–500 μM (Figure 5-2). The bathochromic changes in both of absorption and fluorescence spectra were also observed in a reference compound, zinc methypyropheophorbide-*a* (ZnMPPa), by addition of pyridine (Figure 5-3). A similar bathochromic shift was reported for other zinc chlorophyll derivatives.[15] Therefore, we assigned the bathochromic shift of the absorption and fluorescence spectra to self-coordination of **ZnD**.

The ^{1}H-NMR spectra of **FbD** and **ZnD** in $CDCl_3$ (ca. 10 mM, 298 K) are shown in Figure 5-4. The signals were successfully assigned by use of COSY, NOESY, HMQC, HMBC, and DEPT and by comparison with those of **ZnG0** in Chapter 2. The ^{1}H-NMR signals for the vinylpyridine moiety of **FbD** appeared in the aromatic region, whereas those of **ZnD** were significantly shifted upfield. The amounts of upfield shift of pyridyl protons Pyα and Pyβ are larger (~5.5 ppm for Py; ~1.5 ppm for Py) than those of vinyl group (0.6 ppm for 3^1; 0.9 ppm for 3^2). The signal of the meso-5 proton was also shifted upfield although the signals of other meso protons were not. Similar upfield shifts of ^{1}H-NMR signals for **ZnD** were also observed in C_6D_6 (Figures 5-5, 5-A1–A3). The distances from the nitrogen atom in the pyridine group to the protons correlate with the amounts of the upfield shift for the protons, i.e. the shielding effect is stronger as the displacement is shorter. The results in the absorption, fluorescence, and ^{1}H-NMR measurements are consistent with those for **ZnG0** in Chapter 2, indicating that the intermolecular axial coordination interaction between the nitrogen atom in the pyridine moiety and the zinc center in the zinc chlorophyll molecules involves in their self-assembly, and in turn suggesting that the formation of cyclic tetramers of **ZnD** as was the case for **ZnG0** considering the structural similarity.

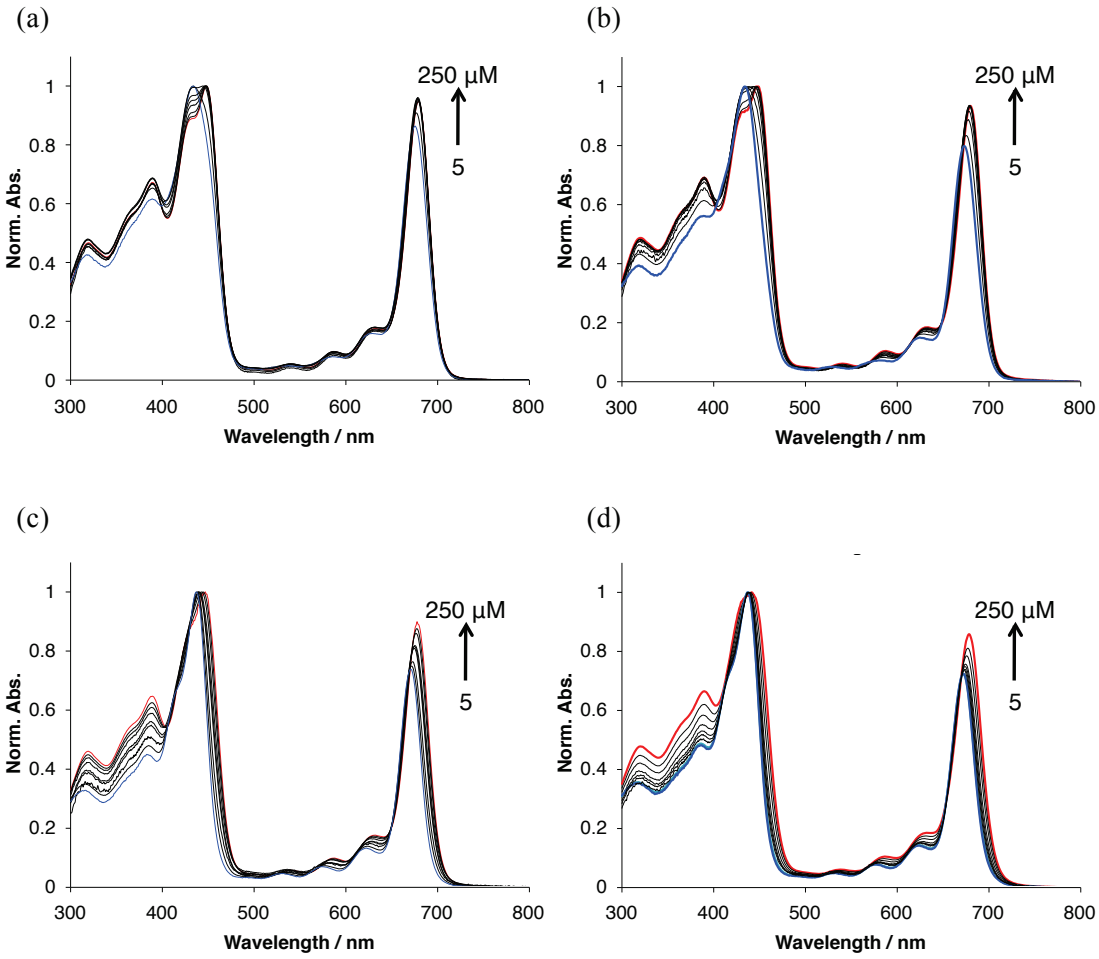

Figure 5-1. Absorption spectra of (a) **ZnG1C12**, (b) **ZnG2C12**, (c) **ZnG1TEG**, and (d) **ZnG2TEG** in benzene in a range of 5–250 µM at 298 K.

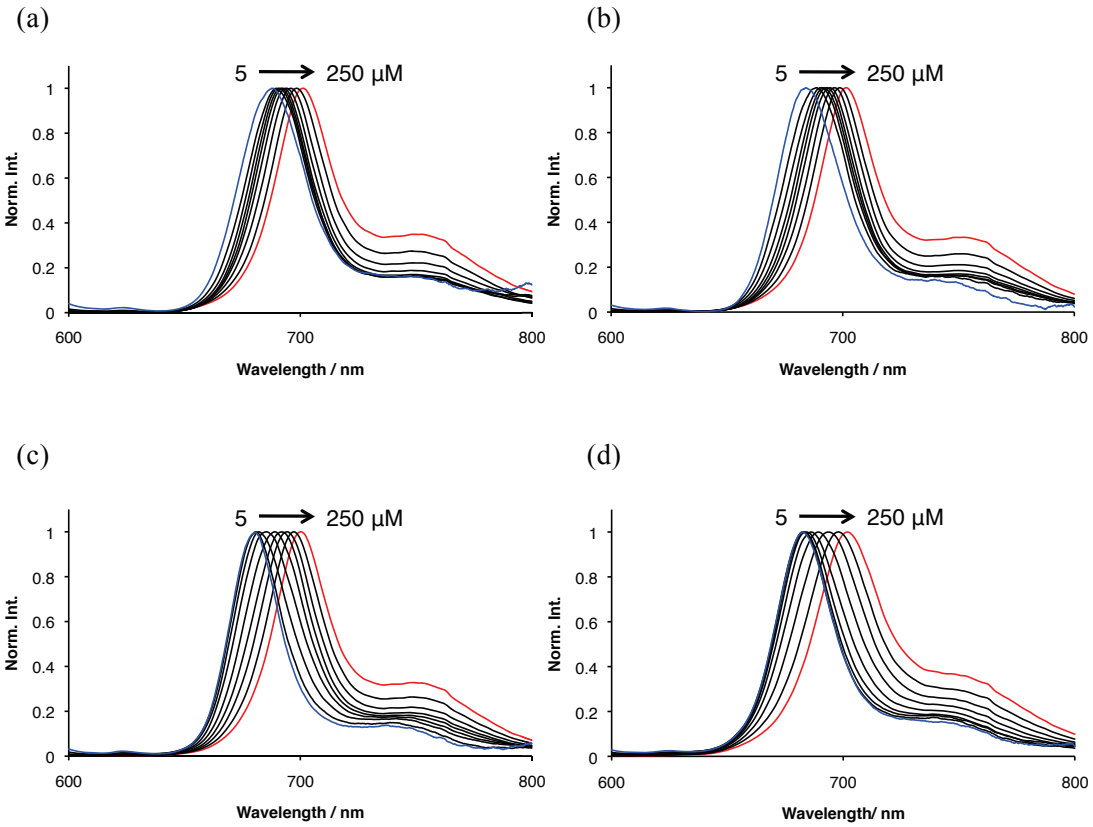

Figure 5-1. Fluorescence spectra of (a) **ZnG1C12**, (b) **ZnG2C12**, (c) **ZnG1TEG**, and (d) **ZnG2TEG** in benzene in a range of 5–250 μM (λ_{ex} = 585 nm) at r.t. These spectra were obtained in a reflection configuration to prevent reabsorption.

(a)

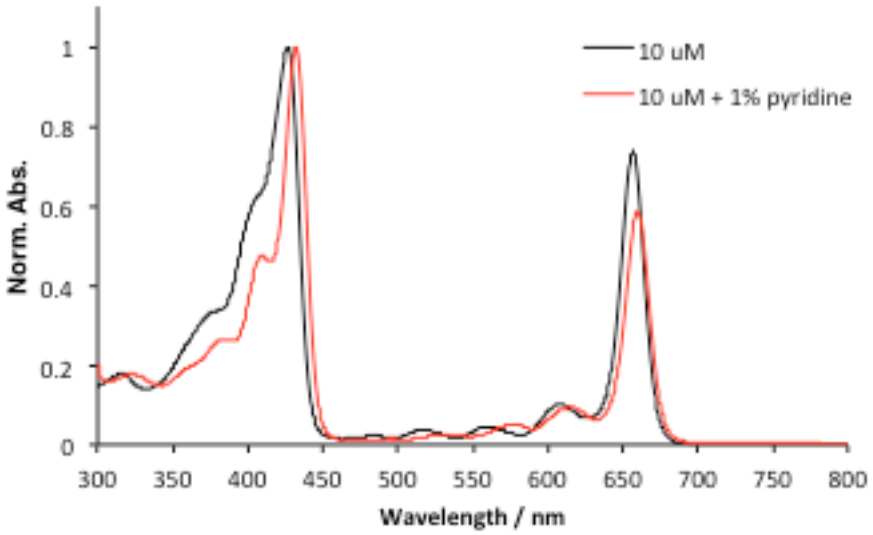

(b)

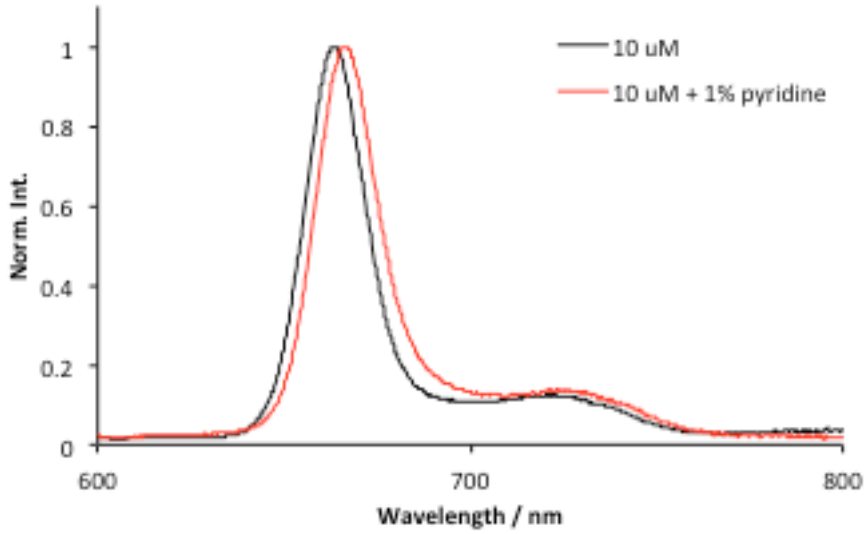

Figure 5-3. (a) Absorption and (b) fluorescence spectra of ZnMPPa (10 μM) in benzene and those after addition of 1% pyridine. The absorption and fluorescence spectra were measured at 298 K and r.t., respectively.

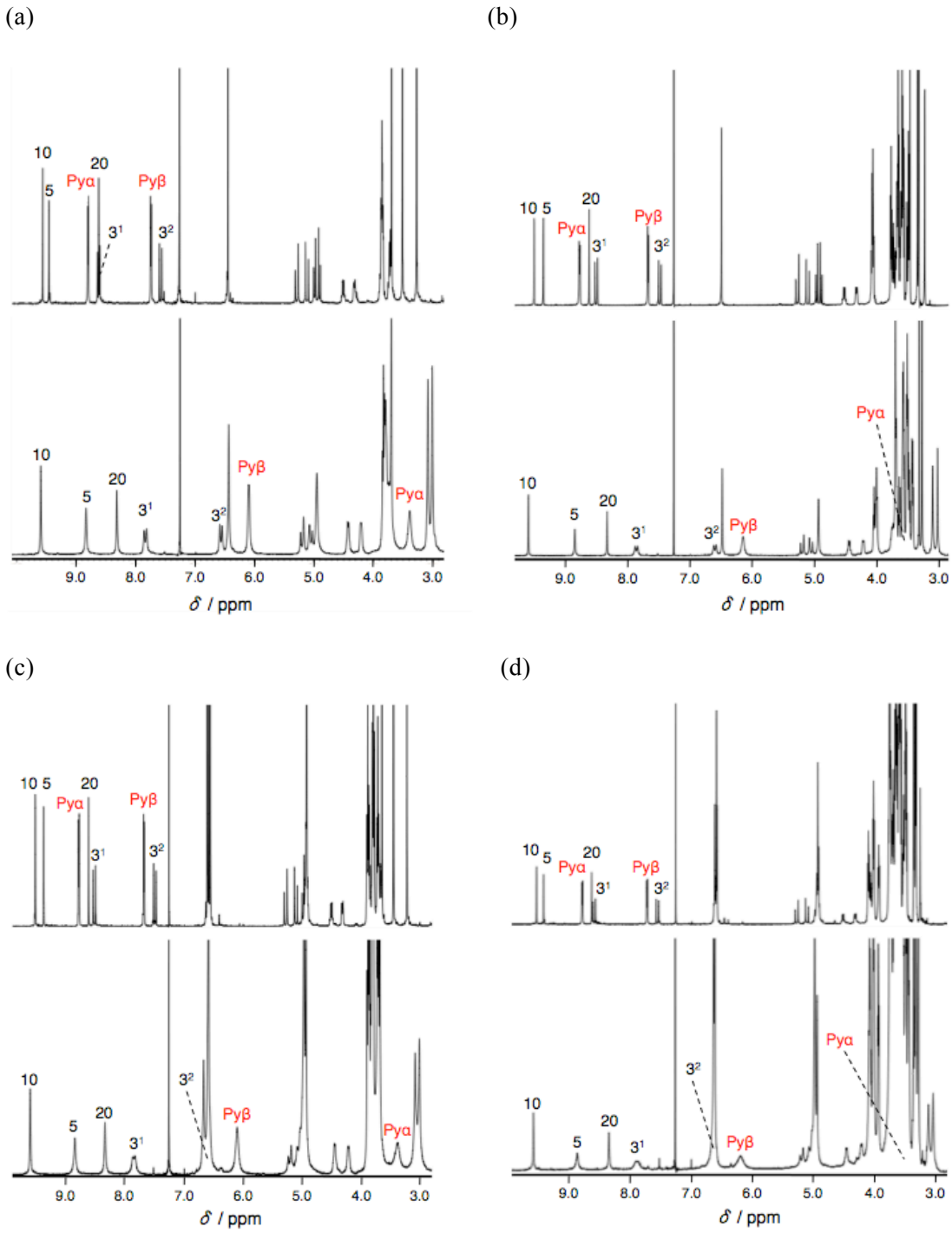

Figure 5-4. ^{1}H-NMR spectra of **FbD** (upper) and **ZnD** (lower) in $CDCl_3$ at 298 K (10 mM). (a) **MG1C12**, (b) **MG1TEG**, (c) **MG2C12**, and (d) **MG2TEG**.

5-2-3 Confirmation of Formation of Cyclic Tetramers

We investigated whether the dendron moiety in the **ZnD** interferes with the formation of the cyclic tetramers in solution by estimation of the stability of the self-aggregate by ^{1}H-NMR measurements, absorption spectroscopy, and circular dichroism spectroscopy.

The ^{1}H-NMR chemical shifts of the vinylpyridine group in **ZnD** in C_6D_6 (10 mM) were almost insensitive to the temperature rising from 298 K to 343 K (Figure 5-5), indicating that the self-association occurs with a large association constant.[16] Although we attempted to qualitatively estimate the stability from the data of concentration dependence of the ^{1}H-NMR chemical shifts of **ZnD** in C_6D_6 in a concentration range of 0.2–10 mM, the exact chemical shifts could not be read upon dilution due to the peak broadening (Figure 5-6). Given that the change of the absorption spectra upon axial coordination is saturated more than 0.2 mM (Figure 5-1), the self-aggregates of **ZnD** formed by the intermolecular axial coordination are the predominant species more than 0.2 mM in C_6D_6. The negative Cotton effect in the CD spectra of **ZnD** rules out the π–π stacking among the zinc chlorophyll molecules (Figure 5-7),[17] indicating the π stacking is not involved for stabilizing the self-aggregates.

The diffusion coefficients (D) of the zinc complexes **ZnD** and the free-base compounds **CHOD** in C_6D_6 (ca. 10 mM) were obtained by the diffusion ordered spectroscopy (DOSY) measurements as summarized in Table 5-1. The hydrodynamic radius (r) were calculated by use of Stokes–Einstein equation

$$r = k_B T / 6\pi\eta D \qquad (1)$$

where k_B, T, and η are the Boltzmann constant, absolute temperature, and viscosity, respectively.[18,19] The radiuses thus obtained are also summarized in Table 5-1. The radius for the free-base compounds **CHOD** is consistent with the dimension of the monomeric species (Figure 5-8), whereas those for the zinc complexes **ZnD** are about twice as large as those for **CHOD**. These results agree well with the cyclic tetramer models of the **ZnD**, which were constructed by use of the MM3 force field calculation, indicating that the dendron moiety in **ZnD** does not interfere the formation of the cyclic tetramers of **ZnD** (Figure 5-9).

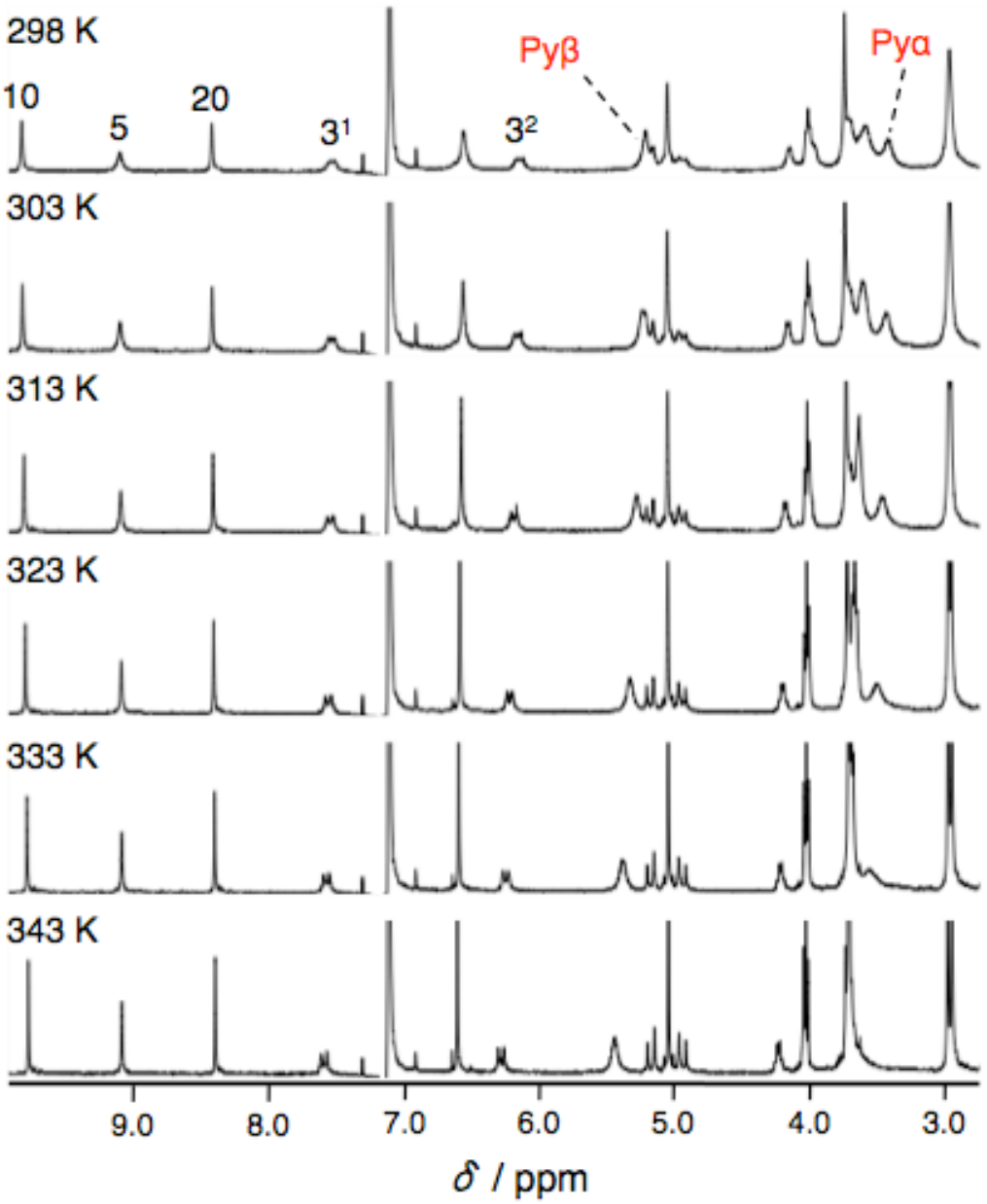

Figure 5-5. VT-^{1}H-NMR spectra of **ZnG1C12** in benzene (10 mM) in a temperature range of 298–343 K. ^{1}H-NMR spectra of other **FbD** and **ZnD** are shown in Figures 5A-1–5A-3.

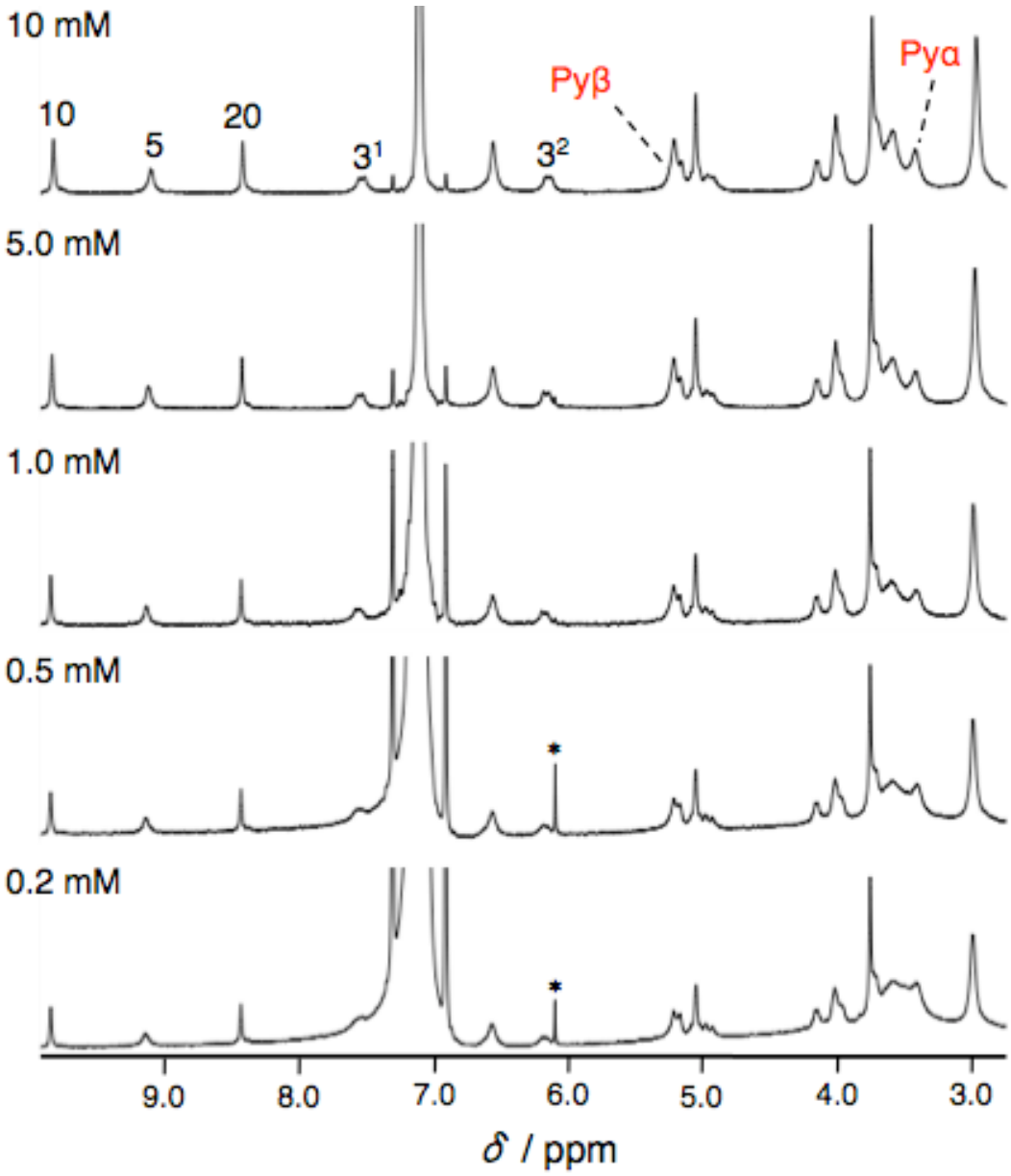

Figure 5-6. ^{1}H-NMR spectra of **ZnG1C12** in C_6D_6 in the concentration range of 10–0.2 mM at 298 K. Asterisk indicates residual $CHCl_3$. ^{1}H-NMR spectra of other **FbD** and **ZnD** are shown in Figures 5A-4–5A-6.

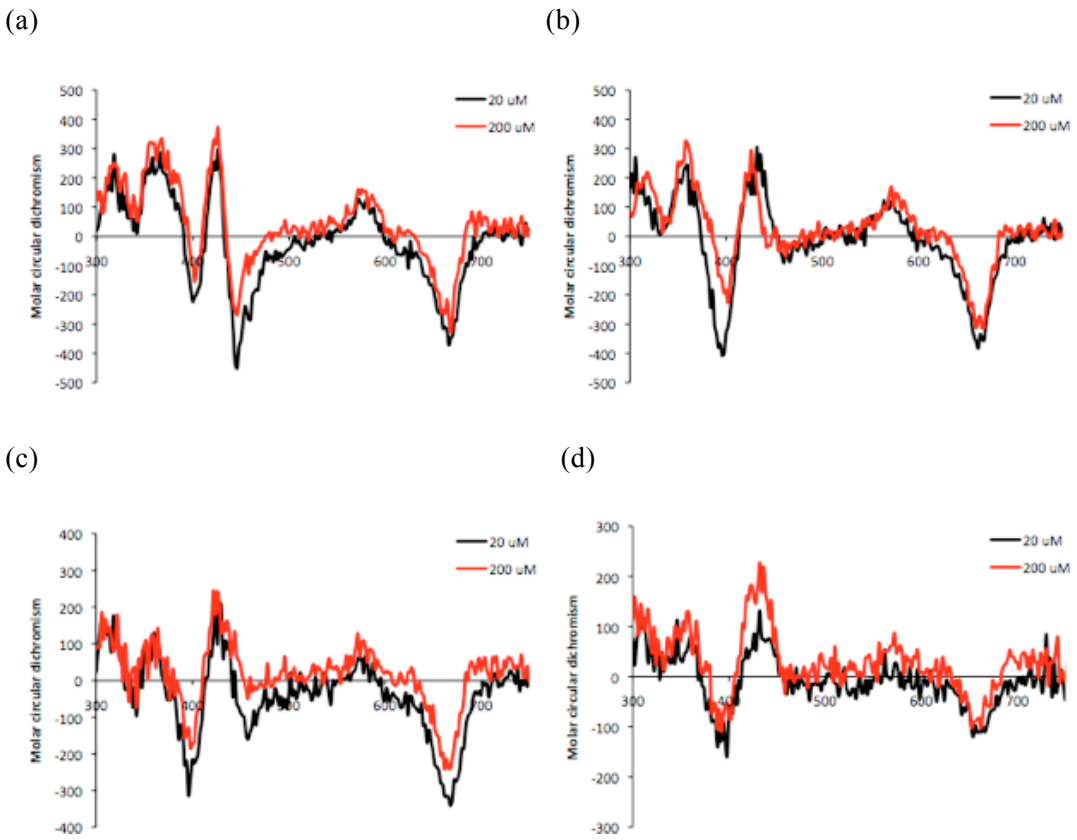

Figure 5-7. CD spectra of (a) **ZnG1C12**, (b) **ZnG1TEG**, (c) **ZnG2C12**, and (d) **ZnG2TEG** in benzene at 20 μM and 200 μM at r.t.

Table 5-1. Diffusion constants (*D*) and hydrodynamic radiuses (*r*) of **CHOD** and **ZnD** in C_6D_6.[a]

Compound	$D\times10^{10}/m^2\ s^{-1}$	*r* / Å [b]	Compound	$D\times10^{10}/m^2\ s^{-1}$	*r* / Å [b]
CHOG1C12	3.67±0.07	9.9±0.2	**ZnG1C12**	1.83±0.02	19.7±0.2
CHOG2C12	2.54±0.01	14.2±0.6	**ZnG2C12**	1.27±0.01	28.4±0.2
CHOG1TEG	3.71±0.01	9.7±0.03	**ZnG1TEG**	1.82±0.02	19.9±0.2
CHOG2TEG	2.60±0.02	13.7±0.1	**ZnG2TEG**	1.47±0.01	24.6±0.2

[a] At 298 K, 10 mM. [b] Calculated by eqn (1).

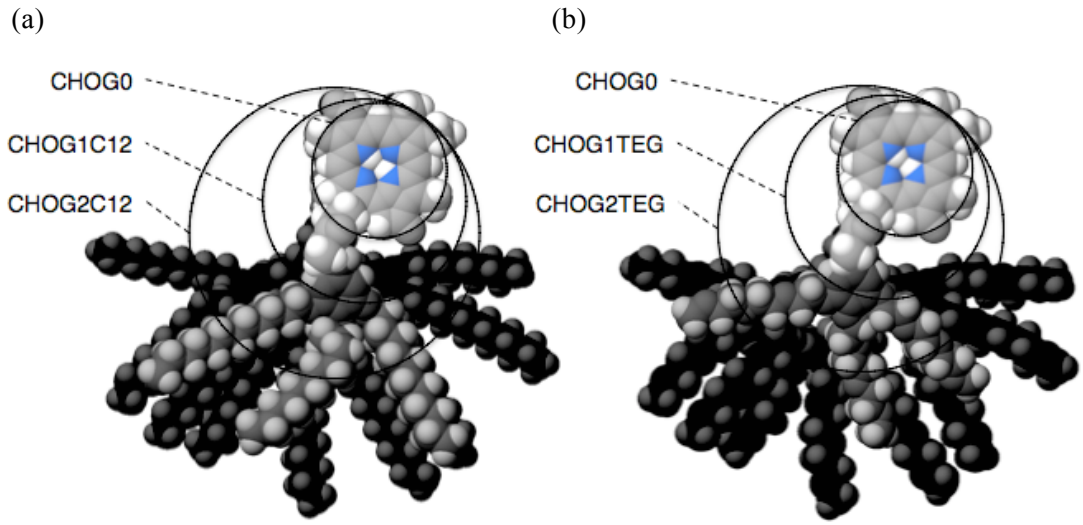

Figure 5-8. Energy-minimized structures (MM3) of **CHOG0** and **CHOD**, superimposed with different shades. The circles are drawn using calculated hydrodynamic radiuses (*r*) on the basis of diffusion constants obtained by DOSY.

(a)

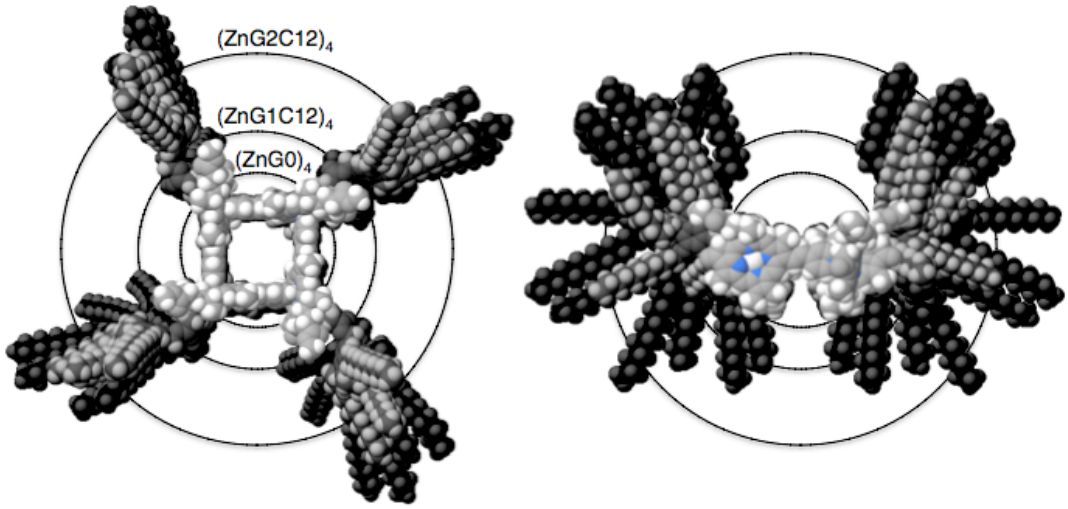

(b)

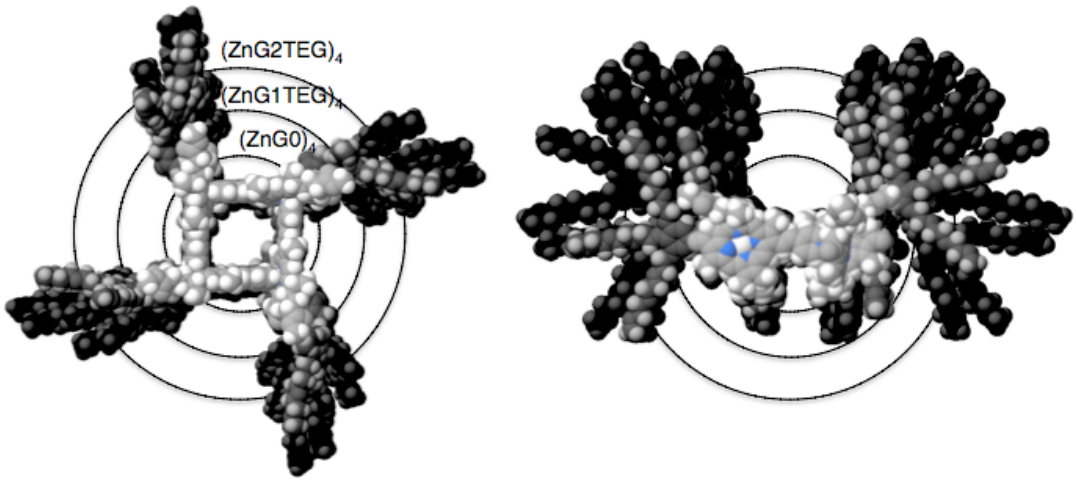

Figure 5-9. Energy-minimized structures (MM3) of **ZnG0** and **ZnD**, superimposed with different shades. The top and side views of the tetrameric models of (a) **ZnG0**, **ZnG1C12**, and **ZnG2C12**, and (b) **ZnG0**, **ZnG1TEG**, and **ZnG2TEG**. The circles are drawn using calculated hydrodynamic radiuses (*r*) on the basis of diffusion constants obtained by DOSY.

5-2-4 Stability of the Cyclic Tetramers

To estimate the stability of the cyclic tetramers, we fitted the absorption data (Figure 5-10). The equilibrium in this system should be represented by the system described in Chapter 3,

$$\begin{array}{ccccccc} \mathrm{M} & \overset{\mathrm{M}}{\rightleftarrows} & \mathrm{M}_2 & \overset{\mathrm{M}}{\rightleftarrows} & \mathrm{M}_3 & \overset{\mathrm{M}}{\rightleftarrows} & \mathrm{M}_4 \overset{\mathrm{M}}{\rightleftarrows} \cdots \\ & & \downarrow\uparrow & & \downarrow\uparrow & & \downarrow\uparrow \\ & & \mathrm{C}_2 & & \mathrm{C}_3 & & \mathrm{C}_4 \end{array} \qquad \begin{cases} K_{\mathrm{i}} = [\mathrm{M}_n]/([\mathrm{M}_{n-1}][\mathrm{M}]) \\ K_{\mathrm{c},n} = [\mathrm{C}_n]/[\mathrm{M}_n] \end{cases}$$

where M_n and C_n represent linear and cyclic n-mers. The K_{i} is the intermolecular binding constant, which we assumed to be independent of the oligomer size. We obtained the equilibrium constants for the axial coordination K_{i} = 11400, 13820, 20800, and 11680 M^{-1} for **ZnG1C12**, **ZnG1TEG**, **ZnG2C12**, and **ZnG2TEG**, respectively by fitting the absorption data as shown in Figure 5-10 by use of the equation (2) generated assuming that the cyclic tetramers selectively form (the detail is described in 3-4-3),

$$[\mathrm{M}]_{\mathrm{T}} = \frac{x}{K_{\mathrm{i}}(1-x^2)} + 4\frac{K_{c,4}}{K_{\mathrm{i}}}x^4 \text{, where } x = K_{\mathrm{i}}[M] \qquad (2)$$

where $[\mathrm{M}]_{\mathrm{T}}$ is the total (initial) concentration of the monomer unit and K_{i} and $K_{\mathrm{c},4}$ were parameterized. These similar values for K_{i} indicate that the axial coordination is not interfered by the dendron moiety. The effective molarities $K_{\mathrm{c},4}$, which signifies the stability of the cyclic species over linear species, were determined to be 6.1, 4.8, 3.4, and 5.5 mM for **ZnG1C12**, **ZnG1TEG**, **ZnG2C12**, and **ZnG2TEG**, respectively. The similarity in $K_{\mathrm{c},4}$ values among **ZnD** suggests that the presence of the dendron moiey and the generation of the dendron do not effect the stability of the cyclic tetramers.

5-3 Conclusion

We successfully constructed the cyclic tetramers soluble in benzene by the introduction of the dendron into the zinc chlorophyll molecules appended by pyridine. The influence of the dendron moiety on the formation of the cyclic tetramer in solution was investigated. While the dendron moiety does not interfere with the formation of cyclic teramers, the dendron moiety

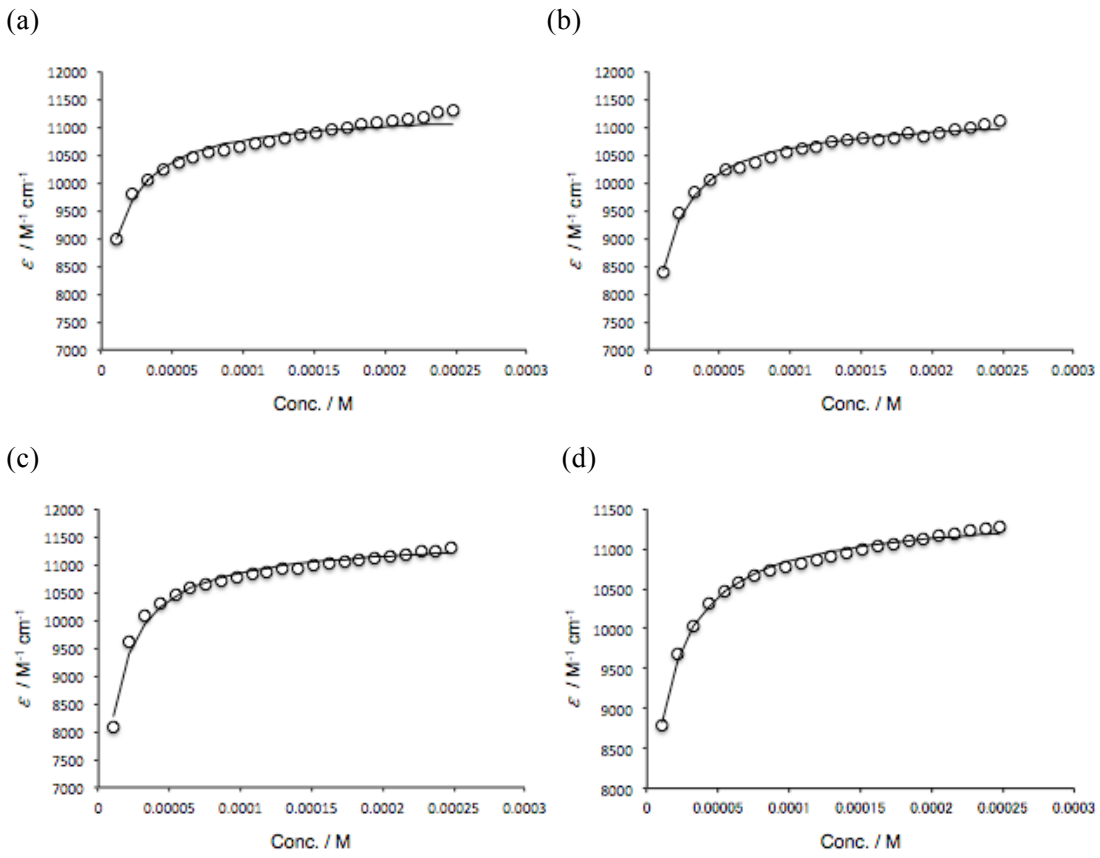

Figure 5-10. Concentration dependence of the molar absorption coefficients of (a) **ZnG1C12**, (b) **ZnG1TEG**, (c) **ZnG2C12**, and (d) **ZnG2TEG**. The fitting curves are described by solid line.

makes the cyclic tetramers soluble in benzene. This solubility in benzene is beneficial for further application of the cyclic tetramers toward construction of the artificial antenna models. We thus demonstrate the utilization of the cyclic tetramers as the light-harvesting antennae in Chapter 6.

5-4 Experiment

5-4-1 General

^{1}H-NMR spectra including DOSY spectra were measured with a JEOL ECX 400 MHz spectrometer. Atmospheric pressure chemical ionization mass spectrometry (APCI-HRMS) and matrix-assisted laser desorption ionization time-of-flight mass spectrometry (MALDI-TOFMS) were performed with Agilent G1969A and Applied Biosystems Voyager RP-PRO spectrometers, respectively. Electronic excitation and circular dichroism spectra were obtained by use of Shimazu UV-2400PC and JASCO FP-8600 spectrometers, respectively. Fluorescence liftetime was measured with a Hamamatsu Photonics Quantaurus Tau system. High performance liquid chromatography (HPLC) and gel permeation chromatography (GPC) were performed with Shimazu HPLC 20A and Japan Analytical Industry LC-9201 apparatuses equipped with Jaigel-2H and Jaigel-1H as column, respectively. Deuterated solvents, $CDCl_3$ and C_6D_6 containing tetramethysilane (TMS) as a standerd were purchased from Sigma and Aldrich, respectively. Spectroscopic grade benzene was purchased from Wako, and was used for optical measurements. All reagents and solvents were used without further purification. The electronic absorption, fluorescence, circular dichroism spectra, and fluorescence lifetime were measured under ambient condition. All reactions were conducted under argon atmosphere.

5-4-2 Syntheses

Esterification: To a solution of pyropheophorbide-*d* (13.6 mg, 0.025 mmol) in dry $CHCl_3$ (20 mL) was added EDC•HCl (35.0 mg, 0.18 mmol), DMAP (41.0 mg, 0.34 mmol), and benzyl alcohol derivative (0.03 mmol) at 0 °C. After stirring overnight at r.t., the mixture was

washed with water. The organic layer was dried with Na_2SO_4, and the solvent was then eliminated *in vacuo*. The crude mixture was purified with column chromatography (silica) to afford **CHOD** as a brown solid.

CHOG2C12: Column chromatography (silica, hexane/EtOAc = 5/1). Yield (50%). ^{1}H-NMR (400 MHz, $CDCl_3$): δ / ppm = 11.50 (s, 1H, CHO), 10.22 (s, 1H, meso), 9.53 (s, 1H, meso), 8.81 (s, 1H, meso), 6.61 (s, 2H, Ph), 6.59 (s, 2H, Ph), 6.56 (s, 4H, Ph), 5.33 (d, J = 19.7 Hz, 1H, 13^2), 5.16 (d, J = 19.7 Hz, 1H, 13^2), 4.98 (d, J = 11.9 Hz, 1H, $\underline{CH_2}$Ph), 4.93 (d, J = 11.9 Hz, 1H, $\underline{CH_2}$Ph), 4.93 (s, 6H, $\underline{CH_2}$Ph), 4.56 (m, 1H, 18-H), 4.38 (m, 1H, 17-H), 3.91–3.64 (m, 26H, ring CH_3, 8$\underline{CH_2}CH_3$, a), 3.25 (s, 3H, ring CH_3), 2.75, 2.63, 2.33 (m, 1H, 1H, 2H, 17^1 and 17^2), 1.83 (d, J = 7.3 Hz, 3H, 18CH_3), 1.71 (m, 18H, CH_2), 1.46–1.23 (m, 162H, CH_2), 0.87 (m, 27H, d), -0.20 (bs, 1H, NH), and -2.14 (bs, 1H, NH). APCI–HRMS: *m/z* = 2604.0056 $[M+H]^+$ (100%), calcd for $C_{168}H_{273}N_4O_{16}$ = 2604.0705.

CHOG1TEG: Column chromatography (silica, $CHCl_3$/MeOH = 50/1). Yield (91%). ^{1}H-NMR (400 MHz, $CDCl_3$): δ / ppm = 11.05 (s, 1H, CHO), 10.22 (s, 1H, meso), 9.53 (s, 1H, meso), 8.82 (s, 1H, meso), 6.49 (s, 2H, Ph), 5.33 (d, J = 20.2 Hz, 1H, 13^2), 5.17 (d, J = 20.2 Hz, 1H, 13^2), 4.96 (d, J = 11.9 Hz, 1H, $\underline{CH_2}$Ph), 4.89 (d, J = 11.9 Hz, 1H, $\underline{CH_2}$Ph), 4.57 (m, 1H, 18-H), 4.38 (m, 1H, 17-H), 4.07 (m, 6H, PhO$\underline{CH_2}$), 3.75 (m, 9H, OCH_2 and ring CH_3), 3.62 (m, 23H, OCH_2, 8$\underline{CH_2}CH_3$, and ring CH_3), 3.50 (m, 6H, OCH_2), 3.35 (s, 3H, ring CH_3), 3.32 (s, 6H, OCH_3), 3.26 (s, 3H, OCH_3), 2.75, 2.63, 2.33 (m, 1H, 1H, 2H, 17^1 and 17^2), 1.84 (d, J = 7.3 Hz, 18CH_3), 1.68 (t, J = 7.8 Hz, 8$CH_2\underline{CH_3}$), -0.22 (bs, 1H, NH), and -2.15 (bs, 1H, NH). APCI–HRMS: *m/z* = 1113.5705 $[M+H]^+$ (100%), calcd for $C_{60}H_{81}N_4O_{16}$ = 1113.5648.

CHOG2TEG: Column chromatography (silica, $CHCl_3$/MeOH = 40/1). Yield (54%). ^{1}H-NMR (400 MHz, $CDCl_3$): δ / ppm = 11.48 (s, 1H, CHO), 10.18 (s, 1H, meso), 9.51 (s, 1H, meso), 8.83 (s, 1H, meso), 6.63 (s, 2H, Ph), 6.60 (s, 4H, Ph), 6.58 (s, 2H, Ph), 5.33 (d, J = 20.2 Hz, 1H, 13^2), 5.17 (d, J =20.2 Hz, 1H, 13^2), 4.98–4.90 (m, 8H, $\underline{CH_2}$Ph), 4.57 (m, 1H, 18-H), 4.39 (m, 1H, 17-H), 4.13–3.93 (m, 18H, PhO$\underline{CH_2}CH_2$), 3.79–3.48 (m, 98H, 8CH_2CH_3, ring CH_3×2, and other CH_2 in TEG), 3.37, 3.36, 3.34, 3.33 (each s, total 27H, terminal CH_3 in TEG), 3.23 (s, 3H, ring CH_3), 2.76–2.72, 2.42–2.26 (m, each 2H, 17^1 and 17^2), 1.84 (d, J = 7.3

Hz, 3H, 18CH_3), 1.67 (t, J = 7.8 Hz, 3H, 8$CH_2\underline{CH_3}$), -0.24 (bs, 1H, NH), and -2.17 (bs, 1H, NH). MALDI-TOF MS (2,5-dihydroxybenzoic acid): *m/z* = 2405 $[M+H]^+$ (100%), calcd for $C_{123}H_{182}N_4O_{43}$ = 2405.

Condensation of pyridine: To a mixture of the aldehyde **CHOD** (0.078 mmol) and large excess 4-picoline (9.9 mL) in acetic acid anhydride (30 mL) was added a catalytic amount of acetic acid (0.1 mL). The resulting mixture was refluxed for 3 h. After cooling to r.t., the solvent and excess 4-picoline were eliminated *in vacuo*. The crude mixture was purified with column chromatography followed by GPC to afford **FbD** as a brown solid.

FbG1C12: Column chromatography (silica, 3% acetone/$CHCl_3$). Yield (32%). ^{1}H-NMR (400 MHz, $CDCl_3$): δ / ppm = 9.56 (s, 1H, meso-10), 9.46 (s, 1H, meso-5), 8.80 (d, J = 6.4 Hz, 2H, Pyα), 8.62 (s, 1H, meso-20), 8.62 (d, J = 16.5, 1H, 3^1), 7.74 (d, J = 6.4 Hz, 2H, Pyβ), 7.59 (d, J = 16.5, 1H, 3^2), 6.45 (s, 2H, Ph), 5.29 (d, J = 19.7 Hz, 1H, 13^2), 5.12 (d, J = 19.7 Hz, 1H, 13^2), 4.99 (d, J = 11.9 Hz, 1H, $\underline{CH_2}$Ph), 4.91 (d, J = 11.9 Hz, 1H, $\underline{CH_2}$Ph), 4.51 (m, 1H, 18-H), 4.32 (m, 1H, 17-H), 3.85 (m, 6H, a), 3.73 (quartet, J = 7.3 Hz, 2H, 8$\underline{CH_2}CH_3$), 3.70 (s, 3H, 12-CH_3), 3.51 (s, 3H, 2-CH_3), 3.27 (s, 3H, 7-CH_3), 2.73, 2.61, 2.34 (m, 1H, 1H, 2H, 17^1 and 17^2), 1.80 (d, J = 7.3 Hz, 3H, 8$CH_2\underline{CH_3}$), 1.69 (m, 9H, 18CH_3 and b), 1.36 (m, 6H, c), 1.23 (m, 48H, alkyl CH_2 except for a, b, and c), 0.86 (m, 9H, d), 0.34 (bs, 1H, NH), and -1.74 (bs, 1H, NH). APCI–HRMS: *m/z* = 1254.8827 $[M+H]^+$ (100%), calcd for $C_{81}H_{116}N_5O_6$ = 1254.8926. GPC (polystyrene, $CHCl_3$): V_R = 149.7 mL.

FbG2C12: Column chromatography (silica, hexane/EtOAc = 4/1). Yield (41%). ^{1}H-NMR (400 MHz, $CDCl_3$, 323 K): δ / ppm = 9.52 (s, 1H, meso), 9.40 (s, 1H, meso), 8.77 (d, J = 6.9 Hz, 2H, Pyα), 8.60 (s, 1H, meso), 8.52 (d, J = 16.1 Hz, 1H, vinyl), 7.67 (d, J = 6.0 Hz, 2H, Pyβ), 7.52 (d, J = 16.1 Hz, 1H, vinyl), 6.61 (s, 2H, Ph), 6.59 (s, 2H, Ph), 6.56 (s, 4H, Ph), 5.26 (d, J = 19.7 Hz, 1H, 13^2), 5.08 (d, J = 19.7 Hz, 1H, 13^2), 4.98 (d, J = 11.9 Hz, 1H, $\underline{CH_2}$Ph), 4.92 (d, J = 11.9 Hz, 1H, $\underline{CH_2}$Ph), 4.92 (s, 6H, $\underline{CH_2}$Ph), 4.50 (m, 1H, 18-H), 4.31 (m, 1H, 17-H), 3.92–3.66 (m, 20H, 8$\underline{CH_2}CH_3$ and a), 3.65 (s, 3H, ring CH_3), 3.46 (s, 3H, ring CH_3), 3.23 (s, 3H, ring CH_3), 2.72, 2.60, 2.35 (m, 1H, 1H, 2H, 17^1 and 17^2), 1.81 (d, J = 7.3 Hz, 3H,

18CH_3), 1.69 (m, 21H, 8$CH_2$$\underline{CH_3}$ and b), 1.46–1.24 (m, 162H, c and other alkyl-CH_2), 0.87 (m, 27H, d), 0.34 (bs, 1H, NH), and –1.73 (bs, 1H, NH). APCI–HRMS: *m/z* = 2679.0857 $[M+H]^+$ (100%), calcd for $C_{174}H_{278}N_5O_{15}$ = 2679.1178. GPC (polystyrene, $CHCl_3$): V_R = 140.6 mL.

FbG1TEG: Column chromatography (silica, $CHCl_3$/MeOH = 50/1). Yield (64%). ^{1}H-NMR (400 MHz, $CDCl_3$): δ / ppm = 9.51 (s, 1H, meso-10), 9.35 (s, 1H, meso-5), 8.77 (d, *J* = 6.0 Hz, 2H, Py), 8.62 (s, 1H, meso-20), 8.51 (d, *J* = 16.5 Hz, 2H, vinyl), 7.67 (d, *J* = 6.0 Hz, 2H, Py), 7.48 (d, *J* = 16.5 Hz, 2H, vinyl), 6.49 (s, 2H, Ph), 5.27 (d, *J* = 19.7 Hz, 1H, 13^2), 5.11 (d, *J* = 19.7 Hz, 1H, 13^2), 4.96 (d, *J* = 11.9 Hz, 1H, $\underline{CH_2}$Ph), 4.89 (d, *J* = 11.9 Hz, 1H, $\underline{CH_2}$Ph), 4.52 (m, 1H, 18-H), 4.32 (m, 1H, 17-H), 4.07 (m, 6H, PhO$\underline{CH_2}$), 3.67 (m, 32H, OCH_2, 8$\underline{CH_2}CH_3$, and ring CH_3), 3.49 (m, OCH_2 and ring CH_3), 3.34 (s, 3H, ring CH_3), 3.32 (s, 6H, OCH_3), 3.23 (s, 3H, OCH_3), 2.73, 2.62, 2.33 (m, 1H, 1H, 2H, 17^1 and 17^2), 1.82 (d, *J* = 7.3 Hz, 3H, 18CH_3), 1.70 (t, *J* = 7.80 Hz, 3H, 8$CH_2$$\underline{CH_3}$), 0.33 (bs, 1H, NH), and -1.79 (bs, 1H, NH). APCI–HRMS: *m/z* = 1188.6065 $[M+H]^+$ (100%), calcd for $C_{66}H_{86}N_5O_{15}$ = 1188.6120. HPLC (octadecylsilyl, MeOH/H_2O = 9/1): T_R = 8.21 min.

FbG2TEG: Column chromatography (silica, hexane/EtOAc = 4/1). Yield (38%). ^{1}H-NMR (400 MHz, $CDCl_3$, 323 K): δ / ppm = 9.52 (s, 1H, meso), 9.40 (s, 1H, meso), 8.77 (d, *J* = 6.9 Hz, 2H, Pyα), 8.60 (s, 1H, meso), 8.52 (d, *J* = 16.1 Hz, 1H, vinyl), 7.67 (d, J = 6.0 Hz, 2H, Pyβ), 7.52 (d, *J* = 16.1 Hz, 1H, vinyl), 6.61 (s, 2H, Ph), 6.59 (s, 2H, Ph), 6.56 (s, 4H, Ph), 5.26 (d, *J* = 19.7 Hz, 1H, 13^2), 5.08 (d, *J* = 19.7 Hz, 1H, 13^2), 4.98 (d, *J* = 11.9 Hz, 1H, $\underline{CH_2}$Ph), 4.92 (d, *J* = 11.9 Hz, 1H, $\underline{CH_2}$Ph), 4.92 (s, 6H, $\underline{CH_2}$Ph), 4.50 (m, 1H, 18-H), 4.31 (m, 1H, 17-H), 3.92–3.66 (m, 20H, 8$\underline{CH_2}CH_3$ and a), 3.65 (s, 3H, ring CH_3), 3.46 (s, 3H, ring CH_3), 3.23 (s, 3H, ring CH_3), 2.72, 2.60, 2.35 (m, 1H, 1H, 2H, 17^1 and 17^2), 1.81 (d, *J* = 7.3 Hz, 3H, 18CH_3), 1.69 (m, 21H, 8$CH_2$$\underline{CH_3}$ and b), 1.46–1.24 (m, 162H, c and other alkyl-CH_2), 0.87 (m, 27H, d), 0.34 (bs, 1H, NH), and –1.73 (bs, 1H, NH). APCI–HRMS: *m/z* = 2679.0857 $[M+H]^+$ (100%), calcd for $C_{174}H_{278}N_5O_{15}$ = 2679.1178. GPC (polystyrene, $CHCl_3$): V_R = 140.6 mL.

Zinc insertion: A saturated solution of $Zn(OAc)_2$•$2H_2O$ in methanol (3.0 mL) was added to a solution of free-base **FbD** (0.014 mmol) in $CHCl_3$ (30 mL), and then the resulting solution

was stirred for 3 h. The reaction was quenched by addition of dil. $NaHCO_3$, and the mixture was then poured into water. The organic layer was separated, and was washed with water. The aqueous layer was thoroughly extracted with $CHCl_3$. The combined organic layer was dried with Na_2SO_4, and the solvent was then eliminated *in vacuo* to afford **ZnD** as a brown solid.

ZnG1C12: Reprecipitation ($CHCl_3$/hexane). Yield (92%). ^{1}H-NMR (400 MHz, $CDCl_3$): δ / ppm = 9.60 (s, 1H, meso-10), 8.83 (s, 1H, meso-5), 8.31 (s, 1H, meso-20), 7.83 (d, J = 16.3 Hz, 1H, 3^1), 6.56 (d, J = 16.3 Hz, 1H, 3^2), 6.43 (s, 2H, Ph), 6.10 (bs, 2H, Pyβ), 5.20 (d, J = 20.2, 1H, 13^2), 5.05 (d, J = 20.2, 1H, 13^2), 4.95 (bs, 2H, $\underline{CH_2}$Ph), 4.42 (m, 1H, 18-H), 4.22 (m, 1H, 17-H), 3.79 (m, 8H, a and 8$\underline{CH_2}CH_3$), 3.70 (s, 3H, 12-CH_3), 3.39 (bs, 2H, Pyα), 3.08 (s, 3H, 2-CH_3), 3.01 (s, 3H, 7-CH_3), 2.64, 2.55, 2.24 (m, 1H, 1H, 2H, 17^1 and 17^2), 1.67 (m, 12H, 8$CH_2\underline{CH_3}$, 18CH_3, and b), 1.27 (m, 54H, alkyl CH_2 except for a and b), and 0.85 (m, 9H, d). APCI–HRMS: *m/z* = 1316.8134 $[M+H]^+$ (100%), calcd for $C_{81}H_{114}N_5O_6Zn$ = 1316.8061.

ZnG2C12: Reprecipitation ($CHCl_3$/CH_3CN). Yield (83%). ^{1}H-NMR (400 MHz, $CDCl_3$): δ / ppm = 9.60 (s, 1H, meso), 8.84 (s, 1H, meso), 8.33 (s, 1H, meso), 7.84 (d, J = 18.8 Hz, vinyl), 6.66 (s, 2H, Ph), 6.58 (m, 7H, vinyl and Ph), 6.10 (s, 1H, Py), 5.21 (d, J = 20.6 Hz, 1H, 13^2), 5.06 (d, J = 20.6 Hz, 1H, 13^2), 4.97, 4.94 (each s, total 8H, O$\underline{CH_2}$Ph), 4.45 (m, 1H, 18-H), 4.22 (m, 1H, 17-H), 3.90–3.69 (m, 23H, a and ring CH_3), 3.39 (s, 2H, Py), 3.09 (s, 3H, ring CH_3), 3.02, (s, 3H, ring CH_3), 2.64, 2.37, 2.21 (m, 2H, 1H, 1H, 17^1 and 17^2), 1.72–1.65 (m, 24H, 18CH_3, 8$CH_2\underline{CH_3}$, and b), 1.44–1.21 (m, 162H, other alkyl-CH_2), and 0.86 (m ,27H, d). APCI–HRMS: *m/z* = 2740.9948 $[M+H]^+$ (100%), calcd for $C_{174}H_{276}N_5O_{15}Zn$ = 2741.0313.

ZnG1TEG: Reprecipitation ($CHCl_3$/hexane). Yield (77%). ^{1}H-NMR (400 MHz, $CDCl_3$, 323 K): δ / ppm = 9.59 (s, 1H, meso-10), 8.87 (s, 1H, meso-5), 8.33 (s, 1H, meso-20), 7.87 (d, J = 16.7 Hz, 1H, 3^1), 6.63 (d, J = 16.7 Hz, 1H, 3^2), 6.49 (s, 2H, Ph), 6.18 (bs, 2H, Pyβ), 5.18 (d, J = 20.2, 1H, 13^2), 5.04 (d, J = 20.2, 1H, 13^2), 4.94 (bs, 2H, $\underline{CH_2}$Ph), 4.44 (m, 1H, 18-H), 4.22 (m, 1H, 17-H), 4.02 (m, 6H, OCH_2), 3.77–3.38 (m, 37H, OCH_2, ring CH_3, 8$\underline{CH_2}CH_3$, Pyα), 3.30 (s, 3H, OCH_3), 3.25 (s, 6H, OCH_3), 3.10 (s, 3H, ring CH_3), 3.02 (s, 3H, ring CH_3), 2.59, 2.27, (m, 2H, 2H, 17^1 and 17^2), and 1.72 (m, 6H, 8$CH_2\underline{CH_3}$ and 18CH_3). APCI–HRMS: *m/z* = 1250.5212 $[M+H]^+$ (100%), calcd for $C_{66}H_{84}N_5O_{15}Zn$ = 1250.5255.

ZnG2TEG: Reprecipitation ($CHCl_3$/Hex). Yield (94%). ^{1}H-NMR (400 MHz, $CDCl_3$): δ / ppm = 9.59 (s, 1H, meso), 8.86 (s, 1H, meso), 8.35 (s, 1H, meso), 7.88 (d, J = 18.8 Hz, vinyl), 6.63–6.61 (m, 9H, vinyl and Ph), 6.20 (s, 1H, Py), 5.19 (d, J = 19.2 Hz, 1H, 13^2), 5.05 (d, J = 19.2 Hz, 1H, 13^2), 4.98, 4.94 (each s, total 8H, O$\underline{CH_2}$Ph), 4.45 (m, 1H, 18-H), 4.21 (m, 1H, 17-H), 4.09–3.92 (m, 18H, PhO$\underline{CH_2}CH_2$), 3.76–3.42 (m, 97H, $8CH_2CH_3$, Py, ring CH_3, and other CH_2 in TEG), 3.37, 3.36–3.28 (m, 27H, terminal CH_3 in TEG), 3.11 (s, 3H, ring CH_3), 3.04 (s, 3H, ring CH_3) 2.65–2.19 (m, total 4H, 17^1 and 17^2), 1.72–1.69 (m, 6H, $18CH_3$, $8\underline{CH_2}CH_3$). MALDI-TOF MS (2,5-dihydroxybenzoic acid): m/z = 2564 $[M+Na]^+$ (100%), calcd for $C_{129}H_{185}N_5NaO_{42}Zn$ = 2564.

5-5 References

(1) Roszak, A. W.; Howard, T. D.; Southall, J.; Gardiner, A. T.; Law, C. J.; Isaacs, N. W.; Cogdell, R. J. *Science* **2003**, *302*, 1969.

(2) McDermott, G.; Prince, S. M.; Freer, A. A.; Hawthornthwaite-Lawless, A. M.; Papiz, M. Z.; Cogdell, R. J.; Isaacs, N. W. *Nature* **1995**, *374*, 517.

(3) Choi, M.-S.; Aida, T.; Yamazaki, T.; Yamazaki, I. *Chem. Eur. J.* **2002**, *8*, 2667.

(4) Choi, M.-S.; Yamazaki, T.; Yamazaki, I.; Aida, T. *Angew. Chem. Int. Ed.* **2004**, *43*, 150.

(5) Kobuke, Y. *Eur. J. Inorg. Chem.* **2006**, 2333.

(6) Aratani, N.; Kim, D.; Osuka, A. *Acc. Chem. Res.* **2009**, *42*, 1922.

(7) Smith, K. M.; Goff, D. A.; Simpson, D. J. *J. Am. Chem. Soc.* **1985**, *107*, 4946.

(8) Tamiaki, H.; Miyata, S.; Kureishi, Y.; Tanikag, R. *Tetrahedron* **1996**, *52*, 12421.

(9) Percec, V.; Wilson, D. A.; Leowanawat, P.; Wilson, C. J.; Hughes, A. D.; Kaucher, M. S.; Hammer, D. A.; Levine, D. H.; Kim, A. J.; Bates, F. S.; Davis, K. P.; Lodge, T. P.; Klein, M. L.; DeVane, R. H.; Aqad, E.; Rosen, B. M.; Argintaru, A. O.; Sienkowska, M. J.; Rissanen, K.; Nummelin, S.; Ropponen, J. *Science* **2010**, *328*, 1009.

(10) Miyatake, T.; Tamiaki, H.; Shinoda, H.; Fujiwara, M.; Matsushita, T. *Tetrahedron* **2002**, *58*, 9989.

(11) Shinozaki, Y.; Richards, G.; Ogawa, K.; Yamano, A.; Ohara, K.; Yamaguchi, K.; Kawano, S.-i.; Tanaka, K.; Araki, Y.; Wada, T.; Otsuki, J. *J. Am. Chem. Soc.* **2013**, *135*, 5262.

(12) Li, J. Z.; Wang, J. J.; Yoon, I.; Cui, B. C.; Shim, Y. K. *Bioorg. Med. Chem. Lett.* **2012**, *22*, 1846.

(13) Sasaki, S.-i.; Mizutani, K.; Kunieda, M.; Tamiaki, H. *Tetrahydron* **2011**, *67*, 6065.

(14) Tamiaki, H.; Holzwarth, A. R.; Schaffner, K. *J. Photochem. Photobiol. B: Biol.* **1992**, *15*, 355.

(15) Tamiaki, H.; Yagai, S.; Miyatake, T. *Bioorg. Med. Chem.* **1998**, *6*, 2171.

(16) Ercolani, G. *J. Phys. Chem. B* **1998**, *102*, 5699.

(17) Numata, M.; Kinoshita, D.; Hirose, N.; Kozawa, T.; Tamiaki, H.; Kikkawa, Y.; Kanesato, M. *Chem. Eur. J.* **2013**, *19*, 1592.

(18) Oliva, A. I.; Gómez, K.; Gonzáleza, G.; Ballester, P. *New J. Chem.* **2008**, *32*, 2159.

(19) Sprafke, J. K.; Odell, B.; Claridge, T. D. W.; Anderson, H. L. *Angew. Chem. Int. Ed.* **2011**, *50*, 5572.

5-6 Appendix

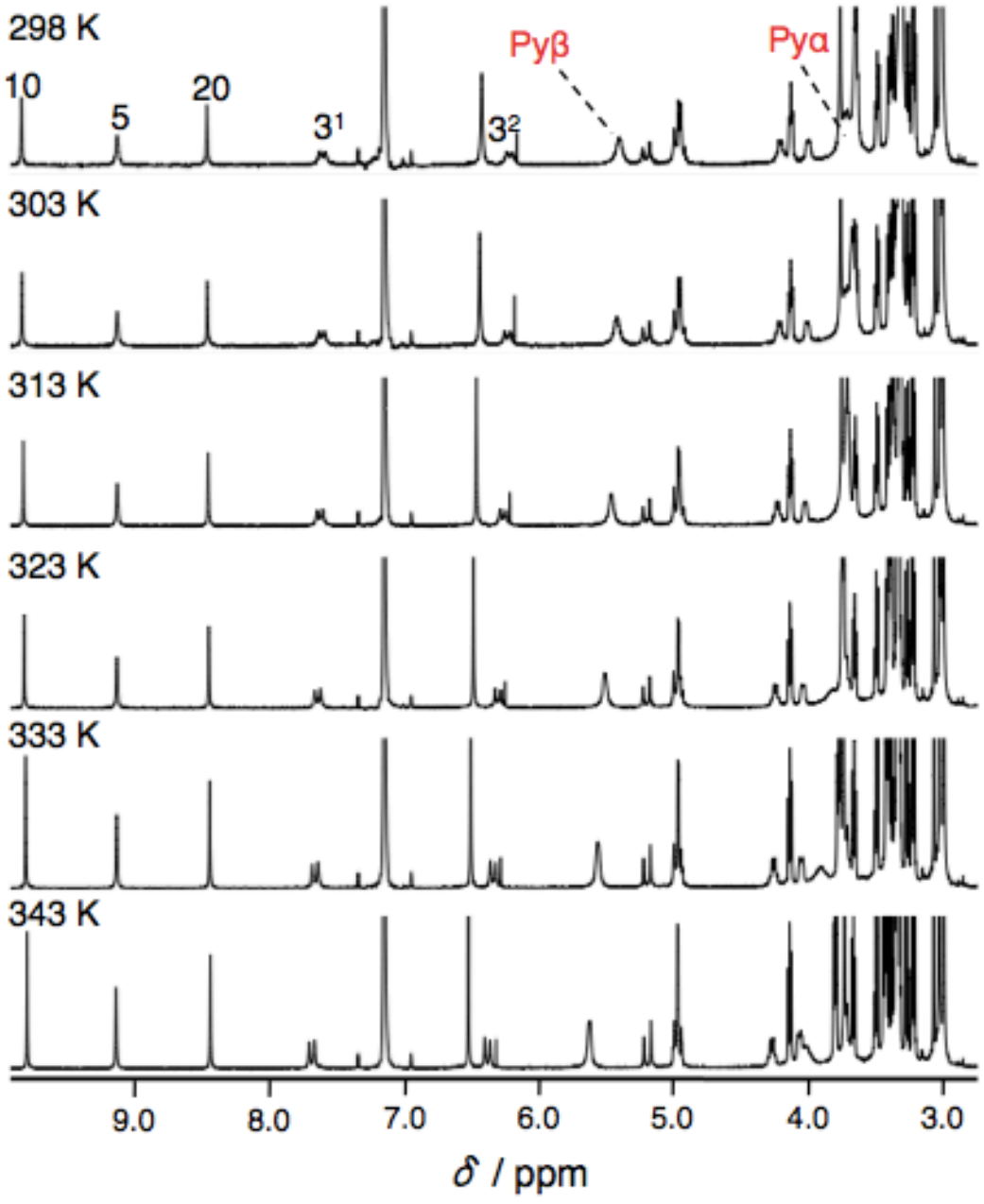

Figure 5A-1. ^{1}H-NMR spectra of **ZnG1TEG** in C_6D_6 (10 mM) in a range of 298–343 K.

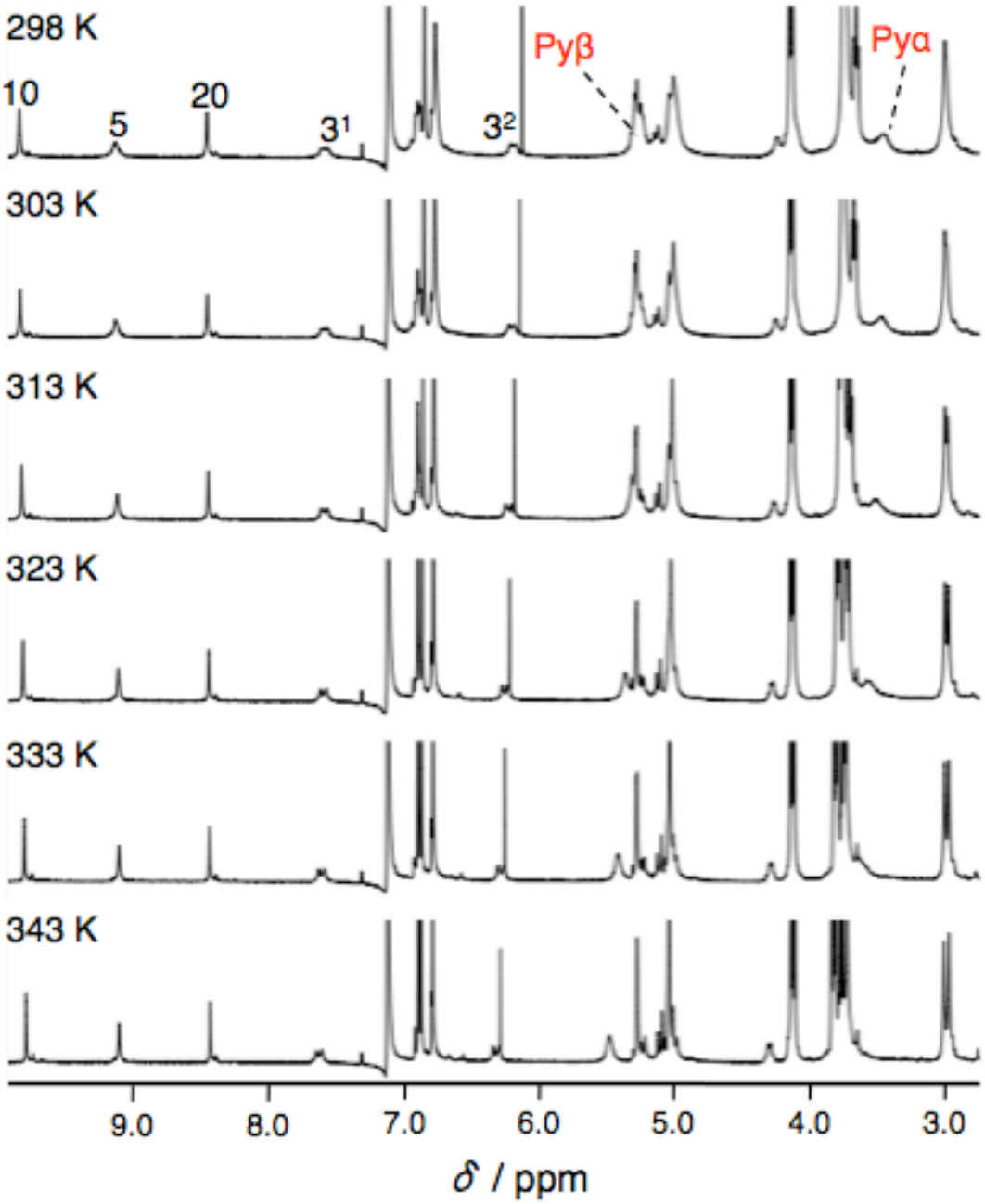

Figure 5A-2. ^{1}H-NMR spectra of **ZnG2C12** in C_6D_6 (10 mM) in a range of 298–343 K.

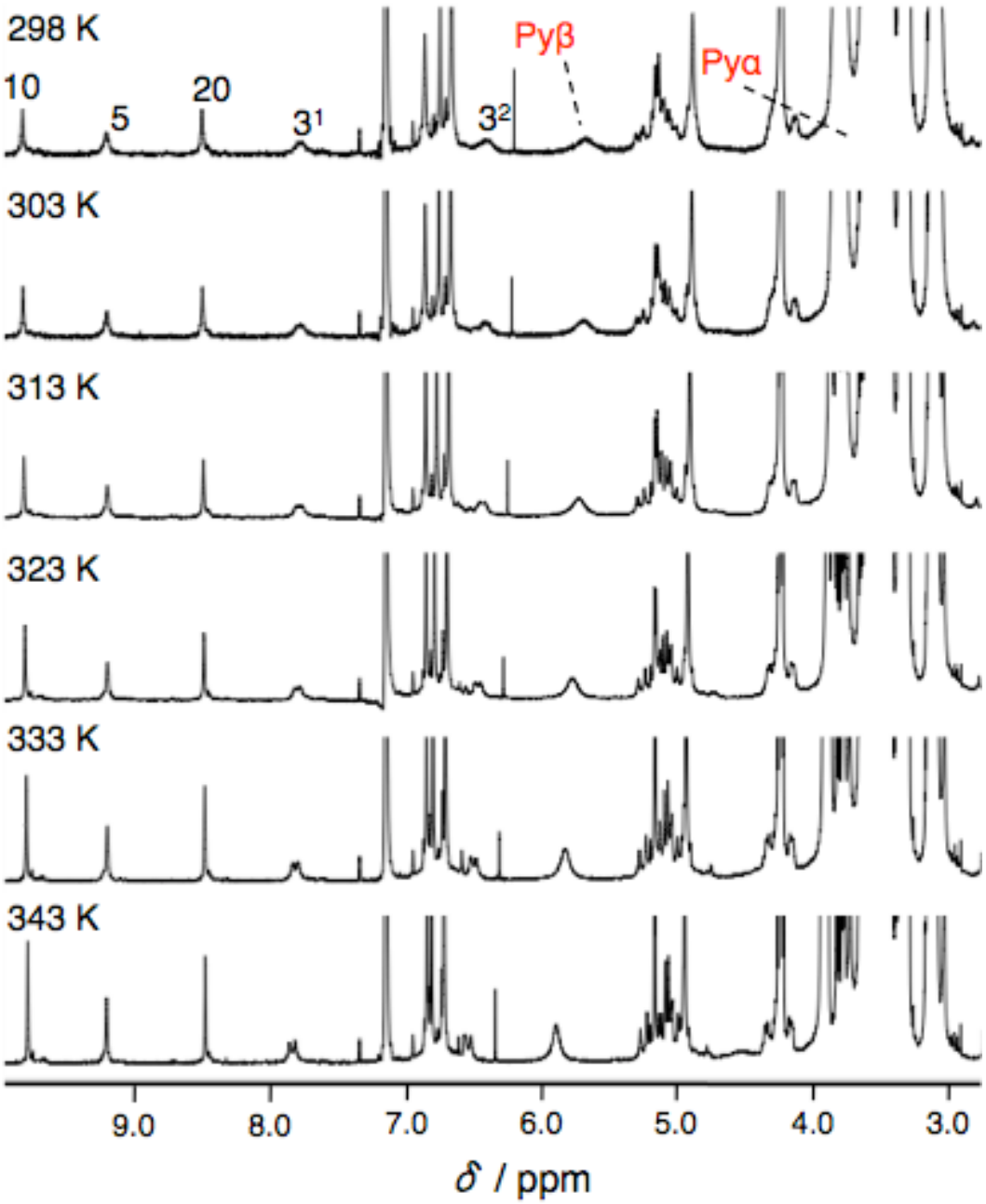

Figure 5A-3. ^{1}H-NMR spectra of **ZnG2TEG** in C_6D_6 (10 mM) in a range of 298–343 K.

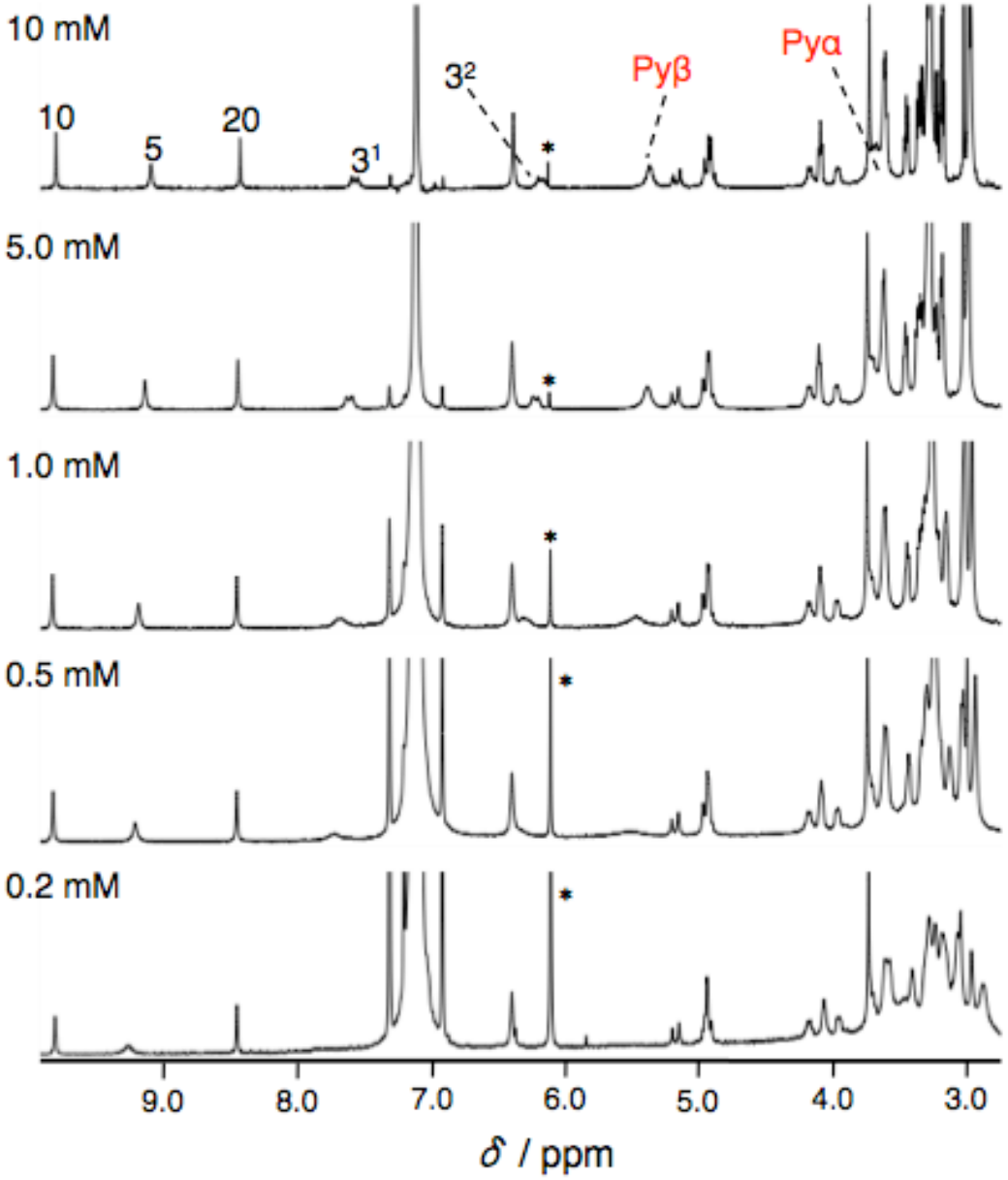

Figure 5A-4. ^{1}H-NMR spectra of **ZnG1TEG** in C_6D_6 in the concentration range of 10–0.2 mM at 298 K. Asterisk indicates residual $CHCl_3$.

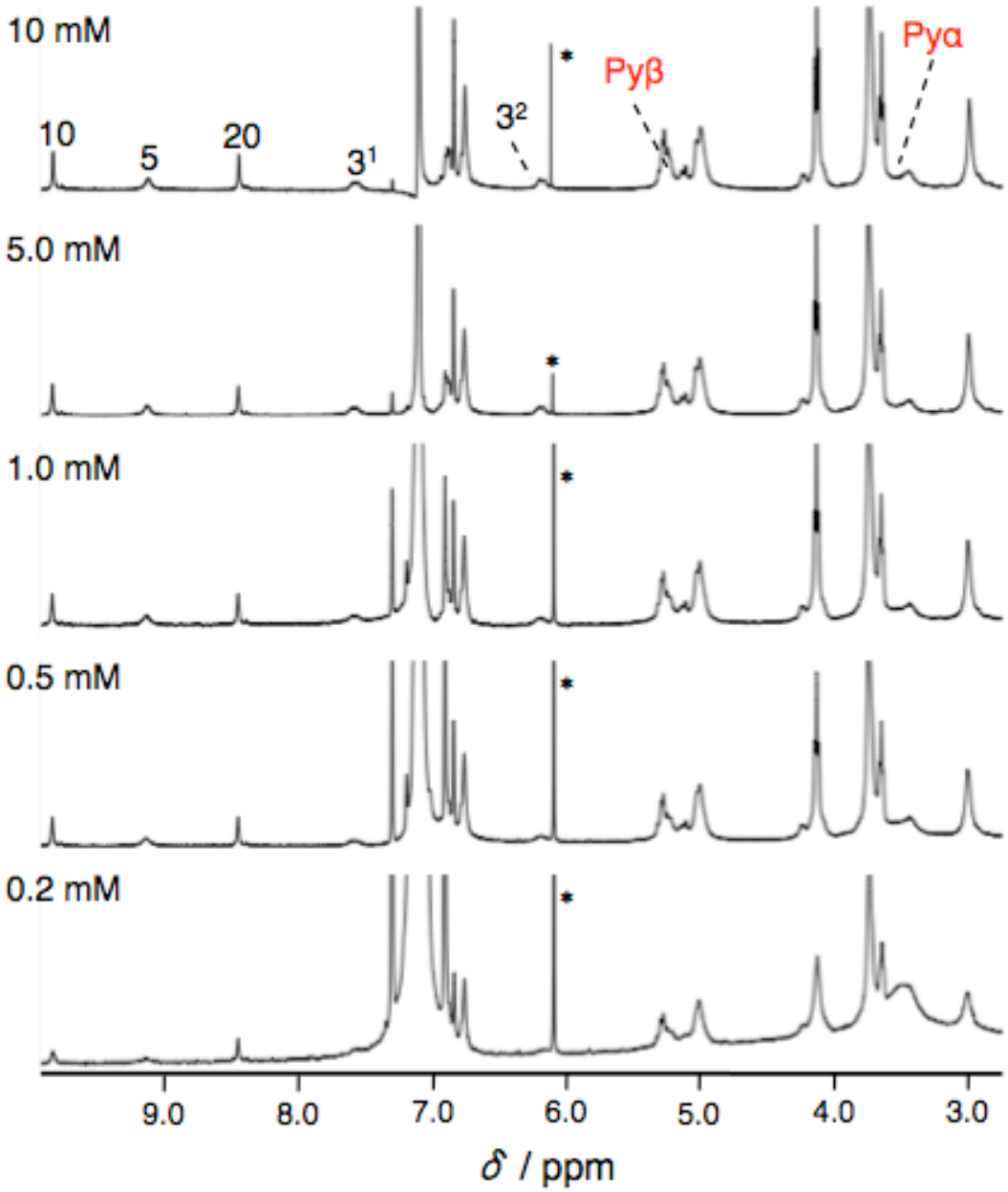

Figure 5A-5. ^{1}H-NMR spectra of **ZnG2C12** in C_6D_6 in the concentration range of 10–0.2 mM at 298 K. Asterisk indicates residual $CHCl_3$.

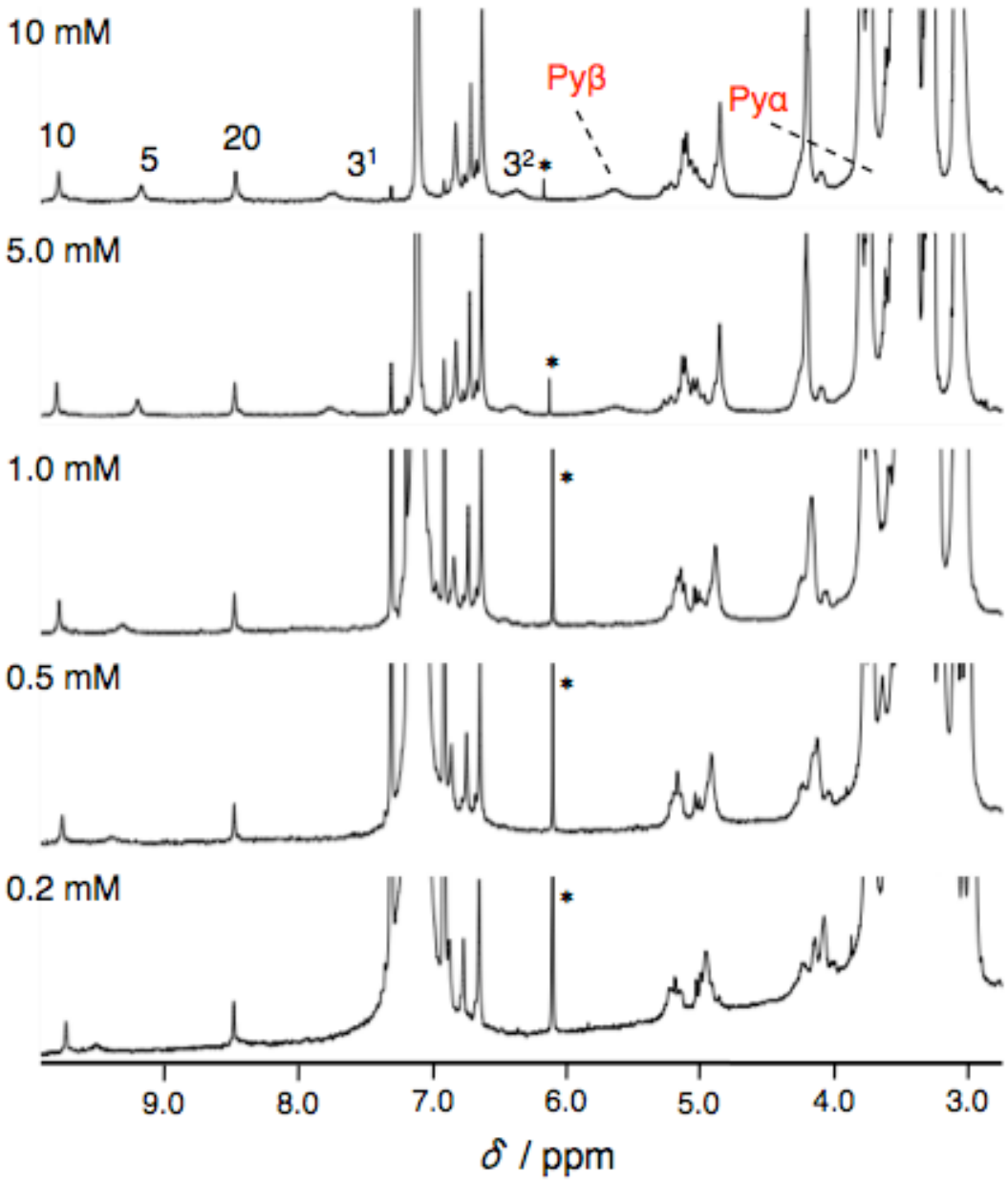

Figure 5A-6. ^{1}H-NMR spectra of **ZnG2TEG** in C_6D_6 in the concentration range of 10–0.2 mM at 298 K. Asterisk indicates residual $CHCl_3$.

Chapter 6

Demonstration of Antenna Function of Zinc Chlorophyll Cyclic Tetramers

6-0 Summary

We demonstrated the antenna function of the cyclic tetramers by coassembly of the pyridine-appended zinc chlorophyll derivative **Zn4Py** and its fullerene dyad **Zn4PyC$_{60}$** *via* intermolecular coordination interaction between the nitrogen atom in the pyridine group and the zinc center in chlorophyll ring. The coassembly into the cyclic tetramers was proved by antenna effect arising from the energy transfer within the zinc chlorophyll moiety in the cyclic tetramers followed by the fluorescence quenching within **Zn4PyC$_{60}$** components in the cyclic tetramers.

6-1 Introduction

Natural light-harvesting system converts the light energy into the chemical potential.[1-3] The excitation energy of the chlorophyll molecules in the LH1 and LH2 pigment–protein complexes are transferred to the reaction center (RC) residing at the center of LH1. The excited special pair in the RC, which resulted in the consecutive energy transfer in the light-harvesting system, initiates the multiple electron transfer reactions in the RC (1-2). While a number of researchers has attempted to construct the LH model (1-2),[4,5] to imitate the RC-LH system has been one of the significant challenges.[6] For example, Kobuke and coworkers reported the haxagonal assembly of a zinc porphyrin dimer (1-2) incorporating fullerene as an electron acceptor from the porphyrins, in which the excitation energy migrates among the porphyrin dimer units followed by the electron transfer from the porphyrin array to the fullerene.[7]

We have described until here the construction of light-harvesting antenna models by self-assembly of zinc chlorophyll derivatives appended by *N*-heterocycles *via* intermolecular axial coordination between the nitrogen atom in the heterocycle and the zinc atom in the center of the chlorophyll ring (Chapter 2–5). The zinc chlorophyll derivatives appended by *N*-heterocycles form the cyclic oligomers in solution while they form the coordination polymers in their crystals as described in Chapters 2 and 3.[8,9] We particularly focused on the coordination polymers, suggesting their application potentiality for the antennae in Chapters

2–4.[8-10] The cyclic oligomers are also promising arrays for the antenna model beside the coordination polymers due to their cyclic geometry reminiscent of LHs in purple bacteria (1-1 and 1-2). We addressed the improvement of the solubility of the cyclic oligomers in Chapter 5 since the poor solubility of the cyclic oligomers presented until Chapter 4 limits further modification and investigation of detailed photochemistry of the oligomers. The dendron moiety was required in the zinc chlorophyll structure to solubilize the cyclic oligomers. We herein demonstrate the construction of the cyclic tetramers with LH-RC function by coassembly of a zinc chlorophyll derivative appended by pyridine and dendron **Zn4Py** and its fullerene dyad **Zn4PyC$_{60}$** (Chart 6-1) in solution and their potentiality for the light-harvesting antennae.

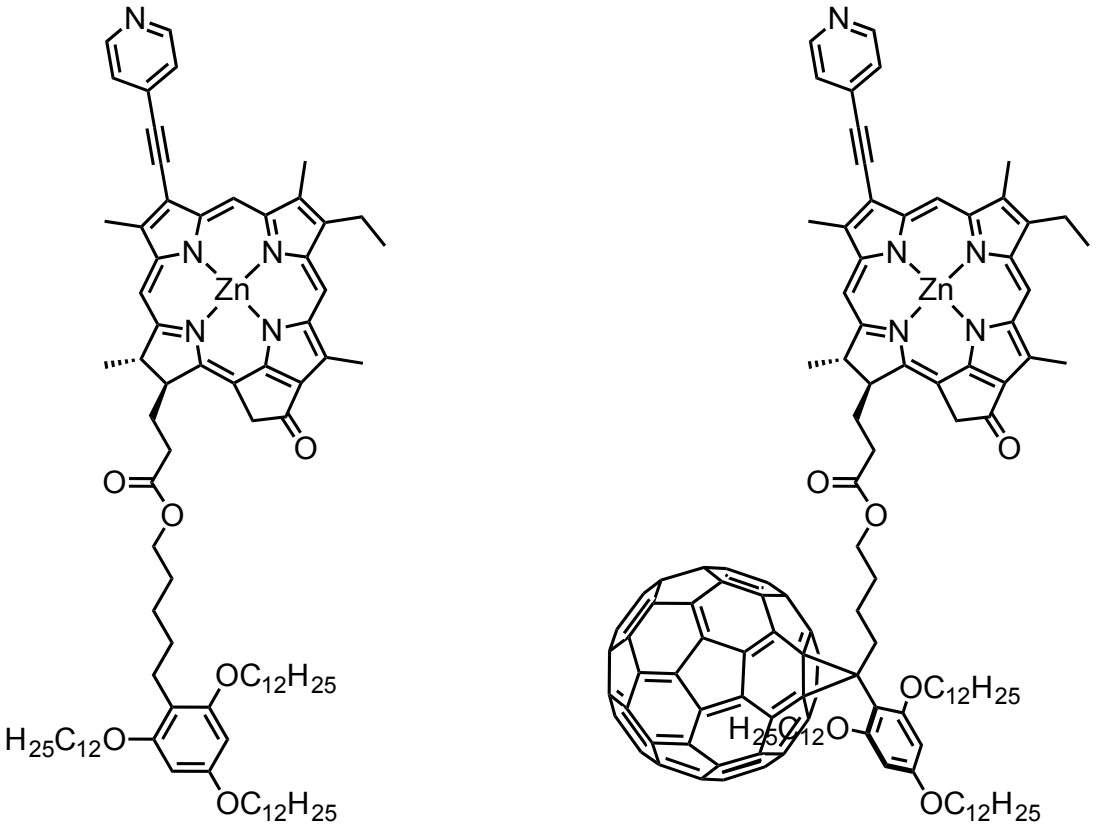

Chart 6-1. Chemical structures of the zinc chlorophyll derivative appended by pyridine **Zn4Py** and its fullerene dyad **Zn4Py C$_{60}$.**

6-2 Results and Discussion

6-2-1 Syntheses

The synthetic procedures of the zinc chlorophyll derivative appended by pyridine **Zn4Py** and its fullerene dyad **Zn4PyC$_{60}$** are shown in Schemes 6-1 and 6-2. The fullerene moiety in **Zn4PyC$_{60}$** was synthesized through seven steps from 2,4,6-trihydroxybenzene **1** as the starting compound. The hydroxyl groups in 1,3,5-trihydroxybenzene were etherified by 1-bromododecane to give 1,3,5-tridodecanoxybenzne **2**. The Friedel–Crafts acylation of the alkoxybenzne using glutaric anhydride to give the 4-benzoylbutylic acid **3**. The methyl ester **4** was obtained by use of the Fischer esterification of the acid **3** in methanol in the presence of catalytic amount of sulfuric acid. The substitution of the carbonyl group of **4** with tosyl hydrazide in methanol did not proceed probably due to the steric repulsion of the alkoxy groups. Alternatively, the tosyl hydrazone **7** was almost quantitatively obtained by the general condition for the imine synthesis using *p*-toluene sulfonic acid (*p*TsOH) as an acid catalyst. The 1,3-dipolar addition of a diazo compound *in situ* generated by the base-induced decomposition of the hydrazone **7** to fullerene gave the [5,6] isomers **8**. The isomerization of the [5,6] isomers to the [6,6] isomer **9** was accomplished by heating in *o*-dichlorobenzene for five days. The total conversion of the [5,6] isomers **8** was confirmed by HPLC analysis using a reverse-phase column (ODS). The methyl ester group in **9** was reduced by use of diisobutyl aluminum hydride (DIBAL-H) to afford an alcoholic fullerene **10**.

The conjugation of the alcoholic fullerene **10** with the chlorophyll was explored in three routes (Scheme 6-3): (i) the hydrolysis of the methyl ester group in the ethynyl chlorophyll **18** (see Chapter 4)[11] followed by the esterification of resulting free carboxylic acid with the alcoholic fullerene **10**; (ii) the formyl group in pyropheophorbide-*d* **20** which has the free carboxylic acid group at the 17^2 position is converted to the ethynyl group followed by the Sonogashira coupling with 4-iodopyridine and the esterification with the alcoholic fullerene **10**; and (iii) the transesterification of the methyl ester group in the chlororphyll **15** or **19**[12] with the alcoholic fullerene **10**. The first route was unsuccessful probably due to *cis*-addition of hydrochloric acid to the ethynyl group in the ethynyl chlorophyll **18** during the

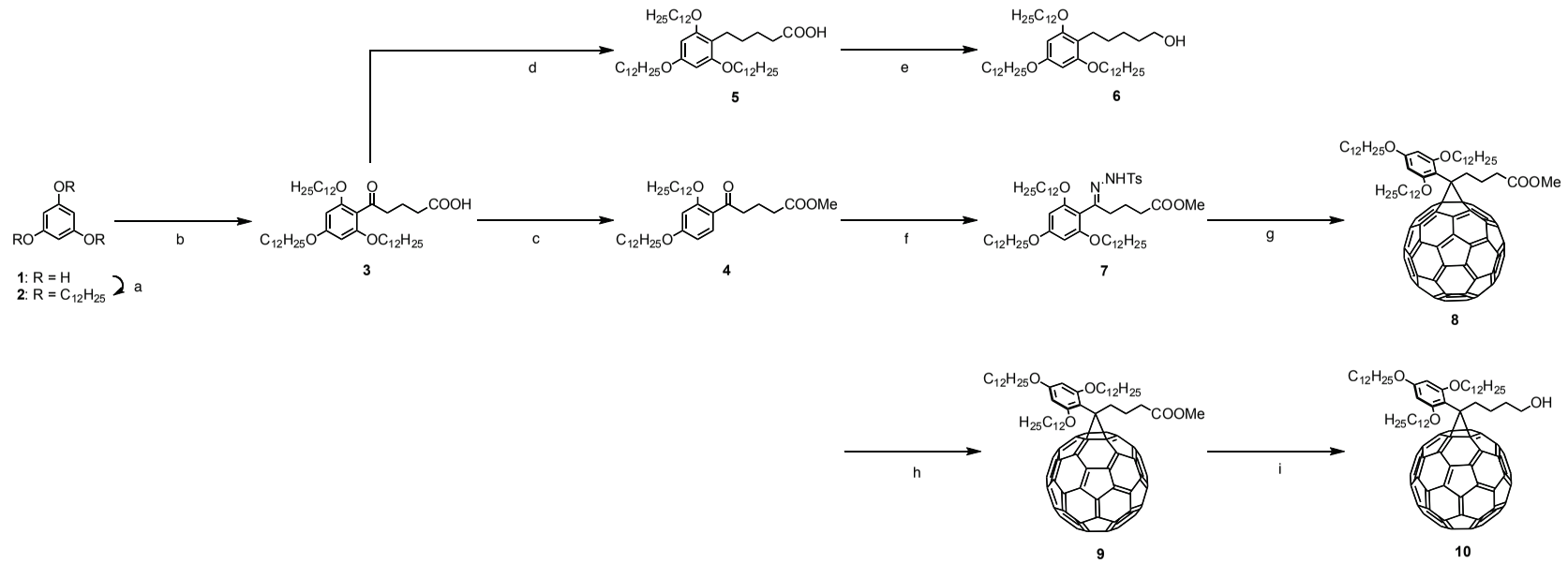

Scheme 6-1. Synthetic procedures of dendron moiety in the **Zn4Py** and **Zn4PyC$_{60}$**. a) $BrC_{12}H_{25}$, K_2CO_3, DMF, reflux, 24 h. b) Glutaic anhydride, $AlCl_3$, CH_2Cl_2, 0 ^oC, 10 min, r.t. overnight. c) H_2SO_4, MeOH, reflux, overnight. d) H_2, Pd/C, AcOH, EtOH, overnight. e) LiAlH, THF, reflux, 3.5 h. f) *p*TsNHNH$_2$, *p*TsOH•H_2O, toluene, reflux, 2.5 h. g) NaOMe, pyridine, 1 h, C_{60}, *o*-DCB, reflux, overnight. h) *o*-DCB, reflux, 5 days. i) DIBAL-H, heptane, toluene, overnight.

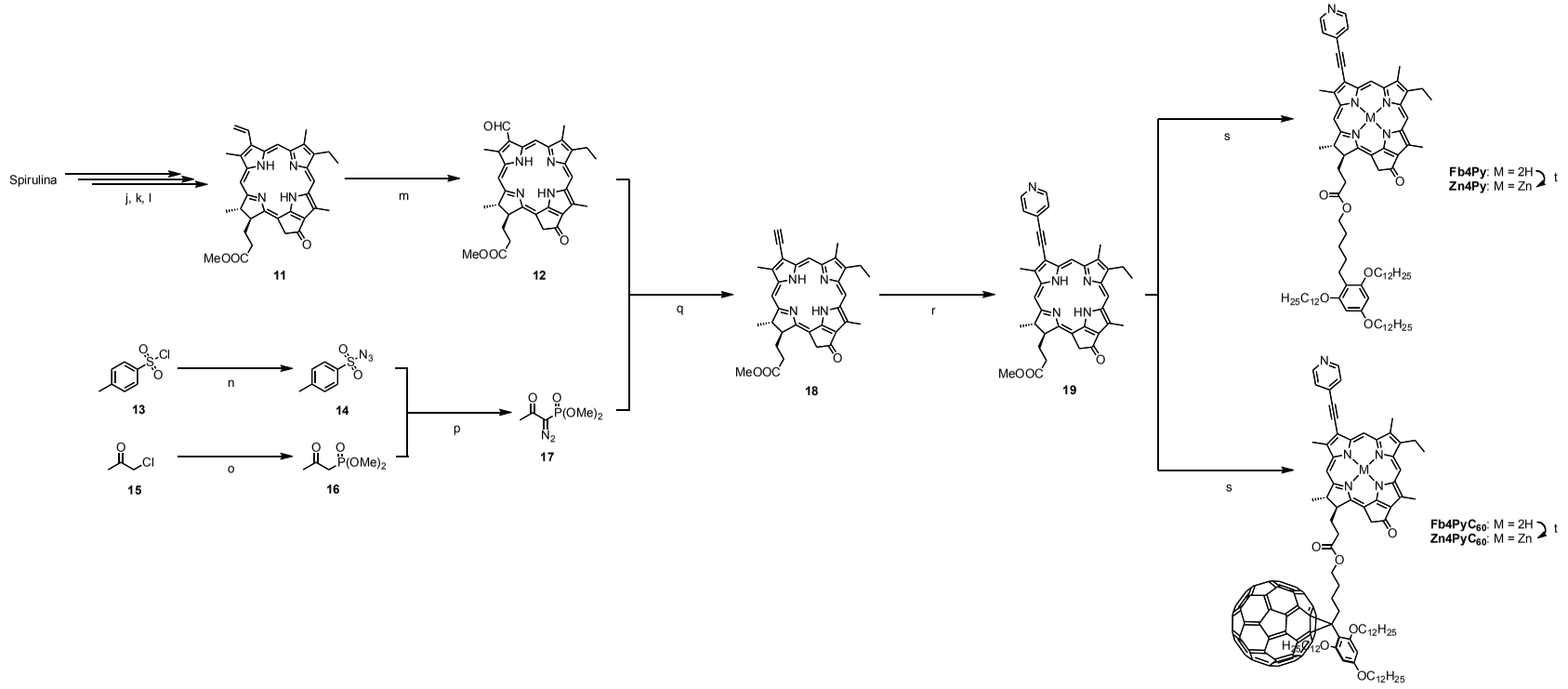

Scheme 6-2. Synthetic procedures of the **Zn4Py** and **Zn4PyC$_{60}$**. j) acetone, reflux, 10 days. k) H_2SO_4, MeOH, overnight. l) 2,4,6-collidine, reflux, 3 h. m) OsO_4, $NaIO_4$, AcOH, THF, H_2O, overnight. n) NaN_3, acetone, 2 h. o) KI, CH_3CN, acetone, $P(OMe)_3$, 22 h, 50 ^oC, 30 min. p) K_2CO_3, CH_3CN, 6 h. q) $CsCO_3$, THF, MeOH, 3 h. r) $Pd_2(dba)_3$, P(*o*-tolyl)$_3$, Et_3N, toluene, reflux, overnight. s) **6** or **10**, bis(dibutylchlorotin(IV))oxide, toluene, reflux, overnight. t) $Zn(OAc)_2 \bullet 2H_2O$, MeOH, $CHCl_3$, 3 h.

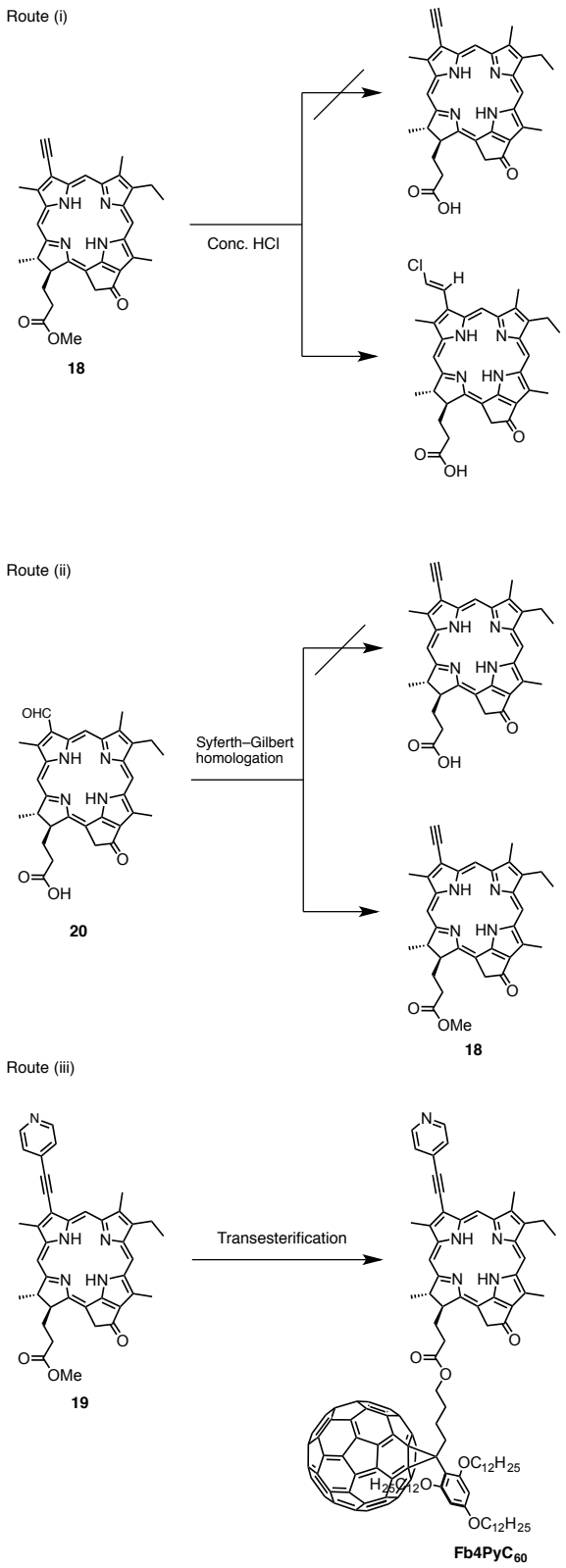

Scheme 6-3. Exploration of the synthetic route to **FbPyC$_{60}$**.

attempted hydrolysis of the methyl ester with conc. HCl (Route (i), Scheme 6-3). Although the hydrolysis under basic condition could be also considered, it is known that the condition using lithium hydroxide generally used for the hydrolysis of chlorophyll compounds gave several by-products resulting in low yield.[13] The transformation of the formyl group in pyropheophorbide-*d* **20** by the Syferth–Gilbert homologation gave the methy ester **18** due to the esterification with methanol used as the solvent (Route (ii), Scheme 6-3). We successfully obtained the fullerene–zinc chlorophyll conjugate **Fb4PyC$_{60}$** following the route (iii) (Scheme 6-2 and Scheme 6-3 Route (iii)). The methyl ester group in pyridylchlorophyll **19** which was prepared by the Sonogashira coupling of the ethynyl chlorophyll **18** with 4-iodopyridine in the copper-free condition was transesterified with the alcoholic fullerene **10** using bis(dibutylchlorotin(IV)) oxide to afford the fullerene–free-base chlorophyll dyad **Fb4PyC$_{60}$** (77%).[14] The zinc insertion to the free-base compound using zinc acetate dihydrate ($Zn(OAc)_2$•$2H_2O$) almost quantitatively afforded the zinc complex **Zn4PyC$_{60}$**.[15] The zinc pyridylchlorophyll **Zn4Py** without fullerene was prepared by a similar procedure using 5-phenylpentanol derivative **6**, which was obtained through four steps from 1,3,5-trihydroxybenzene as a starting compound instead of the alcoholic fullerene **10** (Schemes 6-1 and 6-2).

6-2-2 Photophysical Properties

The absorption spectra of the zinc complexes **Zn4PyC$_{60}$** in neat benzene and benzene containing 1% pyridine, which prevent an intermolecular interaction as mentioned later, (~5 μM) are shown in Figure 6-1.[15,16] These spectra of **Zn4PyC$_{60}$** are composed of the absorption of zinc chlorophyll and fullerene moieties. The five peaks in the region longer than ~400 nm is due to absorption of zinc chlorophyll moiety whereas a peak at ~330 nm is that of fullerene moiety. The spectrum of **Zn4PyC$_{60}$** in neat benzene differs from the superimposed spectra of **Zn4Py** and fullerene derivative **9** as indicated by the sigmoidal features around ~450 and ~700 nm in the difference spectrum of **Zn4Py** and **Zn4PyC$_{60}$** (Figure 6-1a), which are ascribed to the self-assembly of the zinc chlorophylls since the absorption spectrum of

(a)

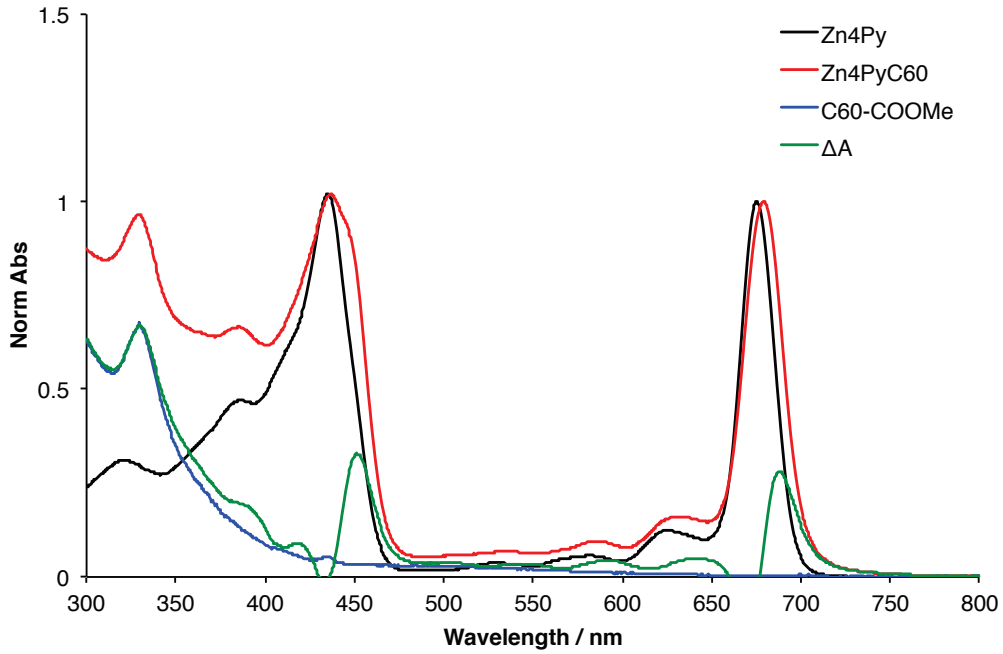

(b)

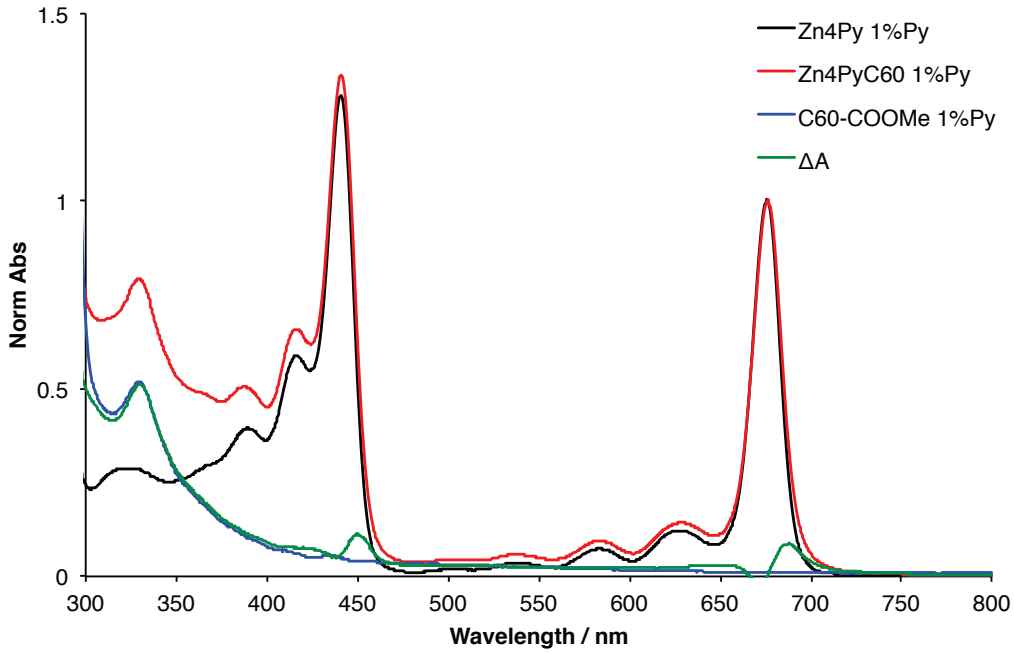

Figure 6-1. Absorption spectra of **Zn4PyC$_{60}$** in (a) neat benzene and (b) benzene containing 1% pyridine (5.0 μM) at 298 K.

in

(a)

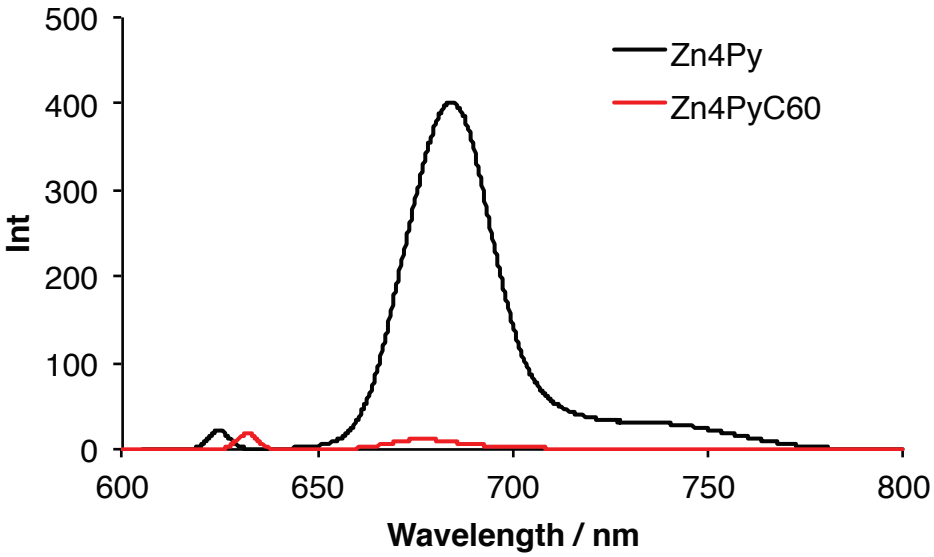

(b)

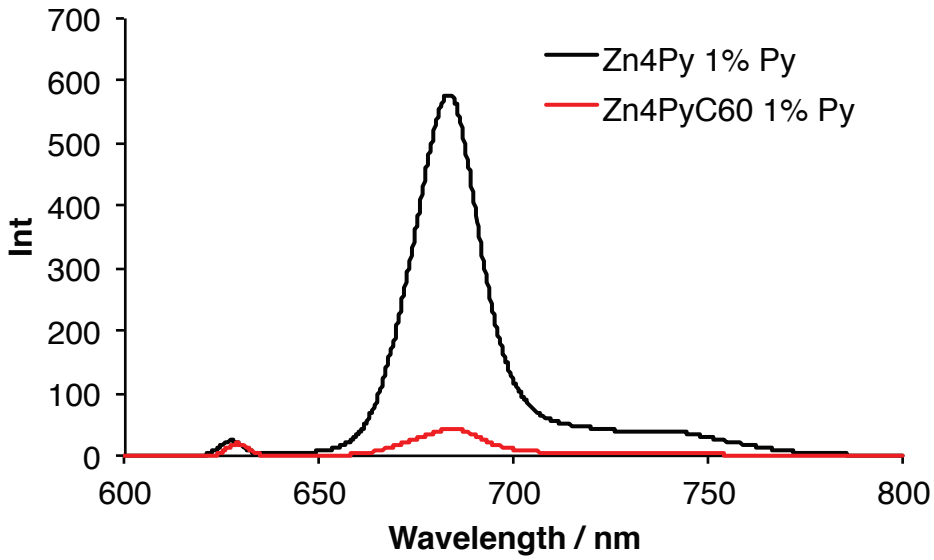

Figure 6-2. Fluorescence spectra of **Zn4Py** and **Zn4PyC$_{60}$** in (a) benzene and (b) benzene containing 1% pyridine (5.0 μM) at r.t.

Zn4PyC$_{60}$ in benzene containing 1% pyridine agrees with the superposition of component spectra (Figure 6-1b), indicating that the zinc chlorophyll and fullerene moieties in **Zn4PyC$_{60}$** molecules do not interact in their ground state. The fluorescence spectra of the zinc complexes **Zn4Py** and **Zn4PyC$_{60}$** are shown in Figure 6-2. The intense fluorescence was observed for **Zn4Py** whereas that of **Zn4PyC$_{60}$** was significantly quenched in both neat benzene (Figure 6-2a) and benzene containing 1% pyridine (Figure 6-2b), suggesting that intramolecular electron transfer (ICT) or energy transfer occurs between the zinc chlorophyll moiety and the fullerene moiety of **Zn4PyC$_{60}$**.[17-19]

6-2-3 Self-Assembly

The self-assembly of the zinc chlorophyll derivatives in solution was confirmed by ^{1}H-NMR measurements including diffusion-ordered spectroscopy (DOSY). The ^{1}H-NMR spectra of the free-base chlorophylls **Fb4Py** and **Fb4PyC$_{60}$** and their zinc complexes **Zn4Py** and **Zn4PyC$_{60}$** in C_6D_6 (10 mM, 298 K) are shown in Figure 6-3. Whereas the signals of pyridyl protons appeared in the aromatic region in the case of the free-base chlorophylls (Pyα 8.64 ppm/**Fb4Py**, 8.64 ppm/**Fb4PyC$_{60}$**, Pyβ 7.40 ppm//**Fb4Py**, 7.40 ppm/**Fb4PyC$_{60}$**), those of the zinc complexes were significantly shifted to the up-field region (Pyα 3.45 ppm/**Zn4Py**, 3.52 ppm/**Zn4PyC$_{60}$**, Pyβ 5.42 ppm//**Zn4Py**, 5.46 ppm/**Zn4PyC$_{60}$**). Further the magnitude of the up-field shift of the signals increased with decreasing the distance between the proton and nitrogen atom in the pyridine ring. These trends are consistent with self-assembly of the zinc chlorophyll derivatives appended by pyridine as a coordination site in Chapters 2, 4, and 5, which is induced by an intermolecular coordination interaction between the nitrogen atom in pyridine ring (N_{Py}) to the zinc center in chlorin ring as mentioned in those chapters, indicating that **Zn4Py** and **Zn4PyC$_{60}$** molecules interact *via* N_{Py}–Zn axial coordination in solution. The chemical shift of these upfield-shifted signals was almost insensitive to the wide range of temperature (298–343 K, Figure 6-4), The insensitivity of the chemical shifts over the wide temperature range together with the upfield-shifted signals were results generally observed when the zinc chlorophyll derivatives form the cyclic oligomers as shown in Chapters 2,3, and

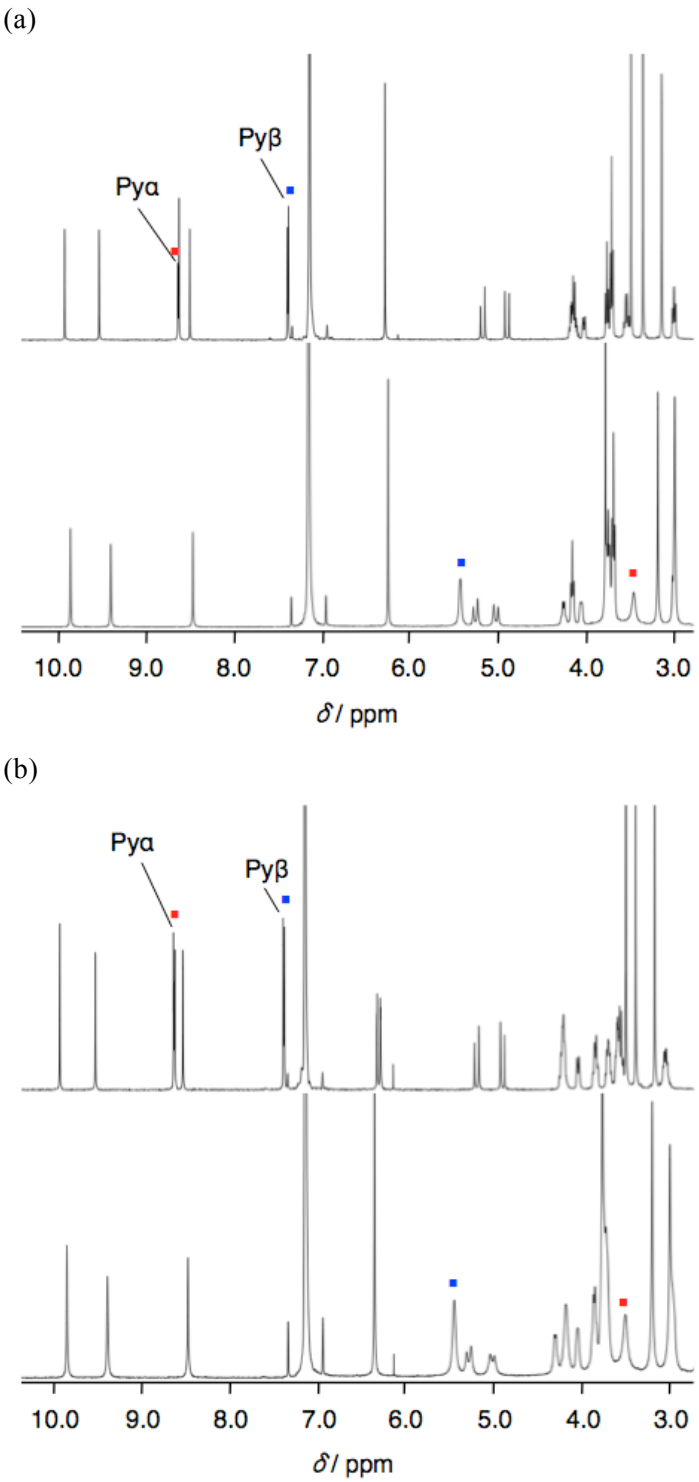

Figure 6-3. ^{1}H-NMR spectra of the free-base chlorophyll (upper) and the zinc complexes (lower) in C_6D_6 (10 mM, 298 K). (a) **Fb4Py** and **Zn4Py**. (b) **Fb4PyC$_{60}$** and **Zn4PyC$_{60}$**.

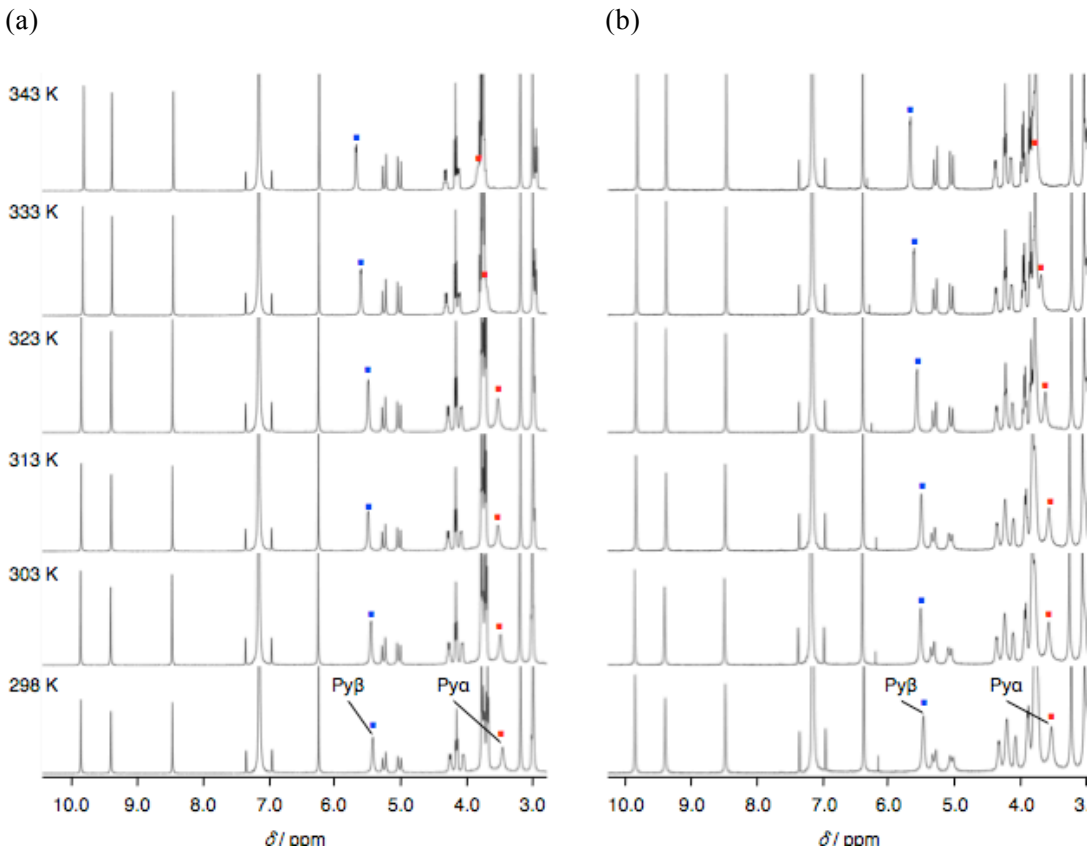

Figure 6-4. ^{1}H-NMR spectra of (a) **Zn4Py** and (b) **Zn4PyC$_{60}$** in C_6D_6 (10 mM) in the temperature range of 298–343 K. The red and blue dots indicate the α and β proton signals of the pyridine moiety, respectively.

5, suggesting that **Zn4Py** and **Zn4PyC$_{60}$** also form the cyclic oligomers.

The diffusion constant (D) of the zinc complexes was obtained by DOSY measurement in C_6D_6 (10 mM, 298 K). The D values for the zinc complexes **Zn4Py** and **Zn4PyC$_{60}$** were determined to be (2.81±0.01) $\times 10^{-10}$ m^2 s^{-1} and (2.28±0.01)$\times 10^{-10}$ m^2 s^{-1}, respectively, while the free-base compounds **Fb4Py** and **Fb4PyC$_{60}$** gave the D values of (4.23±(0.02)$\times 10^{10}$ m^2 s^{-1}) and (3.58±(0.01) $\times 10^{10}$ m^2 s^{-1}), respectively. The smaller D values of the zinc complexes than those of the free-base compounds indicate that the zinc complexes form the self-aggregates in solution. The hydrodynamic radiuses (r) were estimated by use of the Stokes–Einstein equation (1),[20,21]

$$r = k_B T / 6\pi\eta D \quad (1)$$

where k_B, T, and η are the Boltzmann constant, absolute temperature, and viscosity of the medium, respectively. While the r values of the free-base compounds **Fb4Py** and **Fb4PyC$_{60}$** were determined to be 8.5 Å and 10.1 Å, respectively, which are in accordance with the dimensions of their monomeric models which were constructed with MM3 force-field calculation, the value of the zinc complexes were obviously larger (12.9 Å/**Zn4Py**, 15.9 Å/**Zn4PyC$_{60}$**), reflecting the self-assembly of the zinc complexes. The larger radius of the fullerene conjugates **Fb4PyC$_{60}$** and **Zn4PyC$_{60}$** than those of **Fb4Py** and **Zn4Py** is due to the presence of fullerene. Given that the intermolecular N_{Py}–Zn axial coordination generally occurs with the angle of ~ 90° according to the crystal structures of the zinc chlorophyll derivatives in Chapters 2 and 4, we can safely assume that the cyclic tetramers formed. Indeed, the hydrodynamic radiuses of **Zn4Py** and **Zn4PyC$_{60}$** are consistent with the dimensions of their cyclic tetrameric models (Figure 6-5).

6-2-4 Coassembly of the Zinc Chlorophyll Derivatives

The coassembly of **Zn4Py** and **Zn4PyC$_{60}$** into the cyclic tetramers was investigated by the fluorescence quenching at various composition ratios of a mixture of **Zn4Py** and **Zn4PyC$_{60}$** in benzene (1.0 mM) as shown in Figure 6-6. The fluorescence intensity of **Zn4Py** significantly decreased with increasing the molar fraction of **Zn4PyC$_{60}$** (Figure 6-6a). The plot of the

(a)

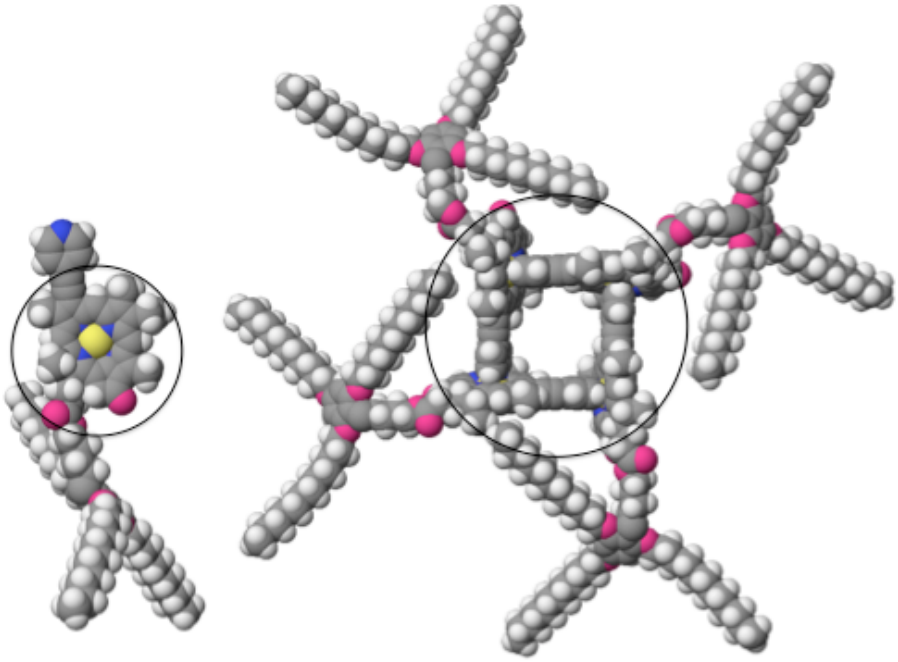

(b)

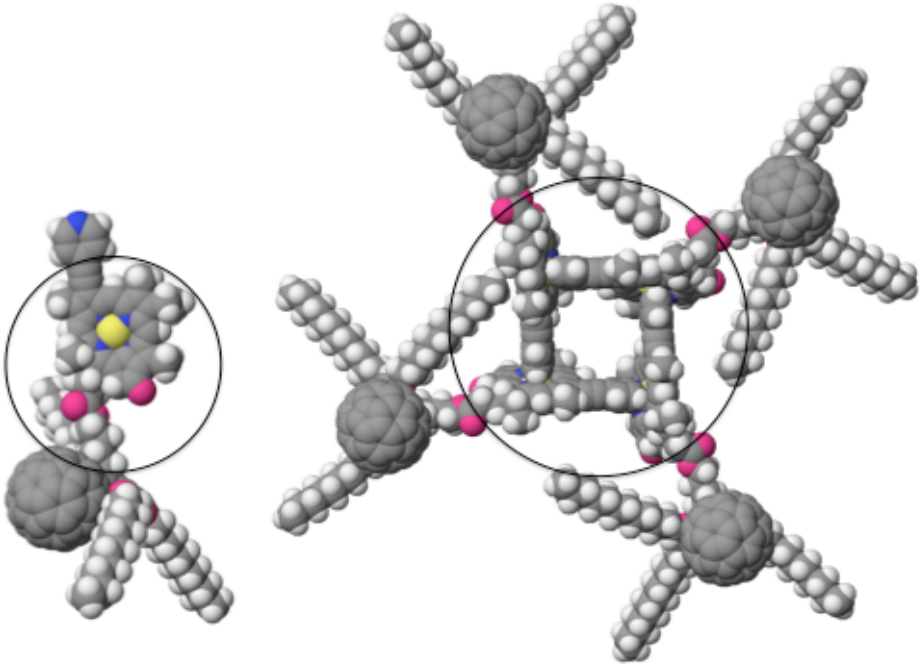

Figure 6-5. Molecular models of monomeric and tetrameric (a) **Zn4Py** and (b) **Zn4PyC$_{60}$**. The circles were drawn by use of the calculated hydrodynamic radiuses.

(a)

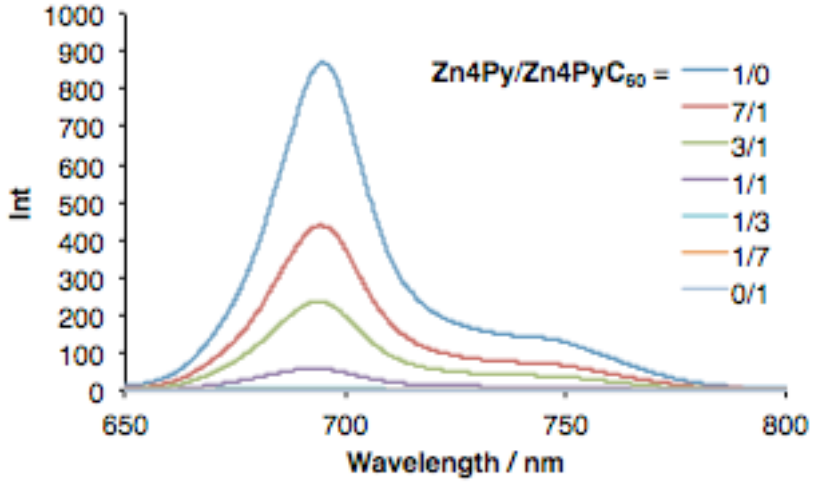

(b)

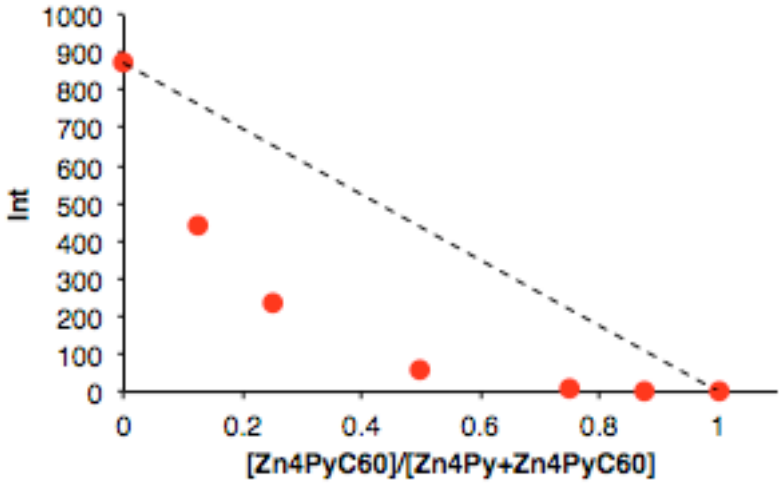

Figure 6-6. (a) Fluorescence spectra of the mixtures of **Zn4Py** and **Zn4PyC$_{60}$** in benzene (1.0 mM, r.t.). (b) The plot of the fluorescence intensity in (a) against the composition of **Zn4PyC$_{60}$**. The dashed line indicates the intensity if there were no interaction among **Zn4Py** and **Zn4PyC$_{60}$** molecules.

(a)

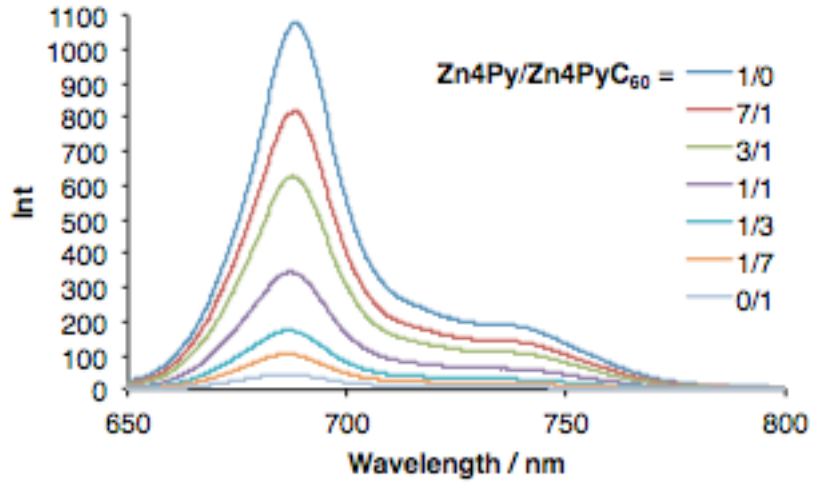

(b)

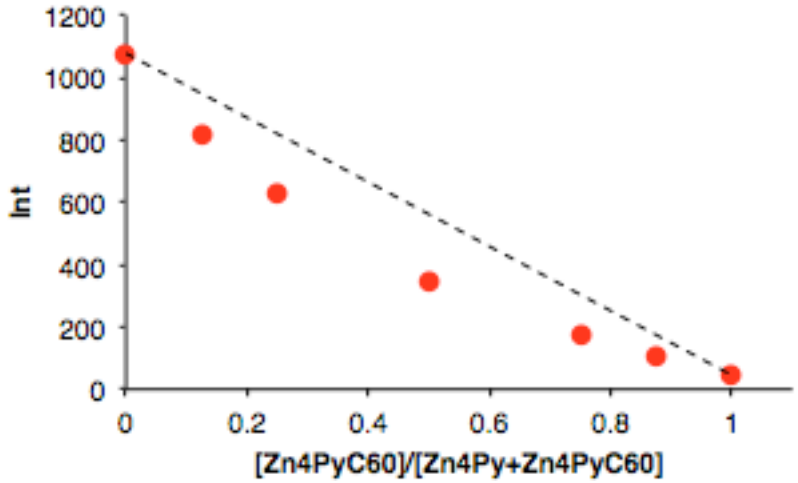

Figure 6-7. (a) Fluorescence spectra of the mixtures of **Zn4Py** and **Zn4PyC$_{60}$** in benzene containing 1% pyridine (1.0 mM, r.t.). (b) The plot of the fluorescence intensity in (a) against the composition of **Zn4PyC$_{60}$**. The dashed line indicates the intensity if there were no interaction among **Zn4Py** and **Zn4PyC$_{60}$** molecules.

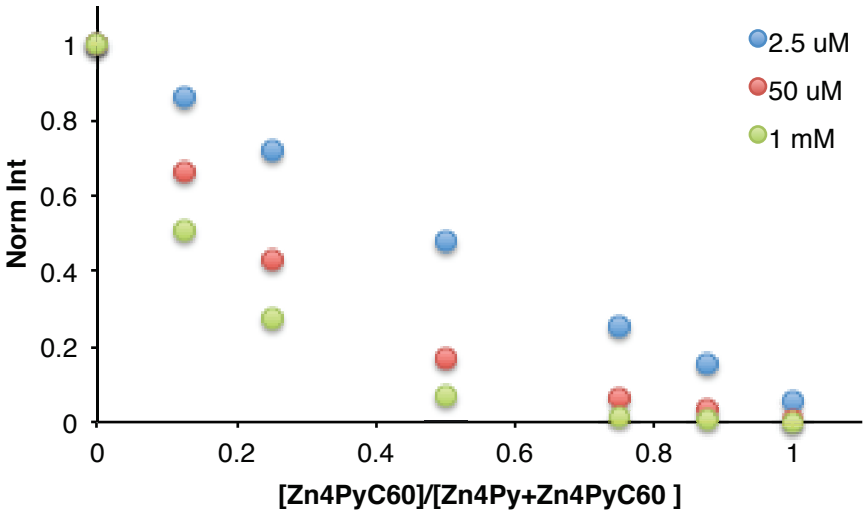

Figure 6-8. Concentration dependence of the fluorescence intensity of a mixture of **Zn4Py** and **Zn4PyC$_{60}$** in benzene.

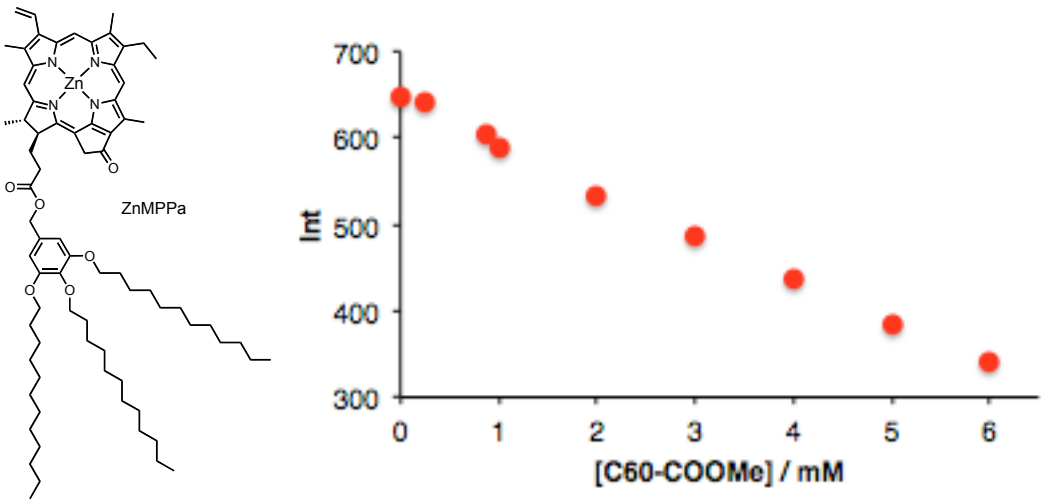

Figure 6-9. (a) Fluorescence intensity of the mixtures of **ZnMPPa** (1.0 mM) and **C_{60}** derivative **9** in benzene at r.t.

the fraction of **Zn4PyC$_{60}$** (Figure 6-6b). Because the fluorescence intensity should linearly decrease against the ratio of **Zn4PyC$_{60}$** if there was no interaction among **Zn4Py** and **Zn4PyC$_{60}$** molecules, the steeper decrease of the fluorescence intensity may thus be attributed to the energy transfer among the zinc chlorophyll moiety in the cyclic tetramers consisting of **Zn4Py** and **Zn4PyC$_{60}$** molecules followed by fluorescence quenching within **Zn4PyC$_{60}$**. Indeed, the addition of 1% pyridine, which prevent self-assembly, to the mixture of **Zn4Py** and **Zn4PyC$_{60}$** (1.0 mM) inhibited the fluorescence quenching (Figure 6-7). Further the fluorescence quenching of **Zn4Py** was smaller as decreasing the concentration of the zinc chlorophylls (Figure 6-8) because of decrease of the concentration of the cyclic tetramers upon dilution (see Figure 5-10), indicating that the significant quenching of **Zn4Py** in neat benzene is resulted in the energy transfer within the cyclic tetramers consisting of **Zn4Py** and **Zn4PyC$_{60}$** molecules.

The contribution of dynamic quenching as a consequence of direct collision of the chlorophyll moiety in **Zn4Py** and the fullerene moiety in **Zn4PyC$_{60}$** on the fluorescence quenching was investigated by the titration of the fullerene derivative **9** into a solution of a zinc chlorophyll derivative **ZnMPPa** in benzene (1.0 mM, Figure 6-9). The fluorescence intensity of **ZnMPPa** decreased with increasing the concentration of **9** due to the dynamic quenching. The fluorescence intensity of **ZnMPPa** decreased by ~8% in the presence of the equimolar amount of **9** (1 mM). This situation is equal to the presence of **Zn4PyC$_{60}$** only in solution (Figure 6-6b). Since the rate of fluorescence quenching of **Zn4Py** in a mixture of **Zn4Py** and **Zn4PyC$_{60}$** is obviously large, the dynamic quenching of the chlorophyll moiety in **Zn4Py** and the fullerene moiety in **Zn4PyC$_{60}$** can be ignored.

6-2-5 Energy Transfer within the Cyclic Tetramers

The order of magnitude of energy transfer rates in the cyclic tetramers consisting of **Zn4Py** and **Zn4PyC$_{60}$** were estimated using a model, in which the energy transfer within the tetramers occurs (i) between a zinc chlorophyll molecule and the neighbor chlorophyll molecule (k_{en1}) and (ii) between a zinc chlorophyll molecule and the next neighbor chlorophyll

molecule (k_{en2}) followed by the fluorescence quenching in **Zn4PyC$_{60}$** molecule. The experimentally obtained decay carves were fitted by the carves calculated using this model. Here we assumed the rates k_{en1} and k_{en2} are equal for simplicity (hereafter k_{en} collectively). The excited state decay rate constant (k_0) and the quenching rate constant (k_q) of **Zn4PyC$_{60}$** was determined to be 2.3×10^8 s^{-1} and 2.3×10^9 s^{-1} by use of

$$k_0 = \frac{1}{\tau_{\mathrm{Zn4Py}}} \qquad k_\mathrm{q} = \frac{1 - \tau_{\mathrm{Zn4PyC60}}\, k_0}{\tau_{\mathrm{Zn4PyC60}}}$$

where τ_{Zn4Py} and $\tau_{Zn4PyC60}$ are the lifetime of **Zn4Py** (4.3 ns) and **Zn4PyC$_{60}$** (0.4 ns), respectively, which were used as the fixed parameters for the calculation. The fitting carves at any composition ratios of **Zn4Py** and **Zn4PyC$_{60}$** were in a range of those at k_{en} = 1.0×10^8–1.0×10^9 s^{-1}, indicating that the energy transfer within the cyclic tetramers occurs with such order (Figure 6-10).

The energy transfer rate constants k_{en1} and k_{en2} were obtained by use of the formula (2)

$$k_\mathrm{en} = \frac{9\ln 10}{128\pi^5 n^4 N_\mathrm{A}\tau} \cdot \frac{\kappa^2}{r^6}\phi \int f(\lambda)\,\varepsilon(\lambda)\,\lambda^4 \mathrm{d}\lambda \qquad (2)$$

where κ^2, n, N_A, τ, r, ϕ, λ are the orientation factor, the refractive index, the Avogadro constant, the lifetime of **Zn4Py**, the center-to-center distance, the fluorescence quantum yield of **Zn4Py**, and the wavelength, respectively, in which κ^2 and r were obtained using a cyclic tetrameric model consisting of a zinc chlorophyll derivative appended by vinyl pyridine (Chapter 2) generated by DFT calculation (B3LYP, 6-31G(d)), while ϕ was determined to be 0.31 in air-saturated benzene by use of tetraphenylporphyrin as a reference compound (0.11).[22] The k_{en1} and k_{en2} values were calculated to be ~2.0×10^8 s^{-1} and ~5.0×10^8 s^{-1}, respectively, which are in the same order of magnitude with the experimentally estimated k values. Because the calculated decay curves using these k_{en} values (Figure 6-10, dashed line) are approximately consistent with the measured curves, and we thus concluded that the energy transfer within the cyclic tetramers occurs at a rate in the order of k_{en} = 1.0×10^8–1.0×10^9 s^{-1}. The slight deviation between the calculated and the measured curves could be ascribed to the structural fluctuation of the tetramers due to their flexibility and/or the contribution of other

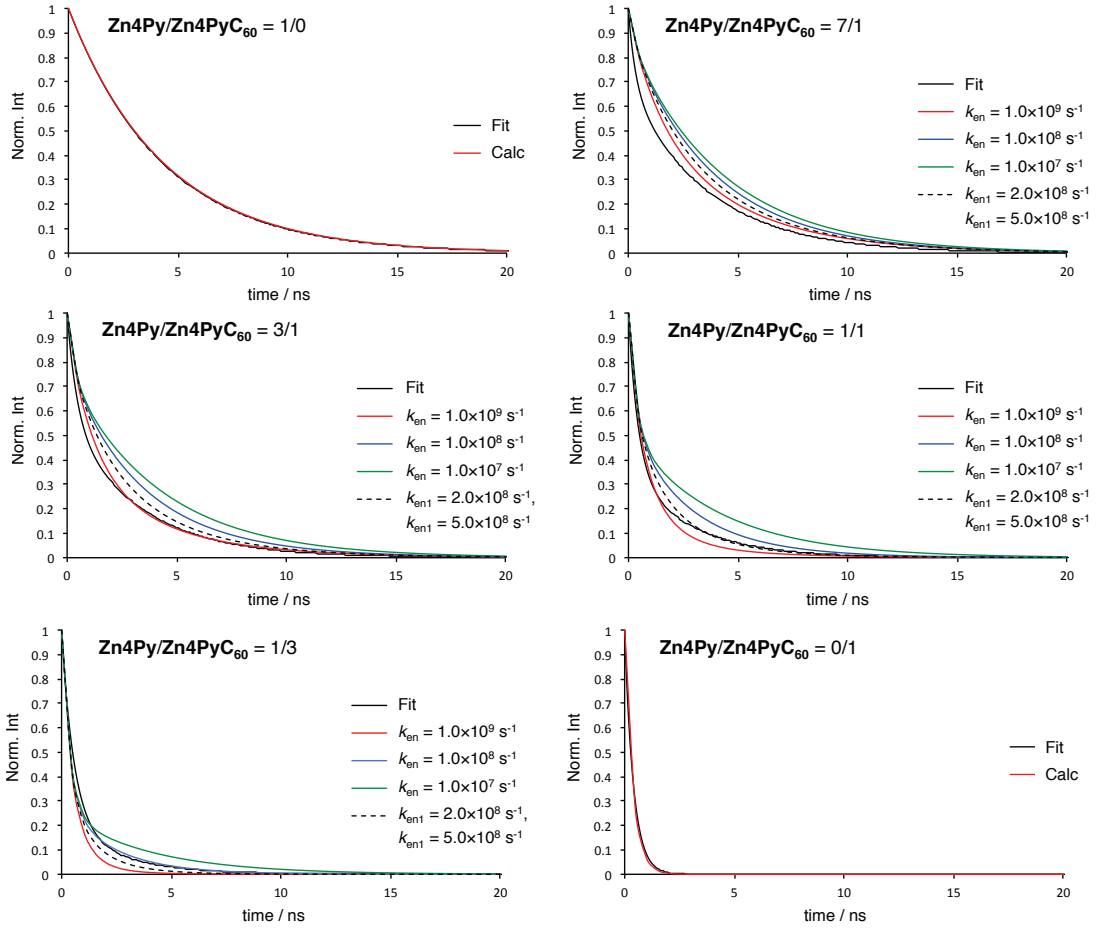

Figure 6-10. Fluorescence decay curves of the mixtures of **Zn4Py** and **Zn4PyC$_{60}$** in benzene (1.0 mM) at different composition ratios.

The slight deviation between the calculated and the measured curves could be ascribed to the structural fluctuation of the tetramers due to their flexibility and/or the contribution of other energy transfer pathways.

6-3 Conclusion

We successfully constructed the cyclic tetramers by coassembly of the zinc chlorophyll **Zn4Py** and its fullerene conjugate **Zn4PyC$_{60}$** *via* the intermolecular N_{Py}–Zn axial coordination. The significant fluorescence quenching of **Zn4Py** was observed when it was mixed with **Zn4PyC$_{60}$** as compared with the fluorescence intensity assuming that there was no interaction between **Zn4Py** and **Zn4PyC$_{60}$** molecules, indicating the antenna effect in the cyclic tetramers consisting both of **Zn4Py** and **Zn4PyC$_{60}$** molecules. Further we suggested that the energy transfer within the cyclic tetramers occurs with the rate constant in the order of of 1.0×10^{8}–1.0×10^{9} s^{-1}.

6-4 Experiment

6-4-1 General

All solvents and reagents as purchased were used for the reactions without further purification.

Spectroscopic grade benzene was purchased from Wako. $CDCl_3$ was C_6D_6 purchased from Sigma-Aldrich. ^{1}H NMR and DOSY spectra were recorded with a 400 MHz JEOL ECX 400 spectrometer, and chemical shifts were reported in ppm relative to internal tetramethylsilane (TMS). The peaks were assigned using COSY, NOESY, HMQC, HMBC, and DEPT. Mass spectrometry analysis was performed with an Agilent G1969A mass spectrometer using APCI ionization method in the positive mode. HPLC was performed with a Shimadzu HPLC 20A apparatus using a solvent system consisting of MeOH and $CHCl_3$, and the flow rates was 0.5 mL/min. UV-vis spectra and fluorescence spectra were obtained using a Shimadzu UV-2400PC spectrometer and a JASCO FP-8600 fluorometer, respectively. Fluorescence lifetimes were measured by a Hamamatsu Photonics Quantaurus Tau system. The molecular

models were obtained with MM3 using CAChe software (version 6.1.12.33).

6-4-2 Syntheses

3. To a mixture of **2** (7.6 g, 12 mmol) and glutaric anhydride (2.3 g, 20 mmol) in CH_2Cl_2 (20.0 mL) was added $AlCl_3$ (3.7 g, 20 mmol) at 0 °C, and the resulting mixture was then stirred for 10 min at 0 °C. After stirring overnight at r.t., the mixture was pored into the mixture of ice and 1N HCl (100 mL) to quench the reaction. The aqueous layer was extracted with $CHCl_3$/THF (1/2, 100 mL×3) followed by washing with brine. The solvent was eliminated after drying with $MgSO_4$ to give brown oil (9.6 g). The crude mixture was purified by column chromatography (silica, hexane/EtOAc = 19/1→9/1) to afford **3** as a pale yellow solid (1.8 g, 2.4 mmol, 20%) which solidified by standing.

^{1}H-NMR ($CDCl_3$, 298 K): δ = 6.05 (s, 2H, Ph), 3.94–3.88 (m, 6H, CH_2), 2.81 (t, J = 6.9 Hz, 2H, CH_2), 2.43 (t, J = 7.3 Hz, 2H, CH_2), 1.99 (quintet, J = 7.2 Hz, 2H, CH_2), 1.80–1.67 (m, 6H, CH_2), 1.48–1.26 (m, 55H, CH_2), and 0.90–0.86 (m, 9H, CH_3) ppm; HRMS: m/z = 745.6350 $[M+H]^+$ (100%), calcd for $C_{47}H_{85}O_6$ 745.6346.

4. To a suspension of **3** (1.0 g, 1.4 mmol) in MeOH (100 mL) conc. H_2SO_4 (5.0 mL) was added, and the resulting white cloudy mixture was heated to reflux overnight. The solvent was eliminated to give yellow oil (1.4 g). The crude mixture was purified by column chromatography (silica, hexane/EtOAc = 19/1) to afford **4** (1.0 mg, 1.3 mmol, 97%) as pale yellow oil.

^{1}H-NMR ($CDCl_3$, 298 K): δ = 6.04 (s, 2H, Ph), 3.94–3.88 (m, 6H, CH_2), 3.65 (s, 3H, COOMe), 2.78 (t, J = 7.1 Hz, 2H, CH_2), 2.38 (t, J = 7.6 Hz, 2H, CH_2), 1.98 (quintet, J = 7.3 Hz, 2H, CH_2), 1.78–1.69 (m, 6H, CH_2), 1.46–1.26 (m, 55H, CH_2), and 0.88 (t, J = 6.9 Hz, 9H, CH_3) ppm; HRMS: m/z = 759.6509 $[M+H]^+$ (100%), calcd for $C_{48}H_{87}O_6$ 759.6503.

5. To a vessel containing 10% Pd/C (55% wet, 249 mg) was added dropwise a solution of **4** (862 mg, 1.2 mmol) in EtOH/AcOH (3/1, mL) under H_2 atmosphere. After the mixture was stirred overnight at r.t., Pd/C was eliminated by suction filtration. The solvent was evaporated to give pale yellow oil (883 mg). The crude mixture was purified by column chromatography

(silica, hexane/EtOAc = 9/1) to afford **5** (774 mg, 1.1 mmol, 91%) as colorless oil.

^{1}H-NMR ($CDCl_3$, 298 K): δ = 6.07 (s, 2H, Ph), 3.92–3.88 (m, 6H, CH_2), 2.58 (t, J = 7.3 Hz, 2H, CH_2), 2.36 (t, J = 7.6 Hz, 2H, CH_2), 1.76 (quintet, J = 6.9 Hz, 6H, CH_2), 1.65 (quintet, J = 7.4 Hz, 2H, CH_2), 1.55–1.26 (m, 57H, CH_2), and 0.88 (t, J = 6.9 Hz, 9H, CH_3) ppm; HRMS: m/z = 731.6572 $[M+H]^+$ (100%), calcd for $C_{47}H_{87}O_5$ 731.6554.

6. To a vessel containing a suspension of LiAlH (148 mg, 4.2 mmol) in THF (10 mL) was added slowly dropwise a solution of **5** (774 mg, 1.1 mmol) in THF (10 mL), and the mixture was stirred at r.t. for 1 h followed by reflux for 3.5 h. After quenching the reaction by addition of H_2O (1.0 mL) and MeOH (1.0 mL) after cooling to r.t., the solid was removed by suction filtration. The solvent was eliminated to give pale yellow oil (772 mg). The crude mixture was purified by column chromatography (silica, $CHCl_3$/hexane = 2/1) to afford **6** as colorless oil (603 mg, 0.84 mmol, 79%) which solidifies after standing.

^{1}H-NMR ($CDCl_3$, 298 K): δ = 6.08 (s, 2H, Ph), 3.92–3.88 (m, 6H, CH_2), 3.62 (t, J = 6.6 Hz, 2H, CH_2), 2.58 (t, J = 7.3 Hz, 2H, CH_2), 1.76 (quintet, J = 6.9 Hz, 6H, CH_2), 1.60 (quintet, J = 7.1 Hz, 2H, CH_2), 1.53–1.26 (m, 59H, CH_2), and 0.88 (t, J = 6.9 Hz, 9H, CH_3) ppm; HRMS: m/z = 717.6766 $[M+H]^+$ (100%), calcd for $C_{47}H_{89}O_4$ 717.6761.

7. A solution of **6** (269 mg, 0.35 mmol), *p*-toluenesulfonyl hydrazide (69 mg, 0.37 mmol), and *p*-TsOH•H_2O (5.9 mg, 0.034 mmol) in toluene (7.5 mL) was heated to reflux for 2.5 h. The solvent was eliminated to give a mixture of a white slid and oil (321 mg). The crude mixture was purified by column chromatography (silica, hexane/EtOAc = 9/1) to afford **7** (242 mg, 0.26 mmol, 75%) as yellow oil.

^{1}H-NMR ($CDCl_3$, 298 K): δ = 7.82 (d, J = 8.0 Hz, 2H, Ph), 7.28 (d, J = 8.0 Hz, 2H, Ph), 6.04 (s, 2H, Ph), 3.93 (t, J = 6.4 Hz, 2H, CH_2), 6.78 (t, J =6.6 Hz, 4H, CH_2), 3.63 (s, 3H, COOMe), 2.47 (t, J = 7.1 Hz, 2H, CH_2), 2.42 (s, 3H, CH_3), 2.23 (t, J = 7.8 Hz, 2H, CH_2), 1.76 (septet, J = 7.3 Hz, 4H, CH_2), 1.49–1.27 (m, 60H, CH_2), and 0.88 (t, J = 6.9 Hz, 9H, CH_3) ppm; HRMS: m/z = 927.6886 $[M+H]^+$ (100%), calcd for $C_{55}H_{95}O_7S$ 927.6860.

9. To a solution of **7** (647 mg, 0.70 mmol) in dry pyridine (3.0 mL) was added NaOMe (53 mg, 0.99 mmol), and the mixture was stirred at r.t. for 1 h. A solution of fullerene (358.2 mg,

0.50 mmol) in *o*-dichlorobenzene (19 mL) was added to the mixture, and the resulting purple mixture was heated to reflux overnight. The solvent was eliminated *in vacuo* to give a brown viscous material (1.2 g). The fraction containing the [5,6] isomers **8** and the [6,6] isomer **9** as the major and the minor products, respectively, was separated by column chromatography (silica, hexane/chlorobenzene = 3/1→2/1) to give a brown viscous material (379 mg). The brown mixture was dissolved in *o*-dichlorobenzene (20 mL), and the solution was heated to reflux for 5 days. The solvent was eliminated *in vacuo* to give a brown viscous matter (447 mg), which was purified by column chromatography (silica, hexane/EtOAc = 50/1) to afford **9** (328 mg, 0.27 mmol, 45% over 2 steps) as a brown viscous material.

^{1}H-NMR ($CDCl_3$, 298 K): δ = 6.27 (s, 2H, Ph), 4.11–4.01 (m, 4H, CH_2), 3.97–3.91 (m, 2H, CH_2), 3.67 (s, 3H, COOMe), 2.53 (t, J = 7.6 Hz, 2H, CH_2), 2.27–2.19 (m, 2H, CH_2), 1.95–1.78 (m, 6H, CH_2), 1.62–1.22 (m, 55H, CH_2), and 0.90–0.85 (m, 9H, CH_3) ppm; HRMS: *m/z* = 1463.6560 $[M+H]^+$, calcd for $C_{108}H_{87}O_5$ 1463.6553.

10. To a solution of **9** (803 mg, 0.55 mmol) in toluene (150 mL) was added dropwise DIBAL-H (1.0 M in heptane, 4.0 mL), and the mixture was stirred overnight. After quenching the reaction by addition of sat. NH_4Cl (15 mL), the reaction mixture was poured into brine (50 mL). The aqueous layer was extracted with $CHCl_3$ (50 mL×3), and the combined organic layer was washed with brine (100 mL×3). The solvent was evaporated after drying with Na_2SO_4 to give a brown viscous material (793 mg). The crude mixture was purified by column chromatography (silica, hexane/EtOAc = 15/1) to afford **10** (694 mg, 0.48 mmol, 88%) as a brown viscous material.

^{1}H-NMR ($CDCl_3$, 298 K): δ = 6.27 (s, 2H, Ph), 4.11–4.01 (m, 4H, CH_2), 3.96–3.91 (m, 2H, CH_2), 3.75–3.71 (m, 2H, CH_2), 2.87–2.82 (m, 2H, CH_2), 2.01–1.73 (m, 10H, CH_2), 1.65–1.22 (m, 55H, CH_2), and 0.90–0.85 (m, 9H, CH_3) ppm; HRMS: *m/z* = 1435.6596 $[M+H]^+$, calcd for $C_{107}H_{87}O_4$ 1435.6604.

General Procedure of Transesterification. To a solution of the methyl ester **19** (30 mg, 0.048 mmol) and an alcohol (0.057 mmol) in toluene (7.5 mL) was added

bis(dibutylchlorotin(IV)) oxide (10 mg, 0.018 mmol), and the mixture was heated to reflux overnight. The solvent was evaporated to give a brown solid. The crude mixture was purified by column chromatography (silica, 2% acetone/$CHCl_3$) to afford the transesterified compound as a brown solid.

Fb4Py. Yield: 76%; ^{1}H-NMR ($CDCl_3$, 298 K): δ = 9.59 (s, 1H, meso), 9.57 (s, 1H, meso), 8.82 (d, J = 5.5 Hz, 2H, Py), 8.66 (s, 1H, meso), 7.77 (d, J = 5.5 Hz, 2H, Py), 6.02 (s, 2H, Ph), 5.31 (d, J = 19.7 Hz, 1H, 13^2-H), 5.15 (d, J = 19.7 Hz, 1H, 13^2-H), 4.56–4.51 (m, 1H, 18-H), 4.36–4.29 (m, 1H, 17-H), 4.09–3.98 (m, 2H, CH_2), 3.87–3.80 (m, 6H, CH_2), 3.75–3.70 (m, 5H, ring CH_3, 8$\underline{CH_2}CH_3$), 3.56 (s, 3H, ring CH_3), 3.30 (s, 3H, ring CH_3), 2.76–2.68 (m, 1H, 17^1-H or 17^2-H), 2.61–2.48 (m, 3H, 17^1-H or 17^2-H, CH_2), 2.33–2.24 (m, 2H, 17^1-H or 17^2-H), 1.84 (d, J = 7.3 Hz, 3H, 18-CH_3), 1.74–1.54 (m, 15H, 8$CH_2\underline{CH_3}$, CH_2), 1.44–1.54 (m, 55H, CH_2), 0.89–0.81 (m, 9H, CH_3), 0.17 (bs, 1H, NH), and -1.91 (bs, 1H, NH) ppm; HRMS: *m/z* = 1308.9410 $[M+H]^+$ (100%), calcd for $C_{85}H_{122}N_5O_6$ 1308.9395; GPC V_R = 147.4 mL (100%).

Fb4PyC$_{60}$. Yield: 77%; ^{1}H-NMR ($CDCl_3$, 298 K): δ = 9.56 (s, 1H, meso), 9.54 (s, 1H, meso), 8.82 (dd, J = 5., 1.8 Hz, 2H, Py), 8.62 (s, 1H, meso), 7.77 (dd, J = 5.5, 1.8 Hz, 2H, Py), 6.19 (d,J = 2.3 Hz, 2H, Ph), 5.28 (d, J = 19.3 Hz, 1H, 13^2-H), 5.12 (d, J = 19.3 Hz, 1H, 13^2-H), 4.53–4.48 (m, 1H, 18-H), 4.33–4.31 (m, 1H, 17-H), 4.22–4.10 (m, 2H, CH_2), 4.00–3.90 (m, 4H, CH_2), 3.86–3.79 (m, 2H, CH_2), 3.74–3.67 (m, 5H, ring CH_3, 8$\underline{CH_2}CH_3$), 3.54 (s, 3H, ring CH_3), 3.30 (s, 3H, ring CH_3), 2.77–2.68 (m, 3H, 17^1-H or 17^2-H, CH_2), 2.62–2.54 (m, 1H, 17^1-H or 17^2-H), 2.37–2.22 (m, 2H, 17^1-H or 17^2-H), 1.95–1.62 (m, 9H, CH_2), 1.85 (d, J =7.3 Hz, 3H, 18-CH_3), 1.72 (t, J = 7.3 Hz, 3H, 8$CH_2\underline{CH_3}$), 1.48–1.06 (m, 55H, CH_2), 0.89–0.80 (m, 9H, CH_3), 0.15 (bs, 1H, NH), and -1.93 (bs, 1H, NH) ppm; HRMS: *m/z* = 2026.9260 $[M+H]^+$, calcd for $C_{145}H_{120}N_5O_6$ 2026.9238; GPC V_R = 155.0 mL (100%).

General Procedure of Zinc Insetion. To a solution of the free-base chlorophyll (0.025 mmol) in $CHCl_3$ (30 mL) was added a saturated solution of $Zn(OAc)_2$•$2H_2O$ in MeOH (5.0 mL). After stirring for 4 h, sat. $NaHCO_3$ (10 mL) was added and the mixture was stirred for 10 min. The organic layer was separated, and was then washed with brine (50 mL×3), and was

dried with Na_2SO_4. The solvent was evaporated to a give deep green solid. The crude mixture was purified by filtration through a short plug of silica (3% acetone/$CHCl_3$) to afford the zinc complex as a deep green solid.

Zn4Py. Yield: 74%; ^{1}H-NMR ($CDCl_3$, 298 K): δ = 9.62 (s, 1H, meso), 8.94 (s, 1H, meso), 8.35 (s, 1H, meso), 6.11 (d,*J* = 4.6 Hz, 2H, Py), 5.99 (s, 2H, Ph), 5.23 (d, *J* = 19.7 Hz, 1H, 13^2-H), 5.08 (d, *J* = 19.7 Hz, 1H, 13^2-H), 4.49–4.44 (m, 1H, 18-H), 4.25–4.23 (m, 1H, 17-H), 4.22–4.10 (m, 2H, CH_2), 4.04 (t, *J* = 6.0 Hz, 4H, CH_2), 3.87–3.71 (m, 7H, CH_2, ring CH_3, and 8$\underline{CH_2}CH_3$), 3.35 (bs, 2H, Py), 3.14 (s, 3H, ring CH_3), 3.01 (s, 3H, ring CH_3), 2.71–2.48 (m, 4H, 17^1-H or 17^2-H, CH_2), 2.37–2.22 (m, 2H, 17^1-H or 17^2-H), 1.76–1.57 (m, 18H, CH_2, 18-CH_3, and 8$CH_2\underline{CH_3}$), 1.44–1.15 (m, 54H, CH_2), and 0.89–0.79 (m, 9H, CH_3) ppm; HRMS: *m/z* = 1370.8536 $[M+H]^+$ (100%), calcd for $C_{85}H_{120}N_5O_6Zn$ 1370.8530.

Zn4PyC$_{60}$. Yield: 99%; ^{1}H-NMR ($CDCl_3$, 298 K): δ = 9.61 (s, 1H, meso), 8.92 (s, 1H, meso), 8.30 (s, 1H, meso), 6.18 (s, 2H, Ph), 6.12 (bs, 2H, Py), 5.22 (d, *J* = 19.7 Hz, 1H, 13^2-H), 5.06 (d, *J* = 19.7 Hz, 1H, 13^2-H), 4.47–4.41 (m, 1H, 18-H), 4.23–4.20 (m, 1H, 17-H), 4.14–4.10 (m, 2H, CH_2), 4.00–3.93 (m, 4H, CH_2), 3.84–3.71 (m, 7H, CH_2, ring CH_3, and 8$\underline{CH_2}CH_3$), 3.42 (bs, 2H, Py), 3.12 (s, 3H, ring CH_3), 3.00 (s, 3H, ring CH_3), 2.70–2.47 (m, 4H, 17^1-H or 17^2-H, CH_2), 2.34–2.17 (m, 2H, 17^1-H or 17^2-H), 1.89–1.67 (m, 16H, CH_2, 18-CH_3, and 8$CH_2\underline{CH_3}$), 1.46–1.10 (m, 54H, CH_2), and 0.88–0.79 (m, 9H, CH_3) ppm; HRMS: *m/z* = 2088.8423 $[M+H]^+$, calcd for $C_{145}H_{119}N_5O_6Zn$ 2088.8373.

6-5 References

(1) Frischmann, P. D.; Mahata, K.; Würthner, F. *Chem. Soc. Rev.* **2013**, *42*, 1847.

(2) Kudo, A.; Miseki, Y. *Chem. Soc. Rev.* **2009**, *38*, 253.

(3) Tachibana, Y.; Vayssieres, L.; Durrant, J. R. *Nat. Photon.* **2012**, *6*, 511.

(4) Kobuke, Y. *Eur. J. Inorg. Chem.* **2006**, 2333.

(5) Choi, M.-S.; Yamazaki, T.; Yamazaki, I.; Aida, T. *Angew. Chem. Int. Ed.* **2004**, *43*, 150.

(6) Gunderson, V. L.; Smeigh, A. L.; Kim, C. H.; Co, D. T.; Wasielewski, M. R. *J. Am. Chem. Soc.* **2012**, *134*, 4363.

(7) Kuramochi, Y.; Satake, A.; Itou, M.; Ogawa, K.; Araki, Y.; Ito, O.; Kobuke, Y. *Chem. Eur. J.* **2008**, *14*, 2827.

(8) Shinozaki, Y.; Richards, G.; Ogawa, K.; Yamano, A.; Ohara, K.; Yamaguchi, K.; Kawano, S.-i.; Tanaka, K.; Araki, Y.; Wada, T.; Otsuki, J. *J. Am. Chem. Soc.* **2013**, *135*, 5262.

(9) Shinozaki, Y.; Yoshikawa, I.; Araki, K.; Ohara, K.; Yamaguchi, K.; Kawano, S.-i.; Tanaka, K.; Araki, Y.; Wada, T.; Otsuki, J. *Chem. Lett.* **2014**, *43*, 862.

(10) Shinozaki, Y.; Yoshikawa, I.; Araki, K.; Sugawa, K.; Otsuki, J. *CrystEngComm* **2014**, *16*, 9155.

(11) Sasaki, S.-i.; Mizutani, K.; Kunieda, M.; Tamiaki, H. *Tetrahydron* **2011**, *67*, 6065.

(12) Yamamoto, Y.; Tamiaki, H. *Tetrahedron* **2014**, *70*, 2731.

(13) Kozyrev, A. N.; Dougherty, T. J.; Pandey, R. K. *Chem. Commun.* **1998**, *4*, 481.

(14) Sasaki, S.-i.; Tamiaki, H. *Tetrahedron Lett.* **2006**, *47*, 4965.

(15) Tamiaki, H.; Holzwarth, A. R.; Schaffner, K. *J. Photochem. Photobiol., B* **1992**, *15*, 355.

(16) Kelley, R. F.; Goldsmith, R. H.; Wasielewski, M. R. *J. Am. Chem. Soc.* **2007**, *129*, 6384.

(17) Tkachenko, N. V.; Tauber, A. Y.; Grandell, D.; Hynninen, P. H.; Lemmetyinen, H. *J. Phys. Chem. A* **1999**, *103*, 3646.

(18) Zheng, G.; J. Dougherty, T.; K. Pandey, R. *Chem. Commun.* **1999**, 2469.

(19) Ohkubo, K.; Kotani, H.; Shao, J.; Ou, Z.; Kadish, K. M.; Li, G.; Pandey, R. K.; Fujitsuka, M.; Ito, O.; Imahori, H.; Fukuzumi, S. *Angew. Chem. Int. Ed.* **2004**, *43*, 853.

(20) Oliva, A. I.; Gómez, K.; Gonzáleza, G.; Ballester, P. *New J. Chem.* **2008**, *32*, 2159.

(21) Sprafke, J. K.; Odell, B.; Claridge, T. D. W.; Anderson, H. L. *Angew. Chem. Int. Ed.* **2011**, *50*, 5572.

(22) Wang, T. Y.; Chen, J. R.; Ma, J. S. *Dyes Pigm.* **2002**, *52*, 199.

Chapter 7

Conclusion

Conclusion

This dissertation described the possibility of the novel types of chromophore array for the artificial light-harvesting antennae. Control of overall three-dimensional structure is one of the critical issues for exploring the efficient antenna model besides selecting individual chromophores. The results obtained in this work are summarized below.

The self-assembled structures of zinc chlorophyll derivatives appended by vinylpyridine as a lead compound were identified in detail in solution and in the crystal in Chapter 2. The nitrogen atom in the *N*-heterocyclic moiety intermolecularly coordinates to the zinc atom at the center of chlorophyll ring, giving two types of molecular assemblies. The self-assembly of the zinc chlorophyll derivative afforded the cyclic tetramers in solution and the double-helical coordination polymers in the crystal. The interstrand energy transfer is expected to be more efficient than intrastrand energy transfer due to the preferable orientations among the zinc chlorophyll molecules being in different strands in the double helix for energy transfer.

We clarified that the altering the *N*-heterocyclic moiety in the zinc chlorophyll derivative influences the higher-order structures of the arrays of zinc chlorophyll derivatives in both solution and the crystal in Chapter 3. The zinc chlorophyll derivative appended by oxazole formed the cyclic trimers as a predominant species in solution while it formed the staircase-like coordination polymers in the crystal.

The fact that the energy transfer efficiency depends on the interchromophore orientation and distance requires the proper design of the higher-order structures of the chromophore arrays. Since the higher-order structures of the coordination polymers dramatically change by altering the *N*-heterocyclic moiety (Chapters 2 and 3), we attempted to control the structures of the polymers by use of the two regioisomeric zinc chlorophyll derivatives appended by 3- or 4-phenylpyridine as a coordination site in Chapter 4. The 4-pyridine derivative formed the staircase-like coordination polymers whereas the 3-pyridine derivative formed the single stranded helical coordination

polymers in the crystals. The energy transfer efficiencies within the polymers changed simultaneously with the change of their higher-order structures as expected. It was clarified that the energy transfer within the helical polymers occurs more than 300 times as efficiently as that within the staircase-like polymers.

From Chapter 5, we focused on the cyclic oligomers formed in solution. Although the cyclic oligomers of the zinc chlorophyll derivatives as described in Chapters 2 and 3 are also promising chromophore array for the light-harvesting antennae, their poor solubility prevented the advanced studies. In this context, we introduced the four different types of dendrons into the zinc chlorophyll derivative appended by pyridine and confirmed the improved solubility of the cyclic tetramers formed by the self-assembly. Further, for appropriately selecting the dendron moiety toward following studies, the effect of the structures of the dendron moiety in the zinc chlorophyll on the stability of the cyclic tetramers was also studied. As no difference in the stability due to different dendron moieties, the smaller dendron is preferable as a solubilizing auxiliary given the synthetical easiness.

We successfully obtained the cyclic tetramers formed by the coassembly of the zinc chlorophyll derivative appended by pyridine and its fullerene dyad, which were designed on the basis of the result that introduction of the dendron into the zinc chlorophyll improves the solubility of the cyclic tetramer in Chapter 5, toward demonstration of the antenna function of the tetramers in Chapter 6. We constructed the cyclic tetramers consisting of two parts: an antenna site comprising the zinc chlorophyll molecules and an electron-accepting site by coassembly of the zinc chlorophyll derivative and its fullerene dyad. The fluorescence quenching of the zinc chlorophyll components in the cyclic tetramers was successfully observed as a consequence of the energy transfer within the tetramers followed by the electron transfer to the fullerene moiety. Therefore we demonstrated that the cyclic tetramers is not only a promising antenna model but also actually behave as an antenna–charge separation system.

The purpose of the control of the higher-order structure of the zinc chlorophyll arrays for exploring the promising antenna model was achieved by the investigation of the self-assembled structures of the zinc chlorophyll derivatives with systematically altered structures. We successfully obtained the three types of coordination polymers, among which the coordination polymers with double-helical motif (Chapter 2) have the most efficient energy transfer pathway among those. Further we demonstrated that the zinc chlorophyll cyclic oligomers are also applicable as the artificial antenna in Chapter 6 by demonstrating the antenna effect in the cyclic tetramers formed by the coassembly of the light-harvesting zinc chlorophyll molecule and its dyad including an electron-accepting moiety. The “exploring the promising antenna model” in this work was performed with a plan in mind for incorporation of our zinc chlorophyll arrays into the actual solar energy conversion system like the solar cells. The issues to be addressed as the next step toward the realization of the artificial light-harvesting antennae have now become clear (i) the construction of the stable coordination polymers in an isolated environment and (ii) the quantitative evaluation of the photophysical processes within the cyclic tetramers. These studies will lay the foundation for the conjugation of the antenna models in this work into the actual photoelectric devices as the final target.

Publication List

(1) Shinozaki, Y.; Richards, G.; Ogawa, K.; Yamano, A.; Ohara, K.; Yamaguchi, K.; Kawano, S.-i.; Tanaka, K.; Araki, Y.; Wada, T.; Otsuki, J. J. Am. Chem. Soc. 2013, 135, 5262.

(2) Shinozaki, Y.; Yoshikawa, I.; Araki, K.; Ohara, K.; Yamaguchi, K.; Kawano, S.-i.; Tanaka, K.; Araki, Y.; Wada, T.; Otsuki, J. Chem. Lett. 2014, 43, 862.

(3) Shinozaki, Y.; Yoshikawa, I.; Araki, K.; Sugawa, K.; Otsuki, J. CrystEngComm 2014, 16, 9155.